

# **Morphological Profiling of Small Molecules for Mode-of-Action Studies using the Cell Painting Assay**

**Dissertation**

zur Erlangung des akademischen Grades eines

**Doktors der Naturwissenschaften**

**(Dr. rer. nat.)**

der Fakultät für Chemie und Chemische Biologie

der Technischen Universität Dortmund

vorgelegt von

M.Sc. Tabea Schneidewind

geboren am 22.09.1990

in Steinheim, Deutschland

Dortmund, 15.03.2021





Die vorliegende Arbeit wurde im Zeitraum von November 2016 bis März 2021 unter der Anleitung von Prof. Dr. Dr. h.c. Herbert Waldmann und Dr. Slava Ziegler an der Fakultät für Chemie und Chemische Biologie der Technischen Universität Dortmund und dem Max-Planck-Institut für molekulare Physiologie in Dortmund angefertigt.

1. Gutachter: Prof. Dr. Dr. h.c. Herbert Waldmann
2. Gutachter: Dr. Leif Dehmelt

**Publication list:**

T. Schneidewind, S. Kapoor, G. Garivet, G. Karageorgis, R. Narayan, G. Vendrell-Navarro, A. P. Antonchick, S. Ziegler, H. Waldmann, "The Pseudo Natural Product Myokinasib is a Myosin Light Chain Kinase 1 Inhibitor with Unprecedented Chemotype", *Cell Chem. Biol.* **2019**, 26, 512-523.

A. Friese, S. Kapoor, T. Schneidewind, S. R. Vidadala, J. Sardana, A. Brause, T. Förster, M. Bischoff, J. Wagner, P. Janning, S. Ziegler, H. Waldmann, "Chemical Genetics Reveals a Role of dCTP Pyrophosphatase 1 in Wnt Signaling", *Angew. Chem.* **2019**, 131, 13143-13147.

J. Schulte-Zweckel, T. Schneidewind, J. L. Abad, A. Brockmeyer, P. Janning, G. Triola, "Azide-tagged sphingolipids for the proteome-wide identification of C16-ceramide-binding proteins", *Chem. Commun.* **2018**, 54, 13742-13745.

**Results presented in this thesis contributed to the following publications:**

T. Schneidewind, A. Brause, S. Sievers, A. Pahl, M. G. Sankar, M. Winzker, P. Janning, K. Kumar, S. Ziegler, H. Waldmann, "Combined morphological and proteome profiling reveals target-independent impairment of cholesterol homeostasis", *Cell Chem. Biol.* **2020**, in revision.

T. Schneidewind, A. Brause, A. Pahl, A. Burhop, T. Mejuch, S. Sievers, H. Waldmann, S. Ziegler, "Morphological profiling identifies a common mode of action for small molecules with different targets", *ChemBioChem* **2020**, 21, 1-12.

## Acknowledgements

I am very grateful for the past years as they made me grow as a scientist but also as a person in many ways. I would like to thank all people who contributed to my development. It was a very exciting but also demanding time that I will never forget.

First and foremost, I would like to thank Prof. Dr. Dr. h.c. Herbert Waldmann for giving me the opportunity to join his research group with all the inspiring projects that I worked on. I highly appreciate the continuous access to outstanding equipment and really enjoyed the great working atmosphere, encouraging an independent way of work. I am still impressed by his scientific knowledge and his true passion for science and would like to thank him for his patient guidance and support.

I would like to express my gratitude to Dr. Leif Dehmelt for taking the time and being my second examiner.

My deepest gratitude goes to Dr. Slava Ziegler, my co-supervisor and group leader, for her constant guidance, support and valuable input that contributed to the success of my projects. She always had an open ear and helped with words and deeds if necessary. I also highly appreciate her encouragement to join workshops and seminars to broaden my mind in relation to scientific research but also to develop my soft skills. Furthermore, I would like to thank her for taking the time to proofread my thesis.

My special thanks go to Alexandra Brause, who worked together with me after finishing her trainee. She is really talented and was extremely dedicated to contribute with her own ideas and scientific work to push my projects forward. She really was a great support and assistance, not only in the lab but also as a friend.

I would like to thank the mass spectrometry facility, especially Dr. Petra Janning, Andreas Brockmeyer, Malte Metz and Jens Warmers for labelling and measuring my samples and analyzing the data. I really appreciate the constructive discussions and feedback regarding the experimental set up and data analysis.

I would particularly like to thank the team of the Compound Management and Screening Center in Dortmund for support in terms of compound handling, stability, purity and screening, especially Dr. Sonja Sievers, Dr. Axel Pahl and Dr. Claude Ostermann. Sonja Sievers and Axel Pahl did an excellent job in setting up and performing the Cell Painting Assay as well as processing and analyzing the data. I am deeply grateful that they shared their knowledge and expertise, for valuable discussions, additional screenings, computational data and help in all kinds of analysis issues.

I would also like to thank Annina Burhop, Dr. Tom Mejuch and Dr. Muthukumar G. Sankar for the synthesis of the uncharacterized small molecules presented in this thesis and Prof. Adam Nelson for fruitful discussions.

I would like to express my gratitude to the administration of the Technical University Dortmund and for the variety of offered seminars and workshops. In addition, I gratefully acknowledge the administration and central facilities of the Max Planck Institute of Molecular Physiology. At this point I would also like to thank Brigitte Rose for her constant help and support in administrative issues.

Furthermore, I am grateful and really appreciate the great work of the Max Planck PhDnet. I would like to thank in particular, Dr. Philine Hagel, Dr. Michael Winzker, Dr. Katrin Estel, Annina Burhop, Elisabeth Hennes, Birte Weyers, Georg Niggemeyer, Pascal Lill, Hans Seidel and Davide Tamborrini. At this point I would also like to thank the Students' Chapter Dortmund of the International Chemical Biology Society (ICBS) for scientific exchange and discussions. I really enjoyed being a part of these organizations.

Moreover, I highly appreciate the excellent working atmosphere, scientific discussions, summer BBQs and social events within this large international and highly collegial team of scientists. Especially I would like to thank Dr. Lea Kremer, Alexandra Brause, Annina Burhop, Jana Flegel, Dr. Nadine Kaiser, Dr. Elena Reckzeh, Elisabeth Hennes, Julian Wilke, Lara Dötsch, Aylin Binici, Jens Warmers and Beate Schölermann.

Last but not least, I am deeply grateful for the emotional support from my family, my partner and friends. Their continuous encouragement and motivation throughout my PhD helped me to stay on track and focus on my scientific as well as personal goals. Thank you.

## TABLE OF CONTENTS

|        |  |    |
|--------|--|----|
| 1      | ABSTRACT.....  | 1  |
| 2      | KURZZUSAMMENFASSUNG.....                                       | 3  |
| 3      | INTRODUCTION .....   | 5  |
| 3.1    | Chemical Biology.....  | 5  |
| 3.1.1  | Classical versus chemical genetic approaches.....              | 5  |
| 3.1.2  | Reverse chemical genetics.....                                 | 6  |
| 3.1.3  | Forward chemical genetics .....                                | 7  |
| 3.2    | Bioactivity profiling of small molecules .....                 | 9  |
| 3.2.1  | Gene expression profiling .....                                | 9  |
| 3.2.2  | Genomics .....   | 10 |
| 3.2.3  | Transcriptomics.....   | 11 |
| 3.2.4  | Proteomics .....   | 12 |
| 3.2.5  | Morphological profiling.....                                   | 12 |
| 3.2.6  | Data analysis and application of morphological profiling ..... | 14 |
| 3.2.7  | Cell Painting Assay .....                                      | 18 |
| 4      | AIM OF THE THESIS .....  | 23 |
| 5      | MATERIAL AND METHODS.....                                      | 25 |
| 5.1    | Materials .....  | 25 |
| 5.1.1  | Chemicals and reagents .....                                   | 25 |
| 5.1.2  | Buffers and media.....   | 27 |
| 5.1.3  | Antibodies .....   | 27 |
| 5.1.4  | Plasmids.....  | 28 |
| 5.1.5  | Cell lines.....  | 28 |
| 5.1.6  | Cell culture media and supplements .....                       | 29 |
| 5.1.7  | Kits .....   | 29 |
| 5.1.8  | Instruments and devices.....                                   | 29 |
| 5.1.9  | Software .....   | 30 |
| 5.1.10 | Other material and consumables.....                            | 31 |
| 5.2    | Methods.....   | 32 |



|       |  |     |
|-------|--|-----|
| 5.2.1 | Molecular biology methods .....  | 32  |
| 5.2.2 | Cell biology methods .....   | 32  |
| 5.2.3 | Biochemical methods.....   | 44  |
| 6     | RESULTS .....  | 48  |
| 6.1   | Applicability of the Cell Painting Assay (CPA) to predict non-protein targets.....             | 48  |
| 6.1.1 | Morphological profiling of the iron-chelating agent Deferoxamine (DFO) .....                   | 48  |
| 6.1.2 | Identification of annotated reference compounds biosimilar to DFO.....                         | 50  |
| 6.1.3 | Biological characterization of reference compounds biosimilar to DFO .....                     | 54  |
| 6.1.4 | Identification and biological evaluation of uncharacterized compounds biosimilar to DFO        | 65  |
| 6.1.5 | Hierarchical clustering for mechanism of action deconvolution .....                            | 74  |
| 6.2   | Investigation of the bioactivity of tetrahydroindolo[2,3-a]quinolizines .....                  | 77  |
| 6.2.1 | Morphological profiling of tetrahydroindolo[2,3-a]quinolizines 10-13.....                      | 77  |
| 6.2.2 | Lysosomotropic properties of compounds 10-13 .....   | 80  |
| 6.2.3 | Live-cell imaging of compounds 10-13.....  | 82  |
| 6.2.4 | Proteome profiling of compounds 10-13 .....  | 91  |
| 6.2.5 | Investigation of lysosomotropism-related bioactivity.....                                      | 98  |
| 6.2.6 | Analysis of reference compounds biosimilar to compound 13 .....                                | 105 |
| 7     | DISCUSSION .....   | 116 |
| 7.1   | CPA identified a cluster based on a common MoA .....   | 116 |
| 7.1.1 | Annotated iron-chelating ligands are biosimilar to DFO .....                                   | 116 |
| 7.1.2 | CPA identified a cluster of iron chelators and cell cycle modulators sharing a common MoA..... | 119 |
| 7.2   | Bioactivity of tetrahydroindolo[2,3-a]quinolizines .....                                       | 124 |
| 7.2.1 | Tetrahydroindolo[2,3-a]quinolizines accumulate in lysosomes .....                              | 124 |
| 7.2.2 | Tetrahydroindolo[2,3-a]quinolizines modulate cholesterol homeostasis .....                     | 126 |
| 7.3   | Many well-known drugs and tool compounds modulate cholesterol homeostasis                      | 131 |
| 8     | CONCLUSION AND PERSPECTIVE .....   | 140 |
| 9     | REFERENCES .....   | 143 |
| 10    | FIGURES.....   | 157 |
| 11    | TABLES.....  | 160 |

|        |  |     |
|--------|--|-----|
| 12     | ABBREVIATIONS.....                             | 161 |
| 13     | APPENDIX.....                                  | 166 |
| 13.1   | Additional data related to 6.1 .....           | 166 |
| 13.2   | Additional data related to 6.2 .....           | 169 |
| 13.2.1 | Vector maps.....                               | 195 |
| 14     | EIDESSTÄTTLICHE VERSICHERUNG (AFFIDAVIT) ..... | 198 |



## 1 ABSTRACT

Phenotypic screening is a powerful approach to evaluate the bioactivity of small molecules. However, it is restricted to a phenotype of interest, that is detected in the corresponding assay. Capturing a broader range of bioactivity would require the performance of multiple assays. This limitation may be overcome by the Cell Painting Assay (CPA), which is an unbiased morphological profiling approach. The CPA generates a holistic view on the bioactivity of perturbed cells and enables the prediction of targets and mode-of-actions by morphological fingerprint comparison to reference compounds, i.e. with known targets or mode-of-action (MoA). This is especially important for compounds with non-protein targets as they are difficult to identify with commonly applied approaches like affinity-based chemical proteomics, which are limited to the identification of protein targets.

In order to examine the applicability of the CPA to identify non-protein targets, the morphological fingerprint of the iron chelator Deferoxamine (DFO), as well as references and so far uncharacterized compounds with similar fingerprints, were investigated. Reference compounds, biosimilar to DFO, possess different annotated targets and activities but share a common MoA of cell cycle arrest. This was experimentally confirmed for a representative selection of references. The cluster analysis enabled not only the identification of annotated iron chelators and cell cycle modulators but also novel and so far uncharacterized chelating agents and DNA synthesis modulators. Furthermore, hierarchical clustering, using the CPA fingerprints, revealed a first insight into the different mechanisms of action.

To investigate the bioactivity of a small tetrahydroindolo[2,3-a]quinolizine compound class, a combination of morphological profiling using the CPA and proteome profiling was pursued. The results revealed an altered cholesterol homeostasis induced by the compound's physicochemical properties that led to an accumulation and an increased pH in lysosomes. More than 400 reference compounds and well-characterized drugs with different annotated targets and activities share high biosimilarity to the most active derivative. The majority of the compounds in this cluster also possess physicochemical properties, that are predictive for the accumulation in lysosomes. However, also direct modulators of cholesterol biosynthesis like statins are among them. Modulation of cholesterol homeostasis was experimentally confirmed for a representative selection of references. Therefore, this cluster can be used to identify novel modulators of cholesterol homeostasis but also to associate the regulation of corresponding genes or proteins to an effect induced by the physicochemical properties of the compounds rather than by their annotated primary targets.

## ABSTRACT

---

Compounds with different annotated targets and activities may induce biosimilar morphological fingerprints due to a shared MoA or biological process, in which the targets are involved. However, morphological fingerprint similarity can also be a result of shared physicochemical properties, which is an effect that is independent of the primary annotated target. Bioactivity induced by the physicochemical properties as well as its biological consequences is often disclosed in profiling approaches only because they cover a broad range of bioactivity in an unbiased manner. For these reasons, morphological profiling approaches more often identify MoA rather than direct targets. The findings presented in this thesis emphasize the power of the CPA to evaluate bioactive small molecules and to predict diverse MoA for uncharacterized compounds as well as to uncover and expand so far unknown activity for already characterized small molecules and drugs.

## 2 KURZZUSAMMENFASSUNG

Phänotypisches Screening ist eine leistungsfähige Methode, um die Bioaktivität von niedermolekularen Verbindungen zu charakterisieren. Ein Nachteil dieser Methode ist jedoch die Limitierung auf einen bestimmten Phänotyp, der in dem jeweiligen Assay detektiert wird. Um eine größere Spannbreite an Bioaktivität abzudecken, müssten die niedermolekularen Verbindungen in mehreren Assays getestet werden. Diese Limitierung könnte durch das *Cell Painting Assay* (CPA) überwunden werden, ein Assay zur morphologischen Profilierung, das ein ganzheitliches Bild der Bioaktivität von mit Substanzen behandelten Zellen liefern kann. Das CPA kann Angriffspunkte und Wirkungsweisen von niedermolekularen Verbindungen durch den Vergleich zu Referenzsubstanzen vorhersagen, deren Angriffspunkte und Wirkungsweisen bereits bekannt sind. Das ist insbesondere dann von Vorteil, wenn die Zielmoleküle keine Proteine sind. Diese sind nur sehr schwer mit den gängigen Methoden wie der affinitäts-basierten chemischen Proteomik zu identifizieren, da diese auf die Identifizierung von Proteinen limitiert sind.

Um zu überprüfen, ob das CPA Angriffspunkte vorhersagen kann, die keine Proteine sind, wurden der morphologische Fingerabdruck des Eisenchelators Deferoxamin (DFO) sowie biologisch ähnliche Referenzen und bisher nicht charakterisierte Substanzen untersucht. Referenzen mit hoher Ähnlichkeit zu DFO weisen unterschiedliche Angriffspunkte und Aktivitäten auf, haben aber den Zellzyklusarrest als gemeinsamen Wirkungsmechanismus, der anschließend experimentell für eine Auswahl an Referenzen bestätigt wurde. Dieser Cluster erlaubt nun die Identifizierung von bereits bekannten als auch von neuen und bisher nicht charakterisierten Eisenchelatoren und Zellzyklusmodulatoren. Darüber hinaus hat eine hierarchische Clusteranalyse erste Einblicke in verschiedene Wirkungsmechanismen geliefert.

Um die Bioaktivität von Tetrahydroindolo[2,3-a]chinolizin-Derivaten zu untersuchen, wurde eine Kombination aus dem CPA und einer Proteom-Profilierung zurate gezogen. Das aktivste Derivat führte zu einem veränderten Cholesterol-Gleichgewicht und zur Ansammlung und einem erhöhten pH-Wert in Lysosomen, hervorgerufen durch die physikochemischen Eigenschaften der Substanz. Über 400 Referenzsubstanzen und gut charakterisierte Wirkstoffe mit verschiedenen Angriffspunkten und biologischen Aktivitäten zeigen eine hohe Ähnlichkeit zu dem morphologischen Fingerabdruck des aktivsten Derivates. Der größte Teil der Substanzen in diesem Cluster weist ebenfalls physikochemische Eigenschaften auf, die stark auf eine Ansammlung in den Lysosomen hindeuten. Aber auch direkte Modulatoren der Cholesterolbiosynthese wie z. B. Statine befinden sich in diesem Cluster. Die Modulation der Cholesterol-Homöostase wurde experimentell für eine repräsentative Auswahl an Referenzen

aus diesem Cluster bestätigt. Aus diesem Grund kann der Cluster dafür verwendet werden neue Modulatoren der Cholesteroll-Homöostase zu identifizieren und die Regulierung von dazugehörigen Proteinen und Genen auf einen Effekt zurückzuführen, der durch die physikochemischen Eigenschaften induziert wird, unabhängig von der annotierten primären Bioaktivität.

Substanzen mit verschiedenen Angriffspunkten und Aktivitäten können aufgrund einer gemeinsamen Wirkungsweise oder eines gemeinsamen biologischen Prozesses, in den die Angriffspunkte involviert sind, einen ähnlichen morphologischen Fingerabdruck induzieren. Ähnlichkeit im morphologischen Fingerabdruck kann allerdings auch durch gemeinsame physikochemische Eigenschaften hervorgerufen werden. Dieser Effekt ist unabhängig von den primären annotierten Angriffspunkten der Substanzen und wird häufig nur in Profilierungen entdeckt, da sie unvoreingenommen eine große Spannbreite an Bioaktivität abdecken. Aus diesem Grund werden in morphologischen Profilierungen häufiger Wirkungsweisen als Angriffspunkte identifiziert. Die Erkenntnisse, die in dieser Arbeit präsentiert werden, unterstreichen den Wert des CPA, bioaktive Substanzen zu evaluieren und diverse Wirkungsweisen für nicht charakterisierte Substanzen vorherzusagen, als auch unbekannte Aktivität für bereits charakterisierte Substanzen aufzudecken und ihre Annotation zu erweitern.

## 3 INTRODUCTION

### 3.1 Chemical Biology

Chemical biology is a relatively new and growing field that links chemical, biological and medical sciences. Researchers from multiple disciplines work in this field and utilize chemical tools to study biological systems. Historically, classical genetics has played a central role in elucidating biology by manipulating a genetic sequence to study the gene-phenotype correlation. The chemical biology approach ‘chemical genetics’ operates in analogy to classical genetics but uses small molecules to perturb biological systems.<sup>[1, 2]</sup> The discovery and characterization of small-molecule perturbagens of a biomolecule’s function or cellular processes are at the heart of chemical biology and pharmaceutical research. Small molecules are inevitable as tools to study human physiology and more importantly, as therapeutics.<sup>[3, 4]</sup>

#### 3.1.1 Classical versus chemical genetic approaches

Classical genetics, typically applied by biologists to understand biological processes, uses mutagenesis to examine how the perturbation of a protein’s function affects the phenotype. There are two fundamental approaches illustrated in Figure 1, a hypothesis-generating (forward) and a hypothesis-based (reverse) approach. In forward classical genetics, a gene responsible for an altered or abnormal phenotype is identified by random mutagenesis. *Vice versa*, reverse classical genetics selectively alters a gene of interest to characterize its function via detection of the altered phenotype.<sup>[2]</sup> Classical genetics has long proven to be a valuable tool for biologists and helped to reveal the molecular basis of fundamental processes like cell division and programmed cell death.<sup>[5]</sup> However, also techniques for genetic manipulation have their advantages and disadvantages. RNA interference (RNAi)<sup>[6]</sup> for example is one of the most applied methods for genetic perturbation<sup>[7]</sup> and silences a gene as a consequence of the degradation of messenger RNA (mRNA) into short RNAs that activate ribonucleases to target homologous mRNA<sup>[8]</sup>. RNA is easy to synthesize and apply to cells. On the other hand, RNAi is limited in *in vivo* applications and may possess off-target effects. Likewise, conditional knockout animals, in which a targeted gene is deleted<sup>[9, 10]</sup>, allow gene- and even tissue-specific manipulation of protein function. However, creating knockout animals is not only labor-intensive but also leads to a total functional loss of the deleted gene.<sup>[2]</sup>



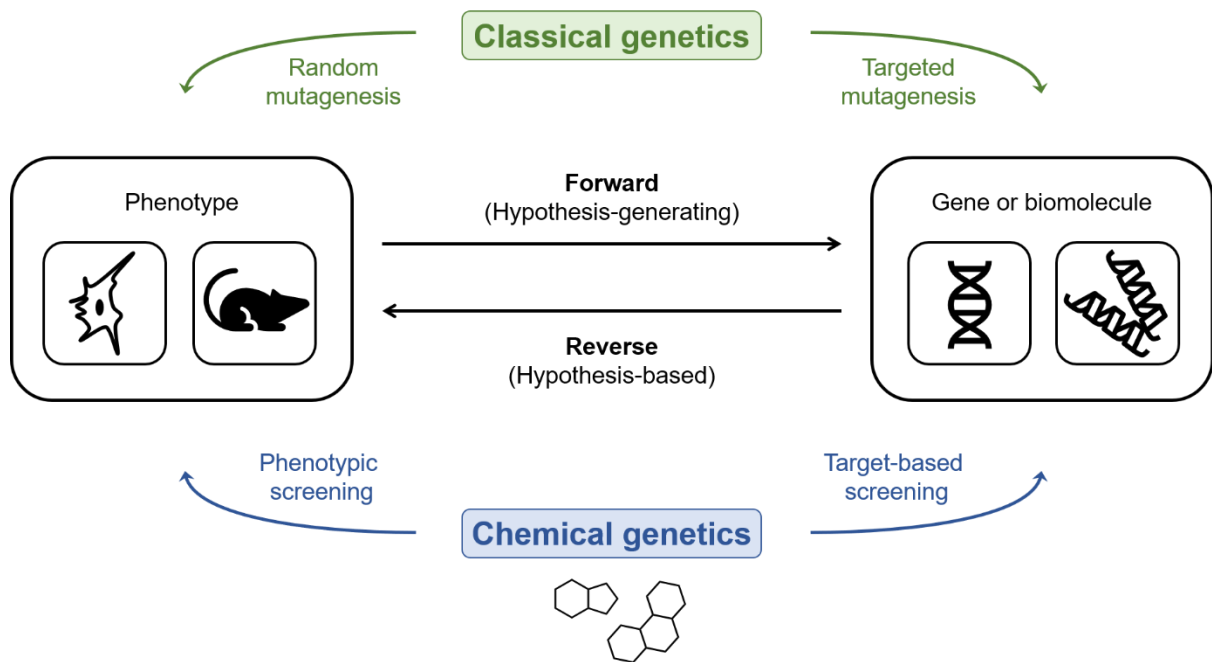


**Figure 1: Classical versus chemical genetics to study biological systems. Adapted from Kawasumi and Nghiem.<sup>[2]</sup>**

A reverse study is a hypothesis-driven approach in which a molecular target of interest is selectively manipulated by using genetics (classical genetics) or small molecules (chemical genetics). A forward study is a hypothesis-generating approach through which a gene (classical genetics) or a small molecule (chemical genetics), responsible for a phenotype of interest, is identified.

Chemical genetics has emerged in the past 20 years as a complementary approach and replaces the genetic removal by small molecules to intervene in biological systems. Like RNAi, small molecules may have the drawback to be unspecific but they also overcome many disadvantages of classical genetics. Small molecules act rapidly and mostly reversibly, as they can often be washed out of the system again. They are typically active across cell types and species and are not limited to protein targets. But especially in the case of a protein target, they may selectively modulate only one function of a multifunctional protein and they may also have the potential to disrupt protein-protein interactions.<sup>[2]</sup>

### 3.1.2 Reverse chemical genetics

Reverse chemical genetics, also referred to as target-based drug screening, starts with the manipulation of a defined molecular target, that is assumed to play an important role in a disease state. Due to the development of molecular genetics in the twentieth century, target-based screening has long been the method of choice for the discovery of new medicines.<sup>[11]</sup>

Sequencing of the human genome and further genetic achievements like RNAi as well as recombinant technologies have led to an increase in disease-relevant molecular targets, for which small-molecule interaction partners can be identified by high-throughput screening of large compound libraries.<sup>[2]</sup> The modulation of target molecules is typically monitored in *in vitro* setups like biochemical or biophysical assays, which are often fast and simple to execute. Diverse methods like crystallography, kinetic or molecular pharmacology studies, available to examine the drug-target interaction, offer excellent opportunities for hit optimization and lead discovery. However, simplified systems using, e.g., recombinant proteins neither reflect the immense biological complexity nor the potential polypharmacology<sup>[12, 13]</sup>, i.e., the interaction of a small molecule with multiple targets. Targets engineered into simplified biochemical or cell-based systems do not always behave as in their physiological environment resulting in a poor translation when tested in a more complex system like animals or humans. Besides, drugs are rarely selective for only one target, but initial target-based screenings are limited to the detection of the desired bioactivity and even this may be influenced by the drug's promiscuity.<sup>[14]</sup>

### 3.1.3 Forward chemical genetics

Forward chemical genetics is also referred to as 'phenotypic screening'. A phenotype describes the composition of observable traits of a cell or a higher organism like morphological properties, gene and protein expression pattern or anatomy and behavior. Phenotypes drive much of the research in life sciences and remain the primary data used to define a pathological condition.<sup>[15, 16]</sup> The rise of forward chemical genetics began with advancements in phenotypic readouts, automated microscopes, and when image analysis algorithms became available. While these technologies were rather innovative at that time, the approach as a whole was established long ago. Before the implementation of target-based screens, bioactive small molecules have already been discovered by evaluating them in complex biological systems such as animals or cells. And within the last decade, phenotypic screening has again gained growing attention.<sup>[11, 17]</sup> In this approach, a specific biological process or phenotype is selected for a high-throughput study to identify small-molecule perturbagens. Phenotypic assays may utilize primary cells, tissues or animals and can be conducted using sophisticated culturing techniques such as co-cultures or spheroids.<sup>[14]</sup> The desired phenotype can be detected using marker genes or proteins, e.g., in reporter gene assays, antibody-based cellular immunoassays, functional assays that directly monitor cellular activities such as cell division, metabolism or apoptosis, or by imaging.<sup>[18]</sup> Unlike target-based screening, forward chemical genetics offers the opportunity to identify novel targets related to the desired phenotype as

there is no bias towards a specific target. Furthermore, the approach features a higher degree of physiological relevance as it enables capturing a broader complexity of a biological system compared to biochemical and biophysical assays. Thereby novel targets and mechanisms and even side effects can be identified.<sup>[14]</sup>

Analysis of FDA-approved first-in-class small-molecule drugs illustrated that between 1999 and 2008 more drugs were discovered by phenotypic screening than by target-based approaches.<sup>[17]</sup> This was a period of time, when the focus of drug discovery was actually on target-based approaches. It was proposed that the lower productivity is a result of the neglected molecular complexity of a drugs' molecular mechanism of action (MMoA) and that the development of best-in-class medicines is facilitated by phenotypic assays to not only identify bioactive small molecules but also their MMoA.<sup>[17]</sup> A mechanism of action can be described at the level of the biomolecule by identifying a target or a cellular entity that is bound by the compound, at the level of a biochemical pathway, at the level of the cell or an organism.<sup>[19]</sup> However, the broader biological complexity of phenotypic screening may at the same time be the bottleneck of this approach as target or mode-of-action (MoA) identification remains unknown. Their identification poses a major challenge, which is often labor- and time-intensive and requires many resources.<sup>[20]</sup> Moreover, small molecules are often promiscuous, i.e., they interact with more than one target. Non-specific interactions can induce assay artifacts like pan-assay interference compounds<sup>[21]</sup> and eventually lead to unwanted off-target effects. However, compound promiscuity is not always undesired as the therapeutic efficiency can also rely on the simultaneous modulation of multiple targets and biological pathways.<sup>[22]</sup> To more precisely describe this process, the term "target deconvolution" was introduced.<sup>[23]</sup>

The identification of novel targets and MoA not only expands the biological space targeted by small molecules but also enhances the understanding of human disease mechanisms and the ability to modulate cellular systems.<sup>[24]</sup> The typically employed target identification process comprises methods such as affinity-based chemical proteomics, protein microarrays or computational approaches.<sup>[20, 23]</sup> However, except for computational approaches, they all share a major limitation as they are restricted to the identification of protein targets. *In silico* approaches predict bioactivity based on reported ligand-target interactions or based on structural similarity of ligands and target molecules, which are then extracted and re-assigned to the query ligands.<sup>[23, 25, 26]</sup> Those approaches are mainly focused on the interaction between a small molecule and a protein, but compounds can also target other biomolecule classes.<sup>[2, 27-29]</sup> Modulating lipids<sup>[30]</sup>, DNA<sup>[31]</sup> or RNA<sup>[32, 33]</sup> by small molecules developed as a new research field in recent years. Conventional phenotypic screening assays are limited to the phenotype of interest and only monitor the sought bioactivity. Hence, to capture a wider range of bioactivity and to explore selectivity and potential toxicity, compounds must be screened in

multiple phenotypic and target-based assays. This limitation can be overcome by using less biased profiling approaches that look at a broad range of bioactivity including whole pathways and processes. These approaches are also crucial for the identification of compounds with non-protein targets, which are difficult to discover with usually employed target identification methods, as they can predict a target or MoA based on biological similarity alone.<sup>[34]</sup>

### 3.2 Bioactivity profiling of small molecules

A central objective and challenge of chemical biology is to find a way to receive a comprehensive bioactivity profile of compound libraries as early as possible. On- and off-target interaction networks provide a valuable resource to map the bioactivity profile of a small molecule and to enhance the understanding and make use of polypharmacological effects.<sup>[35]</sup> Conventional phenotypic screens are mainly used to detect a single bioactivity of interest, addressing the already known drug targets, for example, GPCRs, kinases and enzymes. In contrast, high-content image-based screening and ‘omics approaches, like transcriptomics or proteomics, enable profiling as they collect a myriad of parameters.<sup>[36]</sup> Profiling means, firstly, to represent a sample by a profile, which is a collection of features, and secondly, to make a prediction about the sample based on the profile.<sup>[37]</sup> Profiling is a powerful approach for target or MoA deconvolution as it generates an unbiased and more holistic view of the compound’s influence on a biological system. Compared to conventional phenotypic screening, profiling approaches offer an even higher degree of physiological relevance and the chance to analyze the perturbed cell as a whole. As profiling approaches are less restricted in terms of the detected bioactivity, they may not deliver direct information about a molecular target, but offer insight into various alterations induced by small-molecule perturbators.<sup>[36]</sup> However, the complexity may at the same time represent a drawback as it can add useless noise or the data may be more difficult to interpret than a single selected phenotypic feature.<sup>[7, 37]</sup>

#### 3.2.1 Gene expression profiling

The so-called “central dogma” of molecular biology, depicted in Figure 2, describes the flow of genetic information from the gene to the protein level. DNA can be sequenced and investigated by genomic approaches. Genes are transcribed and processed into functional RNA, which can be explored by transcriptomics. mRNA transcripts are then translated into proteins, the end product of gene expression, which can be profiled by means of proteomic approaches. Thus, the term gene expression profiling comprises analysis on different levels depending on the specific research objective.

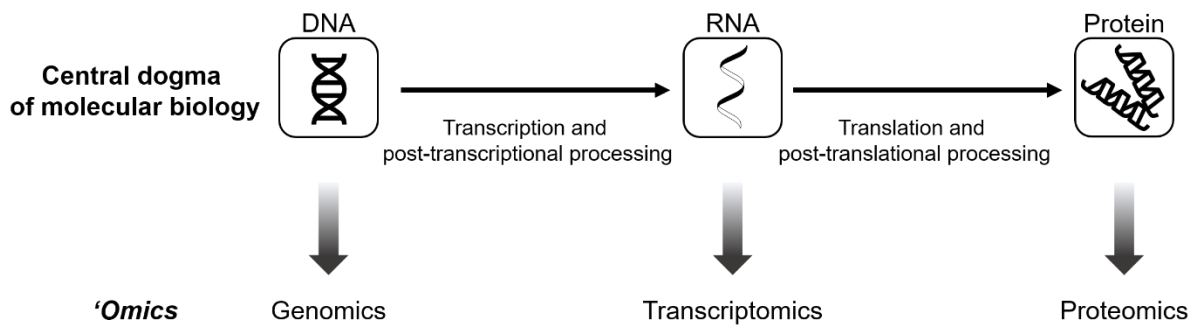


**Figure 2: Schematic illustration of the central dogma of molecular biology. Adapted from M. P. Richards.<sup>[38]</sup>**

Flow of genetic information from the genome to the proteome. DNA is transcribed and processed by, e.g., alternative splicing into functional RNA. mRNA is translated into a protein and can further be modified by, e.g., proteolytic cleavage or post-translational modification.

The human genome consists of around 30-40 thousand genes but the estimated number of unique proteins within a cell is 10 times higher (10,000-100,000). This is due to post-transcriptional and post-translational modifications that RNA transcripts and proteins undergo, which are not investigated by genomics. Hence, it is crucial to have different techniques in hand to fully assess activity and function at the level of protein, RNA and DNA.<sup>[38]</sup>

### 3.2.2 Genomics

Functional genomics has evolved as a new research field in the “post-genomic” era and deals with the identification and characterization of genes to explore their function under different conditions like health and disease states or certain environmental conditions, as well as the connections between different expression profiles of single genes or gene networks. Functional genomics also allows relating this information to a certain phenotype.<sup>[38]</sup> The central technology of genomics is DNA sequencing, which underwent a long and fruitful development over the past 50 years. The first-generation Sanger sequencing, developed in the mid-1900s, was replaced by massively sequencing in parallel using Next-Generation Sequencing (NGS) techniques and this, in turn, was replaced by third-generation real-time single-molecule sequencing. Still, NGS, as well as single-molecule sequencing methods, can be optimized regarding cost and throughput and there are even additional concepts in the pipeline.<sup>[39]</sup>

### 3.2.3 Transcriptomics

Transcriptome studies investigate if and at which level specific mRNA sequences are present in certain biological samples like chemically perturbed cells. This can be done using a single-gene transcript, small related groups, and even thousands of unique transcripts to study gene activity and function. For this, RNA can either directly be used or it needs to be converted into complementary DNA (cDNA) by reverse transcription before amplification via polymerase chain reaction (PCR). All high-throughput techniques to study gene transcripts on a global scale rely on the conversion from RNA into cDNA and hence, on high-throughput DNA sequencing.

Gene expression signatures can be obtained from different biological states including physiological and disease states or a state induced by chemical perturbation or gene editing. Therefore, these signatures can also be used to discover the mechanism of action of a small molecule, to identify and connect small molecules with a shared target, or to discover an unexpected activity of a compound that might, e.g., lead to an off-target effect. Technically genomic signatures could arise from DNA methylation pattern, mRNA level, protein expression, or metabolite profiles. However, only mRNA expression assayed on DNA microarrays offers to receive genomic signatures on a large scale, generated from a small number of cells at low cost but with sufficient complexity to provide a meaningful biological output.<sup>[40, 41]</sup> Advances in genome studies led to a great many of microarray data available in public databases.<sup>[42]</sup> For example, the Connectivity Map (CMap)<sup>[40]</sup>, established in 2006, provides a large reference collection of gene expression profiles from human cells, treated with 164 FDA-approved drugs and bioactive tool compounds as well as a pattern-matching tool to detect signature similarities. This collection was afterwards expanded by reducing the representation of the transcript to 1000 landmark genes to prevent the high costs of commercial gene expression microarrays. Those landmark genes (L1000) are sufficient to recover 82 % of the information in the full transcriptome and are part of the NIH Library of Integrated Network-Based Cellular Signatures (LINCS) initiative.<sup>[41]</sup> Over the last decade, the CMap has been used in numerous applications with a focus in drug discovery and development. It was used to identify novel phenotypic relations and new therapeutic drug targets<sup>[43]</sup> as well as to discover clusters of compounds with a shared MoA like anti-psychotics and calcium channel binders that both lead to the modulation of genes involved in cholesterol biosynthesis<sup>[42, 44]</sup>. Moreover, the CMap can be used to repurpose already known drugs that reverse the gene expression signature of another disease state.<sup>[45, 46]</sup> This underlines the power of the CMap to allow the generation of a target or MoA hypothesis even without experimental lab work<sup>[46, 47]</sup>, which, e.g., led to the successful identification of a novel casein kinase inhibitor<sup>[41]</sup>.

However, the transcriptome, the sum of all RNA transcripts in an organism, only captures a snapshot in time and therefore the analysis of the proteome, the sum of all proteins in an organism, provides additional information about the genotype-phenotype relationship.<sup>[38, 48]</sup>

### 3.2.4 Proteomics

Translation is the last step of gene expression, in which the genetic information is transferred from mRNA to proteins. Compared to genomics and transcriptomics, proteome profiling, i.e., the expression analysis of the proteome is more challenging as proteins are further processed or modified into various forms. Proteome profiling can for example also be performed using protein arrays, however, mass-spectrometry-based approaches became a central technology in profiling the proteome.<sup>[38]</sup> Chemical proteomics was originally used to study unknown function of proteins by small-molecule perturbation.<sup>[49]</sup> However, in recent years it turned into the other way around and chemical proteomics is used to study the function of a small molecule, the small molecules-phenotype relation as well as to identify the target of small molecules.<sup>[50-53]</sup> Although proteins are the target of most drugs and therefore, proteome responses can be more specific than gene expression profiles, less efforts are made to establish connectivity maps based on proteome signatures.<sup>[54]</sup> ProTargetMiner<sup>[55]</sup> is one of a few publicly available and expandable library of proteome signatures induced by anti-cancer molecules.<sup>[54]</sup> This study demonstrated that proteomic signatures cluster by compound targets and MoA and thus, can be used for bioactivity predictions. For example, a group of kinase inhibitors with different targets clustered together based on a shared MoA that relies on an off-target effect, which is the modulation of the cholesterol biosynthesis.<sup>[54]</sup>

All in all, public databases of gene expression profiles are very valuable to gain a first insight into the potential bioactivity of a small molecule by signature comparison. In general '*omic*' studies are well suitable to provide a holistic view of the bioactivity space, however, most approaches do not facilitate the screening of large compound libraries.<sup>[36, 37]</sup>

### 3.2.5 Morphological profiling

In the past two decades, morphological profiling, also known as image-based or cytological profiling, received rising attention in academia and pharmaceutical research.<sup>[37]</sup> Images are rich in data compared to a single readout, target-based, or cell reporter approaches. Furthermore, microscopy imaging is one of the most direct methods to monitor a phenotype. Morphological profiling is the least expensive profiling approach and compatible with different biological species and samples like cells, tissues, or organisms.

Technological and analytical innovations in high-throughput microscopy have enabled the screening of large compound libraries to generate morphological profiles providing information on a putative target, MoA, or toxicity. To this end, algorithms detect morphological patterns and differences, which are often invisible to the human eye, and hundreds of morphological features are extracted to explore small molecule-related bioactivity.<sup>[7, 36, 56-58]</sup>

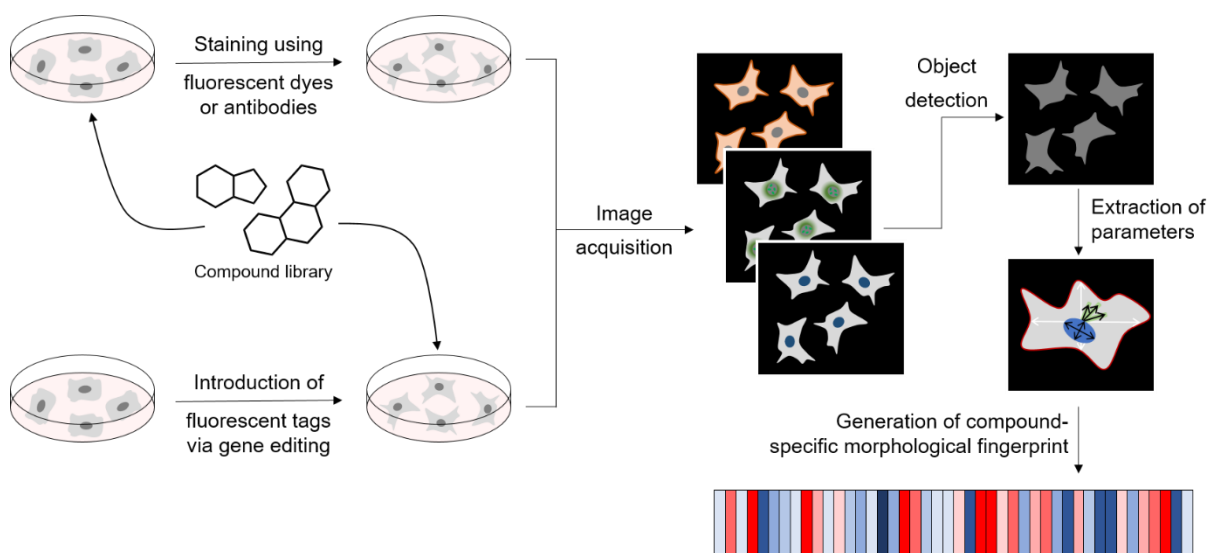


**Figure 3: General workflow of morphological profiling of small molecules adapted from Ziegler *et al.***<sup>[36]</sup>

Cells are treated with small molecules prior to staining of different organelles and cell components with fluorescent dyes or antibodies. Fluorescent tags can also be introduced by gene editing receiving a reporter cell line. Image acquisition and processing is conducted automatically. Single cells and cellular regions are identified (object detection) and cellular features are extracted and combined into a morphological profile.

A general workflow of morphological profiling is depicted in Figure 3. First, cells are treated with small molecules and afterwards cellular organelles and cell components are visualized by a multiplexed staining with fluorescent dyes or antibodies to detect morphological changes compared to the control. As an alternative, reporter cell lines can be used, where different combinations of fluorescent tags are introduced by gene editing.<sup>[57]</sup> Automated image acquisition and processing is required due to the enormous number of acquired images and measured features. The analysis is done on a single-cell level by detecting cells and cellular regions as objects utilizing, for example, the nucleus and the cytoplasm staining.<sup>[36, 58, 59]</sup> Based on the staining, hundreds of cellular features like size, shape, intensity and texture are extracted as numerical descriptors of the phenotype and combined into a morphological profile. These profiles represent high-dimensional readouts of numerous features and comprehensively capture the bioactivity of a small molecule.



### 3.2.6 Data analysis and application of morphological profiling

The idea of morphological profiling was first implemented by Boland and Murphy<sup>[60]</sup> twenty years ago. They aimed for an automated image analysis process to achieve an objective, reliable and reproducible approach to describe the subcellular localization pattern of proteins. Although they were still imaging their samples manually, they successfully set up an automated image analysis workflow. Upon staining HeLa cells for DNA and one cellular organelle or compartment, they extracted and selected 84 features per image and were able to localize and distinguish pattern of proteins in ten different subcellular compartments.<sup>[60]</sup> At that time, Boland and Murphy<sup>[60]</sup> already foresaw that automated image analysis will become an increasingly important tool. Since then, morphological profiling has proven its value in many studies and can be used to address a broad range of scientific questions in the field of chemical biology and medicinal chemistry.<sup>[7]</sup>

In general, morphological profiling can be used to assess the bioactivity of a small molecule, i.e., the ability to induce a morphological change. Of note, compounds that do not induce a morphological change are not necessarily inactive, when their bioactivity is not linked to a morphological change. Furthermore, the data can be used to assess toxicity of screened compounds but also to guide small-molecule library synthesis efforts.<sup>[7, 37]</sup>

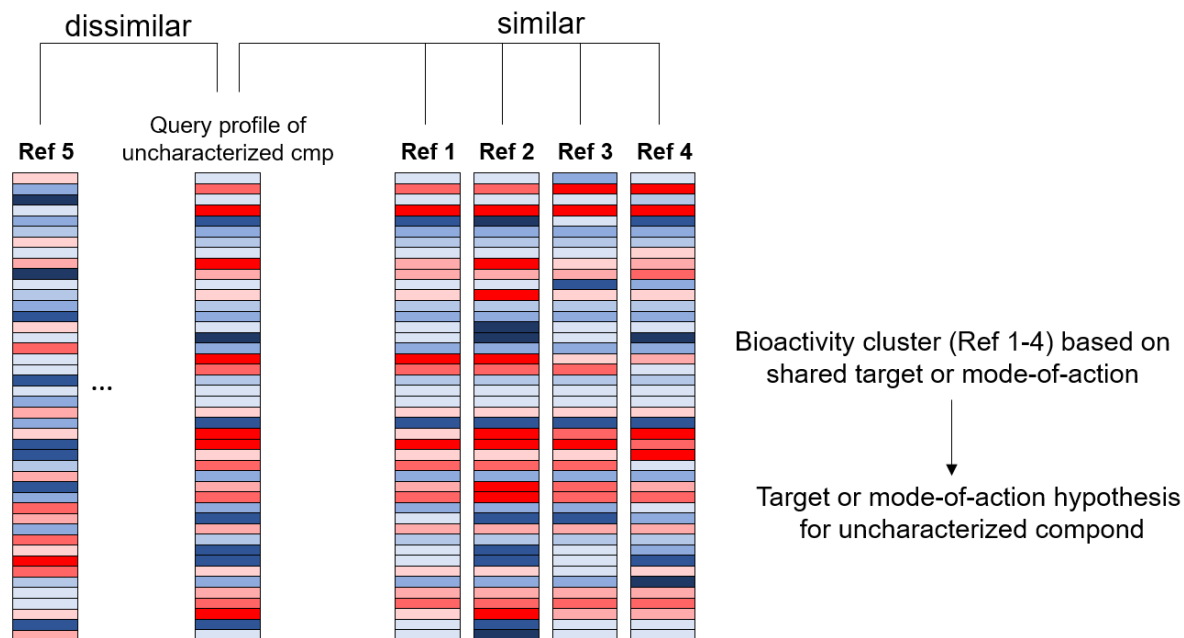


**Figure 4: Target or mode-of-action prediction for uncharacterized compounds (cmp) based on comparison of morphological profiles to annotated reference (ref) compounds.**

The inclusion of a set of annotated reference compounds allows target or MoA prediction by morphological fingerprint comparison presuming that compounds sharing a target or MoA also

induce a similar morphological change (Figure 4).<sup>[7, 61-64]</sup> However, this nearest-reference approach strongly relies on the composition of the reference set as well as on the comprehensiveness of their annotated bioactivity. Besides, the references must be sufficiently active and fairly selective because not every morphological change is necessarily related to the primary target. Compounds are often promiscuous and the *a priori* annotation of a compound is solely based on anticipated targets and disregards off-target effects.<sup>[54]</sup> Therefore, it remains a major challenge to deconvolute a target or MoA of a promiscuous compound when functionally unrelated targets are as well reflected in the profile.<sup>[37, 57]</sup> A report by J. Simm *et al.*<sup>[65]</sup> demonstrated that a supervised machine learning model could help to overcome this issue and predict bioactivity by repurposing images from high-throughput phenotypic screens. The researchers combined image-based profiles of small molecules out of existing data on compound activity from other phenotypic screens. Based on the data, a supervised machine learning approach was able to make useful bioactivity predictions.<sup>[65]</sup> However, this approach is quite elaborative and requires, besides the expertise in machine learning, a sufficient number of reference compounds that have been tested in other phenotypic-, target- or MoA-specific assays.<sup>[57]</sup>

In general, the embedding of supervised and unsupervised machine learning pipelines into the image analysis process of large data sets can help to identify pattern, relationships and cluster of compounds with a shared target, mode- or mechanism-of-action.<sup>[66-69]</sup> Supervised machine learning approaches require the generation of a training data set. This is generated by annotating representative samples of predefined classes, e.g., different phenotypes. Afterwards, the machine-learning algorithm can automatically apply the learned rules to the whole data set and distinguish between the defined classes based on the measured features. Unsupervised machine learning does not require training of the algorithm. This approach extracts information by similarity measures or facilitates data mining by reducing its complexity. Unsupervised machine learning is commonly used to cluster compound profiles based on their similarity, e.g., by hierarchical clustering.<sup>[68, 69]</sup>

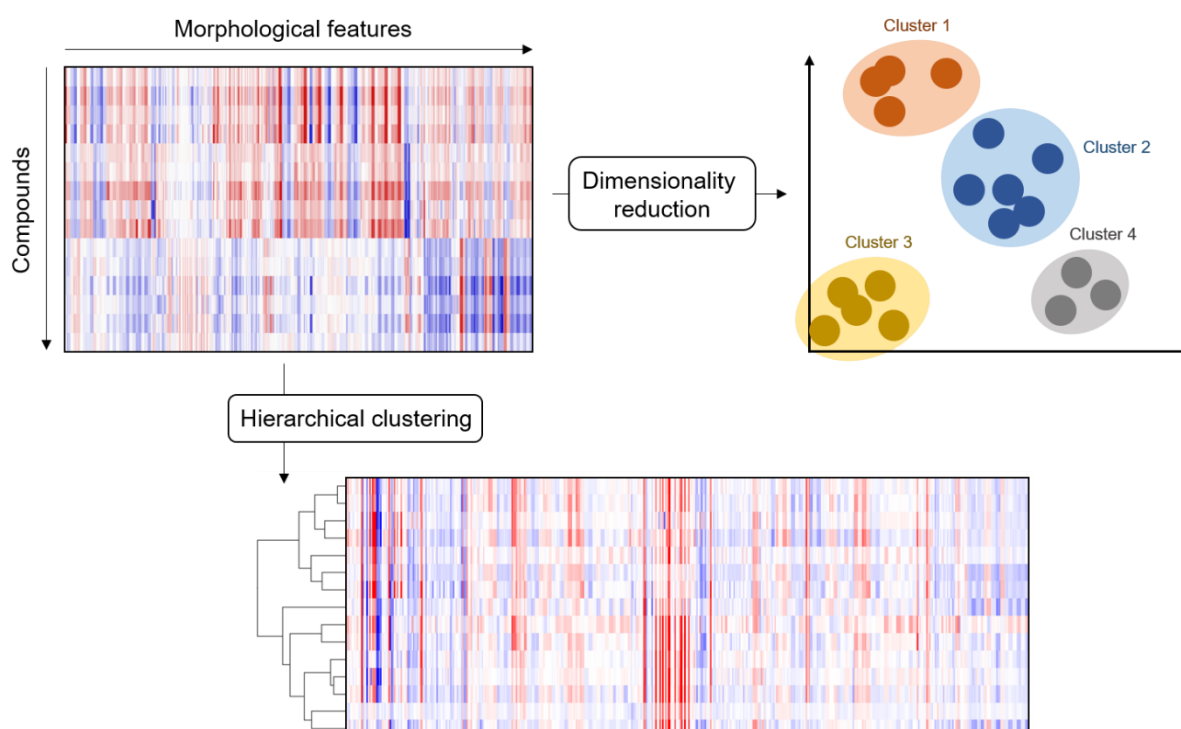


**Figure 5: Schematic representation of morphological profiles subjected to hierarchical clustering or dimensionality reduction used for the clustering of low-dimensional profiles.**

The high-dimensional morphological profiles can be subjected to hierarchical clustering or converted into low-dimensional profiles to assist the clustering of similar profiles and assigning bioactivity (Figure 5). Reducing the dimensionality can, e.g., be done by Principal Component Analysis (PCA), which removes features that are redundant or irrelevant but keeps the variance of the data set. Thereby bioactivity can be mapped and MoAs can be assigned to clusters. This has been successfully used to identify clusters enriched for individual targets, e.g., histone deacetylase or tubulin, signaling pathways like PIK3/AKT/mTOR and clusters of compounds that share a common MoA like iron chelating agents and DNA synthesis inhibitors, which then could be used to identify novel compound-target associations.<sup>[63, 64, 70]</sup> Furthermore, clustering can be used to analyze the overall contribution of different scaffolds, stereochemistry, residues and chemical properties on the biological performance diversity of compound libraries.<sup>[71]</sup> This enables the generation of structure-phenotype relationships (SPR) and qualitative structure-activity relationships (SAR) that can guide hit triaging efforts.<sup>[57, 72, 73]</sup> Wawer *et al.*<sup>[74]</sup> demonstrated that compounds with diverse morphological profiles led to higher performance diversity in high-throughput phenotypic screens rather than a random selection, or compounds with diverse chemical structures. Furthermore, they showed that compounds with a strong activity in the morphological profiling assay had larger hit frequencies in

phenotypic screens, which suggests that multiplexed morphological profiling could provide a way to tag potentially promiscuous compounds early on.

Morphological profiling has also been applied to study genetic perturbation using deletion strains, overexpression, CRISPR or RNAi to identify genetic regulators, disease-specific phenotypes, annotate genes by function and group disease-associated alleles.<sup>[7]</sup> However, morphological profiles induced by RNAi, the most applied method for genetic perturbation, revealed that the profiles are dominated by an off-target effect. This is the so-called seed effect, based on a nucleotide sequence, whose short length results in low specificity.<sup>[75]</sup>

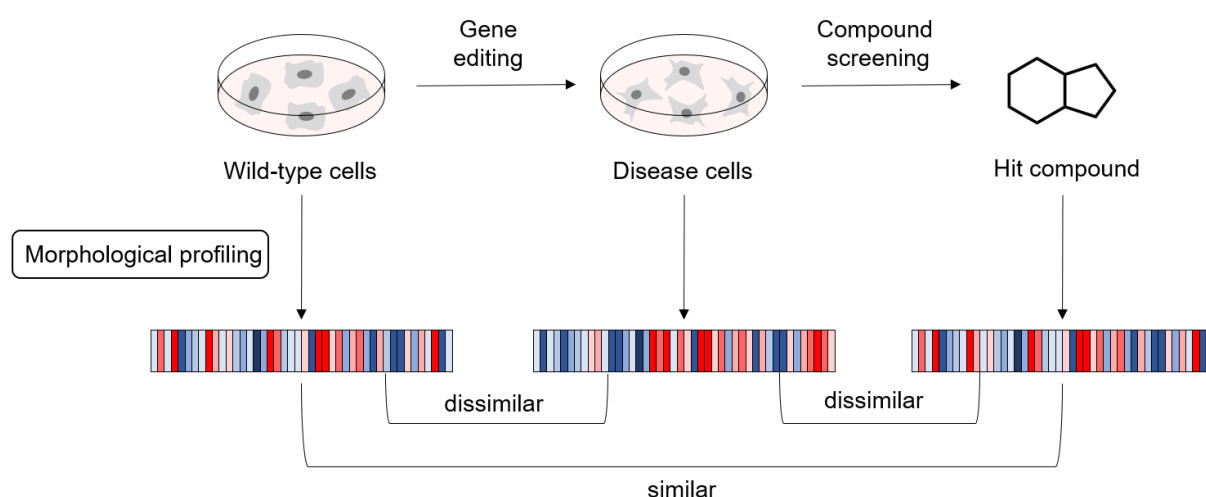


**Figure 6: Schematic representation of morphological profiling for small molecules to reverse disease phenotype.**

As illustrated in Figure 6, morphological profiling can also be used as a combination of chemical and genetic perturbation to screen for small molecules that reverse a disease phenotype of interest.<sup>[7]</sup> As an example, C. C. Gibson *et al.*<sup>[66]</sup> sought for differences between wild-type and disease cells. They knocked down the gene and protein of interest by siRNA (small interfering RNA) to create the disease cells and afterwards screened a large compound library to find a compound that reversed the disease phenotype. Moreover, they demonstrated that hits picked by a machine-learning software outperformed those chosen by human analysis in their secondary screen.

The combination of chemical and genetic perturbation can also be used to determine the MoA for small molecules. For this, the image-based profile of the small molecule is matched to that of cells perturbed via gene editing to predict a target or MoA.

This approach is not widely used but a pioneering study in yeast<sup>[76]</sup> demonstrated that genetic perturbations can be used to identify drug targets based on morphological profile similarity.<sup>[37]</sup>

Taken together, morphological profiling has a variety of applications including target and MoA deconvolution, toxicity testing, library enrichment, hit expansion, and lead optimization. But it is also able to uncover, e.g., unexpected off-target activities and, thus, is a valuable and powerful approach for the evaluation of bioactive small molecules and provides a basis to accelerate the drug discovery process by doing multiple steps at once.<sup>[37, 67]</sup>

### 3.2.7 Cell Painting Assay

The Cell Painting Assay<sup>[77, 78]</sup> is the most commonly used unbiased assay for image-based profiling and has gained increasing interest by academia and the pharmaceutical industry within recent years.<sup>[37]</sup> It was described in 2013 by researchers of the Broad Institute to study various aspects of cell biology as well as genetically and chemically perturbed cells, to predict bioactivity, toxicity, targets and MoAs of small molecules, match drugs with disease states, and to discover and develop new therapeutics.

The CPA multiplexes six fluorescent dyes imaged in five channels to reveal eight different cellular organelles or components. It was established in the U-2OS cell line, and still, most studies use this osteosarcoma cell line for chemical and functional genomic screens. U-2OS cells are especially suitable for imaging cellular structures as they possess large, flat cell bodies, grow in a monolayer, and adhere well to plastic.<sup>[79]</sup> However, the CPA can be performed in many other cell types like A549, MCF7, 3T3, HeLa, HTB-9, ARPE-19, HEKTE, SH-SY5Y, HUVEC or HepG2, including primary cells and coculture systems.<sup>[56, 72, 78]</sup> Warchal *et al.*<sup>[80]</sup> for example applied the CPA to a panel of eight genetically distinct human breast cancer cell lines to identify and rank compounds with distinct responses between the cell types. Cell lines suitable for CPA should in general be adherent, grow in a monolayer, and at best, should be well characterized in the biological area of interest.<sup>[78]</sup>

Since there is no standardized workflow for image processing and data analysis, the following section describes the workflow and data analysis of the CPA performed at the Compound Management and Screening Center (COMAS), Dortmund (Figure 7), which was used to generate the data presented in this thesis.<sup>[59]</sup> However, the workflow closely follows the protocol, which was established by Bray *et al.*<sup>[78]</sup>

# INTRODUCTION

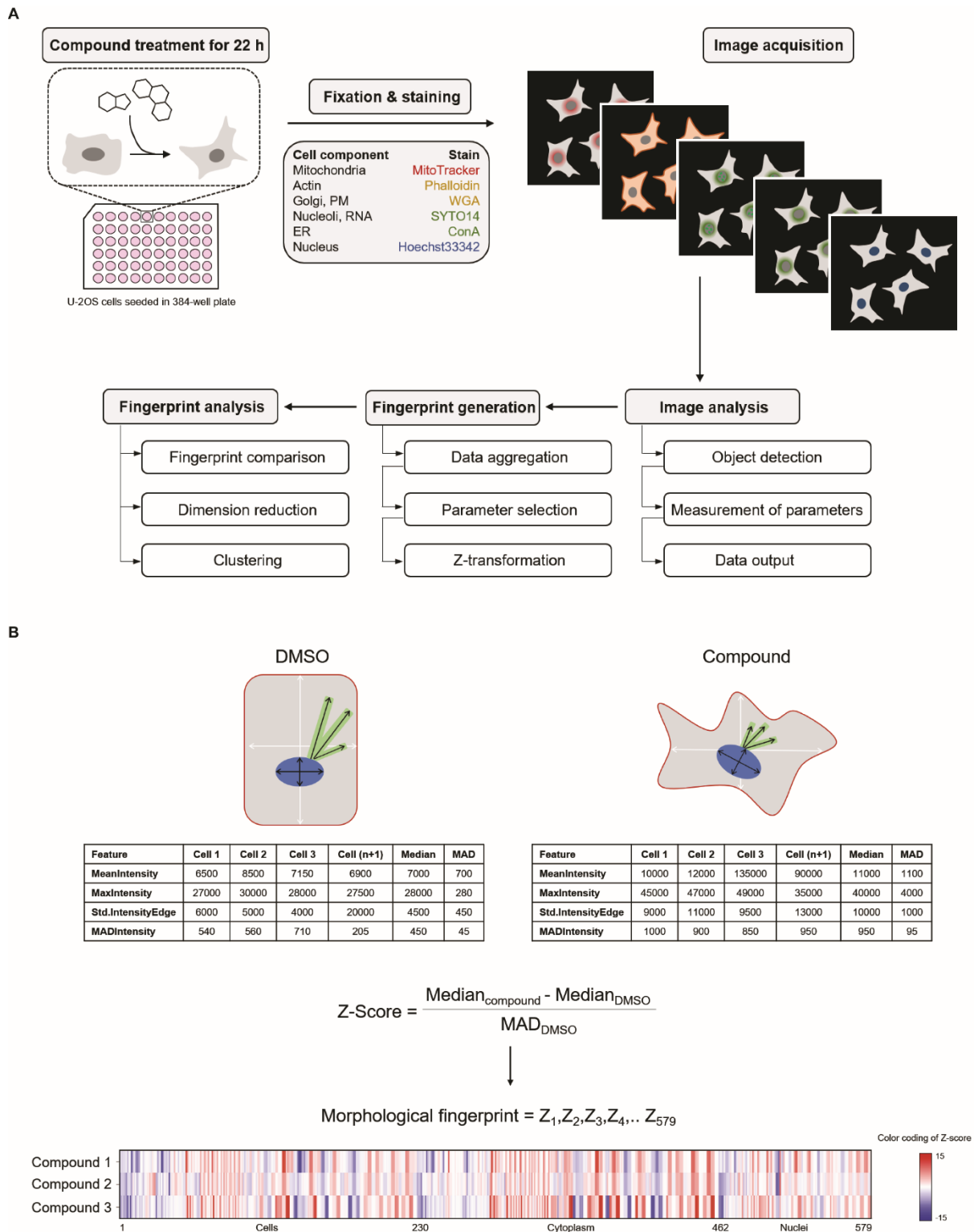


**Figure 7: Workflow of the CPA and data analysis performed at the COMAS and MPI, Dortmund adapted from Ziegler *et al.* [36, 59]**

(A) U-2OS cells are seeded in a 384-well plate and treated for 22 h with annotated reference compounds as well as uncharacterized research compounds at varying concentrations. Before automated image acquisition and processing on a single-cell level, cells are stained with six multiplexed fluorescent dyes to visualize mitochondria, actin, Golgi, plasma membrane, nucleoli/RNA, the endoplasmic reticulum (ER), and the nucleus. Cellular features are measured, extracted and summarized in a morphological fingerprint in form of a heatmap profile. Fingerprints can be compared among small molecules or

reduced into low-dimensional profiles for clustering. (B) The morphological fingerprint is a list of Z-scores, calculated for each feature. To obtain the Z-score, the median value of the DMSO control is subtracted from the median value of the compound for each feature. This difference is afterwards divided by the median absolute deviation (MAD) of the DMSO control to yield the fold change of this feature induced by the small molecule compared to the DMSO control.

For this, U-2OS cells are seeded in a 384 well plate and treated with uncharacterized research compounds or annotated reference compounds for 20 h at 10  $\mu$ M. Kinase inhibitors or particular natural product classes, known to be toxic at high concentrations were screened at lower concentrations of 1-2  $\mu$ M. Before fixing the cells, the mitochondrial staining is performed as the uptake of MitoTracker dyes is dependent on the mitochondrial membrane potential. However, the dye stays well preserved after fixation. After fixing and permeabilization, cells are stained with the remaining five dyes prior to automated image acquisition at 20X magnification. The distinct localization and morphology of the F-actin cytoskeleton and the Golgi and plasma membrane enable their image acquisition using the same filter set. To cover many cells (> 1000 per well) nine microscope sites per well are imaged. To obtain numerical data, image analysis is performed using the open-source software CellProfiler<sup>[81]</sup>, which is especially suitable for high-throughput image analysis. The images are subjected to an image analysis pipeline. This comprises different modules for image processing and object detection to measure features of the cell and its compartments including cell size, shape, intensity, and texture. For each cell, over 1.700 features are measured and aggregated as a median value of each microscope site and afterwards grouped on the median per well and finally over all plates of a screening batch. Irrelevant and highly correlated features are removed, obtaining 579 robust features. Z-scores are calculated for each feature to generate the morphological fingerprint, which is a listing of all relevant and uncorrelated features visualized as a heatmap profile (Figure 7B). The Z-score corresponds to the fold change of the given feature induced by the compound in comparison to the DMSO control. Therefore, the median value of the DMSO control is subtracted from the median value of the compound-treated condition and afterwards the difference is divided by the median absolute deviation (MAD) of the DMSO control. Fingerprints can be compared between small molecules, subjected to hierarchical clustering and they can be reduced into low-dimensional profiles for cluster analysis. Therefore, the similarity between profiles is calculated from the correlation distance<sup>[82]</sup>.

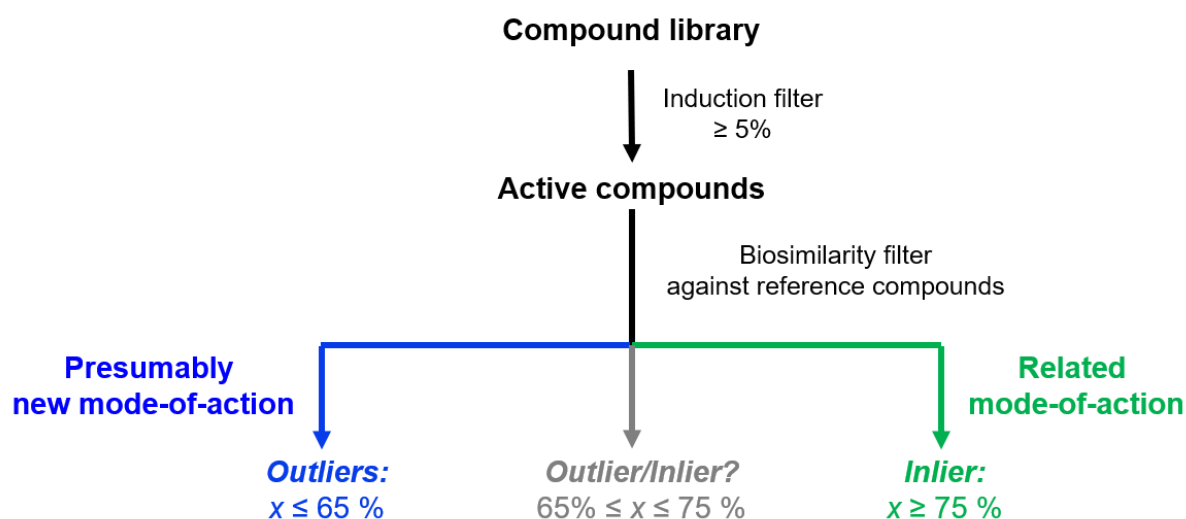


**Figure 8: Workflow for bioactivity prediction performed at the MPI, Dortmund.**

Compounds with an induction value of  $\geq 5\%$  are considered as active, i.e., induce a morphological change in the CPA. Compounds similar ( $\geq 75\%$ ) to annotated reference compounds are called Inliers and presumably possess a related MoA. Compounds not similar  $\leq 65\%$  to any reference are called Outliers and may presumably have a new MoA.

The first step in the workflow for bioactivity prediction (Figure 8) is to filter out inactive compounds. To assess activity in the CPA, an induction value is calculated. The induction is determined as the percentage of significantly changed features within a compound profile compared to the DMSO control. Compounds with an induction  $\geq 5\%$  are considered to be active in the CPA, i.e., they induce a morphological change. In the second step, a similarity filter is applied to evaluate the similarity between the morphological fingerprint of a compound or compound library of interest and reference compounds (biosimilarity). Empirically, fingerprints with a similarity  $\geq 75\%$  are considered biosimilar and therefore presumably share a target or MoA. Uncharacterized compounds biosimilar to a reference compound are called 'Inliers'. Compounds with a similarity  $\leq 65\%$  are considered dissimilar. Uncharacterized small molecules dissimilar to any reference compound potentially possess a new target or MoA and are called 'Outliers'. For compounds with biosimilarity values between 65 and 75 %, it is advisable to decide individually, if those compounds are rather Outliers or Inliers.

This workflow has already led to the successful identification of novel bioactive compounds as well as their targets or MoA.<sup>[73, 83-85]</sup> For example, pyrano-furo-pyridones, a new pseudo-natural product (pseudo-NP) class, were identified to induce mitochondrial superoxide formation based on fingerprint comparison to annotated reference compounds. Furthermore, the analysis of the CPA data, using the induction as a qualitative measure for bioactivity, enabled the establishment of general trends in the structure-phenotype relationship of the pyrano-furo-pyridones.<sup>[73]</sup>



Moreover, Laraia *et al.*<sup>[84]</sup> employed the CPA to identify the MoA of the autophagy inhibitor autoquin. Whereas affinity-based proteomics data were inconclusive in this case, the CPA revealed fingerprint similarity to references that accumulate in lysosomes, a MoA that does not require direct binding to a target protein. However, the proteomics pointed towards the possibility that an altered iron homeostasis may be conducive to the bioactivity of autoquin. This was afterwards experimentally confirmed and again highlights the CPA also as an excellent complementary tool for target or MoA identification.<sup>[84]</sup>

Yet another study, performed by Zimmermann *et al.*<sup>[85]</sup>, revealed an unexpected bioactivity of benzo-sulfonamides using the CPA. The fingerprint of two derivatives of this new compound class, containing a cyclic sulfonamide, showed high biosimilarity to the tubulin modulating agents Fenbendazole and tubulexin A and to a PLK1 (Polo-like kinase 1) inhibitor. Tubulin and PLK1 play crucial roles in mitosis. An increased number of cells in mitosis and an inhibited *in vitro* tubulin polymerization activity in the presence of the two derivatives was afterwards experimentally confirmed. Clustering of tubulin modulating agents is commonly observed.<sup>[63, 64, 86]</sup> Although a substantial amount of bioactive compounds lead to a significant morphological change, a limited number of MoAs can directly be identified by the nearest-reference approach and new clusters are rarely identified. Frequently observed clusters, like tubulin agents or inhibitors of the histone deacetylase, tend to represent bioactivity with a disruptive mechanism. Studies that identified other and more subtle MoA did not increase much in recent years.<sup>[37]</sup>

But also targets were identified using the CPA. For example, Foley *et al.*<sup>[83]</sup> synthesized indocinchona alkaloids, a new class of pseudo-NPs, by merging cinchona alkaloids with the indole ring system. A phenotypic screening assay revealed autophagy inhibiting activity for this new compound class. To gain further insight into the bioactivity, they were subjected to CPA, which uncovered biosimilarity to an inhibitor of the phosphatidylinositol-3 kinase VPS34, namely SAR405. A kinase assay confirmed the inhibitory effect and target engagement in cells was demonstrated by using a cellular thermal shift assay, underlining the potential of CPA to identify targets of small molecules.

## 4 AIM OF THE THESIS

There is a high demand in the field of chemical biology to map and expand bioactivity space. This can be achieved by identifying on- and off-target interaction networks or by the discovery of novel bioactivity. Small molecules and drug candidates addressing cellular structures that go beyond the already known drug targets are particularly interesting.<sup>[36]</sup> Especially the identification of targets, which are not proteins, and MoAs in general, are of interest but difficult to achieve with commonly employed target identification methods.<sup>[20, 34]</sup>

Morphological profiling gains increasing interest in the field and offers an approach with the potential to address all these issues using a single assay. In contrast to conventional phenotypic screens, morphological profiling measures hundreds of features that capture a much broader picture of bioactivity, which is not limited to a specific phenotype, pathway, or biological process of interest. However, researchers are often restricted in their experimental setup and measure only individual features, which leads to a loss of potentially useful and important phenotypic information.

To overcome this limitation, the Compound Management and Screening Center (COMAS), Dortmund, set up the Cell Painting Assay (CPA) in order to assess bioactivity of large compound libraries early on, to guide synthesis efforts, assign so far unknown targets or MoAs to annotated compounds and to identify novel bioactive small molecules and bioactivities.

Therefore, this thesis aimed to evaluate the applicability of the CPA to identify MoAs that are not mediated via small molecule-protein interactions, by investigating iron-chelating compounds. Furthermore, the bioactivity of an example compound class, namely the tetrahydroindolo[2,3-a]quinolizine derivatives, should be explored by means of the CPA.

The ability of the CPA to identify non-protein targets should be assessed using the example of the iron-chelating agent Deferoxamine (DFO). The requirement to use references for activity prediction is, that the morphological fingerprints of references, sharing a target or MoA, are highly biosimilar to ensure that the induced morphological change is related to the annotated target or MoA. Therefore, biosimilar references to DFO should be examined and a potential underlying target or MoA should be experimentally confirmed using secondary assays. If a common target or MoA can be confirmed, this cluster should be used to seek for novel, i.e., uncharacterized and biosimilar compounds that presumably share the same target or MoA.

The tetrahydroindolo[2,3-a]quinolizines are pre-validated by nature as numerous natural products embody the indolo[2,3-a]quinolizine scaffold and possess various biological activities.<sup>[87-89]</sup> To investigate the bioactivity of the tetrahydroindolo[2,3-a]quinolizine derivatives, the morphological fingerprints should be examined and compared to reference

compounds for target or MoA prediction. Depending on the outcome, further experiments to characterize the phenotype and to identify and confirm the potential target or MoA should be performed.

The CPA has the potential to overcome limitations of commonly applied target identification methods, to discover novel bioactive small molecules and new bioactivity areas including targets that are not proteins.

## 5 MATERIAL AND METHODS

### 5.1 Materials

#### 5.1.1 Chemicals and reagents

Compounds used in this thesis but not specified in this section were synthesized by chemists of the department of Chemical Biology at the Max Planck Institute of Molecular Physiology, Dortmund. Annotated reference compounds used in this thesis but not registered in this chapter were obtained from COMAS, Dortmund.

| Name   | Supplier                 | Cat. No          |
|--|--------------------------|------------------|
| 4',6-Diamidin-2-phenylindole (DAPI)              | Sigma Aldrich            | D9542            |
| Acetone  | Carl Roth                | 7328.1           |
| Acrylamide solution (30 %)                       | AppliChem                | A1672            |
| Ammonium persulfate                              | Serva                    | 13375.05         |
| Bovine Serum Albumin (BSA)                       | Serva                    | 11945.03         |
| Bromphenol blue, sodium salt                     | Carl Roth                | A512.1           |
| Chloroquine                                      | Sigma Aldrich            | C6628            |
| cOmplete™, EDTA-free protease inhibitor cocktail | Sigma Aldrich            | 11873580001      |
| Diminazene aceturate (Berenil)                   | Sigma Aldrich            | D7770            |
| Dithioerythritol (DTE)                           | Gerbu                    | 1007.0025        |
| Dithiothreitol (DTT)                             | Gerbu                    | 1008.0005        |
| DNase-free RNase A                               | Thermo Fisher Scientific | EN0531           |
| Dynasore   | Enzo Life Sciences       | ALX-270-502-M005 |
| EDTA   | Gerbu                    | 10341000         |
| EGTA   | AppliChem                | A0878,0100       |
| Ferrozine  | Thermo Fisher Scientific | 10522194         |
| Formaldehyde solution (37 %)                     | AppliChem                | A3592            |
| Glycerol   | Carl Roth                | 3783.1           |
| Glycine  | Carl Roth                | 3790.2           |
| HEPES  | Gerbu                    | 10090250         |
| Hoechst 33342                                    | Sigma Aldrich            | B2261            |
| Hydrochloric acid (HCl)                          | Appllichem               | A0658            |
| Iodoacetamide                                    | AppliChem                | A1666.0025       |
| Iron (II) sulfate heptahydrate                   | Sigma Aldrich            | F8633            |

## MATERIAL AND METHODS

| Name   | Supplier                 | Cat. No          |
|--|--------------------------|------------------|
| Lipofectamine® 2000                                      | Thermo Fisher Scientific | 11668019         |
| LysoTracker® Red DND-99                                  | Thermo Fisher Scientific | L7528            |
| Magnesium chloride hexahydrate                           | AppliChem                | A3618            |
| Methanol   | Sigma Aldrich            | 32213            |
| Nonfat dried milk powder                                 | AppliChem                | A0830            |
| NP-40 alternative  | Calbiochem               | 492016           |
| Opti-MEM™  | Thermo Fisher Scientific | 31985062         |
| PageRuler™ Plus prestained protein ladder, 10 to 250 kDa | Thermo Fisher Scientific | 26620            |
| PBS tablets  | Jena Bioscience          | AK-102P-L        |
| PhosSTOP phosphatase inhibitors                          | Sigma Aldrich            | 04906837001      |
| PIPES  | Sigma Aldrich            | P6757            |
| Propidium iodide   | Sigma Aldrich            | P4864            |
| SDS  | Gerbu                    | 12,120,100       |
| Sodium chloride  | AnalaR NORMAPUR          | 27810295         |
| SuperSignal™ West Femto                                  | Thermo Fisher Scientific | 34095            |
| SuperSignal™ West Pico                                   | Thermo Fisher Scientific | 34580            |
| TEMED  | Carl Roth                | 2367.3           |
| Transferrin from human serum, Alexa Fluor™ 594 (AF594)   | Thermo Fisher Scientific | T13343           |
| Triethylammonium bicarbonate buffer                      | Sigma Aldrich            | T7408            |
| TRIS   | Carl Roth                | 4855.2           |
| TCEP   | Thermo Fisher Scientific | 20491            |
| Triton® X-100  | Serva                    | 39795.02         |
| Trypan Blue Stain (0.4 %)                                | Thermo Fisher Scientific | T10282           |
| Trypsin recombinant, proteomics grade                    | Sigma Aldrich            | 3708969001       |
| Tween™ 20  | Fisher Bioreagents       | BB3337-100       |
| U18666A  | Abcam                    | Ab133116-192test |
| UltraPure™ Calf Thymus DNA Solution                      | Thermo Fisher Scientific | 15633019         |

## MATERIAL AND METHODS

### 5.1.2 Buffers and media

| Description                | Name   | Method                            |
|----------------------------|--|-----------------------------------|
| DNA binding buffer         | 2 mM HEPES, 9.4 mM NaCl, 0.01 mM EDTA, pH 7.0  | DNA binding assay                 |
| Lysis buffer               | 50 mM PIPES (pH 7.4), 50 mM NaCl, 5 mM EGTA, 5 mM MgCl <sub>2</sub> , 0.1 % NP-40, 0.1 % Triton X-100, 0.1 % Tween 20, freshly add: 1 mM DTT, PhosSTOP, cOMplete <sup>TM</sup> , EDTA-free protease inhibitor cocktail | Cell lysis for immunoblot         |
| Lysogeny broth (LB) medium | 10 g/L bacterial tryptophan, 5 g/L yeast extract, 10 g/L NaCl in mH <sub>2</sub> O   | Bacterial culture                 |
| PBS-T                      | 0.1 % Tween 20 in PBS  | General washing buffer            |
| Resolving gel              | 6-12.5 % acrylamide, 1.5 M TRIS-HCl (pH 8.8), 0.1 % SDS, 0.1 % APS, 0.004 % TEMED in mH <sub>2</sub> O   | SDS-PAGE                          |
| Running buffer (10X)       | 250 mM TRIS, 2 M glycine, 1 % SDS in mH <sub>2</sub> O   | SDS PAGE                          |
| SDS sample buffer (5X)     | 0.5 M TRIS, 40 % glycerol, 8 % SDS, 0.4 M DTE, 0.02 % bromphenol blue in mH <sub>2</sub> O   | SDS PAGE                          |
| Stacking gel               | 5 % acrylamide, 1 M TRIS-HCl (pH 6.8), 0.1 % SDS, 0.1 % APS, 0.01 % TEMED in mH <sub>2</sub> O   | SDS PAGE                          |
| Transferrin wash buffer    | 50 mM glycine, 150 mM NaCl, pH 3.0   | Transferrin uptake assay          |
| Wet blotting buffer        | 25 mM TRIS, 190 mM glycine, 10 % (v/v) methanol  | Wet protein transfer (immunoblot) |

### 5.1.3 Antibodies

#### 5.1.3.1 Primary antibodies

| Antigen    | Host   | Supplier                  | Cat. No |
|------------|--------|---------------------------|---------|
| LC3        | Rabbit | Cell Signaling Technology | 2775S   |
| p62/SQSTM1 | Rabbit | MBL Life science          | PM045   |
| Vinculin   | Mouse  | Sigma Aldrich             | V9131   |

#### 5.1.3.2 Secondary antibodies

| Antigen | Conjugate | Host   | Supplier | Cat. No   |
|---------|-----------|--------|----------|-----------|
| Mouse   | 800CW dye | Donkey | Li-COR   | 926-32210 |
| Rabbit  | HRP       | Goat   | Abcam    | Ab97051   |

### 5.1.4 Plasmids

| Name                               | Backbone   | Insert   | Source         |
|------------------------------------|------------|--|----------------|
| pRL-TK                             | pRL        | <i>Renilla luciferase</i>  | Promega E2241  |
| pSyn-SRE-Mut-T-Luc <sup>[90]</sup> | pGL2 basic | HMG-CoA synthase promoter with four point mutations (G → C or A → C) in the SRE binding region | Addgene #60490 |
| pSyn-SRE-T-Luc <sup>[91]</sup>     | pGL2 basic | HMG-CoA synthase promoter  | Addgene #60444 |

### 5.1.5 Cell lines

| Name     | Description  | Culture conditions   | Source  |
|----------|--|--|---|
| HeLa     | Female human adenocarcinoma                        | DMEM supplemented with 10 % (v/v) FBS, 1 mM sodium pyruvate, 1% (v/v) non-essential amino acids  | DSMZ, ACC 57  |
| L        | Male mouse fibroblasts                             | DMEM supplemented with 10 % (v/v) FBS, 1 mM sodium pyruvate, 1% (v/v) non-essential amino acids  | ATCC, CRL-2648  |
| MCF7-LC3 | Human epithelial, stably transfected with eGFP-LC3 | Eagle's MEM supplemented with 10 % (v/v) FBS, 1 mM sodium pyruvate, 1 % (v/v) non-essential amino acids, 0.01 mg/mL human insulin and 200 µg/mL G418 | The cell line was kindly provided by Yaowen Wu. <sup>[92]</sup> |
| U-2OS    | Female human osteosarcoma                          | DMEM supplemented with 10 % (v/v) FBS, 1 mM sodium pyruvate, 1% (v/v) non-essential amino acids  | CLS, 300364   |

### 5.1.6 Cell culture media and supplements

| Description                     | Supplier      | Cat. No    |
|---------------------------------|---------------|------------|
| DMEM                            | PAN Biotech   | P04-03550  |
| Eagle's MEM                     | PAN Biotech   | P04-08500  |
| EBSS                            | Sigma Aldrich | E3024      |
| Fetal bovine serum              | Gibco         | 10500-084  |
| G418                            | Sigma Aldrich | G8168      |
| Insulin                         | Sigma Aldrich | I9278      |
| Non-essential amino acids, 100X | PAN Biotech   | P08-32100  |
| Sodium pyruvate                 | PAN Biotech   | P04-43100  |
| Trypsin/EDTA                    | PAN Biotech   | P10-023100 |

### 5.1.7 Kits

| Description  | Supplier                 | Cat. No          |
|--|--------------------------|------------------|
| Actin Polymerization Kit                                 | Tebu-bio                 | 027BK003         |
| Cholesterol Assay Kit (Cell-Based)                       | Abcam                    | Ab133116-192test |
| Click-it™ Plus EdU Alexa Fluor™ 488 Flow Cytometry Assay | Thermo Fisher Scientific | C10632           |
| DC protein assay   | Bio-Rad                  | 5000112          |
| Dual-Glo® luciferase assay system                        | Promega                  | E2980            |
| EndoFree Plasmid Maxi Kit                                | Qiagen                   | 12362            |
| MycoAlert™ Mycoplasma Detection Kit                      | Lonza                    | LT07-318         |

### 5.1.8 Instruments and devices

| Description                    | Name                                 | Supplier                 |
|--------------------------------|--------------------------------------|--------------------------|
| Automated cell counter         | Countess™ II Automated Cell Counter  | Thermo Fisher Scientific |
| Automated screening microscope | Axiovert 200 M                       | Carl Zeiss               |
| Cell freezing container        | CoolCell® LX cell freezing container | BioCision                |
| Centrifuge                     | Table-top centrifuge, 5415D          | Eppendorf                |
| Centrifuge                     | Table-top centrifuge, 5415R          | Eppendorf                |
| Centrifuge                     | Large table-top centrifuge, 5810R    | Eppendorf                |



## MATERIAL AND METHODS

| Description                                  | Name                                    | Supplier                 |
|--|---|--------------------------|
| Clean bench for cell culture                 | NU-437-400E                             | lbs tecnomara            |
| Clean bench for proteomics experiments       | MSC-Advantage 1.2                       | Thermo Fisher Scientific |
| Device for running SDS gels and wet blotting | Mini-PROTEAN® Tetra Cell                | Bio-Rad                  |
| Device for SDS gel preparation               | Mini-PROTEAN® Tetra Cell Casting Module | Bio-Rad                  |
| Fine scale                                   | Analytical Plus                         | Sartorius                |
| Flow Cytometer                               | BD LSRII analyzer                       | Becton Dickinson         |
| Holder for SDS gels                          | Mini-PROTEAN® Tetra Electrode Assembly  | Bio-Rad                  |
| Holder for wet blotting                      | 2-Gel Tetra and Blotting Module         | Bio-Rad                  |
| Live-cell imaging system                     | Incucyte® ZOOM / Incucyte® S3           | Essen BioScience         |
| Multi-channel pipettes, 10 and 100 µL        | Research Plus                           | Eppendorf                |
| Plate reader                                 | Spark®                                  | Tecan                    |
| Scale  | CP3202S                                 | OHAUS                    |
| Spectrophotometer                            | Nanodrop 2000c                          | Thermo Fisher Scientific |
| Thermomixer                                  | Thermomixer comfort 1.5 mL              | Eppendorf                |
| Widefield fluorescence microscope            | Zeiss Observer Z1                       | Zeiss                    |

### 5.1.9 Software

| Description                            | Name                 | Supplier  |
|--|----------------------|---|
| Graphical representation               | GraphPadPrism 6.0    | <a href="https://www.graphpad.com/scientific-software/prism/">https://www.graphpad.com/scientific-software/prism/</a>     |
| Live-cell imaging                      | IncuCyte Software    | <a href="https://www.essenbioscience.com/en/products/incucyte/">https://www.essenbioscience.com/en/products/incucyte/</a> |
| Quantification of filipin staining     | Fiji-ImageJ          | <a href="https://imagej.net/Fiji">https://imagej.net/Fiji</a>   |
| Quantification of LC3 puncta formation | MetaXpress           | Molecular Devices   |
| Quantification of Western blots        | Image Studio Ver 5.2 | LI-COR  |

### 5.1.10 Other material and consumables

| Name  | Supplier                 |
|---|--------------------------|
| 0.5 mL tubes  | Sarstedt                 |
| 1.5 mL tubes  | Sarstedt                 |
| 10 µL pipette tips  | Sarstedt                 |
| 1000 µL pipette tips  | Diagonal                 |
| 15 mL tubes   | Sarstedt                 |
| 2 mL tubes  | Sarstedt                 |
| 200 µL pipette tips   | Diagonal                 |
| 5 mL Round Bottom Tube with Cell Strainer (FACS tubes)                  | Corning                  |
| 50 mL tubes   | Sarstedt                 |
| 6-well plate (transparent, standard)                                    | Sarstedt                 |
| 6-well plate, tissue culture-treated, clear, flat bottom                | Sarstedt                 |
| 96-well plate, black, clear-bottom                                      | Corning                  |
| 96-well plate, tissue culture-treated, clear, flat bottom<br>(standard) | Falcon/Sarstedt          |
| Countess™ Cell Counting Chamber Slides                                  | Thermo Fisher Scientific |
| Cryo vials  | Sarstedt                 |
| Glass slides, 76 x 26 cm  | Diagonal                 |
| Immobilon-DL PVDF Membrane  | Millipore                |
| Mini Cell Buffer Dam  | Bio-Rad                  |
| Mini-PROTEAN® Comb, 10-well, 1.0 mm, 44 µL                              | Bio-Rad                  |
| Mini-PROTEAN® Comb, 15-well, 1.0 mm, 26 µL                              | Bio-Rad                  |
| Mini-PROTEAN® Short Plates  | Bio-Rad                  |
| Mini-PROTEAN® Spacer Plates with<br>1.0 mm Integrated Spacer            | Bio-Rad                  |
| Protein LoBind Tubes 0.5 mL   | Eppendorf                |
| Protein LoBind Tubes 1.5 mL   | Eppendorf                |
| Protein LoBind Tubes 2.0 mL   | Eppendorf                |
| Serological pipette 1 mL  | Sarstedt                 |
| Serological pipette 10 mL   | Sarstedt                 |
| Serological pipette 25 mL   | Sarstedt                 |

| Name                                     | Supplier          |
|--|-------------------|
| Serological pipette 5 mL                 | Sarstedt          |
| T175 cell culture flask                  | Sarstedt          |
| T25 cell culture flask                   | Sarstedt          |
| T75 cell culture flask                   | Sarstedt          |
| Whatman® gel blotting paper, Grade GB005 | Sigma Aldrich     |
| X1000 Round Coverslips, diameter 12 mm   | Fisher Scientific |

## **5.2 Methods**

### **5.2.1 Molecular biology methods**

#### **5.2.1.1 Plasmid amplification, isolation and DNA sequencing**

To amplify a plasmid of interest, bacteria from a glycerol stock were inoculated in LB culture medium containing the respective selection antibiotic and incubated overnight at 37 °C. To prevent contamination, the inoculation was performed close to a Bunsen burner and with sterile equipment. The plasmid was isolated by using the EndoFree Plasmid Maxi Kit according to the manufacturer's protocol. Precipitated DNA was dissolved in autoclaved water and the concentration was determined with the Nanodrop 2000 spectrophotometer. DNA sequencing was performed by StarSEQ using the Sanger sequencing.

### **5.2.2 Cell biology methods**

#### **5.2.2.1 Sub-cultivation of adherent cell lines**

All cell lines were handled under sterile conditions and cultured at 37 °C and 5 % CO<sub>2</sub> until the cells reached 90 % confluence (5.1.5 and 5.1.6). For sub-culturing, medium was removed and cells were carefully washed with PBS. A trypsin/EDTA solution was added to detach the cells and the flask was incubated at 37 °C and 5 % CO<sub>2</sub>. Depending on the cell line, the flask was incubated between 1 and 5 min. Cells were fully detached by gently tapping against the flask. Subsequently, the respective growth medium was added to inactivate the trypsin. To resuspend and collect all cells, the flask was slowly flushed with the suspension three to four times.

**Table 1: Volumes used to wash, detach and resuspend the cells depending on the flask size.**

| Volumes [mL]  | T25 | T75 | T175 |
|---------------|-----|-----|------|
| PBS           | 2   | 5   | 10   |
| Trypsin/EDTA  | 0.5 | 2   | 3    |
| Growth medium | 2   | 8   | 12   |

A suitable volume of cell suspension was transferred into a new flask in a total volume of T25 (5 mL), T75 (12 mL) and T175 (22 mL).

#### 5.2.2.2 Cell counting and seeding

Cells were detached as described in 5.2.2.1 and the cell suspension was collected in a 50 mL tube. 10  $\mu$ L trypan blue were added to 10  $\mu$ L cell suspension and cells were counted in duplicates using an automated cell counter.

#### 5.2.2.3 Cryo-conservation of cells

For long-term storage, cells were preserved in the gas phase of liquid nitrogen. Therefore, cells were collected and counted as described in 5.2.2.1 and 5.2.2.2, respectively. The cell suspension was centrifuged for 3 min at 198 x g, the supernatant was removed and the cells were diluted to  $1 \times 10^6$  cells/mL in growth medium containing 5 % DMSO (v/v) to avoid membrane damage by ice crystals. 1 mL of the cell suspension was then transferred into a cryovial. To assure slow reduction in temperature the cryovials were placed in a freezing container, frozen overnight at -80°C and afterwards transferred to the liquid nitrogen tank.

#### 5.2.2.4 Thawing of cryo-conserved cells

To ensure rapid thawing of the cells, the cryovial was transferred on ice from the liquid nitrogen tank to the cell culture and then directly placed into a water bath (prewarmed to 37 °C) until most of the suspension was thawed. Subsequently, the cells were transferred into a containing 5 mL growth medium and centrifuged for 3 min at 380 x g to remove the DMSO containing freezing medium. The cell pellet was resuspended in 5 mL growth medium and transferred into cell culture flask that contained an appropriate volume of fresh growth media. The cells were cultured until 90 % confluence and passaged for at least one more time before they were used for experiments.

#### 5.2.2.5 Mycoplasma test

Bacterial contamination of cell cultures with mycoplasma can alter cell physiology and metabolism without being noticed because mycoplasma are invisible under a conventional light field microscope. This is mainly due to their small size, the lack of a cell wall and their adherence to the cell surface.<sup>[93]</sup> Therefore, cell cultures were monthly tested for mycoplasma contamination using the MycoAlert™ Mycoplasma Detection Kit according to the manufacturer's protocol.

#### 5.2.2.6 Real-time kinetic live-cell imaging

Live-cell imaging and monitoring of cell growth was performed using the Incucyte® ZOOM or Incucyte® S3 system. Therefore, cells were seeded into a 96-well plate at a density of 4,500 U-2OS/well, 3,500 L cells/well or 4000 HeLa/well in 90 µL medium per well. To let the cells attach to the surface, plates were incubated overnight and treated in triplicates with compound or 0.3 % DMSO as a control the following day. If toxicity was assessed, 16.67 µg/µL propidium iodide was added to the assay medium. Cell growth was monitored by means of confluence and toxicity by means of propidium iodide (PI) fluorescence as a readout through quantitative kinetic processing metrics obtained from the time-lapsed image acquisition using the Incucyte® ZOOM or Incucyte® S3 software.

#### 5.2.2.7 Cell Painting Assay

The Cell Painting Assay was performed by the Compound Management and Screening Center, Dortmund and follows closely the method described by Bray *et al.*<sup>[78, 94]</sup>

Initially, 5 µL U-2OS medium was added to each well of a 384-well plate (PerkinElmer CellCarrier-384 Ultra). Subsequently, U-2OS cells were seeded with a density of 1600 cells per well in 20 µL medium. The plate was incubated for 10 min at the ambient temperature, followed by an additional 4 h incubation (37 °C, 5 % CO<sub>2</sub>). Compound treatment was performed with the Echo 520 acoustic dispenser (Labcyte) at final concentrations of 1, 3 or 10 µM. Incubation with compound was performed for 20 h (37 °C, 5 % CO<sub>2</sub>). Subsequently, mitochondria were stained with Mito Tracker Deep Red (Thermo Fisher Scientific, Cat. No. M22426). The Mito Tracker Deep Red stock solution (1 mM) was diluted to a final concentration of 100 nM in prewarmed medium. The cell medium was removed from the plate leaving 10 µl residual volume and 25 µl of the Mito Tracker solution were added to each well. The plate was incubated for 30 min in the dark (37 °C, 5 % CO<sub>2</sub>). To fix the cells, 7 µL of

18.5 % formaldehyde in PBS were added, resulting in a final formaldehyde concentration of 3.7 %. Subsequently, the plate was incubated for another 20 min in the dark at room temperature (RT) and washed thrice with 70  $\mu$ L of PBS (Biotek Washer Elx405). Cells were permeabilized by the addition of 25  $\mu$ L 0.1 % Triton X-100 to each well, followed by 15 min incubation (RT) in darkness. The cells were washed thrice with PBS leaving a final volume of 10  $\mu$ L. To each well 25  $\mu$ L of a staining solution were added, which contains 1 % BSA, 5  $\mu$ L/mL Phalloidin (Alexa594 conjugate, Thermo Fisher Scientific, A12381), 25  $\mu$ g/mL Concanavalin A (Alexa488 conjugate, Thermo Fisher Scientific, Cat. No. C11252), 5  $\mu$ g/mL Hoechst 33342 (Sigma, Cat. No. B2261-25mg), 1.5  $\mu$ g/mL WGA-Alexa594 conjugate (Thermo Fisher Scientific, Cat. No. W11262) and 1.5  $\mu$ M SYTO 14 solution (Thermo Fisher Scientific, Cat. No. S7576). The plate is incubated for 30 min (RT) in darkness and washed three times with 70  $\mu$ L PBS. After the final washing step, the PBS was not aspirated. The plates were sealed and centrifuged for 1 min at 500 rpm.

The plates were prepared in triplicates with shifted layouts to reduce plate effects and imaged using a Micro XL High-Content Screening System (Molecular Devices) in 5 channels (DAPI: Ex350-400/ Em410-480; FITC: Ex470-500/ Em510-540; Spectrum Gold: Ex520-545/ Em560-585; TxRed: Ex535-585/ Em600-650; Cy5: Ex605-650/ Em670-715) with 9 sites per well and 20X magnification (binning 2).

The generated images were processed with the *CellProfiler* package (<https://cellprofiler.org/>, version 3.0.0) on a computing cluster of the Max Planck Society to extract 1716 cell features per microscope site. The data was then further aggregated as medians per well (9 sites -> 1 well), then over the three replicates.

Further analysis was performed with custom *Python* (<https://www.python.org/>) scripts using the *Pandas* (<https://pandas.pydata.org/>) and *Dask* (<https://dask.org/>) data processing libraries as well as the *Scientific Python* (<https://scipy.org/>) package (separate publication to follow).

From the total set of 1716 features, a subset of highly reproducible and robust features was determined using the procedure described by Woehrmann *et al.*<sup>[63]</sup> in the following way: Two biological repeats of one plate containing reference compounds were analyzed. For every feature, its full profile over each whole plate was calculated. If the profiles from the two repeats showed a similarity  $\geq 0.8$ , the feature was added to the set. This procedure was only performed once and resulted in a set of 579 robust features out of the total of 1716 that was used for all further analyses.

To determine the phenotypic fingerprint for each test compound z-scores were calculated for each feature:

$$z\_score = \frac{value_{meas.} - Median_{Controls}}{MAD_{Controls}}$$

The morphological fingerprint of a compound is then determined as the list of z-scores of all features for one compound.

In addition to the phenotypic fingerprint, an induction value was determined for each compound as the fraction of significantly changed features, in percent:

$$Induction [\%] = \frac{\text{number of features with abs. values} > 3}{\text{total number of features}}$$

Similarities of morphological fingerprints were calculated from the correlation distances<sup>[95]</sup> between two fingerprints (Similarity = 1 - Correlation Distance) and compounds with the most similar fingerprints were determined from a set of 3000 reference compounds that was also measured in the assay.

#### 5.2.2.7.1 Hierarchical clustering

The hierarchical clustering was performed and visualized using the clustermap tool from the seaborn package.<sup>[96]</sup> The tool in turn uses the hierarchical clustering module from the scipy package.<sup>[95]</sup> The linkage method was "complete", the used metric was "correlation" which corresponds to the similarity measure used for profile comparison. The clustermaps were either generated from the full parameter profiles or, to improve the visibility of less pronounced areas of the profiles, by forming sub-profiles in the following way: For all considered profiles, keep only those parameters from the profile, where all of the absolute values over all the rows are less than 10.0.

PseudoCode:

```

cutoff_filter = 10.0
parameters_to_keep = []
for parameter in ALL_PARAMETERS:
    absmax =
abs(dataframe_with_considered_profiles[parameter]).max(
)
    if absmax < cutoff_filter:
        parameters_to_keep.append(parameter)

```

#### 5.2.2.8 Flow Cytometry

To quantify the DNA amount of cells and to determine the percentage of cells in S phase, the Click-it™ Plus EdU Alexa Fluor™ 488 Flow Cytometry Assay Kit was used according to the manufacturer's protocol. Therefore,  $1.25 \times 10^5$  U-2OS cells were seeded in a 6-well plate and incubated overnight. The following day, cells were treated with indicated concentrations of compound or 0.3 % DMSO as a control for 22 h. To determine the percentage of cells in S phase of the cell cycle, cells were pulsed for another 2 h with  $10 \mu\text{M}$  5-ethynyl-2'-deoxyuridine (EdU) or medium as a control. EdU is a thymidine analog that is incorporated into the DNA during active DNA synthesis.<sup>[97]</sup> Cells were washed with PBS, detached using trypsin/EDTA and re-suspended in PBS. Cells were centrifuged at  $1258 \times g$  for 5 min at room temperature and washed with 1 % BSA in PBS. Cells were fixed with 4 % PFA in PBS and subjected to a click-reaction to label incorporated EdU with a fluorophore. Afterwards, cells were stained with a propidium iodide (PI) solution ( $100 \mu\text{g}/\text{mL}$  PI, 0.1% (v/v) Triton X-100 and  $100 \mu\text{g}/\text{mL}$  DNase-free RNase A in PBS) for 30 min at room temperature. PI intercalates into DNA in a 1:1 ratio causing a red shift of the PI excitation maximum and an increase in fluorescence intensity. The DNA amount is proportional to the fluorescence intensity, if PI is used in excess. For the measurement, the cell suspension was filtered to FACS tubes through a nylon mesh. For each sample 10,000 cells were sorted by the BD LSRII analyzer (Becton Dickinson, USA). FlowJo 10.6.1 software was used for quantification and data analysis. For every analysis, FSC and SSC (forward and side scatter, respectively) gating was performed to exclude doublets and debris and to select single cells. All results were plotted using GraphPad Prism 6 software.

#### 5.2.2.9 Sterol Regulatory Element (SRE) reporter gene assay

The SRE reporter gene assay was employed to study the effect of small molecules on sterol regulatory binding protein (SREBP)-dependent transcriptional activation. Therefore, cells were transfected with the pSynSRE-T-Luc plasmid, which contains the promoter of 3-hydroxy-3-methylglutaryl-Coenzyme A (HMG-CoA) synthase harboring the SREBP responsive region linked to a firefly luciferase. As a control, cells were transfected with a mutant version (pSynSRE-Mut-T-Luc) containing four point mutations (A→C or G→C) in the promoter region that abolish SRE-induced firefly luciferase expression. Cells transfected with pSynSRE-T-Luc or pSynSRE-Mut-T-Luc were in addition transfected with a *Renilla* luciferase construct (pRL-TK) as a cell viability and transfection efficiency control. Cells were transfected via lipofection using Lipofectamine 2000 according to the manufacturer's protocol.  $1.42 \times 10^6$  U-2OS cells per T25 flask were transfected with  $3 \mu\text{g}$  of the respective pSyn-SRE plasmid and  $0.3 \mu\text{g}$  pRL-TK using a DNA to Lipofectamine ratio of 1:3. Cells were incubated for 6 h at  $37 \text{ }^\circ\text{C}$  and 5 %



CO<sub>2</sub> and afterwards re-plated in a standard 96-well plate with 2,5 x 10<sup>4</sup> cells per well. Cells were incubated for another hour to allow attachment, treated with compounds and incubated for 24 h. Luciferase activities were measured using the Dual-Glo® Luciferase Assay System according to the manufacturer's instruction. In order to obtain normalized data the expression of the firefly luciferase reporter was divided by the *Renilla* luciferase signal. Modulation of the firefly and *Renilla* luciferase by the compounds was excluded by performing a Luciferase inhibition assay (see 5.2.2.10).

### 5.2.2.10 Luciferase inhibition assay

To identify small molecules that inhibit the activity of the firefly or *Renilla* luciferase, which would falsify the results of the reporter gene assay (see 5.2.2.9), a luciferase inhibition assay was performed. For this purpose, U-2OS cells were transfected with the pRL-TK and pSynSRE-T-Luc plasmid plasmid encoding the *Renilla* and firefly luciferase and re-plated as described in 5.2.2.9. But instead of treating the cells with compounds, cells were incubated overnight and lysed according to the manufacturer's protocol of the Dual-Glo® Luciferase Assay System. Prior to the readout, lysates were incubated with compounds for 1 h to restrict the source of a reduced signal to a direct inhibition by a compound. The readout performed according to the manufacturer's protocol of the Dual-Glo® Luciferase Assay System.

### 5.2.2.11 Lysosomotropism assay

Staining of lysosomes with LysoTracker® Red DND-99 was employed to assess the ability of small molecules to increase lysosomal pH. LysoTracker® Red DND-99 is a weak base linked to a fluorophore for a selective staining of acidic organelles. In the neutral environment of the cytosol, the probe is able to freely permeate through cell membranes. Once protonated in the acidic environment of the lysosome, the charged probe is unable to cross the lysosomal membrane to re-enter the cytoplasm. Lysosomotropic compounds lead to an increase in lysosomal pH which results in a decreased LysoTracker® Red DND-99 staining. For the assay, 7.000 U-2OS cells per well were seeded in 100 µL into a black 96-well plate (clear bottom) and incubated overnight at 37 °C and 5 % CO<sub>2</sub> to let the cells attach. The next day the cells were treated with compounds and incubated for 1 h. 50 µL medium were removed from each well and 50 µL medium containing LysoTracker® Red DND-99 (1 µM) and Hoechst 33342 (10 µg/µL) were added and incubated for 30 min at 37 °C and 5 % CO<sub>2</sub>. The medium was removed, cells were washed with 60 µL PBS and afterwards fixed with 50 µL 3.7 % formaldehyde in PBS by incubating for 10 min at RT in the dark. Cells were washed twice with

PBS prior to imaging using an Axiovert 200 M microscope at 10X magnification. Image analysis was performed using CellProfiler<sup>[81]</sup>, which identified cells via the Hoechst-33342 staining. LysoTracker® Red DND-99 mean intensity was measured per cell. For background correction, the mean intensity of 100  $\mu$ M Chloroquine, which was used as a control, was subtracted from all other conditions and the obtained values were normalized to the corresponding vehicle control.

### 5.2.2.12 Proteome profiling

#### Sample preparation for mass spectrometry

One day prior to treatment with compounds or DMSO as a control,  $1 \times 10^6$  U-2OS cells were seeded in a T75 flask. At the end of the incubation time, the medium was removed and transferred into a 50 mL tube. Cells were washed with 5 mL PBS, which was also collected in the tube, and then cells were detached using 2 mL trypsin/EDTA. Cells were resuspended in 8 mL PBS and the flask was washed with another 5 mL. All fractions were collected in the same falcon. The cells were centrifuged for 5 min at  $652 \times g$ , the supernatant was removed, the cell pellet was washed with 10 mL PBS and centrifuged again. The supernatant was removed and the cells were washed with 5 mL ice-cold PBS, centrifuged and washed again with 1 mL ice-cold PBS. The cell suspension was transferred into a 1 mL tube and again centrifuged. The supernatant was removed and cells were resuspended in 100  $\mu$ L PBS containing protease- and phosphatase inhibitors. Cells were lysed by subjecting them to seven freeze-thaw cycles. Cells were therefore frozen in liquid nitrogen and thawed at 37 °C in a thermomixer until only a small ice clump was visible. Afterwards the samples were centrifuged for 15 min at  $16,000 \times g$  at 4 °C. The protein concentration of the received supernatant was determined by means of the DC protein assay. 75  $\mu$ L of 100 mM triethylammonium bicarbonate (TEAB) buffer was added to each sample containing 50  $\mu$ g protein. 7.5  $\mu$ L 200 mM TCEP were added to each sample, the tubes were directly inverted and all samples were vortexed followed by a short centrifugation at  $10,000 \times g$  to collect the liquid. The samples were incubated for 1 h at 55 °C in a thermomixer to reduce the proteins. To alkylate the proteins 7.5  $\mu$ L of iodoacetamide were added to each sample and incubated for 30 min at RT in the dark. The proteins were precipitated by adding 900  $\mu$ L ice-cold acetone. Precipitation proceeded overnight at -20 °C. Samples were centrifuged for 10 min at  $8,000 \times g$  at 4 °C to collect the precipitated proteins. The supernatant was carefully removed and pellets were dried for 45 min. To digest the proteins, 107.5  $\mu$ L of 0.4  $\mu$ g/mL trypsin in 100 mM TEAB were added to each sample. The tubes were vigorously vortexed for about 20 s followed by a short centrifugation step to collect the liquid. Digestion proceeded overnight at 37 °C in a

thermomixer with shaking at 300 rpm. Afterwards samples were labeled with TMT label (TMT10plex, # 90110 ThermoFisher Scientific) according to the manufacturer's instruction.

*The TMT labeling as well as the nanoHPLC-MS/MS measurement and analysis was performed by the mass spectrometry group of the MPI Dortmund, namely Jens Warmers, Andreas Brockmeyer, Malte Metz and Dr. Petra Janning.*

### Mass spectrometry

Prior to nanoHPLC-MS/MS analysis samples were fractionated into ten fractions on a C18 column using high pH conditions to reduce the complexity of the samples and thereby increase the number of quantified proteins. Therefore, samples were dissolved in 120  $\mu$ L of 20 mM ammonium formate (HCOONH<sub>4</sub>) at pH 11, followed by incubation in an ultra-sonicator for 2 min, subsequent vortexing for 1 min and centrifugation at 8,000 x g for 3 min at room temperature. 50  $\mu$ L of the supernatant were injected onto a XBridge C18 column (130 Å, 3.5  $\mu$ m, 1mm x 150 mm) using a U3000 capHPLC system (ThermoFisher Scientific, Germany). Separation was performed at a flow rate of 50  $\mu$ L/min using 20 mM HCOONH<sub>4</sub> pH 11 in water as solvent A and 40 % 20 mM HCOONH<sub>4</sub> pH 11 in water premixed with 60 % acetonitrile as solvent B. Separation conditions were 95 % solvent A / 5% solvent B isocratic for the first 10 min, to desalt the samples, followed by a linear gradient up to 25 % in 5 min, a second linear gradient up to 65 % solvent B in 60 min, and a third linear gradient up to 100 % B in 10 min. Afterwards, the column was washed at 100 % solvent B for 14 min and re-equilibrated to starting conditions. Detection was carried out at a valve length of 214 nm. The eluate between 15 and 100 min was fractionated into ten fractions (30 s per fraction, circular fractionation using ten vials). Each fraction was dried in a SpeedVac at 30 °C until complete dryness and subsequently subjected to nanoHPLC-MS/MS analysis. For nanoHPLC-MS/MS analysis samples were dissolved in 20  $\mu$ L of 0.1 % TFA in water and 3  $\mu$ L were injected onto an UltiMate™ 3000 RSLCnano system (ThermoFisher scientific, Germany) online coupled to a Q Exactive™ HF Hybrid Quadrupole-Orbitrap Mass Spectrometer equipped with a nanospray source (Nanospray Flex Ion Source, Thermo Scientific). All solvents were LC-MS grade. To desalt the samples, they were injected onto a pre-column cartridge (5  $\mu$ m, 100 Å, 300  $\mu$ m ID \* 5 mm, Dionex, Germany) using 0.1 % TFA in water as eluent with a flow rate of 30  $\mu$ L/min. Desalting was performed for 5 min with eluent flow to waste followed by back-flushing of the sample during the whole analysis from the pre-column to the PepMap100 RSLC C18 nano-HPLC column (2  $\mu$ m, 100 Å, 75  $\mu$ m ID x 50 cm, nanoViper, Dionex, Germany) using a linear gradient starting with 95 % solvent A (water containing 0.1 % formic acid) / 5 % solvent B (acetonitrile containing 0.1 % formic acid) and increasing to 60 % solvent A 0.1 % formic acid / 40 % solvent B in 120 min using a flow rate of 300 nL / min. Afterwards, the column was

washed (95 % solvent B as highest acetonitrile concentration) and re-equilibrated to starting conditions. The nanoHPLC was online coupled to the Quadrupole-Orbitrap Mass Spectrometer using a standard coated SilicaTip (ID 20  $\mu\text{m}$ , Tip-ID 10  $\mu\text{m}$ , New Objective, Woburn, MA, USA). Mass range of  $m/z$  300 to 1,650 was acquired with a resolution of 60,000 for full scan, followed by up to 15 high energy collision dissociation (HCD) MS / MS scans of the most intense at least doubly charged ions using a resolution of 30,000 and a NCE energy of 35 %. Data evaluation was performed using MaxQuant software (v.1.6.3.4)<sup>[98]</sup> including the Andromeda search algorithm and searching the human reference proteome of the Uniprot database. The search was performed for full enzymatic trypsin cleavages allowing two miscleavages. For protein modifications, carbamidomethylation was chosen as fixed and oxidation of methionine and acetylation of the N-terminus as variable modifications. For relative quantification, the type “reporter ion MS2” was chosen and for all lysines and peptide N-termini TMT labels were defined. The mass accuracy for full mass spectra was set to 20 ppm (first search) and 4.5 ppm (second search), respectively and for MS/MS spectra to 20 ppm. The false discovery rates for peptide and protein identification were set to 1 %. Only proteins for which at least two peptides were quantified were chosen for further validation. Relative quantification of proteins was carried out using the reporter ion MS2 algorithm implemented in MaxQuant. The proteinGroups.txt file was used for further analysis. All proteins which were not identified with at least two razor and unique peptides in at least one biological replicate were filtered off. For further data analysis, the “Reporter intensity corrected” corresponding to compound treatment was divided by the “Reporter intensity corrected” of the corresponding vehicle control and the results were written into a new column. This file was stored under a different file name in txt-format. For further data analysis, Perseus version 1.6.2.3<sup>[99]</sup> was used. The calculated ratios of the above-mentioned file were defined as main columns. Proteins resulting from the reverse database search, just identified by site, typical contaminants and not quantified in at least three out of three or four replicates, respectively, were filtered off. The ratios of the “Reporter intensities corrected” were logarithmized ( $\log_2$ ) and normalized to the median. The mean of the replicates was calculated and the outlier test “Significance A” was performed. Proteins with a  $p$ -value  $< 0.05$  were considered as statistically significantly up- or down-regulated, depending on the direction of change.

### 5.2.2.13 Protein levels of LC3 and p62/SQSTM1

Protein levels of LC3 and p62/SQSTM1 are widely used to monitor the autophagic flux. Therefore, MCF7 cells stably expressing the GFP-tagged LC3, were used.  $3 \times 10^5$  MCF7-LC3 cells per well were seeded in a 6-well plate and incubated overnight. The cell line was kindly

provided by Yaowen Wu.<sup>[92]</sup> On the next day, cells were treated with compounds or DMSO as a control for 24 h. As a control, autophagy was induced by amino acid starvation using EBSS (Earle's Balanced Salt Solution). In order to lyse the cells, medium was removed, cells were washed with PBS and detached by adding 250  $\mu$ L trypsin/EDTA per well. Cells were resuspended in 1 mL PBS and transferred into a 15 mL tube. Cells were centrifuged for 5 min at 3,220 x g, washed with 1 mL PBS and transferred into a 1 mL tube. Cells were centrifuged, the supernatant was removed and 50  $\mu$ L lysis buffer for immunoblotting was added. Samples were incubated for 30 min on ice by inverting the tube every 10 min and afterwards centrifuged for 20 min at 15,700 x g at 4 °C. The protein concentration of the received supernatant was determined by means of the DC protein assay (see 5.2.3.3). Proteins were separated by size via a sodium dodecyl sulfate polyacrylamide gel electrophoresis (SDS-PAGE) (see 5.2.3.4) using 15 % SDS polyacrylamide gels and transferred onto a PVDF membrane by the wet blot technique (see 5.2.3.5). Membranes were cut according to the used antibodies and corresponding protein size and blocked in 5 % nonfat dried milk in PBS-T. Antibody treatment (see Table below) and detection of the protein bands was performed as described in section 5.2.3.5.

Table 2: Antibodies, blocking solution and detection method for LC3 and p62 p62/SQSTM1 immunoblot.

| Primary antibody       | Dilution primary antibody | Secondary antibody     | Dilution secondary antibody | Blocking solution             | Detection         |
|------------------------|---------------------------|------------------------|-----------------------------|-------------------------------|-------------------|
| Rabbit anti-p62/SQSTM1 | 1:10,000                  | Anti-rabbit HRP        | 1:10,000                    | 5% nonfat dried milk in PBS-T | Chemiluminescence |
| Rabbit anti-LC3        | 1:1000                    | Anti-rabbit HRP        | 1:10,000                    | 5% nonfat dried milk in PBS-T | Chemiluminescence |
| Mouse anti-Vinculin    | 1:1000                    | Anti-mouse IRDye 800CW | 1:5000                      | 5% nonfat dried milk in PBS-T | Fluorescence      |

#### 5.2.2.14 Transferrin uptake assay

A fluorescently labeled transferrin was used to monitor receptor-mediated endocytosis under compound treatment. For this,  $3 \times 10^4$  U-2OS cells were seeded on round coverslips (12 mm diameter) placed in a 24-well plate. The plate was incubated overnight to let the cells attach. On the next day, cells were washed once with serum-free medium (DMEM without supplements) followed by a 3 h treatment in duplicates in serum-free medium containing

compounds or DMSO as a control. Afterwards, the medium was removed and replaced by fresh serum-free medium containing 25 µg/mL Transferrin-AF594 and the compounds or DMSO. The plate was incubated for 2 min at RT to pause endocytosis and afterwards incubated for 5 min at 37 °C and 5 % CO<sub>2</sub> to initiate the internalization of the labeled transferrin. Coverslips were washed carefully but as fast as possible twice with transferrin wash buffer (see 5.1.2) to remove residual transferrin attached to the cell surface. Subsequently, cells were washed twice with PBS and then fixed in 3.7 % formaldehyde in PBS for 20 min at RT in the dark. A first sample was thereby already taken after the incubation step at RT in order to have a sample at timepoint 0. After fixation, cells were washed twice with PBS and nuclei were stained by incubating the coverslips for 10 min at RT in the dark in PBS containing 1 µg/mL DAPI. Finally, cells were washed again with PBS and mounted on a glass slide for microscopic examination. Images were acquired using the Zeiss Observer Z1 with a 63X oil objective. Image analysis was performed using CellProfiler<sup>[81]</sup>, which identified cells via the DAPI staining. Mean integrated intensity Transferrin-AF594 was determined per image using 12 images per experimental condition.

### 5.2.2.15 Cholesterol staining

The cellular distribution of cholesterol can be visualized using naturally fluorescent filipin, a polyene macrolide antibiotic and antifungal, that binds unesterified cholesterol. Cholesterol staining using filipin was performed using the Cholesterol Assay Kit (Abcam) according to the manufacturer's protocol. Briefly, 4,700 U-2OS cells were seeded in a 96-well glass bottom plate and incubated overnight. Cells were treated with the compounds or DMSO as a control for 3 h prior to fixation and staining with filipin. Images were acquired using the Zeiss Observer Z1 with a 63x oil objective. Fiji-ImageJ was used to determine the stained area per cell.

### 5.2.2.16 GFP-LC3 puncta formation assay

MCF7 cells stably expressing GFP-tagged LC3 were used to detect the formation of autophagosomes during autophagy. The cell line was kindly provided by Yaowen Wu.<sup>[92]</sup> The assay was performed to test compounds for their ability to induce autophagy. As a control autophagy was induced by amino acid starvation using Earle's Balanced Salt Solution (EBSS). MCF7-GFP-LC3 cells were seeded at a density of  $1.5 \times 10^4$  cells per well in a black 96-well plate (clear bottom) and incubated overnight. The next day cells were treated with compounds or DMSO as a control both, in the presence and absence of 50 µM Chloroquine, for 24 h at 37 °C and 5 % CO<sub>2</sub>. The medium was removed and cells were fixed with 3.7 % formaldehyde

in PBS containing Hoechst 33342 (10  $\mu\text{g}/\mu\text{L}$ ) by incubating for 20 min at RT. Cells were washed thrice with PBS and images were acquired using an Axiovert 200 M microscope at 20X magnification. Automated image analysis was performed using the granularity setting of MetaXpress Software (Molecular Devices).

### 5.2.3 Biochemical methods

#### 5.2.3.1 Iron chelation assay

The ability of the compounds to chelate iron was assessed in a colorimetric way by ferrozine-Fe(II)-complex formation. Ferrous ions form a purple complex with the chromogen ferrozine which can be followed spectrophotometrically.<sup>[100]</sup> Chelating compounds will compete with ferrozine for the ferrous ions leading to a restricted complex formation, i.e., reduced absorbance. Therefore, 12.5  $\mu\text{M}$  iron(II) sulfate was incubated with compounds in  $\text{mH}_2\text{O}$  for 10 min at RT in a 96-well plate. DMSO and Deferoxamine were used as controls. Afterwards, 0.5 mM ferrozine was added and absorbance was detected at 561 nm with a plate reader.

#### 5.2.3.2 DNA binding assay

The binding of small molecules to DNA was assessed by performing a competition assay using DAPI as a minor groove binder and propidium iodide (PI) as a DNA intercalator. Binding of a compound to DNA would displace DAPI or PI depending on the binding mode and result in a decreased fluorescence signal. Therefore, 1  $\mu\text{g}$  calf thymus DNA was incubated with different concentrations of the compound and either 0.625  $\mu\text{M}$  DAPI or 0.625  $\mu\text{M}$  PI in DNA binding buffer. Fluorescence was measured immediately. The assay was performed in technical triplicates in black 96-well plates with clear bottom using 100  $\mu\text{L}$  per well. First, the fluorescence of DAPI (ex/em: 350/470 nm) and afterwards the fluorescence of PI (ex/em: 535/617 nm) was measured using a plate reader.

#### 5.2.3.3 DC protein assay

The colorimetric DC protein assay was performed to determine the protein concentration of lysates. The assay is based on the reaction between proteins and copper ions and the folin reagent. Two steps lead to the color development, first the reaction between the proteins and the copper ions at basic pH followed by the reduction of the folin reagent by the copper-treated proteins. The responsible amino acid residues are primarily tyrosine and tryptophan and to a

lesser extent cysteine and histidine. The reduction of the folin reagent by the amino acids results in a species with a characteristic blue color, whose absorbance can be measured at 750 nm.<sup>[101]</sup> For this, lysates were diluted 1:5 in lysis buffer in order to be in the linear range. A BSA dilution series was used as a standard to determine the protein concentration. All samples were measured in duplicates in a standard 96-well plate according to the manufacturer's protocol using a plate reader.

### 5.2.3.4 Sodium dodecyl sulfate polyacrylamide gel electrophoresis (SDS-PAGE)

In preparation for an immunoblot (see 5.2.3.5), proteins, e.g., in lysates need to be separated by size by using an SDS-PAGE. At first, proteins were denatured by reducing disulfide bonds and by boiling the lysate in 5X SDS-sample buffer containing DTE for 5 min at 95 °C and shaking at 350 rpm. SDS covers the intrinsic charge of the proteins enabling the separation in the gel solely based on the size. The Mini-PROTEAN® Tetra Cell was assembled, the comb was removed from the SDS polyacrylamide gel and the tank was filled with 1X running buffer. Protein samples were loaded into the gel pockets including 10 µL of PageRuler™ Plus prestained protein ladder. First, a voltage of 80 V was applied until the proteins passed the stacking gel and the ladder started to separate. Afterwards, the voltage was increased to 120 V until the marker band completely separated or the running front reached the end of the gel.

### 5.2.3.5 Immunoblot

An immunoblot was performed subsequent to an SDS-PAGE. Upon separation by size using an SDS-PAGE, proteins need to be transferred onto a suitable membrane that allows binding of antibodies to detect proteins of interest. In this thesis, wet blotting was performed using the Mini-PROTEAN® Tetra Cell. After electrophoresis, the gel was transferred into water until blotting. The Immobilon-FL PVDF membrane was activated by incubation in methanol for 1 min. The membrane and two filter papers were equilibrated in freshly prepared and pre-chilled wet blotting buffer. The sandwich, consisting of fiber pads, filter papers, the gel and the membrane, was assembled in a tank filled with wet blotting buffer. First, one fiber pad was placed on top of the white side of the plastic holder belonging to the transfer cassette followed by one filter paper, the membrane, the gel, another filter paper and in the end the second fiber pad. Bubbles were removed by flattening the layers with a plastic roller. The plastic holder was closed, inserted into the cassette and placed inside the blotting tank. A thermal pack and a magnetic stirrer were added to the tank to ensure cooling of the sandwich. The tank was filled with wet blotting buffer, placed on top of a magnetic stirrer and the transfer was performed by



applying a voltage of 100 V for 100 min. After blotting, the membrane was placed in a tube and incubated for 1 h at RT in blocking solution. Primary antibodies were diluted in blocking solution and incubated overnight at 4 °C. The membrane was washed thrice for 5 min with PBS-T and afterwards incubated with the secondary antibodies in blocking solution for 1 h at RT. Finally, the membrane was washed once with PBS-T for 5 min and twice with PBS for 5 min and stored in PBS until imaging. The secondary antibodies were either linked to a horseradish peroxidase (HRP) for chemiluminescent detection or to a near-infrared dye (LI-COR antibodies, 680RD or 800CW) for fluorescent detection. For fluorescence detection, the membrane can be directly imaged. For HRP detection, the membrane was incubated with SuperSignal™ Pico or Femto reagent according to the manufacturer's protocol. Imaging was carried out with an Odyssey Fc imaging system. Protein bands were quantified by normalization to a housekeeping protein.

### 5.2.3.6 Actin polymerization assay

The assay was performed to study the effect of small molecules on the polymerization of actin based on the enhanced fluorescence of pyrene-conjugated actin that occurs during polymerization. The experiment was carried out according to the manufacturer's protocol. Briefly, pyrene-conjugated actin was diluted in G-actin buffer (5 mM TRIS-HCl, pH 8.0, 0.2 mM CaCl<sub>2</sub>, 0.2 mM ATP) to a final concentration of 0.4 mg/mL. The actin solution was kept on ice for 1 h for de-polymerization followed by centrifugation at 86,700 g for 30 min at 4 °C. The supernatant was collected in a fresh tube. Pyrene-conjugated actin was added to black bottom 96-well plates at 4 °C. Different concentrations of compounds or DMSO as control were dissolved in 10X actin polymerization buffer (500 mM KCl, 20 mM MgCl<sub>2</sub>, 0.05 M guanidine carbonate, and 10 mM ATP) and added to the actin solution in the 96-well plate at 4 °C. The final concentration of pyrene-conjugated actin in the assay was 0.36 mg/mL. After shaking for 1 min at 600 rpm the time course of actin polymerization was monitored over 100 min by reading the fluorescence (ex/em: 360/410 nm) at 30 °C in a plate reader.

### 5.2.3.7 Topoisomerase activity assay

Topoisomerase activity assays were performed at Inspiralis. In all experiments, the activity of the enzyme was determined prior to the testing of the compounds. 1 U was defined as the amount of enzyme required to fully decatenate or relax the substrate. Compounds were tested at a fixed concentration of 30 µM and added to the reaction before the addition of the enzyme. The final DMSO concentration in the assays was 10 % (v/v).

### *Human DNA Topoisomerase I relaxation assay*

1 U of human DNA topoisomerase I was incubated with 0.5 µg supercoiled plasmid DNA (pBR322) in a 30 µL reaction at 37 °C for 30 min under the following conditions: 20 mM TRIS-HCl (pH 7.5), 200 mM NaCl, 0.25 mM EDTA and 5 % glycerol plus 10 % DMSO. Each reaction was stopped by the addition of 30 µl chloroform/iso-amyl alcohol (24:1) and 30 µl Stop Dye (40 % sucrose, 100 mM TRIS-HCl (pH 7.5), 10 mM EDTA, 0.5 µg/ml bromophenol blue), before being loaded on a 1.0 % TAE (0.04 mM Tris-acetate, 0.002 mM EDTA) gel and run at 80 V for two h.

### *Human DNA topoisomerase II (alpha) decatenation assay*

1 U of human DNA topoisomerase II $\alpha$  was incubated with 200 ng kinetoplast DNA in a 30 µL reaction at 37 °C for 30 min under the following conditions: 50 mM TRIS-HCl (pH 7.5), 125 mM NaCl, 10 mM MgCl<sub>2</sub>, 5 mM DTT, 0.5 mM EDTA, 0.1 mg/mL bovine serum albumin (BSA) and 1 mM ATP in 10 % DMSO. Each reaction was stopped by the addition of 30 µl chloroform/iso-amyl alcohol (24:1) and 30 µL Stop Dye (40 % sucrose, 100 mM TRIS-HCl (pH 7.5), 10 mM EDTA, 0.5 µg/ml bromophenol blue), before being loaded on a 1.0 % TAE (Tris-acetate 0.04 mM, EDTA 0.002 mM) Gels run at 80 V for two h.

### *Data acquisition and analysis*

Bands were visualized by ethidium staining for 10 min, destained for 10 min in water and analyzed by gel documentation equipment (Syngene, Cambridge, UK) and quantitated using Syngene Gene Tools software. Raw gel data (fluorescent band volumes) collected from Syngene, GeneTools gel analysis software were calculated as a % of the control (the fully supercoiled or decatenated band) and converted to % inhibition. Raw gel data were analyzed using SigmaPlot Version 13 (2015). The global curve fit non-linear regression tool was used to calculate IC<sub>50</sub> data using the following equation: Exponential Decay, Single, 2 Parameter  $f = a \cdot \exp(-b \cdot x)$

### 5.2.3.8 CDK/cyclin activity assay

The screening of selected CDK/cyclin complexes was performed by SelectScreen Kinase Profiling Service of Life Technologies according to the instructions provided on the company's website: <https://www.thermofisher.com/de/de/home/products-and-services/services/custom-services/screening-and-profiling-services/selectscreen-profiling-service/selectscreen-kinase-profiling-service.html>

## 6 RESULTS

### 6.1 Applicability of the Cell Painting Assay (CPA) to predict non-protein targets

It is rather difficult to identify a target of a small molecule, which is not a protein because commonly applied target or MoA identification methods are designed to identify proteins only. To evaluate the usefulness of the CPA to predict bioactivity that goes beyond protein targets, morphological fingerprints for the iron chelator Deferoxamine (DFO) were generated and afterwards used as a query profile to examine biosimilar reference compounds.

#### 6.1.1 Morphological profiling of the iron-chelating agent Deferoxamine (DFO)

DFO (Figure 9A) is an FDA-approved drug and has been used for decades in the treatment of iron-overload diseases.<sup>[102]</sup> It is a hexadentate siderophore from *Streptomyces pilosus* with a high affinity for Fe(III).<sup>[103]</sup>

U-2OS cells were exposed to different concentrations of DFO and the CPA was employed to generate morphological fingerprints.<sup>[59, 78]</sup>

## RESULTS

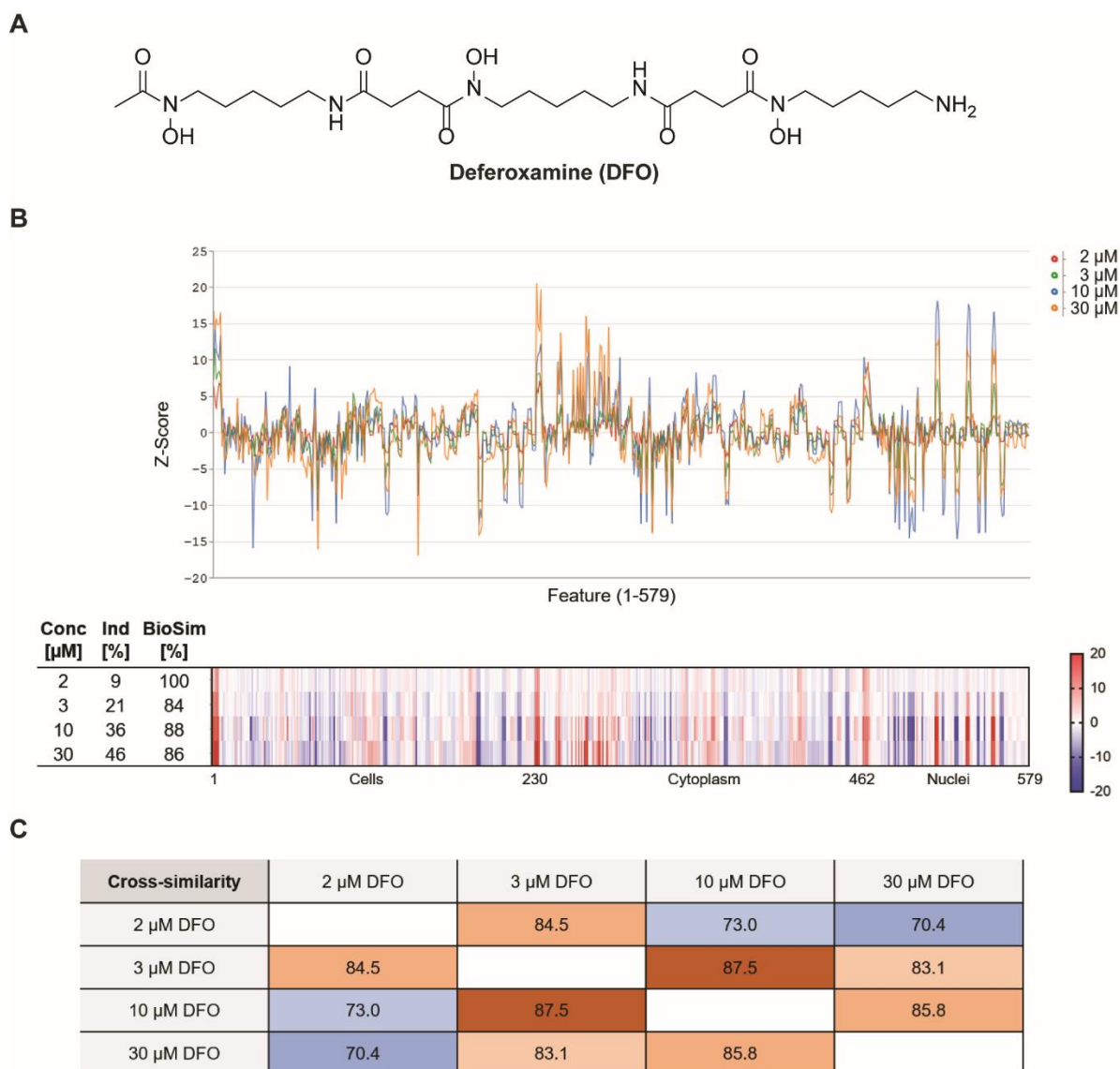


**Figure 9: Morphological fingerprints of DFO.**

(A) Chemical structure of DFO. (B) Morphological fingerprints generated for different concentrations (conc) of DFO visualized as line plots and heatmap profiles. Shown similarities (biosimilarity, BioSim) are relative to the respective previous entry. The set of 579 features is divided into cell (1-229), cytoplasm (230-461) and nuclei (462-579) related features. Values were normalized to the DMSO control. Blue: decreased feature, red: increased feature. Ind: induction. Conc: concentration. (C) Biosimilarity among different concentrations of DFO.

The morphological fingerprints of DFO depicted in Figure 9B displayed a concentration-dependent increase in the induction value. The induction is defined as the fraction of significantly changed features compared to the DMSO control. Even at the lowest concentration of 2 μM, DFO possessed activity in the CPA with an induction value of 9 %. At 3 μM, DFO had an induction of 21 %, at 10 μM the value further increased to 36 % and at the highest concentration of 30 μM, DFO showed an induction of 46 %. The concentration-dependent increase in induction paired with the constant biosimilarity of over 80 % points

## RESULTS

towards a dose-dependent phenotype. This hypothesis is supported by the cross-correlation of the biosimilarity among the different concentrations (Figure 9C) with a median biosimilarity percentage (MBP) of 83.5 %.

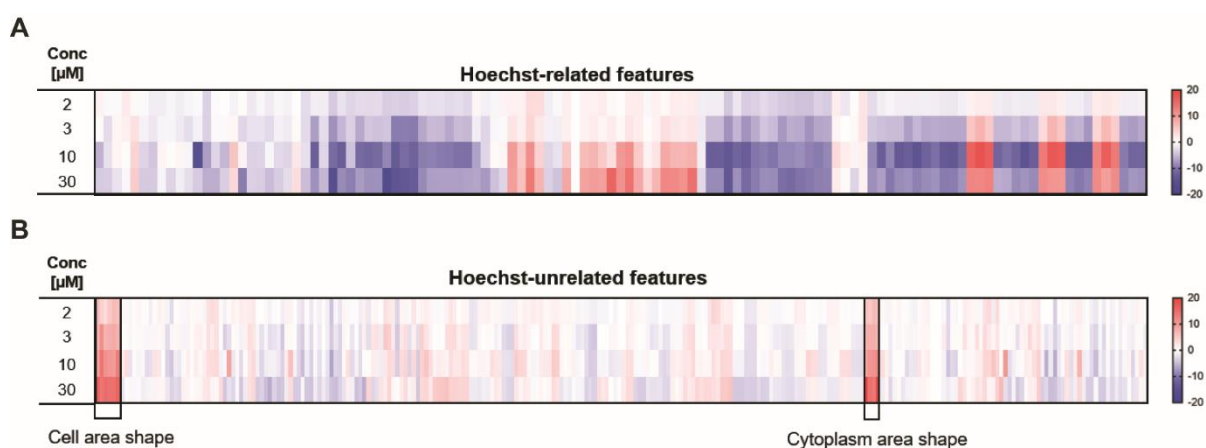


**Figure 10: Selected features of the morphological fingerprints of DFO.**

Nucleus (Hoechst)-related (A) and Hoechst-unrelated (B) features. Values were normalized to the DMSO control. Blue: decreased feature, red: increased feature.

Interestingly, a closer look into the set of measured features revealed that those related to the Hoechst staining of the nucleus (Figure 10A) were induced much stronger than Hoechst-unrelated features (Figure 10B). Among the Hoechst-unrelated features, only those describing the cell and cytoplasm area shape were dose-dependently altered and reached z-score values  $\geq 10$  at the two highest concentrations of 10 and 30  $\mu\text{M}$  (Figure 10B).

Taken together, DFO is active in the CPA and induced concentration-dependent morphological changes, which can be attributed to the same phenotype based on the high cross-similarity among the different concentrations. Furthermore, the phenotype is mainly related to morphological changes in the nucleus and cell size.

### 6.1.2 Identification of annotated reference compounds biosimilar to DFO

3,580 annotated reference compounds were profiled in the CPA to compare their morphological fingerprints to fingerprints of uncharacterized compounds with the aim to predict a target or MoA. Among others, the reference set contained the Library of Pharmacologically Active Compounds (LOPAC)<sup>[104]</sup>, libraries of kinase inhibitors and the Prestwick Chemical Library<sup>[104]</sup>. References that share a target/MoA are supposed to possess high morphological fingerprint similarity, defining a cluster. This is the prerequisite for using references for

## RESULTS

---

bioactivity predictions as this ensures that their morphological fingerprints result from the annotated target/MoA-related bioactivity. If this is not the case, the morphological profile of a reference is most likely influenced by an additional target or off-target effect, which might not be reflected in its annotation.

The fingerprint of 10  $\mu$ M DFO was used as a query profile to investigate if the CPA is able to identify biosimilar references that share the same target/MoA. The analysis revealed that the four metal ion chelating agents Ciclopirox<sup>[105-107]</sup>, 1,10-phenanthroline<sup>[108-110]</sup>, PAC-1<sup>[111]</sup> and catechol<sup>[102, 112]</sup> were among the references with the highest biosimilarity to DFO (Figure 11A, B).

## RESULTS

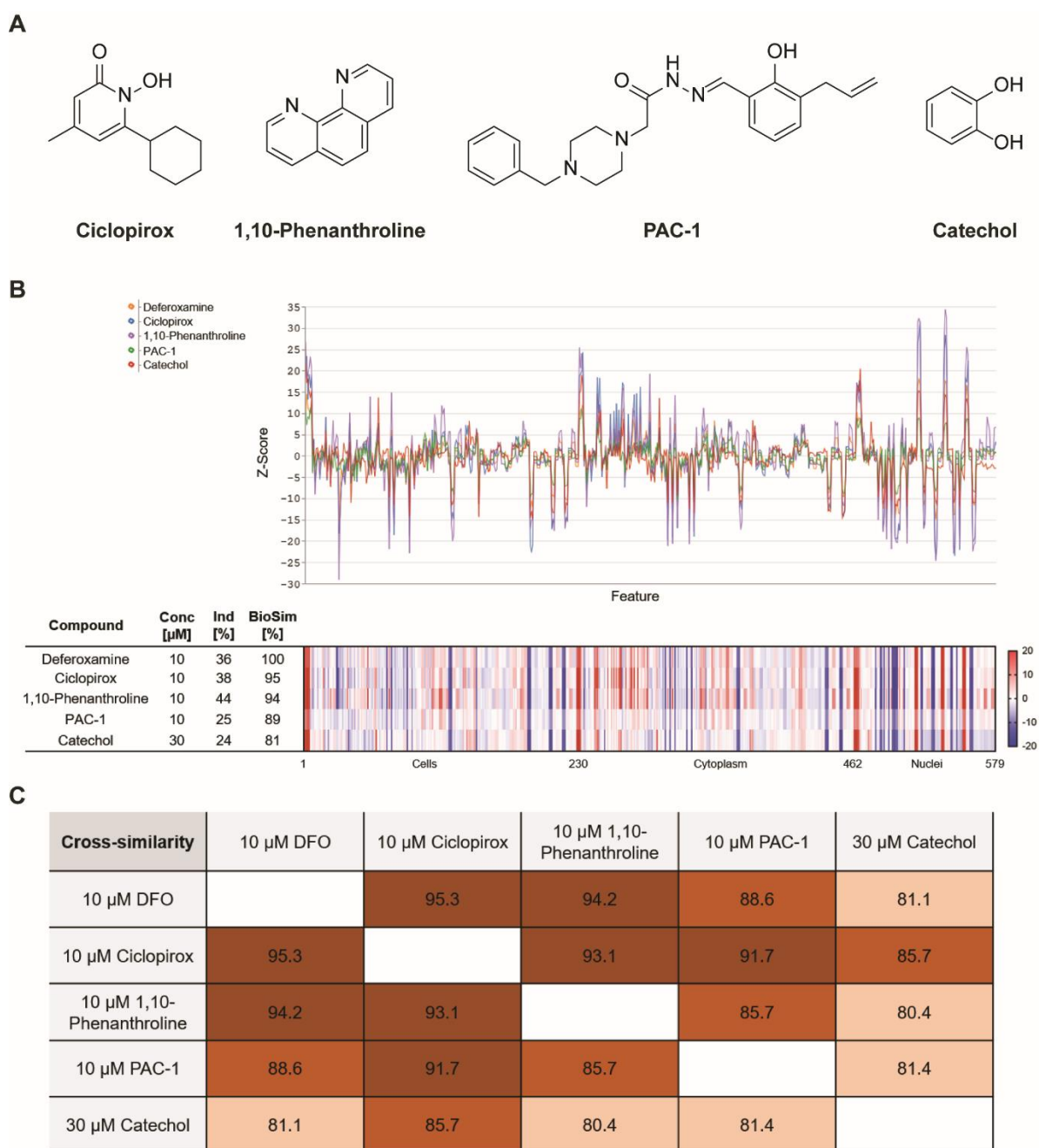


**Figure 11: Morphological profiling of different metal-chelating agents with high biosimilarity to DFO.**

(A) Chemical structures of metal ion chelators. (B) Morphological fingerprints of metal ion chelators visualized as line plots and heatmap profiles. The fingerprint of DFO is set as a reference (100 % biosimilarity, BioSim) to which the following fingerprints are compared. The set of 579 features is divided into cell (1-229), cytoplasm (230-461) and nuclei (462-579) related features. Values were normalized to the DMSO control. Blue: decreased feature, red: increased feature. Conc: concentration. Ind: induction. (C) Biosimilarity among metal ion chelators.

The metal ion chelators Ciclopirox and 1,10-phenanthroline were identified as the top two references sharing the highest biosimilarity to DFO of 95 and 94 %, respectively. Also, their induction values (38 and 44 %, respectively) were within the same range as the values

## RESULTS

recorded for DFO (36 %) at 10  $\mu$ M. PAC-1 and catechol shared high biosimilarity values as well (89 and 81 %, respectively). However, their induction values were slightly lower (25 and 24 %, respectively) although the biosimilar fingerprint of catechol derived from a higher concentration of 30  $\mu$ M (Figure 11B). The metal ion chelating agents did not only exhibit a high biosimilarity to DFO but also among each other. The cross-similarity matrix (Figure 11C) reflects the same trend in biosimilarity, i.e., higher than 80 % among all references.

35 additional references were identified as biosimilar (> 75 %) to the morphological fingerprint of 10  $\mu$ M DFO (Figure 12, for structures, see Table 11 in the appendix). Although the fingerprints of the identified references originate from different concentrations (0.2- 30  $\mu$ M) and cover a broad induction range between 5 and 58 %, they also displayed a high cross-similarity among each other with a MBP of 82.5 %.

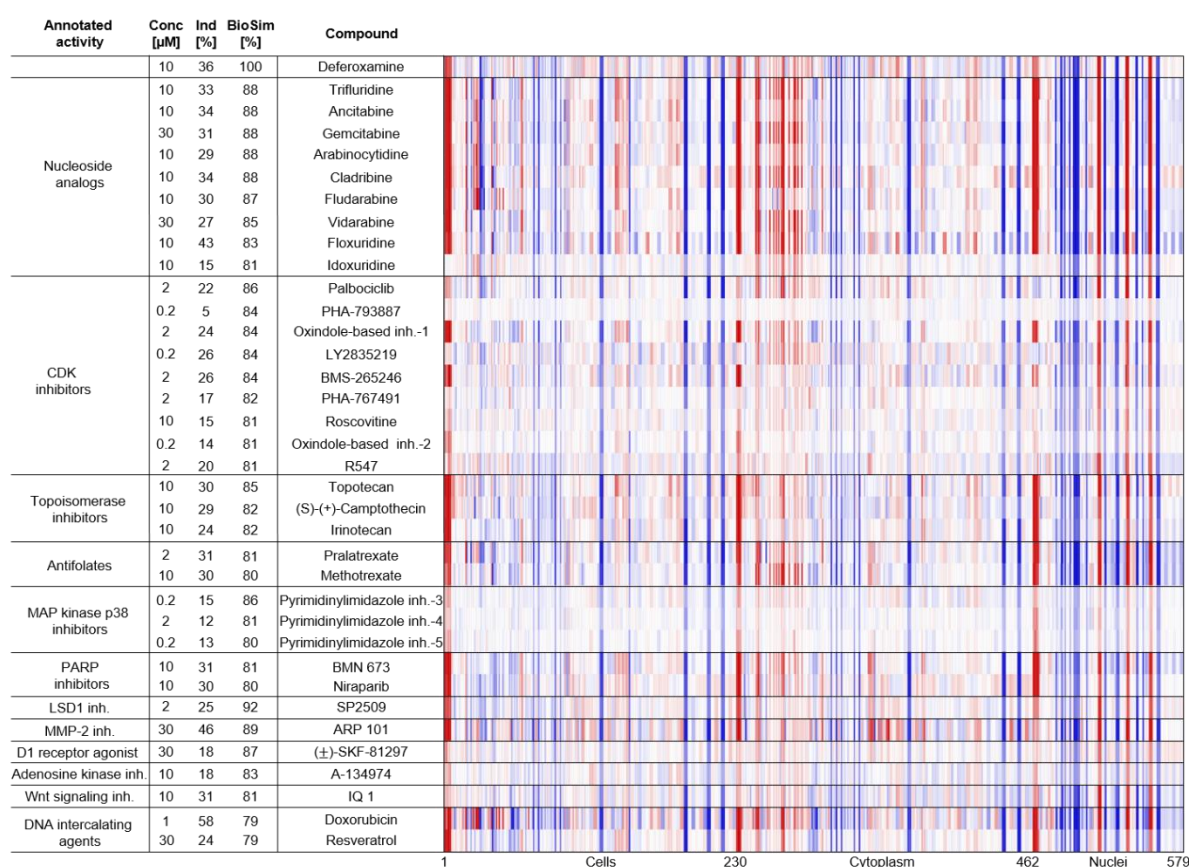


**Figure 12: Morphological fingerprints of reference compounds with high biosimilarity (> 75 %) to 10  $\mu$ M DFO.**

The fingerprint for 10  $\mu$ M DFO is set as a reference fingerprint (100 % biosimilarity, BioSim). The set of 579 features is divided into cell (1-229), cytoplasm (230-461) and nuclei (462-579) related features. Values were normalized to the DMSO control. Blue: decreased feature, red: increased feature. Conc: concentration. Ind: induction. Inh.: inhibitor.



The annotated activities and targets of those references are diverse, comprising nucleoside analogs, cyclin-dependent kinases (CDKs), topoisomerases, folic acid analogs, MAP kinase p38, poly(ADP-Ribose)-polymerase (PARP), lysine-specific histone demethylase 1 (LSD1), matrix metalloproteinase-2 (MMP-2), dopamine 1 receptor, adenosine kinase,  $\beta$ -catenin signaling and DNA intercalation. At first sight, these references are not only chemically diverse but also their annotated bioactivity seemed entirely different from metal ion chelation. However, iron is crucial for various cellular processes, e.g., DNA synthesis and repair, as many enzymes involved in these processes require iron as a cofactor.<sup>[102, 112, 113]</sup> Iron chelators not only inhibit cell growth but also block the cell cycle in G1/S phase.<sup>[114]</sup> Another reason for the cell cycle arrest in the presence of iron-chelating agents is their ability to modulate the expression of a number of cyclins and cyclin-dependent kinases, which are the main cell cycle regulators.<sup>[115]</sup> Hence, the high biosimilarity within this large cluster of diverse annotated reference compounds could be based on a shared MoA, i.e., cell cycle modulation, rather than a shared target.

### **6.1.3 Biological characterization of reference compounds biosimilar to DFO**

To investigate the bioactivity of the reference cluster that shared high biosimilarity with DFO and, hence, to confirm the hypothesis of a shared MoA linked to cell cycle modulation, a representative selection of references was subjected to further biological characterization.

Real-time live-cell imaging at different compound concentrations was performed to monitor cytotoxicity and the influence of the selected references on the growth behavior of U-2OS cells. To determine the ability of the references to chelate iron, the colorimetric reagent ferrozine was used. Ferrozine binds ferrous iron<sup>[100]</sup> and a restricted complex formation, i.e., a decreased absorbance after compound addition is indicative of iron chelation by the tested compounds. Furthermore, to analyze the influence of the references on cell cycle modulation, the nucleoside analog EdU (5-ethynyl-2'-deoxyuridine) was used as cells incorporate EdU into their DNA during S phase.<sup>[97]</sup> Additional staining of cells with propidium iodide (PI) allows the investigation of a compounds' influence on the DNA content.

DFO was subjected to these three experiments (Figure 13), thus serving as a control for the reference cluster.

## RESULTS

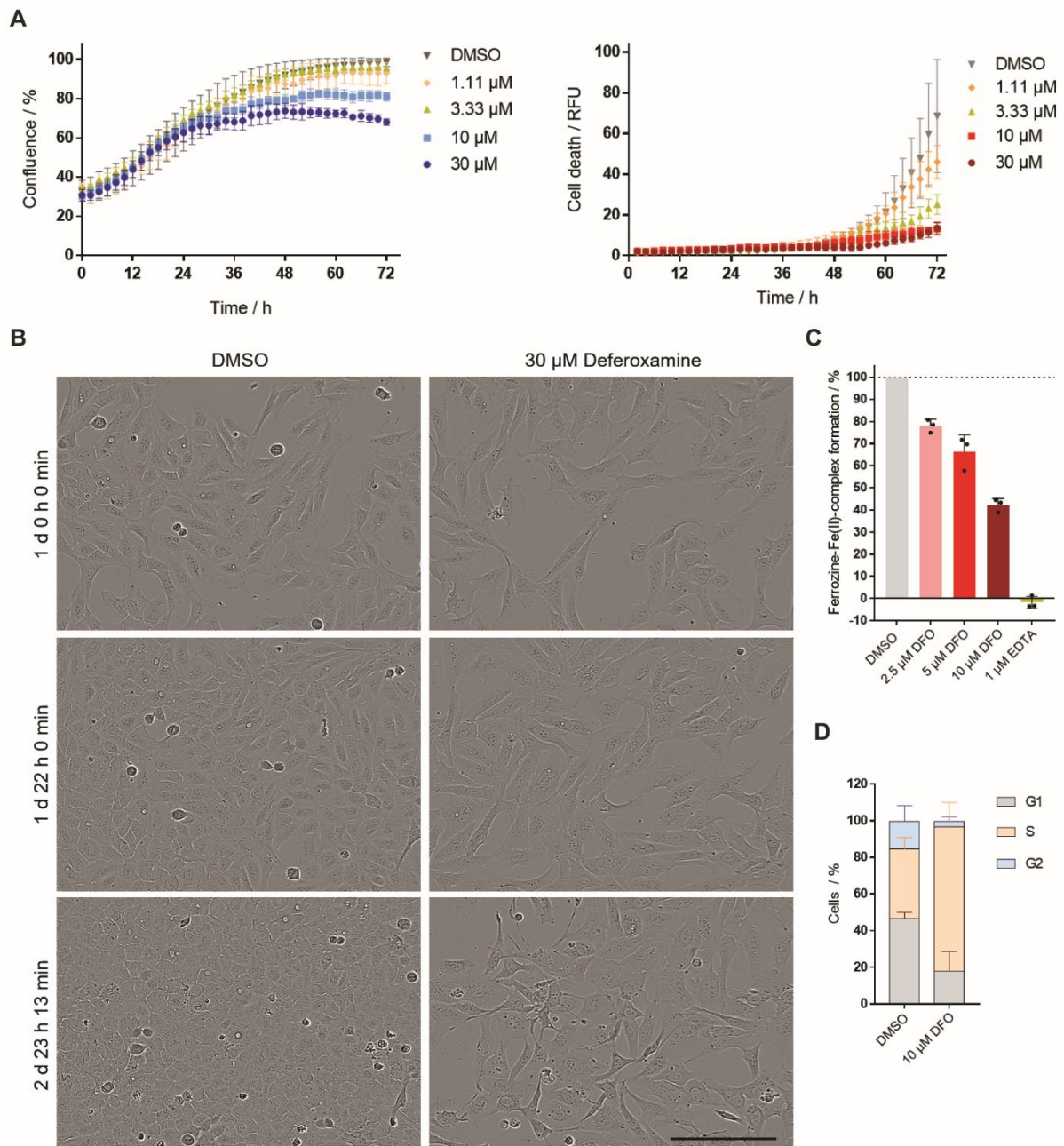


**Figure 13: Influence of DFO on cell growth, iron chelation and cell cycle.**

(A) Influence of DFO on the growth behavior. U-2OS cells were incubated for 72 h with DFO or DMSO as control at indicated concentrations in the presence of propidium iodide (PI) to detect dead cells. Images were acquired in a 2-hour interval using the IncuCyte S3 imaging system. Image-based analysis was used to quantify cell growth through cell confluence as a readout, or dead cells through PI fluorescence. Data (mean values  $\pm$  SD of N=3) are representative of three independent replicates. (B) Representative images from the live-cell imaging using the IncuCyte S3. U-2OS cells were treated with 30  $\mu$ M DFO or DMSO as a control after indicated time points. Scale bar: 200  $\mu$ m. (C) Iron chelation by DFO or EDTA as control at indicated concentrations determined by interference with ferrozine-Fe(II)-complex formation. Data shown are mean values  $\pm$  SD of three independent experiments. (D) Influence of DFO on the cell cycle. U-2OS cells were treated with DFO or DMSO as a control for 22 h and subsequently pulsed for 2 h with 10  $\mu$ M EdU (5-ethynyl-2'-deoxyuridine) prior to fixation and staining of DNA with PI. The number of cells in G1, S and G2 phase was determined by means of flow cytometry. Data shown are mean values  $\pm$  SD of three independent experiments. The percentage values of cells in the G1 (DNA content of 2N), S (2N-4N) and G2 phase (4N) of the cell cycle are shown in the appendix (Table 12).

## RESULTS

---

Figure 13A illustrates that DFO dose-dependently restricted the growth of U-2OS cells after 24 h of treatment. At the highest concentration of 30  $\mu\text{M}$  and after 72 h of compound incubation, the cell confluence was at 68 %, which corresponds to a reduction of approx. 30 % compared to the DMSO control. However, this degree of confluence was already reached after 24 h (62 % confluence) indicating either a cytotoxic or cytostatic effect. The PI staining revealed that the growth reduction was not a result of cytotoxicity as the PI fluorescence of cells treated with DFO was decreasing in a concentration-depend manner compared to the DMSO control. Cells that were treated with DMSO reached 100 % confluence after three days and the number of dead cells was increasing within the last twenty hours as space and nutrients became increasingly limited. The restricted growth paired with the low number of dead cells was not only suggesting a cytostatic effect for DFO but also the phenotypic appearance was pointing towards a cell cycle arrest. Images taken from cells treated with DMSO after one, two and three days of treatment exhibited a small proportion of round cells, which is normal under physiological conditions and indicative for cells that reside in mitosis (Figure 13B). However, images of cells treated with 30  $\mu\text{M}$  DFO from the same time points showed, if at all, a far lower number of round cells, pointing towards a cell cycle arrest in either G1, S or G2 phase of the cell cycle. In addition, the cell shape changed upon treatment with 30  $\mu\text{M}$  DFO. The cells were shaped homogenously after 24 h, whereas a substantial number of cells were smaller and more elongated after 72 h of treatment. As expected for an iron-chelating agent, DFO dose-dependently decreased the formation of the ferrozine-Fe(II)-complex (Figure 13C). The cell cycle analysis (Figure 13D) revealed that DFO treatment led to a strong enrichment of cells in S phase, thus, confirming reported literature references and is in line with the growth reduction observed in the live-cell imaging experiment (Figure 13A, B).

The four nucleoside analogs Trifluridine<sup>[116]</sup>, Arabinocytidine<sup>[117]</sup>, Cladribine<sup>[118]</sup> and Fludarabine<sup>[118]</sup>, depicted in Figure 14A, were explored for their influence on cell viability and growth, their ability to chelate iron and their influence on the cell cycle.

## RESULTS

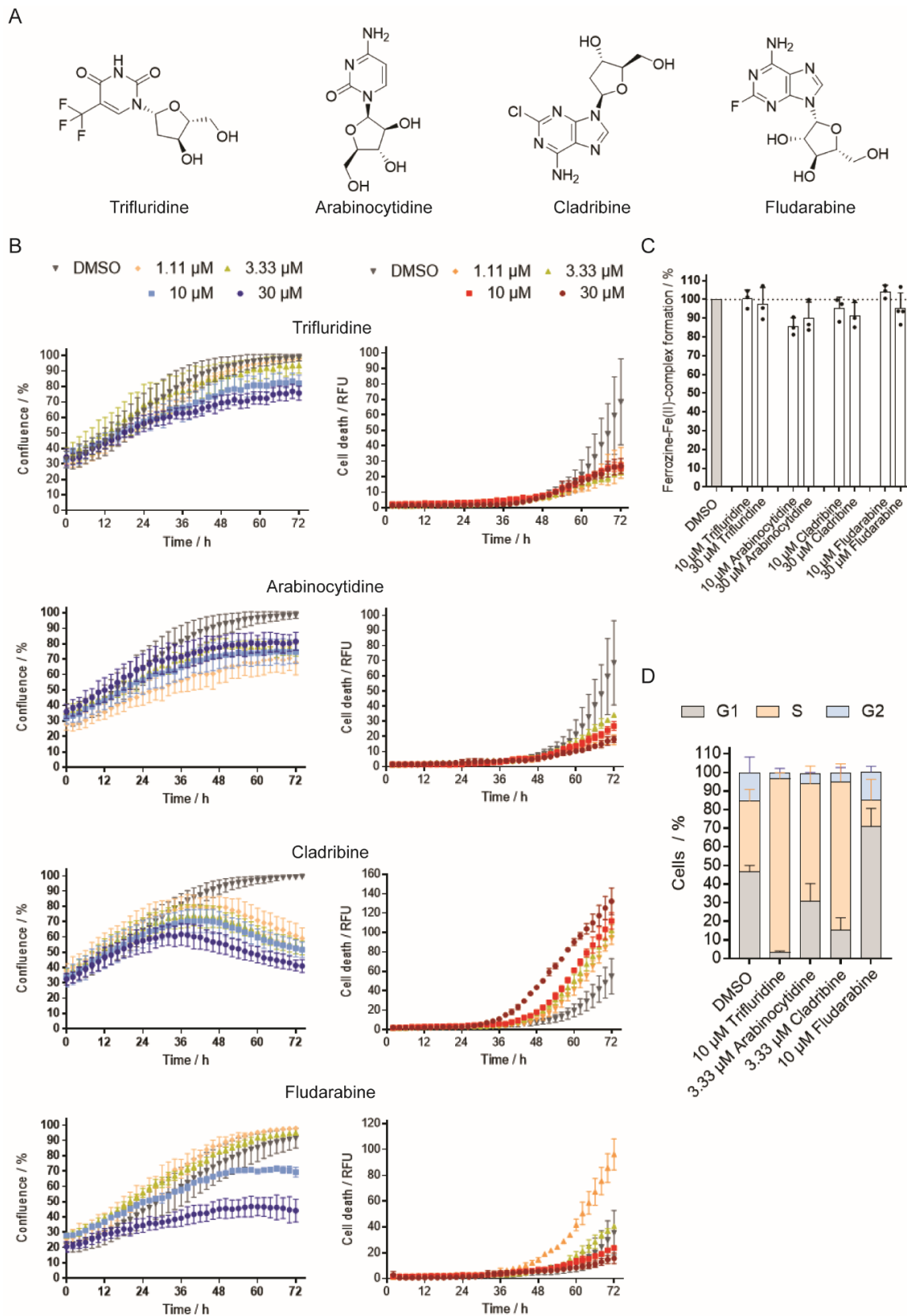


**Figure 14: Influence of selected nucleoside analogs on cell growth, iron chelation and cell cycle.**

(A) Chemical structures of nucleoside analogs. (B) Influence of selected nucleoside analogs on the growth behaviour of U-2OS cells. Cells were incubated for 72 h with compounds or DMSO as a control at indicated concentrations in the presence of propidium iodide (PI) to detect dead cells. Images were

## RESULTS

---

acquired every two hours using the IncuCyte S3 imaging system. Image-based analysis was used to quantify cell growth through cell confluence as a readout, or dead cells through PI fluorescence. Data (mean values  $\pm$  SD of N=3) are representative of three independent replicates. (C) Iron chelation by the compounds at indicated concentrations determined by interference with ferrozine-Fe(II)-complex formation. Data shown are mean values  $\pm$  SD of three independent experiments. (D) Influence of selected nucleoside analogs on the cell cycle. U-2OS cells were treated with the compounds or DMSO as a control for 22 h and subsequently pulsed for 2 h with 10  $\mu$ M EdU (5-ethynyl-2'-deoxyuridine) prior to fixation and staining of DNA with PI. The number of cells in G1, S and G2 phase was determined by means of flow cytometry. Data shown are mean values  $\pm$  SD of three independent experiments. The numerical percentage values of cells in the G1 (DNA content of 2N), S (2N-4N) and G2 phase (4N) of the cell cycle can be reviewed in the appendix (Table 12).

Trifluridine reduced the growth of U-2OS cells after 24 h of treatment by 20 and 25 % at concentrations of 10 and 30  $\mu$ M, respectively (Figure 14B). Like DFO, the restricted growth was a result of a cytostatic effect rather than cytotoxicity as the number of dead cells was lower compared to cells treated with DMSO. Arabinocytidine reduced cell growth after 24 h of treatment by approx. 20 % at all four measured concentrations without cytotoxic effects. Cladribine decreased cell growth by approx. 50 % at all measured concentrations, as already implied by the bell-shaped confluence curve. It was also cytotoxic after 36 hours of treatment. Fludarabine led to a growth reduction by approx. 50 % at 30  $\mu$ M and by approx. 20 % at 10  $\mu$ M after 72 h of treatment without showing cytotoxic effects. At the lower concentrations of 1.11 and 3.33  $\mu$ M, Fludarabine did not reduce cell growth. As expected, none of the four nucleoside analogs showed iron-chelating properties (Figure 14C) but all of them induced cell cycle arrest (Figure 14D). Trifluridine, Arabinocytidine and Cladribine, like DFO, caused a strong enrichment of cells in S phase, whereas Fludarabine increased the number of cells in G1 phase.

Two CDK inhibitors PHA-793887<sup>[119]</sup> and roscovitine<sup>[120]</sup> and the topoisomerase I inhibitor Topotecan<sup>[121]</sup> were tested for their influence on cell growth, iron chelation and cell cycle modulation (Figure 15).

## RESULTS

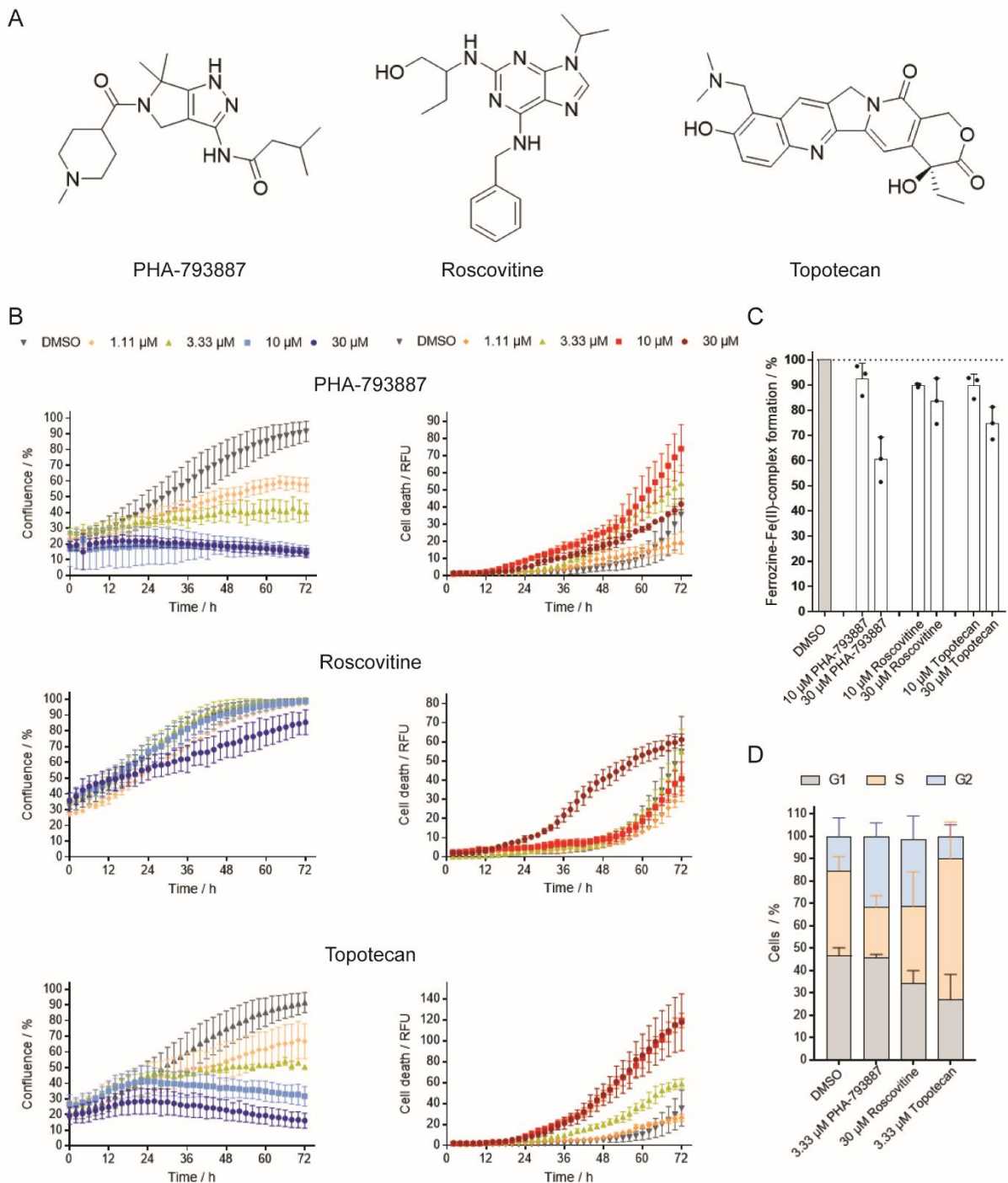


**Figure 15: Influence of PHA-793887, roscovitine and Topotecan on cell growth, iron chelation and cell cycle.**

(A) Chemical structures of PHA-793887, roscovitine and Topotecan. (B) Influence on the growth behavior of U-2OS cells. Cells were incubated for 72 h with compounds or DMSO as a control at the indicated concentrations in the presence of propidium iodide (PI) to detect dead cells. Images were acquired every two hours using the IncuCyte S3 imaging system. Image-based analysis was used to quantify cell growth through cell confluence as readout, or dead cells through PI fluorescence. Data (mean values  $\pm$  SD of N=3) are representative of three independent replicates. (C) Iron chelation by the compounds at the indicated concentrations determined by interference with ferrozine-Fe(II)-complex formation. Data shown are mean values  $\pm$  SD of three independent experiments. (D) Influence of the references on the cell cycle. U-2OS cells were treated with the compounds or DMSO as a control for 22 h and afterwards pulsed for another 2 h with 10  $\mu$ M EdU (5-ethynyl-2'-deoxyuridine) prior to fixation

## RESULTS

---

and staining of DNA with PI. The number of cells in S phase was determined by means of flow cytometry. Data shown are mean values  $\pm$  SD of three independent experiments. The numerical percentage values of cells in the G1 (DNA content of 2N), S (2N-4N) and G2 phase (4N) of the cell cycle can be reviewed in the appendix (Table 12).

Treatment of U-2OS cells with PHA-793887 and Topotecan resulted in a concentration-dependent growth reduction and cytotoxicity at concentrations  $\geq$  3.33  $\mu$ M after 24 h of treatment (Figure 15B). Even the lowest concentration of 1.11  $\mu$ M reduced cell growth by approx. 30 %, however, without cytotoxic influence. Roscovitine only led to a minor growth reduction at 30  $\mu$ M of approx. 15 %, however, increased the number of dead cells. Iron chelating properties of the CDK inhibitor PHA-793887 are not reported in the literature, but 30  $\mu$ M PHA-793887 reduced the ferrozine-Fe(II)-complex formation by approx. 40 % (Figure 15C). The EdU pulse-chase assay for PHA793887 was performed at 3.33  $\mu$ M and showed enrichment in cells that reside in the G2 phase of the cell cycle (Figure 15D). As PHA-793887 did not possess iron-chelating properties at 10  $\mu$ M, the G2 phase arrest was therefore most likely not a result of the iron-chelating ability. Roscovitine and Topotecan did not influence the ferrozine-Fe(II)-complex formation, neither at 10 nor at 30  $\mu$ M, but both led to cell cycle arrest. Alike the CDK inhibitor PHA-793887, roscovitine-treatment enriched the cells in the G2 phase, whereas Topotecan led to an S phase arrest. In general, an increase in the number of cells with a double amount of DNA (4N) can emerge from cytokinesis failure or a cell cycle arrest in the G2 or M phase. However, time-resolved live-cell imaging (representative images are shown in Figure 16) did not reveal an accumulation of round cells, which would be an indication of a mitotic arrest or failed cytokinesis. Moreover, the accumulation of round cells, i.e., a shrinkage in cell size, would also lead to a drop in cell confluence as it represents the growth area of the well, which is covered by the cells. Therefore, the increase in 4N after treatment with the two CDK inhibitors is most likely attributed to a cell cycle arrest in G2 phase.

## RESULTS

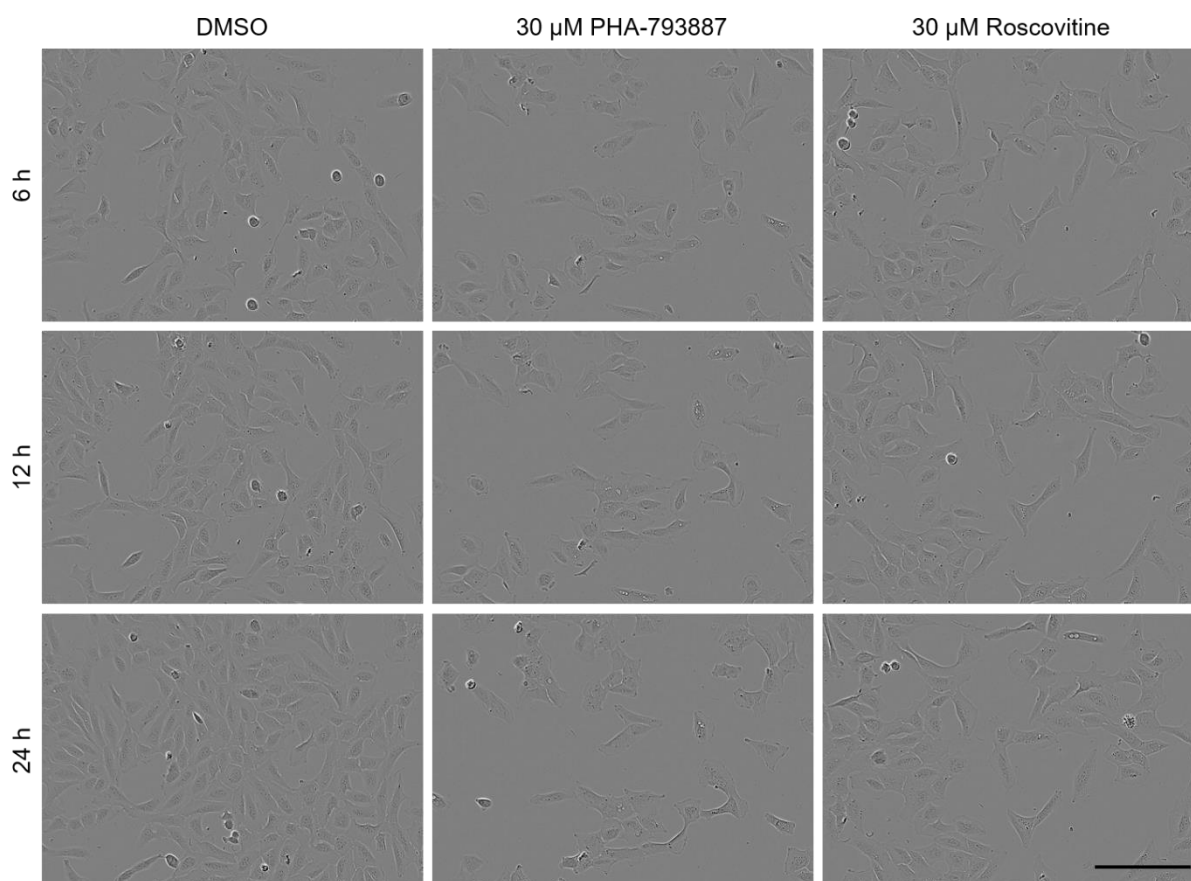


**Figure 16: Images of U-2OS cells treated with PHA-793887 and roscovitine.**

Representative images from live-cell imaging using the IncuCyte S3. U-2OS cells were treated with 30  $\mu\text{M}$  of the compounds of DMSO as a control. Images at the indicated time points after compound addition are shown. Scale bar: 200  $\mu\text{m}$ .

The last group of tested references contained the iron chelator Ciclopirox<sup>[106]</sup> and the two DNA intercalating agents resveratrol<sup>[122]</sup> and Doxorubicin<sup>[123]</sup> (Figure 17). Similar to DFO, Ciclopirox reduced the growth of U-2OS cells in a dose-dependent manner without exhibiting cytotoxic effects (Figure 17B). Resveratrol at 30  $\mu\text{M}$  only slightly reduced cell growth by approx. 17 % and to an even lesser extent at 10  $\mu\text{M}$  and was not cytotoxic. Doxorubicin already induced cell death at 3.33  $\mu\text{M}$  within the first 24 h of treatment. Also, a concentration of 1.11  $\mu\text{M}$  was cytotoxic, however, only after 24 h of treatment. The lower concentrations of 0.37  $\mu\text{M}$  and 0.12  $\mu\text{M}$  were not cytotoxic but reduced cell growth by approx. 40 and 20 %, respectively.



## RESULTS

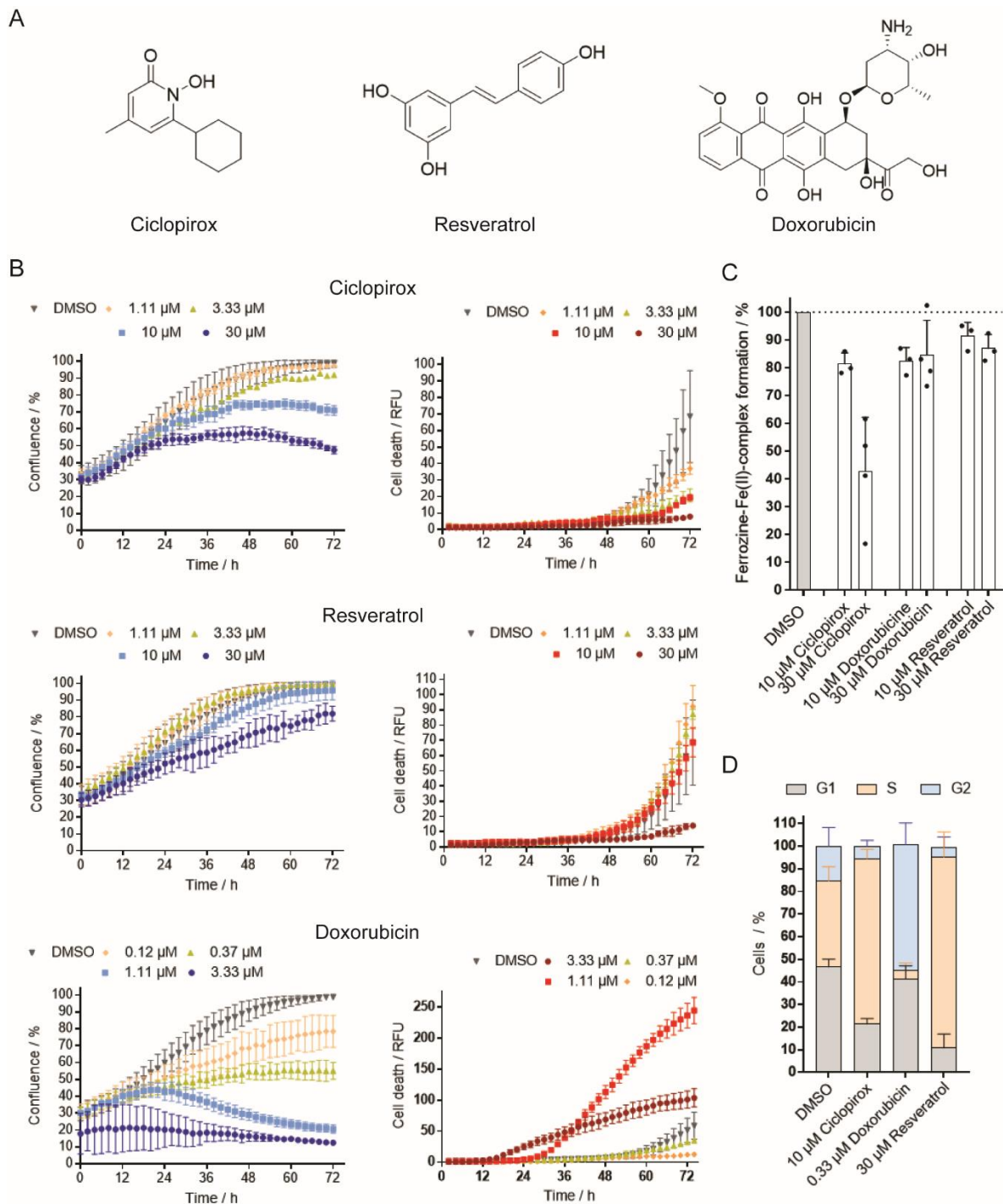


**Figure 17: Influence of Ciclopirox, resveratrol and Doxorubicin on cell growth, iron chelation and cell cycle.**

(A) Chemical structures of selected references. (B) Influence on the growth behavior of U-2OS cells. Cells were incubated for 72 h with compounds or DMSO as control at indicated concentrations in the presence of propidium iodide (PI) to detect dead cells. Images were acquired every two hours using the IncuCyte S3 imaging system. Image-based analysis was used to quantify cell growth through cell confluence as readout, or dead cells through PI fluorescence. Data (mean values  $\pm$  SD of N=3) are representative of three independent replicates. (C) Iron chelation by compounds at indicated concentrations determined by interference with ferrozine-Fe(II)-complex formation. Data shown are mean values  $\pm$  SD of three independent experiments. (D) Influence of selected references on the cell cycle. U-2OS cells were treated with compound or DMSO as a control for 22 h and subsequently pulsed

## RESULTS

for 2 h with 10  $\mu\text{M}$  EdU (5-ethynyl-2'-deoxyuridine) prior to fixation and staining of DNA with PI. The number of cells in G1, S and G2 phase was determined by means of flow cytometry. Data shown are mean values  $\pm$  SD of three independent experiments. The numerical percentage values of cells in the G1 (DNA content of 2N), S (2N-4N) and G2 phase (4N) of the cell cycle can be reviewed in the appendix (Table 12).

As expected, 30  $\mu\text{M}$  Ciclopirox inhibited the ferrozine-Fe(II)-complex formation by approx. 60 %; which is in line with the reported iron chelation. No iron complexing ability was detected for the two DNA intercalating agents resveratrol and Doxorubicin (Figure 17C). As anticipated all three compounds modulated the cell cycle (Figure 17D). Ciclopirox and resveratrol strongly enriched the cells in S phase whereas Doxorubicin led to an accumulation of cells in the G2 phase. As previously mentioned, an increase in the number of cells with a double amount of DNA (4N) can emerge from cytokinesis failure or a cell cycle arrest in the G2 or M phase

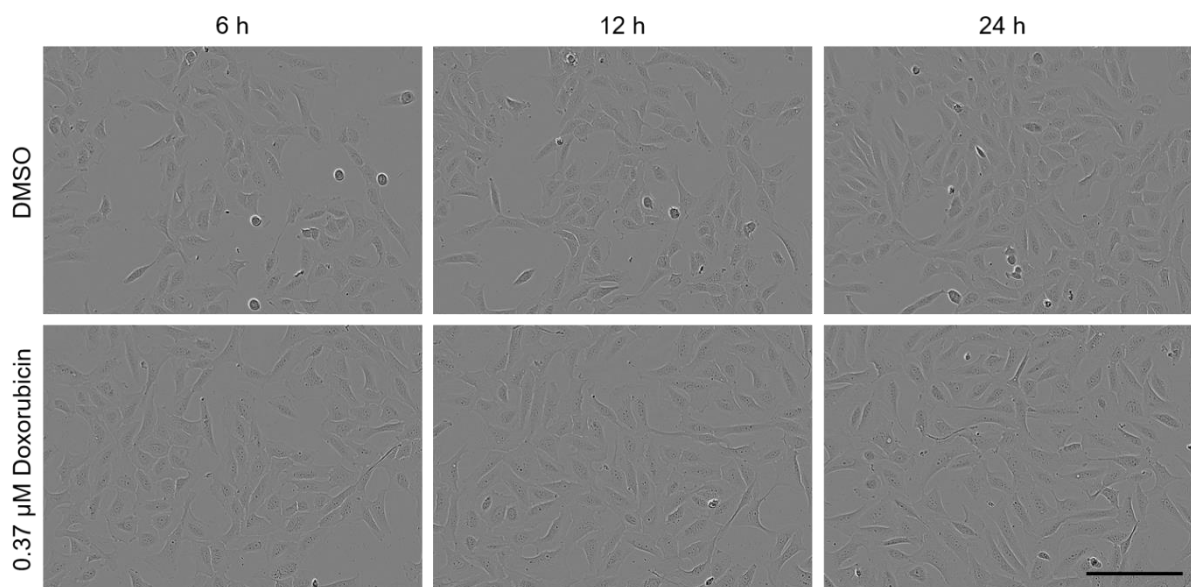


**Figure 18: Images of U-2OS cells treated with 0.37  $\mu\text{M}$  Doxorubicin.**

Representative images from live-cell imaging using the IncuCyte S3. U-2OS cells were treated with 0.37  $\mu\text{M}$  Doxorubicin or DMSO as a control. Images at the indicated time points after compound addition are shown. Scale bar: 200  $\mu\text{m}$ .

Time-resolved live-cell imaging of Doxorubicin-treated cells did not reveal accumulation of round cells or failed cytokinesis, hence, G2 phase arrest can be assumed (Figure 18).

Collectively, the results confirmed the hypothesis that the cluster of references (Figure 12) with diverse annotated activities but high biosimilarity to the iron chelator DFO shares a common MoA that is independent of chemical similarity or the cellular target. All selected references of the cluster led to an accumulation of cells in either the S or G2 phase.

## RESULTS

Besides the annotated iron chelator Ciclopirox, the CDK inhibitor PHA-793887 showed a weak iron-chelating ability at 30  $\mu\text{M}$ . The G2 arrest induced by PHA-793887 was however already detected at a concentration of 10  $\mu\text{M}$  and is, therefore, most likely not a result of iron chelation (Figure 15).

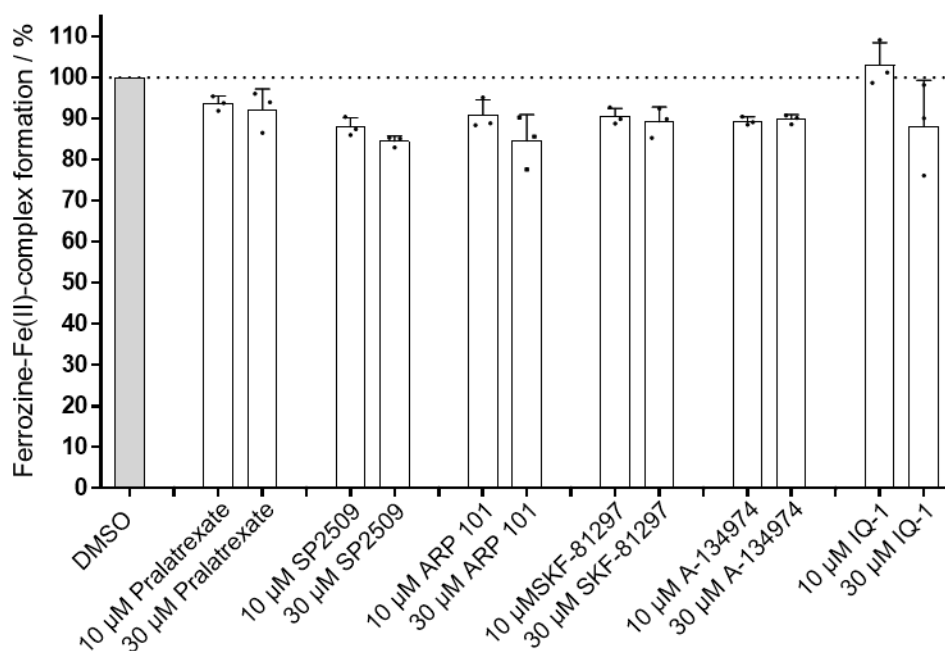


**Figure 19: Iron chelation by compounds with high biosimilarity to DFO.**

Iron chelation by reference compounds at indicated concentrations determined by ferrozine-Fe(II)-complex formation. Data shown are mean values  $\pm$  SD of three independent experiments.

The bioactivity of the antifolate Pralatrexate, the LSD1 inhibitor SP2509, the MMP-2 inhibitor ARP 101, the D1 dopamine receptor agonist ( $\pm$ )-SKF-81297, the adenosine kinase inhibitor A-134974 and the  $\beta$ -Catenin/p-300 signaling inhibitor IQ 1 is at first sight not directly related to the cell cycle. Therefore, those references were additionally tested for their ability to chelate iron. However, none of the references showed a restriction in the ferrozine-Fe(II)-complex formation (Figure 19).

### 6.1.4 Identification and biological evaluation of uncharacterized compounds biosimilar to DFO

Morphological fingerprint similarity based on a shared target or MoA is the requirement to use a cluster of references for bioactivity prediction. The common MoA of cell cycle arrest in G1, S or G2 phase was experimentally confirmed for the large cluster of references biosimilar to DFO (see 6.1.3). Therefore, the morphological fingerprint of DFO was used as a query profile to search for uncharacterized biosimilar compounds within the in-house library of 9619 novel and structurally diverse natural product-inspired compounds<sup>[124, 125]</sup> or pseudo-natural products<sup>[126]</sup>.

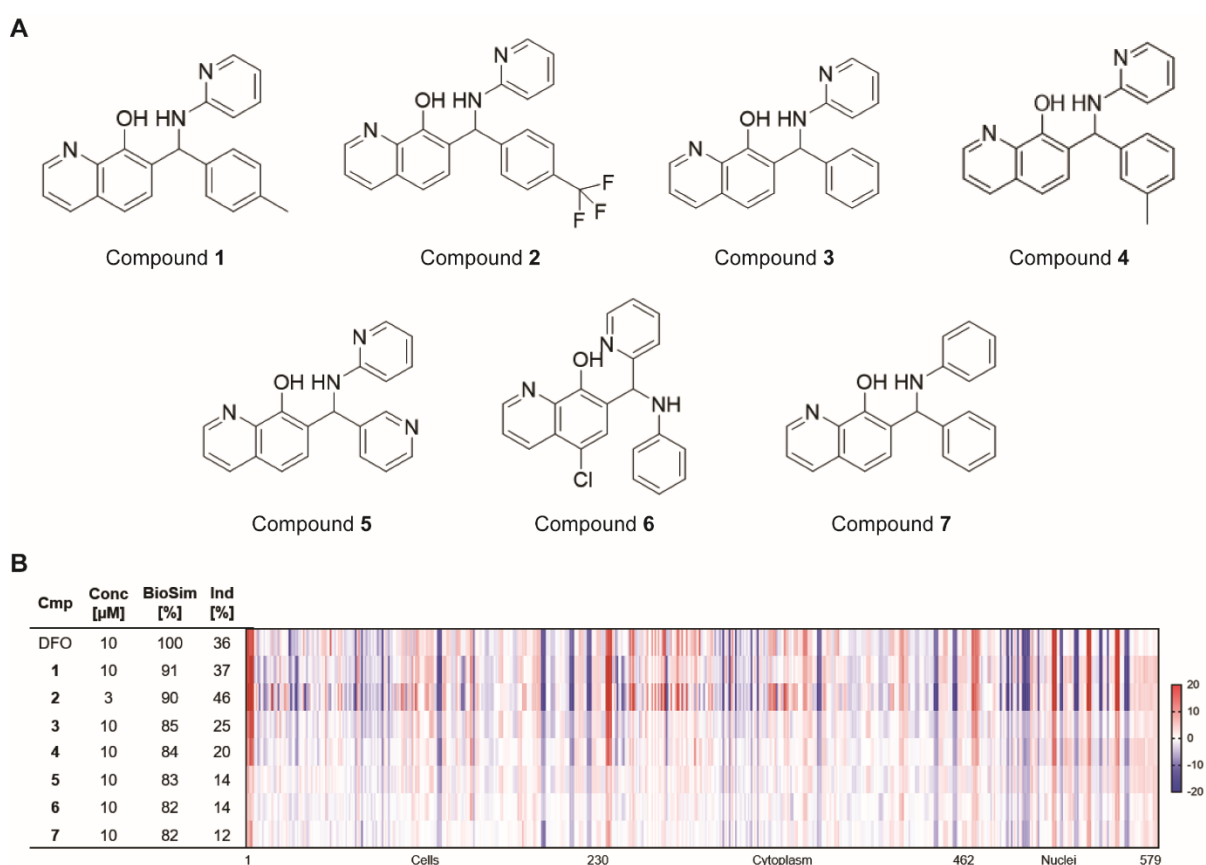


**Figure 20: Morphological profiling of 8-hydroxyquinoline derivatives 1-7 with high biosimilarity to DFO.**

(A) Chemical structures of compounds (cmp) 1-7. (B) Morphological fingerprints of 8-hydroxyquinolines at indicated concentrations (Conc) visualized as line plots and heatmap profiles. The fingerprint of DFO is set as a reference (100 % biosimilarity, BioSim) to which the following fingerprints are compared. The set of 579 features is divided into cell (1-229), cytoplasm (230-461) and nuclei (462-579) related features. Values were normalized to the DMSO control. Blue: decreased feature, red: increased feature. Conc: concentration. Ind: induction.

## RESULTS

---

Several derivatives of 8-hydroxyquinoline, which is a known motif for a metal-chelating ligand<sup>[102, 127]</sup>, displayed high biosimilarity ( $\geq 82\%$ ) to the morphological fingerprint of 10  $\mu\text{M}$  DFO (Figure 20A, B). Compound **1-3**, whose induction values (37, 46 and 25 %, respectively) were within the same induction range as 10  $\mu\text{M}$  DFO (approx.  $\pm 10$ ), were also the top three biosimilar compounds.

## RESULTS

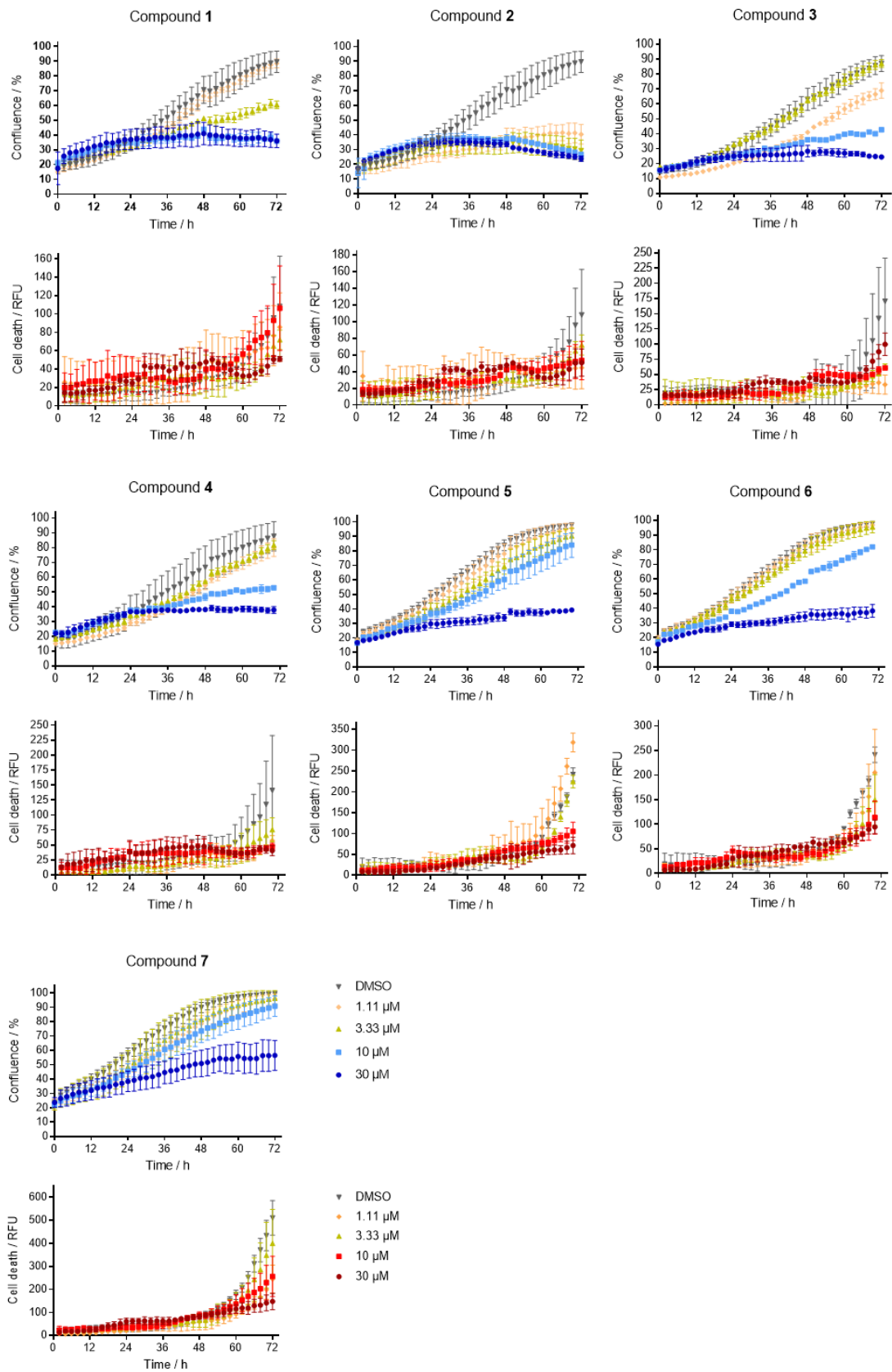


**Figure 21: Influence of compounds 1-7 on cell growth.**

U-2OS were incubated for 72 h with the compounds or DMSO as a control at the indicated concentrations in the presence of PI to detect dead cells. Images were acquired in a 2-hour interval

## RESULTS

using the IncuCyte S3 imaging system. Image-based analysis was used to quantify cell growth through cell confluence as readout, or dead cells through PI fluorescence. Data (mean values  $\pm$  SD of N=3) are representative of three independent replicates.

Live-cell imaging of compounds **1-7** (Figure 21) revealed a strong reduction in cell growth at 30  $\mu$ M after 24 h of treatment. However, no cell death was detected, indicating that the compounds induce cell cycle arrest. Cells treated with a dose of 10  $\mu$ M also affected the cell growth and thereby reflecting the trend in induction (Figure 20). Compounds **1-4** that possessed the highest induction of  $\geq 20\%$  also showed the strongest inhibition in cell growth. Whereas no changes were observed for any of the compounds at the lowest concentration of 1.11  $\mu$ M compared to the DMSO control, compound **1** and **2** suppressed cell growth at 3.33  $\mu$ M. The confluence of cells treated with 1.11  $\mu$ M compound **3** and **4** was lower than DMSO, however, this effect most likely originated from an initial deviation in the seeding density and not from an inhibited cell growth.

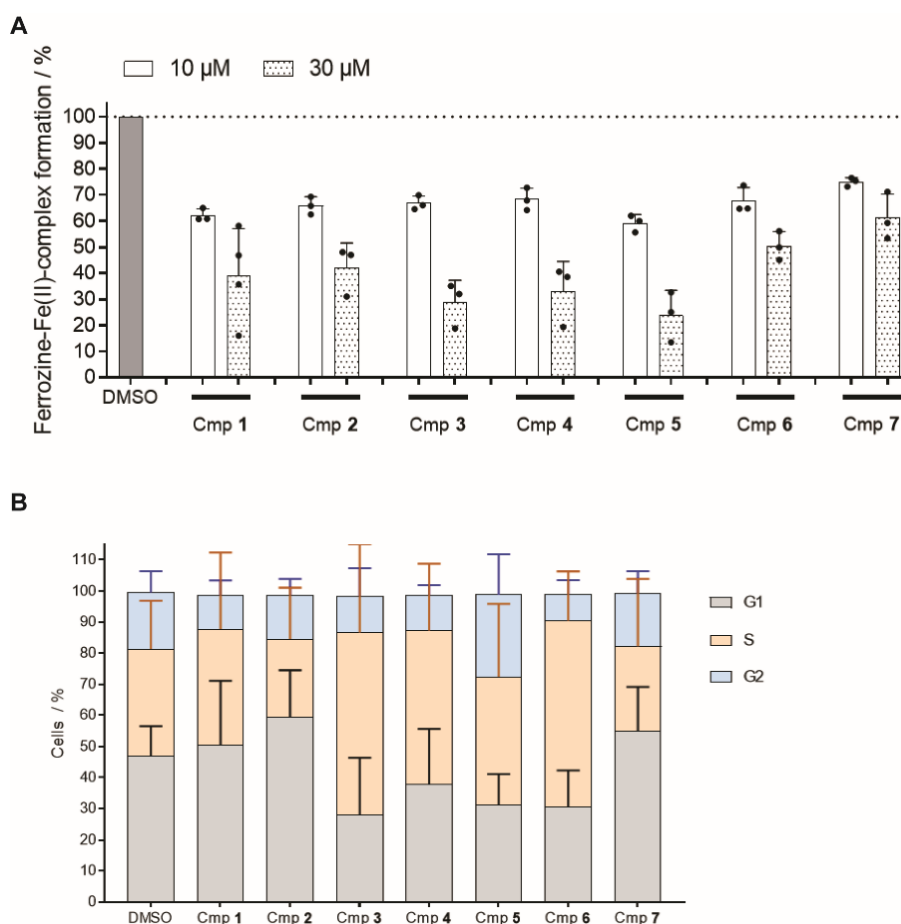


**Figure 22: Influence of compounds 1-7 on iron chelation and cell cycle.**

(A) Iron chelation by compounds (cmp) **1-7** at indicated concentrations determined by interference with ferrozine-Fe(II)-complex formation. Data shown are mean values  $\pm$  SD of three independent

## RESULTS

experiments. (B) Influence of 10  $\mu\text{M}$  compounds **1-7** on the cell cycle. U-2OS cells were treated with the compounds or DMSO as a control for 22 h and afterwards pulsed for another 2 h with 10  $\mu\text{M}$  EdU (5-ethynyl-2'-deoxyuridine) prior to fixation and staining of DNA with PI. The number of cells in S phase was determined by means of flow cytometry. Data shown are mean values  $\pm$  SD of three independent experiments. The numerical percentage values of cells in the G1 (DNA content of 2N), S (2N-4N) and G2 phase (4N) of the cell cycle can be reviewed in the appendix (Table 13).

As expected for an annotated iron-chelating scaffold, all 8-hydroxyquinoline derivatives **1-7** restricted the ferrozine-Fe(II)-complex formation exhibiting iron-chelating abilities (Figure 22A). Whereas only a minor influence was observed at 10  $\mu\text{M}$  (approx. 30 % reduction), all compounds, except for compound **7**, reduced the complex formation to more than 50 % at 30  $\mu\text{M}$ . The EdU pulse-chase assay revealed that 10  $\mu\text{M}$  compound **1**, **3-5** and **6** led to an accumulation of cells in S phase. However, the effect of compound **1** and **5** was only weak. Compound **2** and **7** induced a cell cycle arrest in the G1 phase (Figure 22B).

In addition, the macrocycle **8**<sup>[128]</sup> and the natural product-inspired<sup>[126]</sup> compound **9** exhibited high biosimilarity ( $\geq 80$  %) to the morphological fingerprint of 3  $\mu\text{M}$  DFO with induction values of 41 and 45 %, respectively (Figure 23A, B).

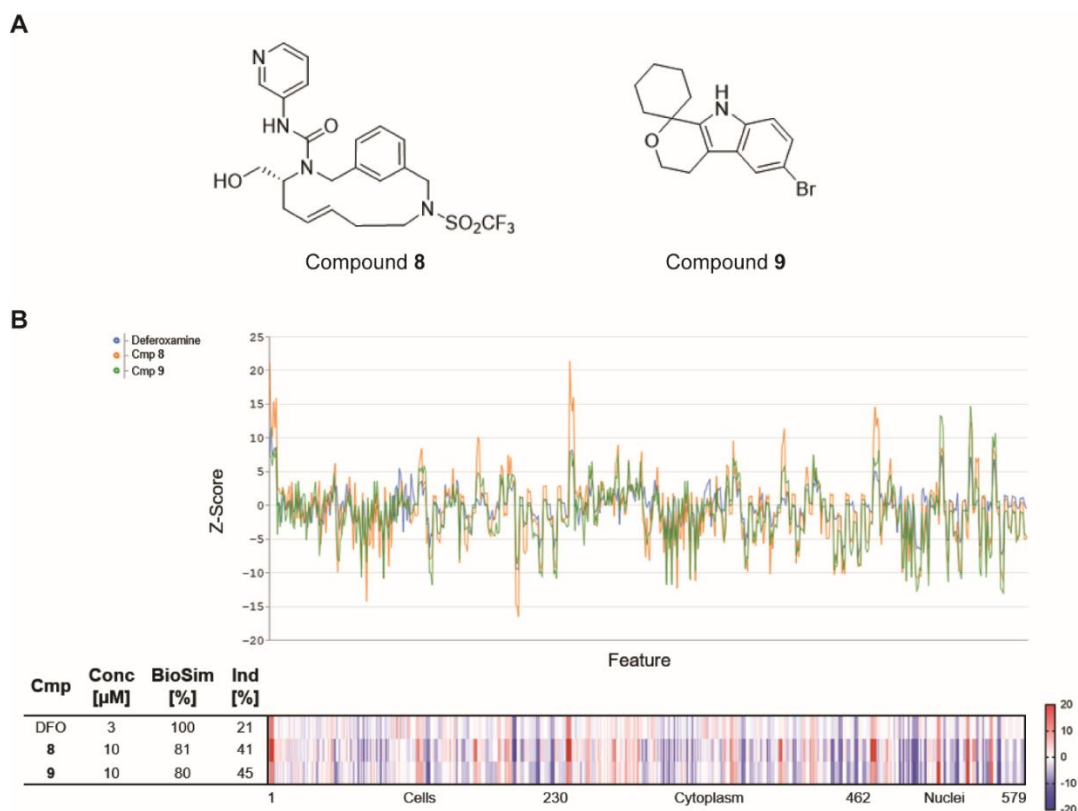


**Figure 23: Morphological profiling of compounds **8** and **9** with high biosimilarity to DFO.**

(A) Chemical structures of compounds (cmp) **8** and **9**. (B) Morphological fingerprints of compounds **8** and **9** visualized as line plots and heatmap profiles. The fingerprint of DFO is set as a reference (100



## RESULTS

---

% biosimilarity, BioSim) to which the following fingerprints are compared. The set of 579 features is divided into cell (1-229), cytoplasm (230-461) and nuclei (462-579) related features. Values were normalized to the DMSO control. Blue: decreased feature, red: increased feature. Conc: concentration. Ind: induction.

The exploration of the phenotype induced by compounds **8** and **9** revealed that both compounds restricted cell growth at 30  $\mu\text{M}$  (Figure 24A). Compound **8** suppressed cell growth by approx. 60 % at 30  $\mu\text{M}$  and compound **9** only by approx. 30 %. The PI staining revealed toxic effects for both small molecules. Whereas the cytotoxicity by compound **8** appeared only after 24 h of treatment at concentrations  $\geq 3.33 \mu\text{M}$ , compound **9** increased the number of dead cells within the first four hours of treatment but remained constant over the whole 72 h of treatment.

## RESULTS

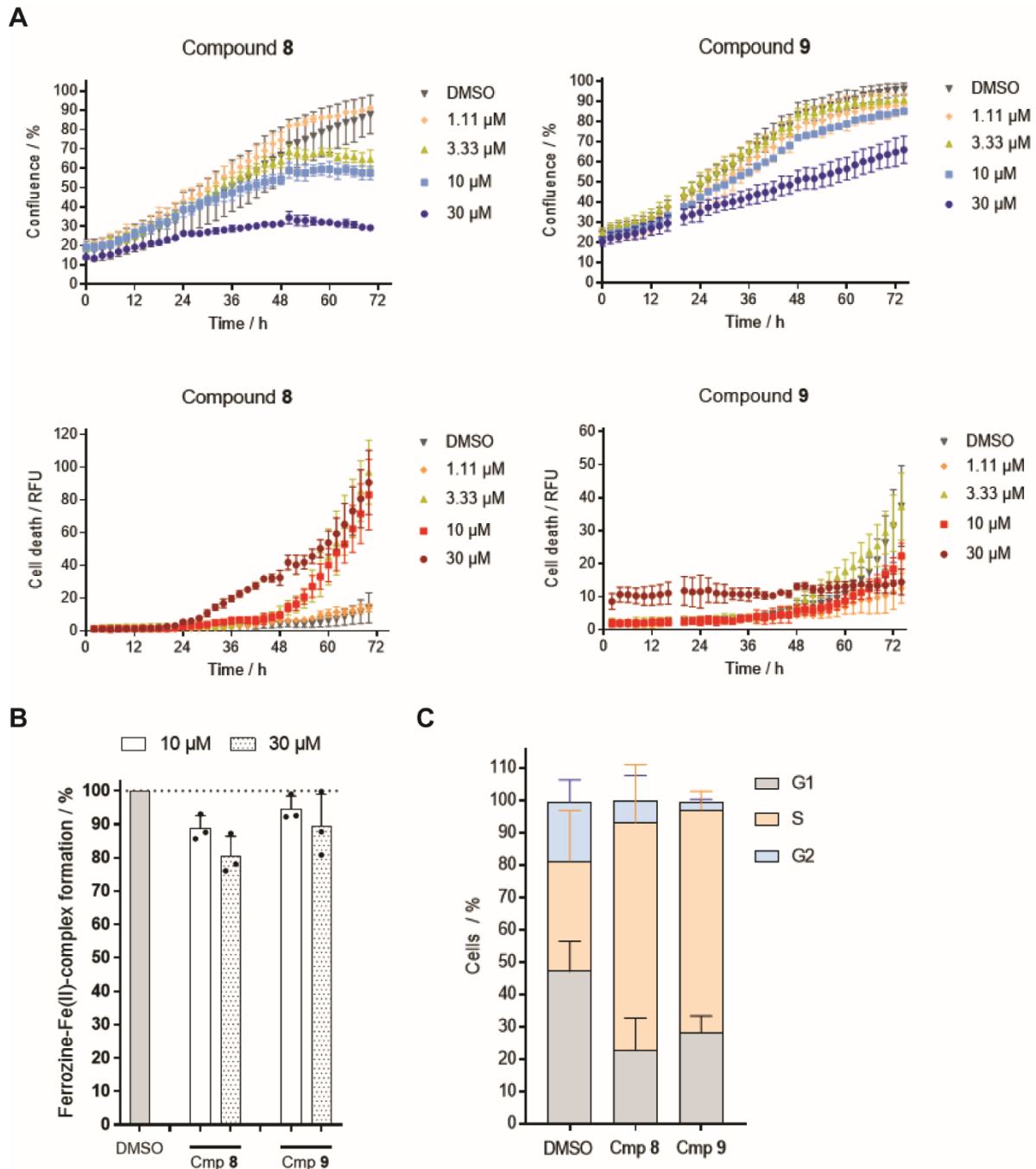


**Figure 24: Influence of compounds 8 and 9 on cell growth, iron chelation and cell cycle.**

(A) Influence on the growth behavior of U-2OS cells. Cells were incubated for 72 h with the compounds or DMSO as a control at the indicated concentrations in the presence of propidium iodide (PI) to detect dead cells. Images were acquired every two hours using the IncuCyte S3 imaging system. Image-based analysis was used to quantify cell growth through cell confluence as readout, or dead cells through PI fluorescence. Data (mean values  $\pm$  SD of N=3) are representative of three independent replicates. (B) Iron chelation by the compounds at the indicated concentrations determined by interference with ferrozine-Fe(II)-complex formation. Data shown are mean values  $\pm$  SD of three independent experiments. (C) Influence of compounds 8 and 9 on the cell cycle. U-2OS cells were treated with the compounds or DMSO as a control for 22 h and subsequently pulsed for 2 h with 10  $\mu$ M EdU (5-ethynyl-2'-deoxyuridine) prior to fixation and staining of DNA with PI. The number of cells in G1, S and G2 phase was determined by means of flow cytometry. Data shown are mean values  $\pm$  SD of three

## RESULTS

independent experiments. The numerical percentage values of cells in the G1 (DNA content of 2N), S (2N-4N) and G2 phase (4N) of the cell cycle can be reviewed in the appendix (Table 13).

Figure 24B and C illustrate that neither compound **8** nor **9** displayed an iron-chelating ability but both of them led to an accumulation of cells in S phase that was twice as high as compared to the DMSO control.

Collectively, these findings demonstrate that the cluster of references around the iron chelator DFO enables the identification of new iron complexing small molecules in particular and new modulators of the G1, S or G2 phase in general. Therefore, the cluster is hereinafter referred to as Fe/DNA synthesis cluster.

The cell cycle arrest induced by compounds **1-7** is most likely a result of their iron chelating activity. In contrast, the reason for the accumulation of cells in S phase induced by compounds **8** and **9** is unknown. To get a deeper insight into the possible mechanism of action, compounds **8** and **9** were investigated for their ability to bind DNA.

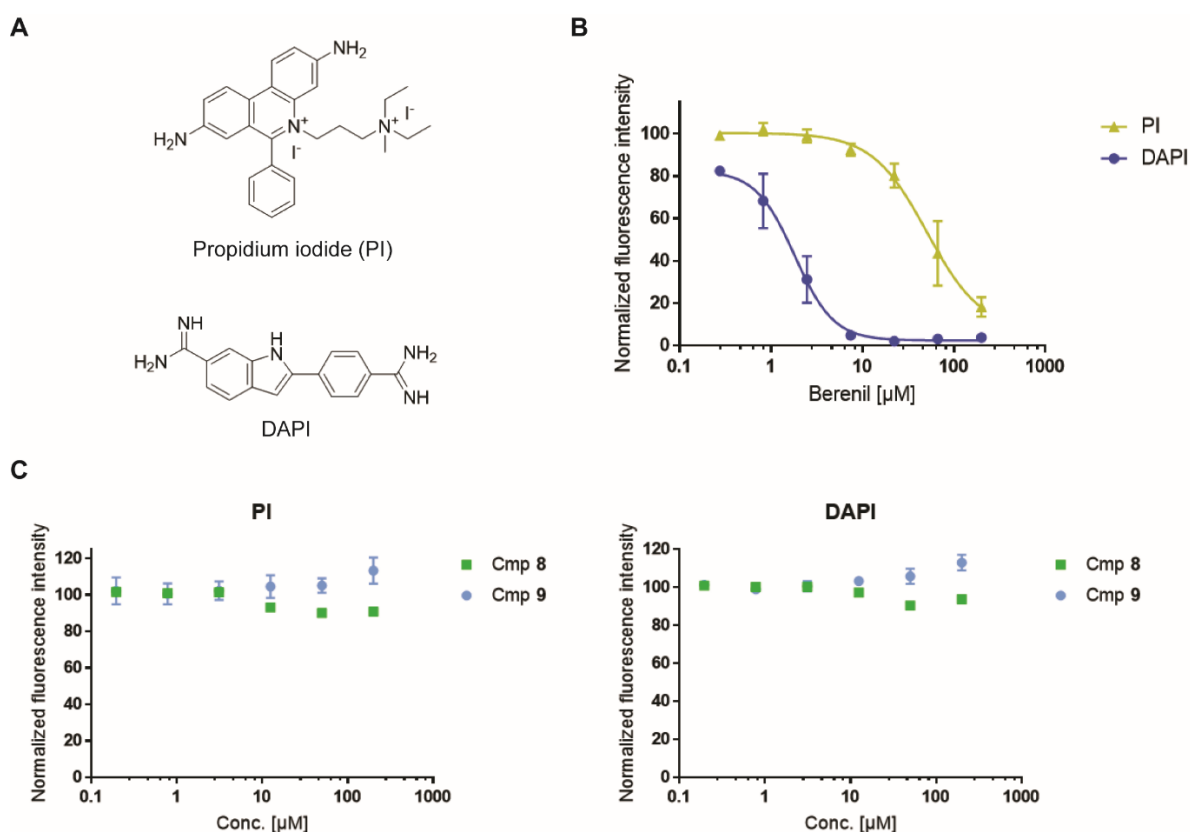


**Figure 25: DNA binding of compounds **8** and **9**.**

(A) Chemical structures of PI and DAPI. (B and C) Calf thymus DNA was incubated with the minor groove binder DAPI and the intercalator PI in the presence of the positive control Berenil (B) or compounds **8** and **9** (C).

## RESULTS

Two different binding modes were analyzed. Binding to the minor groove by DAPI, which increases its fluorescence or DNA intercalation by PI. Compounds with similar binding modes are expected to decrease DAPI- and/or PI-related fluorescence. Berenil, which was used as a control, displaced DAPI and less potently also PI. However, compounds **8** and **9** did neither displace the minor groove binder DAPI nor the DNA intercalator propidium iodide (Figure 25) and hence, do not bind to DNA. However, based on the annotated bioactivity of the references from the cluster, further mechanisms of action like topoisomerase or CDK inhibition are possible. Therefore, compounds **8** and **9** were further tested for modulation of topoisomerase I and II.

**Table 3: Inhibition of human topoisomerase I relaxation and topoisomerase II $\alpha$  decatenation by 30  $\mu$ M compounds **8** and **9**.**

Measurements were performed by Inspiralis. Data are mean values of two replicates.

| Topoisomerase I relaxation     |               | Topoisomerase II $\alpha$ decatenation |                   |
|--------------------------------|---------------|--|-------------------|
| Compound                       | % Relaxed DNA | Compound                               | % Decatenated DNA |
| Camptothecin, 10 $\mu$ M       | 97.72         | Etoposide, 10 $\mu$ M                  | 90.28             |
| Camptothecin, 30 $\mu$ M       | 94.24         | Etoposide, 30 $\mu$ M                  | 36.23             |
| Camptothecin, 50 $\mu$ M       | 78.25         | Etoposide, 50 $\mu$ M                  | 27.89             |
| Camptothecin, 100 $\mu$ M      | 41.42         | Etoposide, 100 $\mu$ M                 | 19.77             |
| Compound <b>8</b> , 30 $\mu$ M | 97.97         | Compound <b>8</b> , 30 $\mu$ M         | 99.70             |
| Compound <b>9</b> , 30 $\mu$ M | 98.89         | Compound <b>9</b> , 30 $\mu$ M         | 80.55             |

Compared to the known inhibitors camptothecin and etoposide, 30  $\mu$ M compound **8** and **9** did neither inhibit topoisomerase I induced relaxation of DNA nor topoisomerase II $\alpha$ -mediated DNA decatenation. Both small molecules displayed residual activity  $\geq 80$  % at 30  $\mu$ M in both assays (Table 3). For this reason, compounds **8** and **9** were further analyzed for their modulation of selected CDK/cyclin complexes (Table 4).

## RESULTS

**Table 4: Inhibition or binding of selected CDK/cyclin complexes by 30  $\mu$ M compounds 8 and 9.**

Measurements were performed by the SelectScreen Kinase Profiling Service of Life Technologies. Data are mean values of two technical replicates.

| Kinase         | % Inhibition compound 8  | % Inhibition compound 9  | [ATP] / $\mu$ M | Technology           |
|----------------|--------------------------|--------------------------|-----------------|----------------------|
| CDK4/cyclin D1 | 8                        | -11                      | 10              | Adapta               |
| CDK4/cyclin D3 | -11                      | -12                      | 10              | Adapta               |
| CDK6/cyclin D1 | -13                      | -3                       | 10              | Adapta               |
| CDK1/cyclin B  | 3.5                      | 1                        | Km app          | Z'Lyte               |
| CDK2/cyclin A  | 2                        | 0.5                      | Km app          | Z'Lyte               |
| Kinase         | % Replacement compound 8 | % Replacement compound 9 | [ATP] / $\mu$ M | Technology           |
| CDK2/cyclin A1 | 5.5                      | 4                        | -               | LanthaScreen Binding |
| CDK2/cyclin E1 | 5                        | 9                        | -               | LanthaScreen Binding |

The screening results depicted in Table 4 illustrate that both compounds did not inhibit the activity or bind to selected CDK/cyclin complexes *in vitro*.

### 6.1.5 Hierarchical clustering for mechanism of action deconvolution

Hierarchical clustering, performed by Dr. Axel Pahl (COMAS, Dortmund), was conducted to explore the applicability of the CPA to differentiate between the different mechanisms of action within the cluster of references biosimilar to DFO. Therefore, the reference compounds biosimilar to DFO as well as compound 4, representing the 8-hydroxyquinoline derivatives and compounds 8 and 9 were analyzed.

## RESULTS

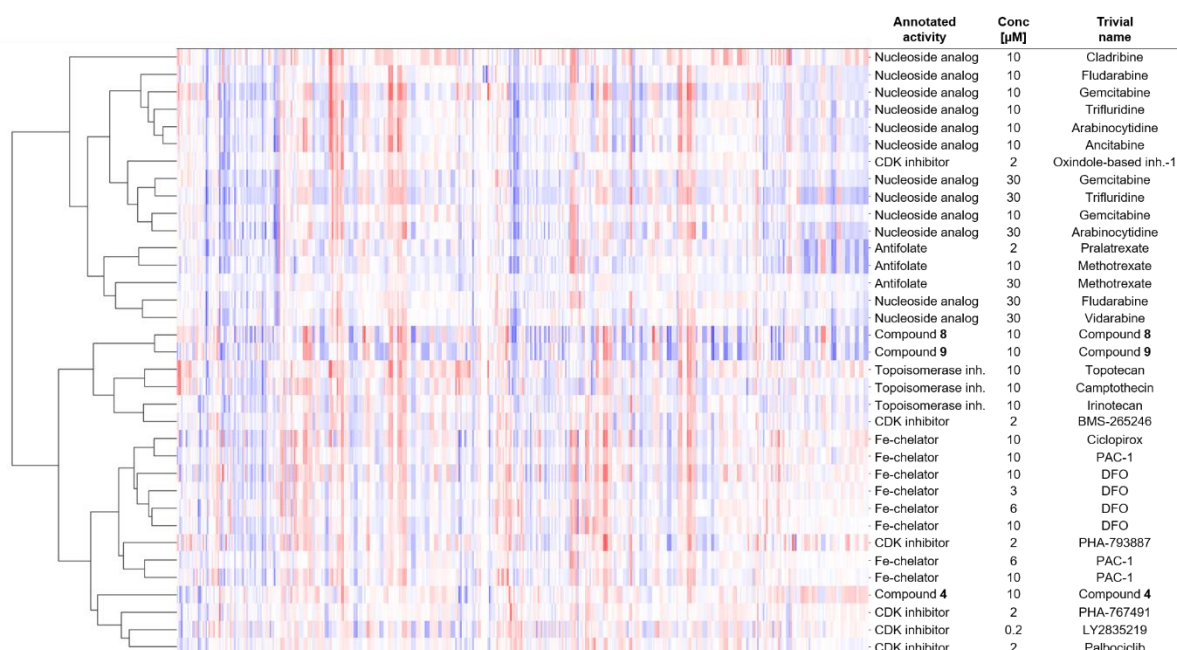


**Figure 26: Hierarchical clustering of fingerprints from compounds biosimilar (> 80 %) to 10 μM DFO.**

Compounds biosimilar (> 80 %) to 10 μM DFO, including different concentrations and compound batches, were subjected to hierarchical clustering performed by Dr. Axel Pahl (COMAS, Dortmund). For this, the list of similar compounds was further filtered for compounds with an induction between 17 and 37 % to mitigate induction effects and was restricted to references with a reported MoA of iron chelation or cell cycle arrest that is shared by the Fe/DNA synthesis cluster. To improve the visibility of less pronounced areas of the fingerprints, the hierarchical clustering was performed using sub-profiles, where only those features were kept, for which the Z-score was less than 10. Inh: inhibitor.

The hierarchical clustering of the fingerprints showed a separation in two subclusters (Figure 26). The upper subcluster contained the nucleoside analogs and antifolates, which function as mimetics of biological macromolecules, and the lower subcluster included the iron chelators, topoisomerase and CDK inhibitors, which modulate the activity of a protein. Only the CDK inhibitor oxindole-based inhibitor-1 was an outlier as it was assigned to the group of mimetics. Compounds **4**, **8** and **9** were assigned to the lower subcluster of iron chelators, topoisomerase and CDK inhibitors. However, compound **4** was distinguishable from compounds **8** and **9** and clustered together with the other annotated iron-chelating agents, which is in line with the experimentally observed iron-chelating activity (Figure 22A).

Clusters of iron chelators and DNA synthesis modulators have been identified in previous morphological studies, however, with a reduced number of stains.<sup>[64, 129]</sup> To examine if there is a benefit, for the assignment of a mechanism of action, in using a reduced number of stains, the hierarchical clustering was additionally performed with only three stains.

## RESULTS

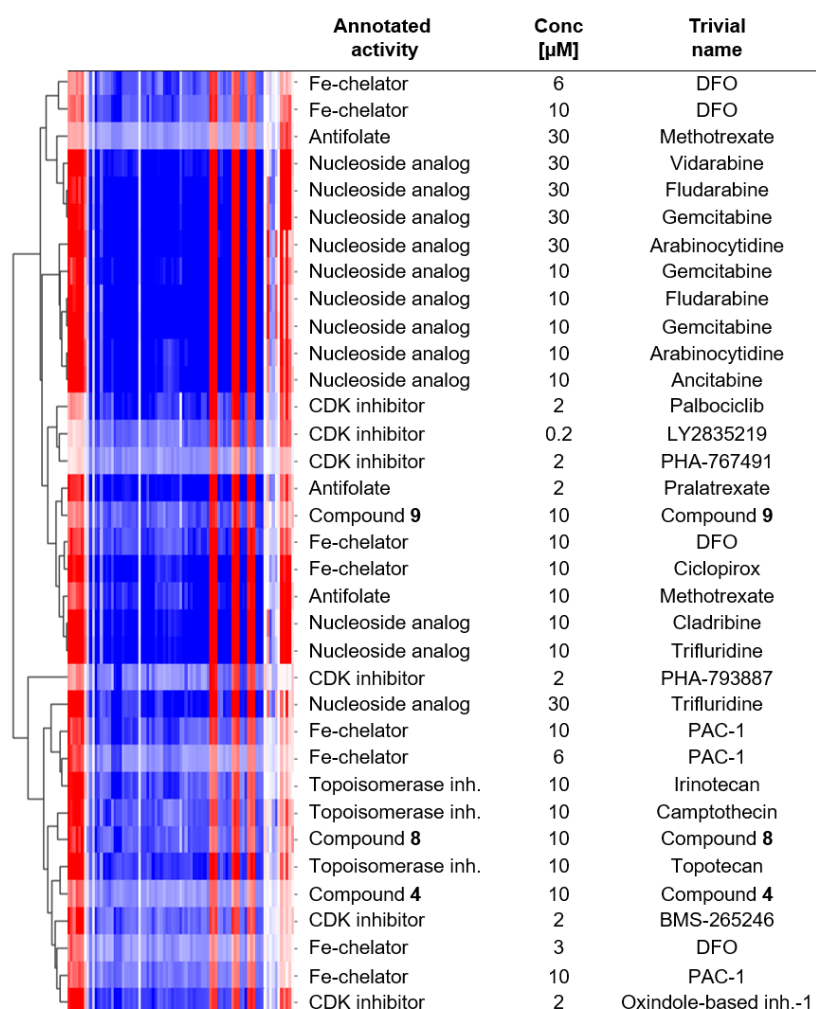


**Figure 27: Hierarchical clustering of fingerprints from compounds biosimilar (> 80 %) to DFO based on selected features.**

Only features that are related to Hoechst-33342, Phalloidin-Alexa Fluor 568 and WGA-Alexa Fluor 555) staining were used for clustering performed by Dr. Axel Pahl (COMAS, Dortmund). Compounds biosimilar (> 80 %) to DFO, including different concentrations and compound batches, were subjected to hierarchical clustering. For this, the list of similar compounds was further filtered for compounds with an induction between 17 and 37 % to mitigate induction effects and was restricted to references with a reported MoA of iron chelation or cell cycle arrest that is shared by the Fe/DNA synthesis cluster. To improve the visibility of less pronounced areas of the fingerprints, the hierarchical clustering was performed using sub-profiles, where only those features were kept, for which the Z-score was less than 10. Inh: inhibitor.

Figure 27 illustrates that hierarchical clustering exclusively based on the staining of DNA, actin and plasma membrane/Golgi did not result in a separation of relevant subcluster.

## 6.2 Investigation of the bioactivity of tetrahydroindolo[2,3-a]quinolizines

The indolo[2,3-a]quinolizine scaffold is present in many natural products that exhibit a variety of biological activities.<sup>[87-89]</sup> Hence, tetrahydroindolo[2,3-a]quinolizine derivatives represent a pre-validated compound class and they have not yet been investigated in terms of their biological activity.<sup>[130]</sup>

### 6.2.1 Morphological profiling of tetrahydroindolo[2,3-a]quinolizines 10-13

To assess a broad range of possible bioactivities, four selected tetrahydroindolo[2,3-a]quinolizines<sup>[130]</sup> were subjected to morphological profiling using the CPA (Figure 28).

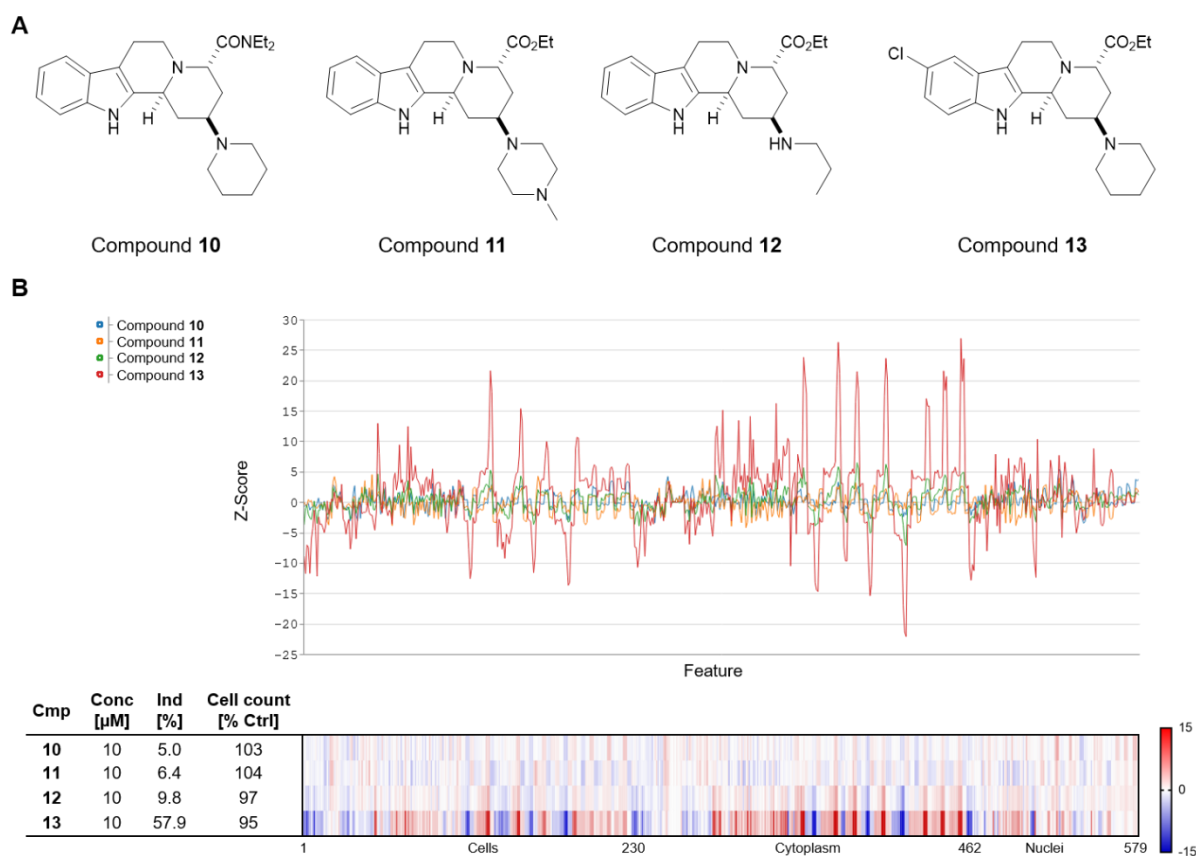


**Figure 28: Morphological fingerprints of tetrahydroindolo[2,3-a]quinolizines 10-13.**

(A) Chemical structures of compounds **10-13**. (B) Morphological fingerprints of compounds **10-13** at 10 μM visualized as line plots and heatmap profiles including the induction value (ind). The set of 579 features is divided into cell (1-229), cytoplasm (230-461) and nuclei (462-579) related features. Values were normalized to the DMSO control. Blue: decreased feature, red: increased feature.



## RESULTS

Compounds **10-13** displayed bioactivity in the CPA without affecting the cell count. While the activity of 10  $\mu\text{M}$  compound **10**, **11** and **12** was weak, with induction values below 10 %, 10  $\mu\text{M}$  compound **13** led to greater morphological changes with an induction value of 57.9 %. For this reason, compound **13** was selected for MoA deconvolution.

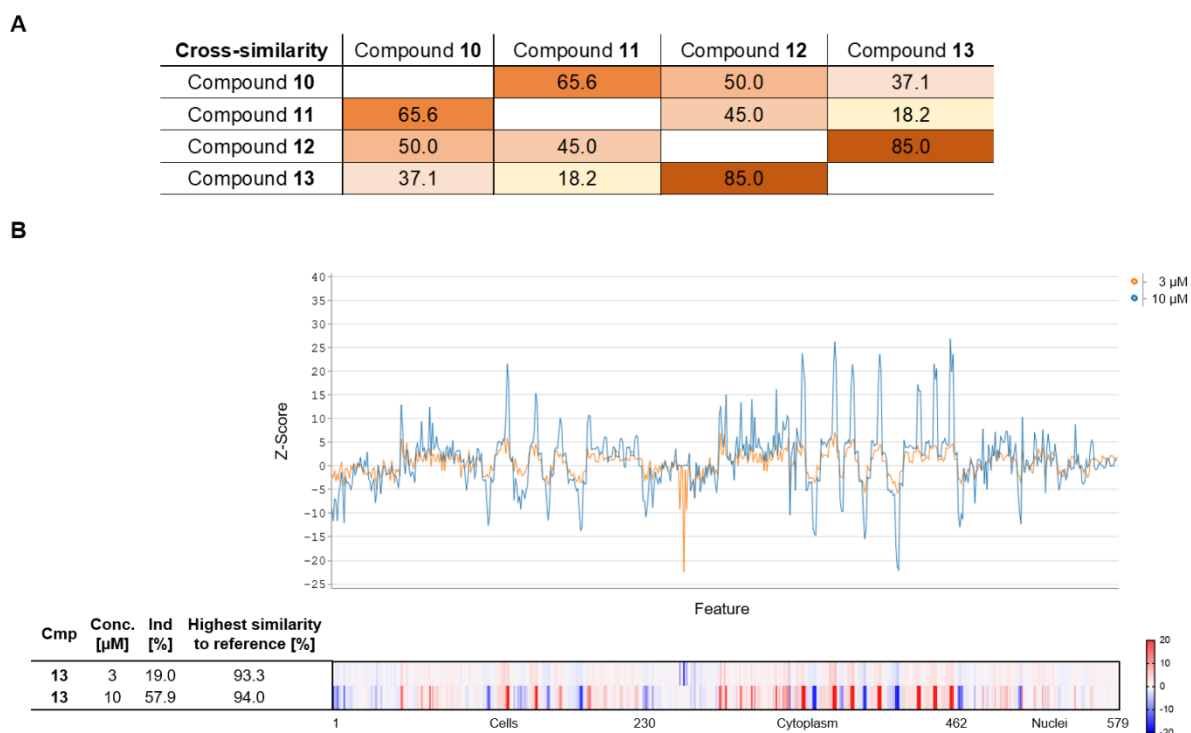


**Figure 29: Morphological profiling of compounds 10-13.**

(A) Biosimilarity among compounds **10-13** at 10  $\mu\text{M}$ . (B) Morphological fingerprints visualized as line plots and heatmap profiles including the induction value (ind). The set of 579 features is divided into cell (1-229), cytoplasm (230-461) and nuclei (462-579) related features. Values were normalized to the DMSO control. Blue: decreased feature, red: increased feature.

The median biosimilarity percentage (MBP) of 47.5 % illustrates a low biosimilarity among the derivatives **10-13** at 10  $\mu\text{M}$  (Figure 29A). Only the two most active compounds **12** and **13** possessed high biosimilarity (85 %) indicating a similar target or MoA. The most active compound **13** was screened at a lower concentration of 3  $\mu\text{M}$  and was still active with an induction value of 19 % (Figure 29B). To predict bioactivity for compound **13**, the morphological fingerprint was compared to the set of measured reference compounds. Surprisingly, the fingerprint, induced by 10  $\mu\text{M}$  compound **13**, showed high biosimilarity ( $\geq 75$  %) to more than 400 references that can be reviewed in the appendix (Table 14). This large reference cluster comprised compounds with diverse annotated targets and

## RESULTS

activities but was predominantly enriched in G protein-coupled receptor (GPCR) ligands, including anti-psychotics, and kinase inhibitors (Figure 30).

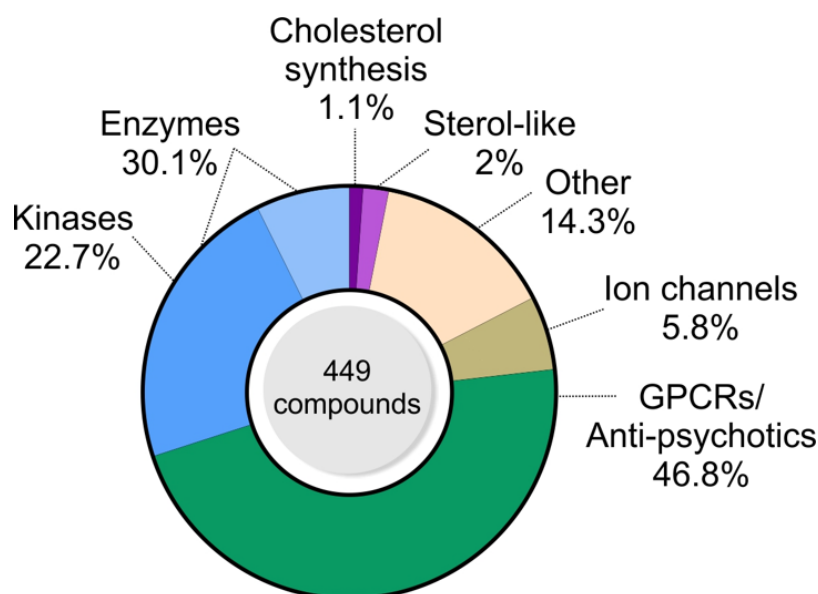


**Figure 30: Distribution of target classes among references biosimilar to 10  $\mu$ M compound 13.**

GPCRs are the largest family of membrane receptors and targeted by around 30 % of the marketed drugs.<sup>[131, 132]</sup> This includes anti-psychotics, that need to cross the blood-brain barrier in order to exert their therapeutic effect. Therefore, they need a cationic amphiphilic character comprising a hydrophobic part and a hydrophilic side chain containing basic amines.<sup>[133, 134]</sup> However, these structural, i.e., physicochemical properties often result in promiscuity for off-targets.<sup>[135, 136]</sup> Small molecules can intercalate and accumulate in membrane structures if they are highly lipophilic. Moreover, this increases the chance of binding to multiple targets. Accumulation of compounds in acidic organelles is primarily associated with a basic pKa. This effect is called lysosomotropism.<sup>[44, 134, 137]</sup> For simplicity reasons, the term 'lysosomes', to relate to acidic organelles, is often used, like in this thesis, however, it also includes other acidic organelles like endosomes and Golgi. Lysosomotropic compounds can freely pass through membranes within the neutral pH of the cytoplasm but once they become protonated in acidic organelles they are trapped due to the low retro-diffusion of protonated species.<sup>[138]</sup> This effect is largely species- and cell type-independent and also independent of the compound and its target class because the effect is determined by the physicochemical properties.<sup>[139]</sup> Compounds possessing physicochemical properties of a logP value above 2 and a bpKa between 6.5 and 11 are prone to accumulate in lysosomes.<sup>[140]</sup>

To investigate the physicochemical properties of the reference cluster, their logP and bpKa values were calculated<sup>[141]</sup> (Figure 31).

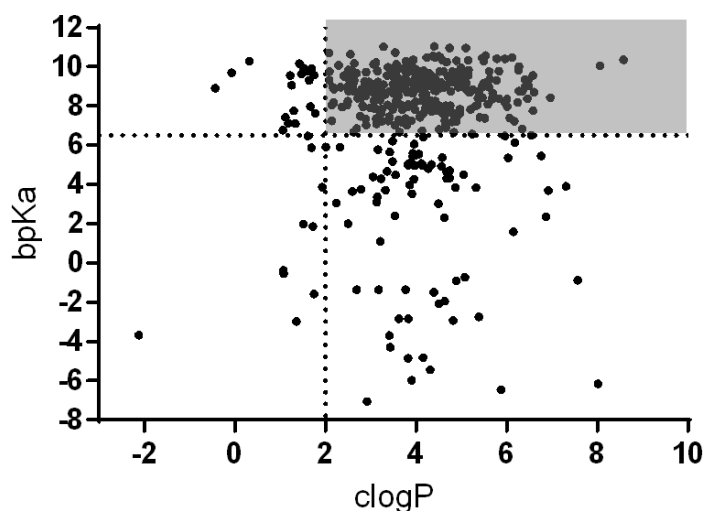


**Figure 31: Physicochemical properties of references biosimilar to compound 13.**

Calculated<sup>[141]</sup> clogP value of references biosimilar ( $\geq 75\%$ ) to 10  $\mu\text{M}$  compound **13** plotted against their calculated basic pKa (bpKa) value. Grey region corresponds to clogP > 2 and bpKa > 6.5.

Interestingly, the properties of 75.7 % of the references biosimilar to 10  $\mu\text{M}$  compound **13** were assigned to the physicochemical properties of lysosomotropic compounds (clogP > 2, bpKa > 6.5, Figure 31, grey box). The calculated<sup>[141]</sup> physicochemical properties of compound **13** were as well predictive for lysosomal accumulation (clogP: 3.7, bpKa: 9.1).

### 6.2.2 Lysosomotropic properties of compounds 10-13

To validate the potential lysosomotropic activity of compound **13**, which was suggested by the analysis of biosimilar references, the tetrahydroindolo[2,3-a]quinolizine derivatives **10-13** were subjected to a lysosomotropism assay using the fluorophore LysoTracker<sup>TM</sup> Red DND-99. This dye is itself a weak base and therefore gets trapped in acidic compartments upon protonation and thus, selectively stains acidic organelles. Chloroquine was used as a positive control as it is reported to be lysosomotropic<sup>[142]</sup>, leading to an increase in lysosomal pH and subsequently to a decreased LysoTracker<sup>TM</sup> Red DND-99 staining (Figure 32).

## RESULTS

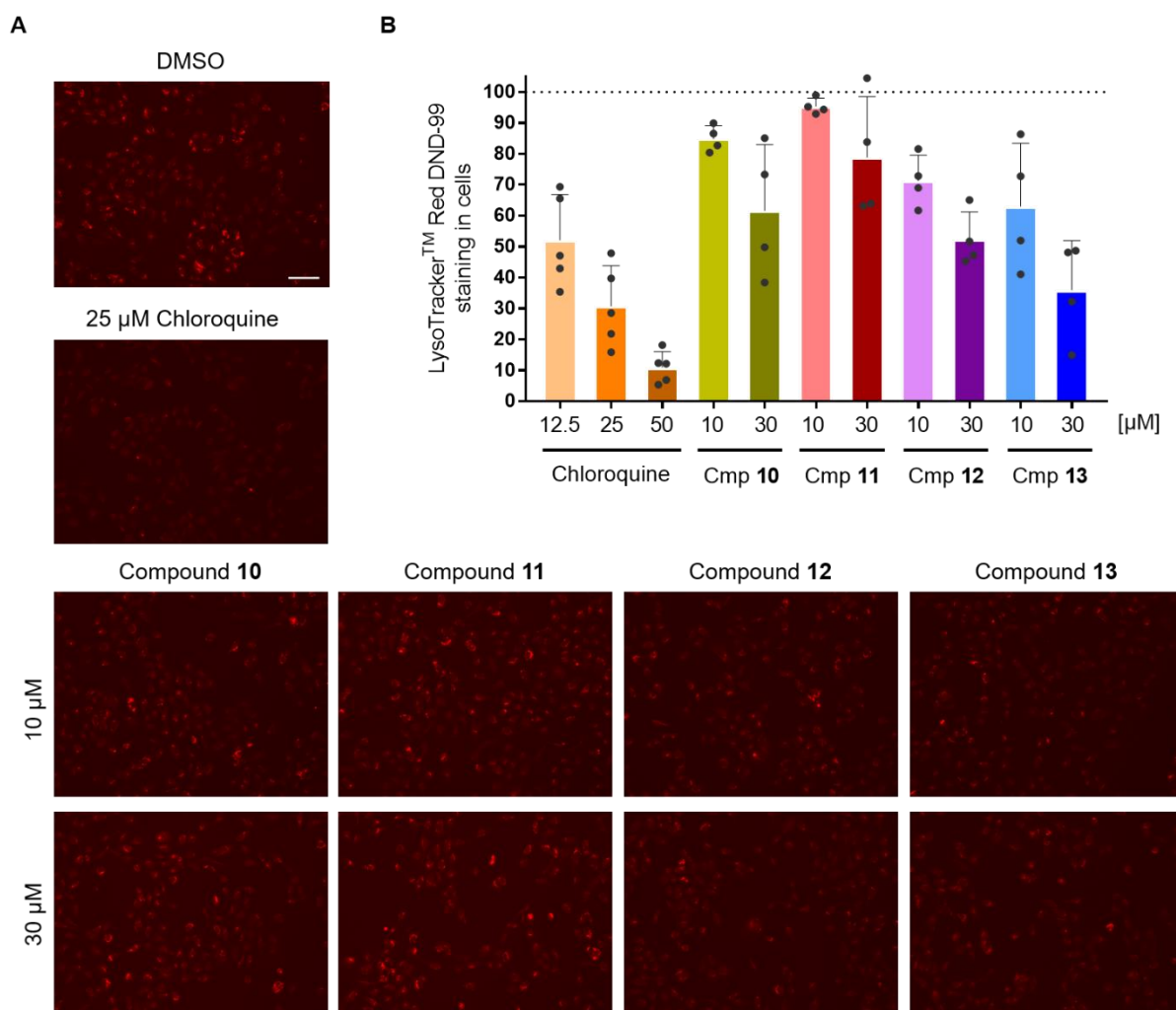


**Figure 32: Influence of compounds 10-13 on lysosomal accumulation of LysoTracker™ Red DND-99.**

(A) Representative images and (B) quantification of U-2OS cells incubated for 1 h with the compounds (cmp) or DMSO or Chloroquine as controls prior to staining with LysoTracker™ Red DND-99 and fixation. Scale bar: 100 μm. Data are mean values ± SD of four independent experiments.

The images as well as the quantification of the LysoTracker™ Red DND-99 staining (Figure 32) illustrate that compound **13** led to a concentration-dependent decrease in staining and hence, most likely to an increase in lysosomal pH. At 10 μM the staining was reduced by 37 % and at 30 μM by 64 %. Also, compound **12**, which showed a high biosimilarity to compound **13**, reduced the staining by 48 % at 30 μM. Compound **11** was inactive, whereas compound **10** showed weak lysosomotropic activity at 30 μM, reducing the signal by 38 %.

### **6.2.3 Live-cell imaging of compounds 10-13**

Lysosomotropism may lead to cell death for various reasons, e.g., due to lysosomal cell death<sup>[143-145]</sup> or the influx of water into lysosomes yielding enlarged vacuoles, which may cause irreversible cellular injuries<sup>[146]</sup>. To investigate the influence of the compounds on cell growth, viability and morphology, a real-time live-cell analysis was performed.

## RESULTS

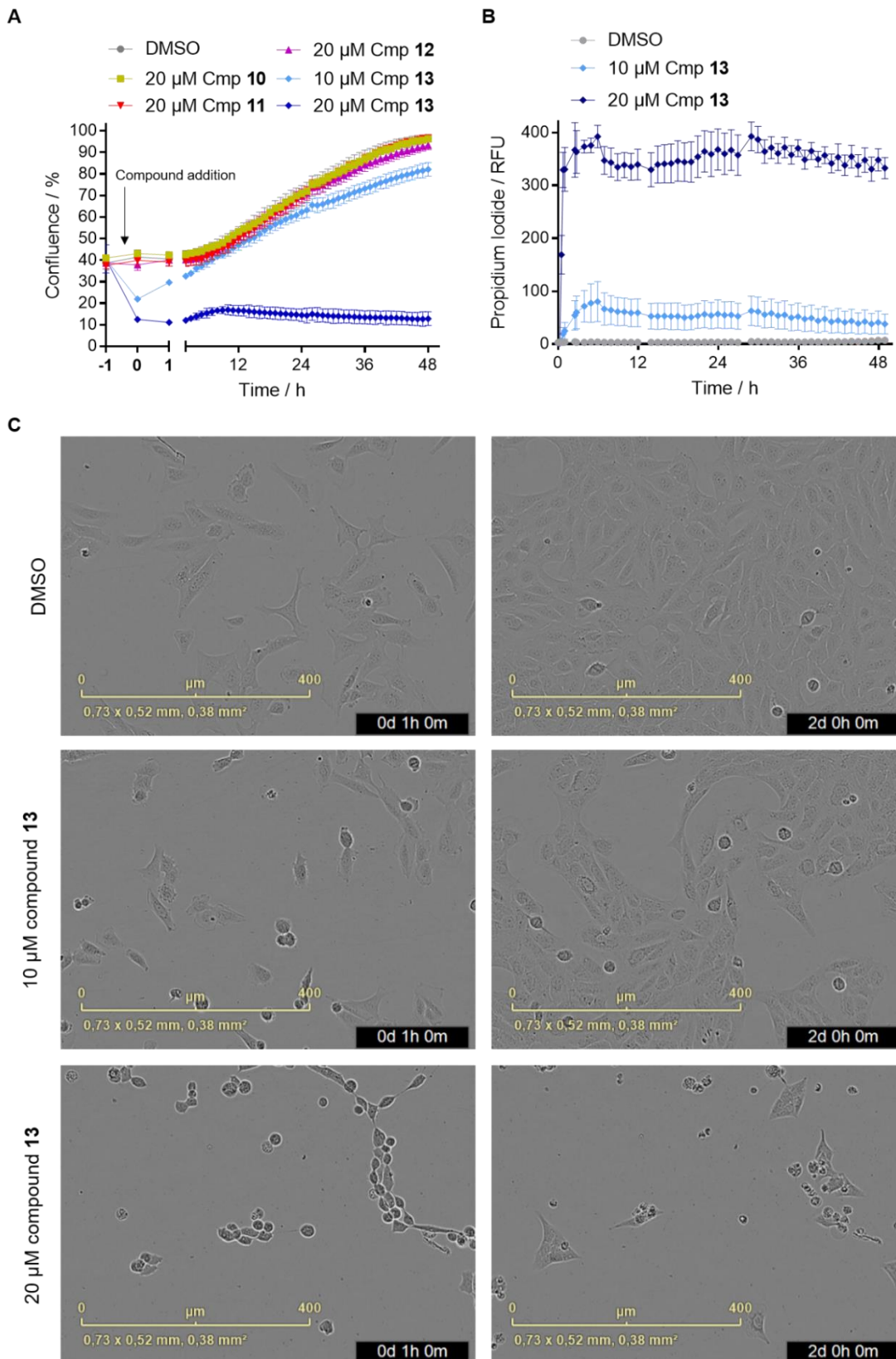


**Figure 33: Influence of compounds 10-13 on cell growth and morphology.**

(A-C) U-2OS cells were incubated with compounds or DMSO as a control for 48 h and (B) in the presence of propidium iodide (PI) to detect dead cells. Images were acquired in a 1-hour interval over 48 h using the IncuCyte S3 imaging system. Image-based analysis was used to quantify cell growth

## RESULTS

through cell confluence as a readout, or dead cells through PI fluorescence. (C) Representative images of treated cells after 1 h and 2 days. Data (mean values  $\pm$ SD of N=3) are representative of three independent replicates.

Only compound **13** affected the cell growth (Figure 33A). Whereas 10  $\mu$ M only led to a slight reduction, 20  $\mu$ M completely inhibited cell growth. However, at both concentrations, a drop in the confluence curve was detected within the first hour of compound treatment. The corresponding morphological phenotype of cells 1 h after treatment are depicted in representative images in Figure 33C, which show that the initial drop in the curve was a result of cell shrinkage and rounding. The confluence determined with the IncuCyte S3 imaging system represents the growth area, which is covered by the cells. Cell shrinkage and rounding lead to a smaller covered area and hence, to a decrease in the curve, which is therefore not necessarily linked to an inhibited cell growth or cytotoxicity. Images taken 48 h after compound treatment at a dose of 20  $\mu$ M depict cell debris and only a few primarily rounded cells, indicating cytotoxicity. The propidium-iodide staining confirmed the cytotoxic effect of 20  $\mu$ M compound **13** as the fluorescence, i.e., number of dead cells increased already 1 h after treatment compared to the DMSO control (Figure 33B). In contrast, cells treated with 10  $\mu$ M compound **13** only displayed a minor reduction in confluence (Figure 33C), reflecting the course of the growth curve. Moreover, the propidium-iodide staining revealed only a slight increase in dead cells upon treatment with 10  $\mu$ M compound **13** (Figure 33B).

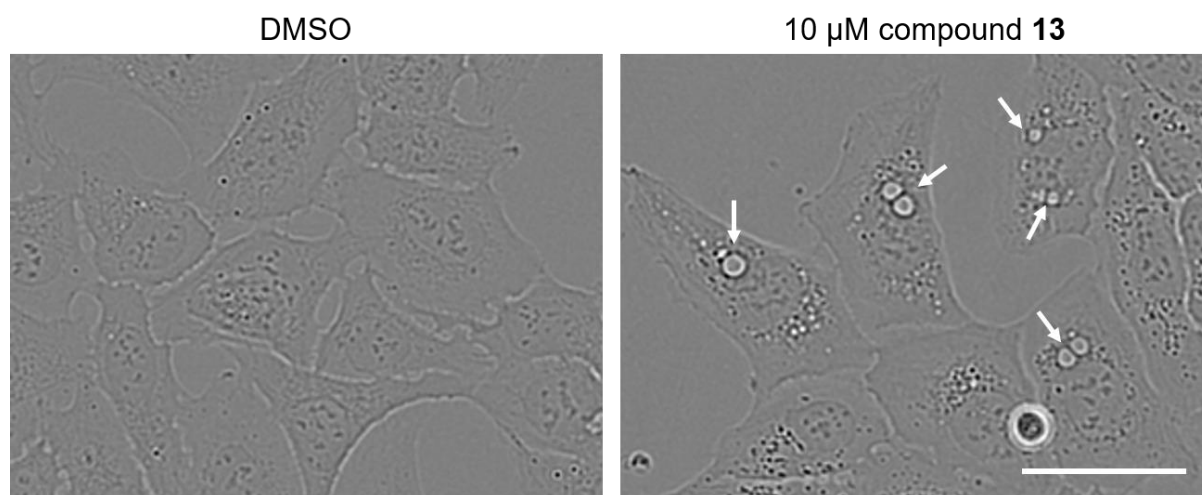


**Figure 34: Influence of compound 13 on cell morphology.**

Cells were incubated with the compound or DMSO for 1 hour. Images were acquired at 20X magnification using the IncuCyte S3 imaging system. White arrows indicate vacuolar structures. Scale bar: 50  $\mu$ m.

## RESULTS

At the first glance, no changes in morphology, e.g., cell shape, were observed for cells treated with 10  $\mu\text{M}$  compound **13** (Figure 33C). However, cells that were treated with compound **13** (Figure 34) contained vacuoles, which are most likely enlarged acidic organelles that gained volume due to the influx of water as a consequence of the treatment with a lysosomotropic agent<sup>[147]</sup>.

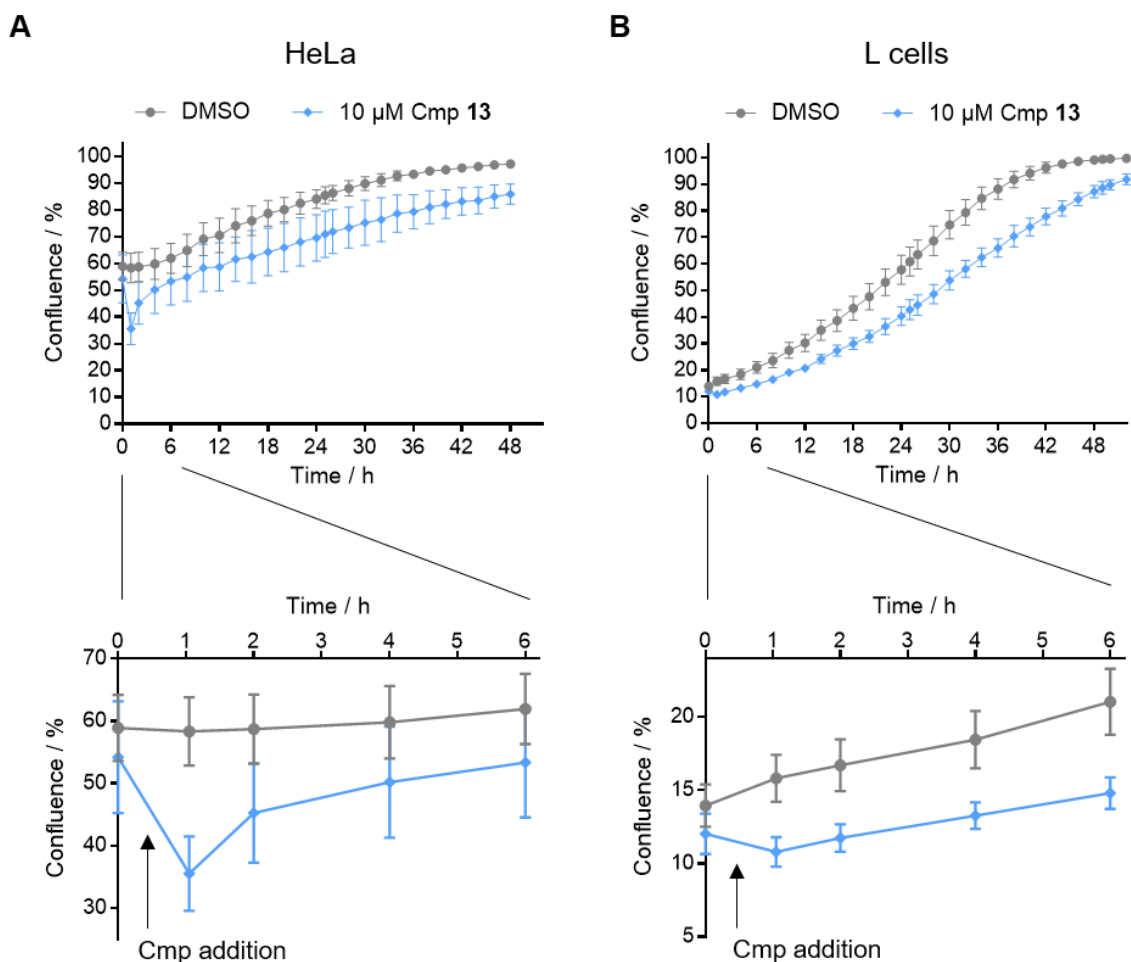


**Figure 35: Influence of compound 13 on the growth of HeLa and L cells.**

(A) HeLa and (B) L-cells were treated with 10  $\mu\text{M}$  compound (cmp) **13** or DMSO as a control. Images were acquired in a 2-hour interval for 48 h using the IncuCyte S3 imaging system. Image-based analysis was used to quantify cell growth through cell confluence as readout. Data (mean values  $\pm$ SD of N=3) are representative of three independent replicates.

As lysosomotropism is largely cell-type independent, compound **13** was tested for its influence on the cell growth of the cervix carcinoma cell line HeLa and the mouse fibroblast L cells (Figure 35). Similar to U-2OS cells, 10  $\mu\text{M}$  compound **13** slightly reduced the cell growth of HeLa and L cells. Furthermore, the same initial drop in confluence, related to cell shrinkage and rounding, was detected directly after compound treatment.



## RESULTS

To investigate if the initial shrinkage and rounding of the cells is related to lysosomotropism, a co-treatment with Bafilomycin A (Baf A1) was performed. Baf A1 is an inhibitor of the lysosomal proton-transporting V-type ATPase (v-ATPase), a proton pump, that is responsible for the acidic pH in lysosomes.<sup>[148]</sup> Inhibition of the v-ATPase by Baf A1 leads to an increase in lysosomal pH and may therefore abolish lysosomotropic-related effects induced by a compound.

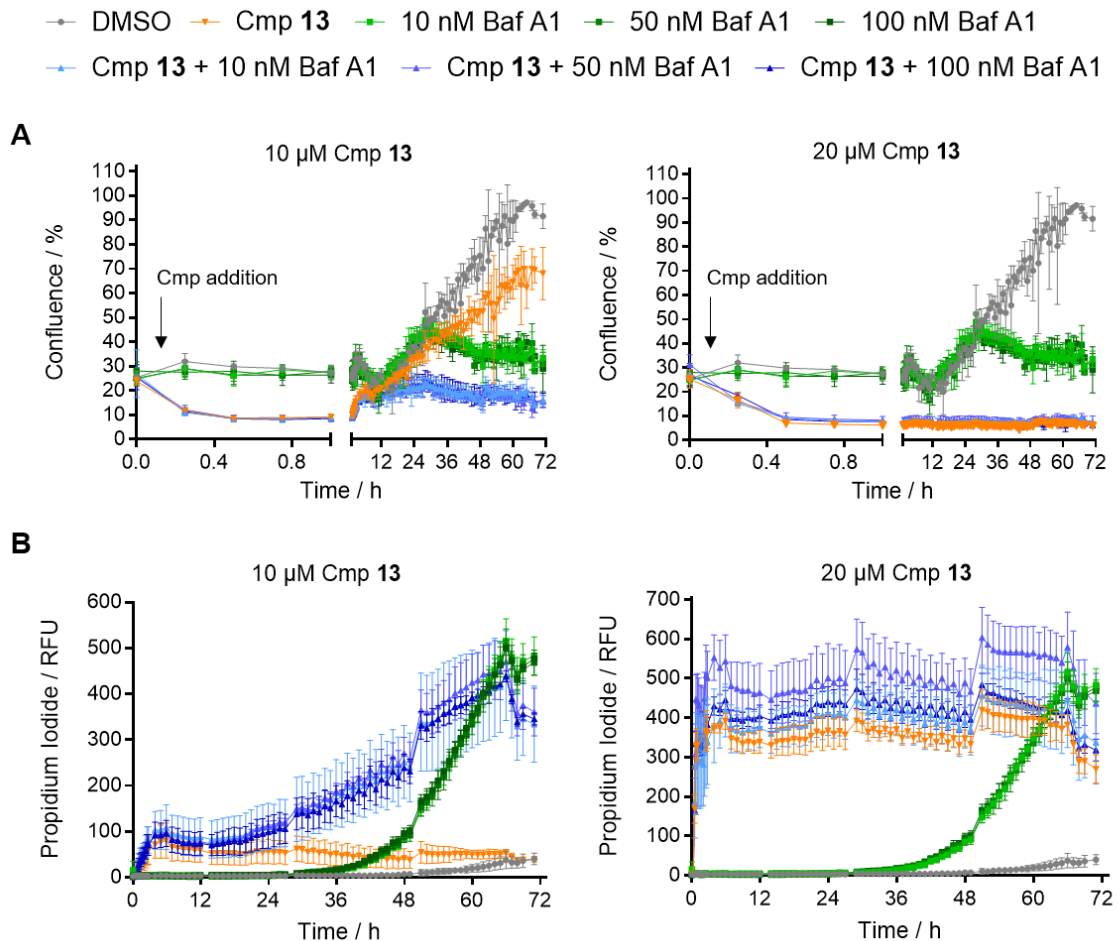


**Figure 36: Influence of Bafilomycin A1 co-treatment on cell morphology and viability of U-2OS cells that were treated with compound 13.**

(A and B) U-2OS cells were treated with the indicated concentrations of Bafilomycin A1 (Baf A1) and 10  $\mu\text{M}$  compound 13 or DMSO as a control in the presence of propidium iodide. Images were acquired using the IncuCyte S3 imaging system. Image-based analysis was used to quantify cell growth (A) through cell confluence as readout, or dead cells through PI fluorescence (B). Data (mean values  $\pm$  SD of N=3) are representative of three independent replicates.

Figure 36 illustrates that Baf A1 was cytotoxic after 36 hours of treatment as the confluence decreased along with an increased number of dead cells within the concentration range of 10-100 nM.

Compound **13** alone showed the same effect as in the previous experiment (Figure 33). A dose of 10  $\mu\text{M}$  led to a slight reduction in confluence and a slight increase in dead cells as well as to the initial drop in the confluence due to cell shrinkage and rounding within the first 30 min of treatment. A dose of 20  $\mu\text{M}$  compound **13** was cytotoxic within the first hour of treatment. The co-treatment of 10  $\mu\text{M}$  and 20  $\mu\text{M}$  compound **13** with different concentrations of Baf A1 (10-100 nM) led as well to immediate cell death. Therefore, the co-treatment did neither rescue the initial cell shrinkage and rounding induced by 10  $\mu\text{M}$  compound **13** nor the cytotoxic effect induced by 20  $\mu\text{M}$  compound **13**, suggesting a lysosomotropic-independent mechanism for the cell rounding and cytotoxicity.

### 6.2.3.1 Influence of compound 13 on the actin cytoskeleton

The cytoskeleton is a major determinant of cellular shape.<sup>[149]</sup> As compound **13** led to initial cell shrinkage and rounding, its influence on the *in vitro* actin polymerization and the actin cytoskeleton in cells was investigated.

## RESULTS

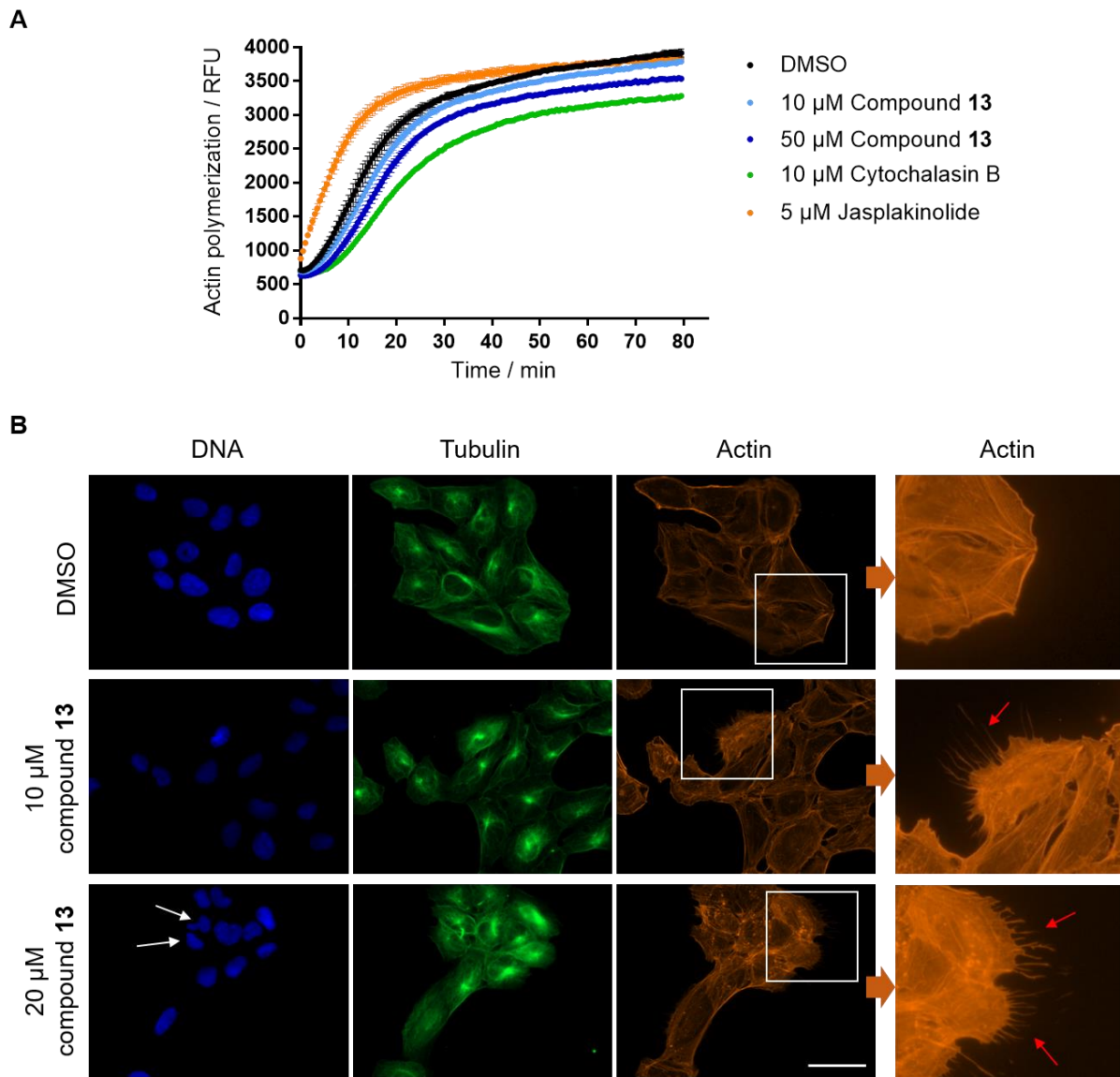


**Figure 37: Influence of compound 13 on actin dynamics.**

(A) Influence on the *in vitro* actin polymerization. Pyrene-conjugated actin was incubated with compound **13** or DMSO, cytochalasin B or jasplakinolide as controls and polymerization was monitored by measuring the fluorescence intensity (ex/em: 360/410 nm). Results are representative of three independent experiments. (B) Influence on the actin cytoskeleton. U-2OS cells were treated with compound **13** or DMSO as a control for 25 min prior to fixation and staining with DAPI (blue), anti- $\alpha$ -tubulin antibody (green) and phalloidin (orange) for visualizing DNA, microtubules, and actin, respectively. White arrows indicate deformed nuclei. Red arrows indicate actin fibers in cropped and enlarged images (adjusted brightness) of the area within the white box. Representative images of three independent replicates. Scale bar: 50  $\mu\text{m}$ .

Cytochalasin B reduces the actin polymerization rate by inhibiting actin monomer addition<sup>[150]</sup> and jasplakinolide induces actin filament polymerization and stabilizes F-actin.<sup>[151]</sup> Whereas 10  $\mu\text{M}$  compound **13** did not affect actin polymerization, 50  $\mu\text{M}$  slightly reduced the polymerization rate.

## RESULTS

---

In contrast, the staining of the actin cytoskeleton in cells revealed that compound **13** led to a concentration-dependent formation of fibers 25 min after treatment (Figure 37B, red arrows, right column). These are most likely retraction fibers, whose formation is a concomitant of de-adherence, and they are extending from the cell margin to the original site of adhesion<sup>[152]</sup>, which is in line with the observed cell rounding induced by compound **13** (Figure 33). Compound **13** did not influence the tubulin network but led to deformed nuclei (white arrows), which can also be related to alterations in the cytoskeleton<sup>[153, 154]</sup>. The formation of fibers and deformed nuclei was not observed after a treatment time of six hours (Figure 38A). However, the formation of actin aggregates was detected for the highest concentration of 20  $\mu$ M compound **13** (Figure 38A, red arrows).

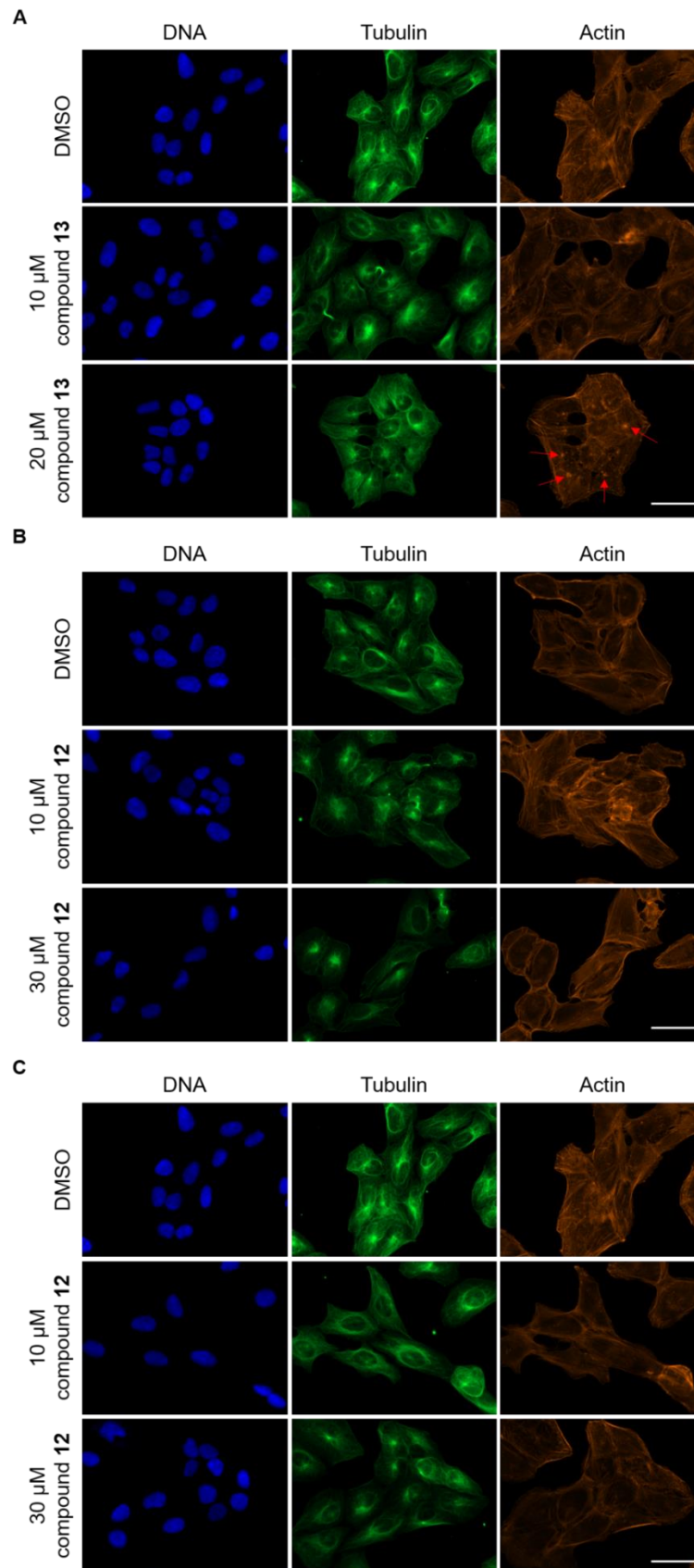


**Figure 38: Influence of compounds 12 and 13 on the actin cytoskeleton.**

(A-C) Representative images of U-2OS cells treated with the compounds or DMSO as a control prior to fixation and staining with DAPI (blue), anti- $\alpha$ -tubulin antibody (green) and phalloidin (orange) for

## RESULTS

---

visualizing DNA, microtubules, and actin, respectively. Representative images of three independent replicates. Scale bar: 50  $\mu\text{m}$ . (A) 6 h treatment with compound **13**. Red arrows indicate actin aggregates. (B) 25 min treatment with compound **12**. (C) 6 h treatment with compound **12**.

For comparison, the influence of compound **12** on the actin dynamics was explored as its morphological fingerprint was biosimilar to compound **13**. Compound **12** was also lysosomotropic, although, less potent. However, treating cells for 25 min and 6 h with 10 and 30  $\mu\text{M}$  compound **12** did neither lead to the formation of fibers and aggregates nor to deformed nuclei. Moreover, the tubulin network was not affected by compound **12**.

### 6.2.4 Proteome profiling of compounds 10-13

To gain deeper insight into the bioactivity of the tetrahydroindolo[2,3-a]quinolizines **10-13** and potential regulated pathways and proteins, a global proteome profiling was performed. U-2OS cells were treated with the compounds or DMSO as control and lysed 24 h later. The lysates were reduced, alkylated, and digested into peptides. Afterwards, peptides were labeled with tandem mass tags, which enable peptide quantification by nanoHPLC-MS/MS analysis.

## RESULTS

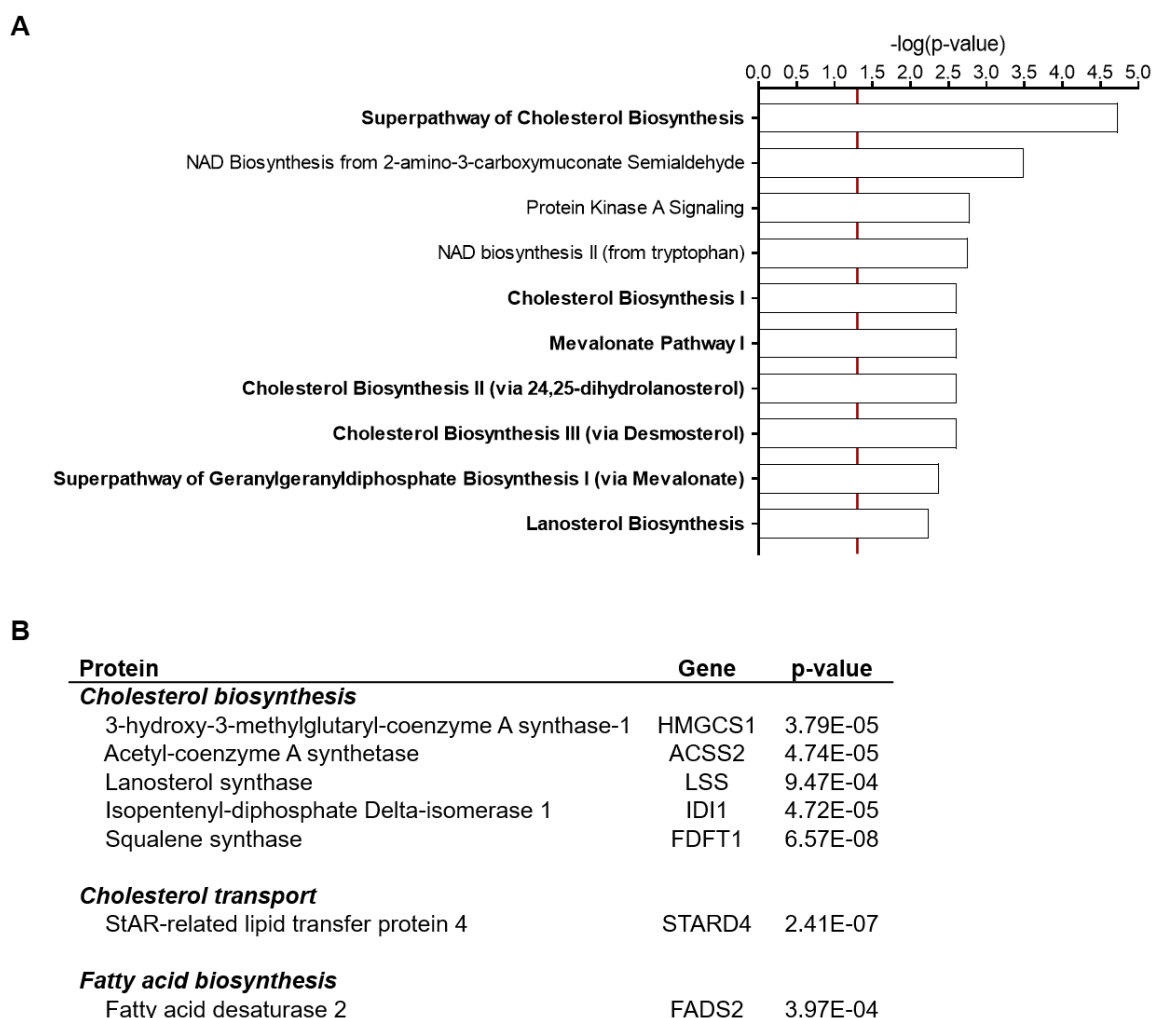


**Figure 39: Proteome profiling analysis of compound 13.**

(A and B) U-2OS cells were treated for 24 h with 10  $\mu$ M compound **13** prior to proteome profiling using tandem mass tags for quantification by nanoHPLC-MS/MS. Data are mean values  $\pm$  SD of three independent experiments. Pathway enrichment analysis was performed using the Ingenuity Pathway Analysis software to determine significantly affected pathways (FDR < 0.05, Benjamini-Hochberg corrected). (A) Top 10 enriched pathways. Red line:  $p = 0.05$ . (B) List of proteins that were significantly upregulated by **13** and are involved or related to cholesterol homeostasis.

Treatment with 10  $\mu$ M compound **13** led to the significant up- or downregulation of 118 proteins (FDR < 0.05, Benjamini-Hochberg corrected), which can be reviewed in the appendix (Table 15). To identify potentially affected signaling pathways, the data set was analyzed for pathway enrichment with the Ingenuity Pathway Analysis (IPA) software (QIAGEN Inc., <https://www.qiagenbioinformatics.com/products/ingenuity-pathway-analysis>). The analysis revealed an enrichment in proteins involved in the biosynthesis of cholesterol (Figure 39A, depicted in bold). Five proteins are directly involved in the biosynthesis of cholesterol: 3-hydroxy-3-methylglutaryl-coenzyme A synthase (HMGCS1), acetyl-coenzyme A synthetase (ACSS2), lanosterol synthase (LSS), isopentyl-diphosphate delta-isomerase 1 (IDI1) and

## RESULTS

squalene synthase (FDFT1) (Figure 39B).<sup>[155-158]</sup> In addition, compound **13** upregulated the protein amount of the cholesterol transport protein STARD4 (StAR-related lipid transport protein 4)<sup>[159]</sup> and the fatty acid desaturase 2 (FADS2), which is part of the fatty acid biosynthesis<sup>[160]</sup> (Figure 39B).

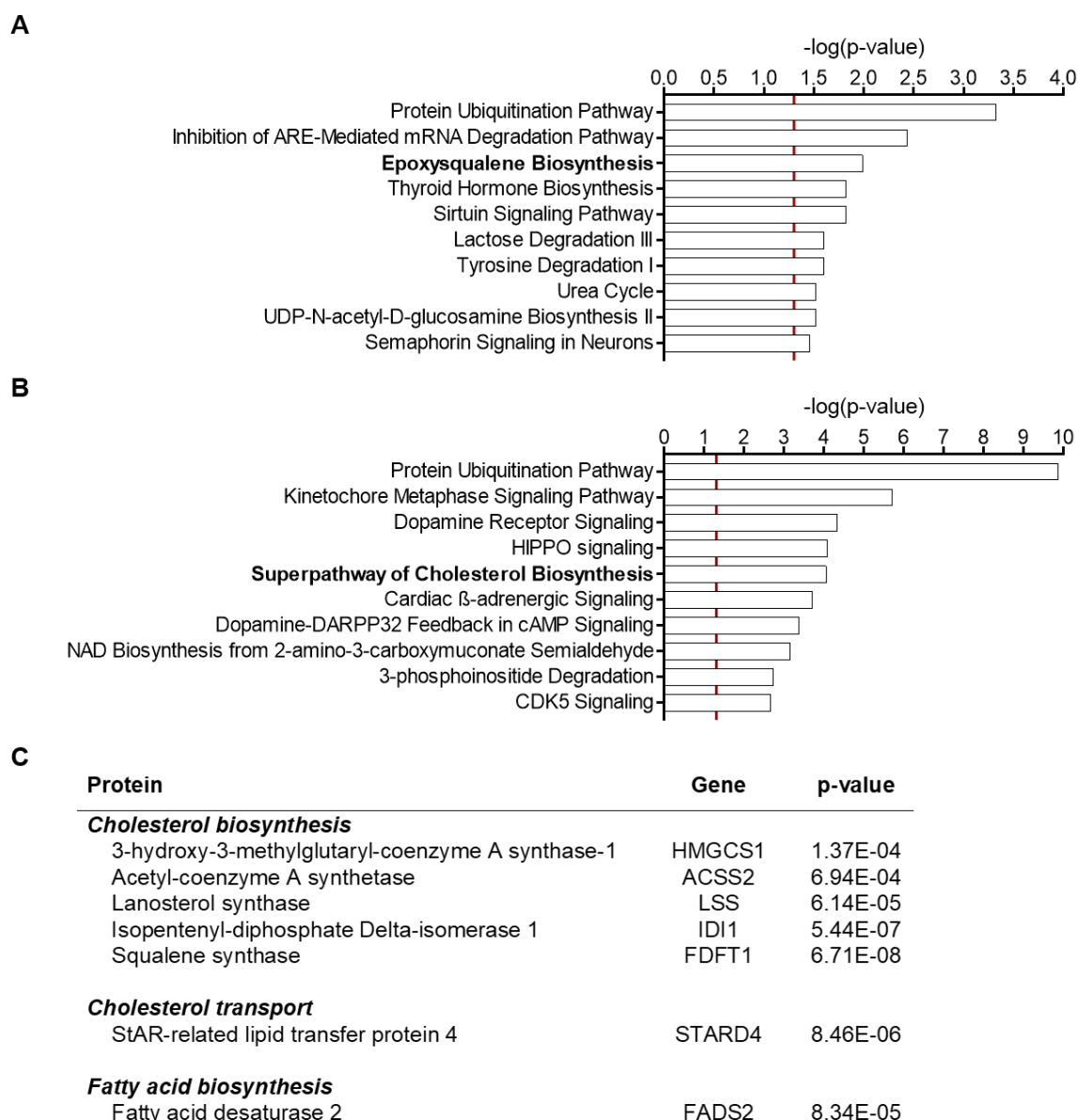


**Figure 40: Proteome profiling analysis of compound 12.**

(A-C) U-2OS cells were treated for 24 h with compound **12** prior to proteome profiling using tandem mass tags for quantification by nanoHPLC-MS/MS. Data are mean values  $\pm$  SD of three independent experiments. Pathway enrichment analysis was performed using IPA to determine significantly (FDR < 0.05, Benjamini-Hochberg corrected) affected pathways. (A and B) Top 10 enriched pathways. Red line:  $p = 0.05$ . (A) 10  $\mu$ M compound **12**. (B) 30  $\mu$ M compound **12**. (C) List of proteins that were significantly upregulated by 30  $\mu$ M compound **12** and are involved or related to cholesterol biosynthesis.



## RESULTS

---

In total, 107 proteins were significantly up- or down-regulated (FDR < 0.05, Benjamini-Hochberg corrected) by 10  $\mu$ M compound **12** and 99 proteins by 30  $\mu$ M compound **12** (data can be reviewed in the appendix (Table 16)). Whereas the IPA analysis revealed that 10  $\mu$ M compound **12** increased the level of FDFT1 (epoxysqualene biosynthesis, Figure 40A) as the only protein involved or related to the biosynthesis of cholesterol, 30  $\mu$ M compound **12** led, similar to 10  $\mu$ M compound **13**, to an upregulation of the same proteins involved in the biosynthesis of cholesterol, namely HMGCS1, ACSS2, LSS, IDI1 and FDFT1 (Figure 40B, C). In addition, STARD4 and FADS2 were as well upregulated by 30  $\mu$ M compound **12** (Figure 40C). However, besides modulated proteins involved or related to cholesterol homeostasis, the top pathway for 10 and 30  $\mu$ M compound **12** is the protein ubiquitination pathway containing, amongst others, several subunits of the proteasome.

## RESULTS

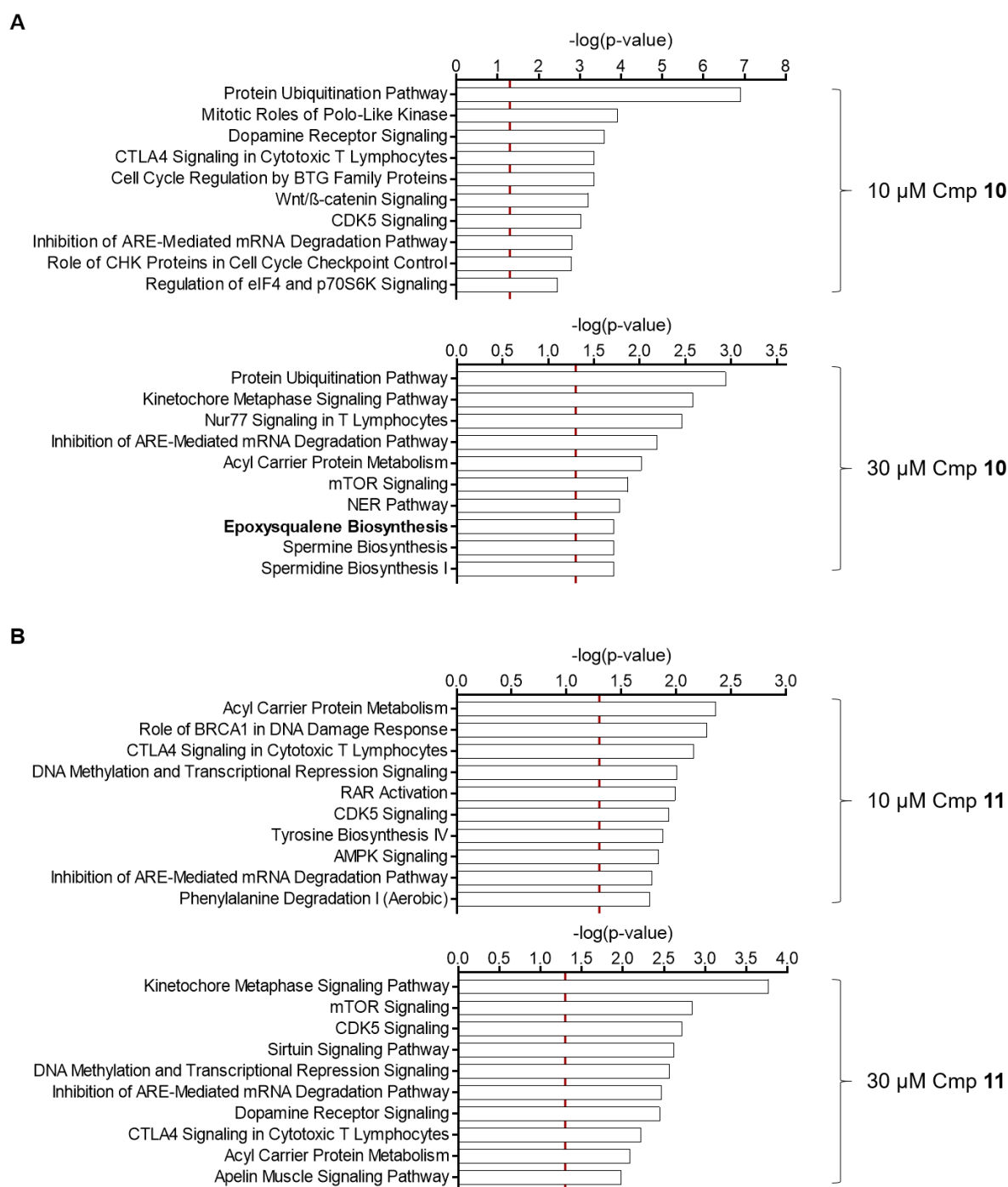


**Figure 41: Proteome profiling analysis of compounds 10 and 11.**

(A and B) U-2OS cells were treated for 24 h with compounds (cmp) **10** and **11** prior to proteome profiling using tandem mass tags for quantification by nanoHPLC-MS/MS. Data are mean values  $\pm$  SD of three independent experiments. Pathway enrichment analysis was performed using IPA to determine significantly (FDR < 0.05, Benjamini-Hochberg corrected) affected pathways. Top 10 enriched pathways. Red line:  $p = 0.05$ . (A) 10 and 30  $\mu$ M compound **10**. (B) 10 and 30  $\mu$ M compound **11**.

In total, 88 proteins (FDR < 0.05, Benjamini-Hochberg corrected) were significantly up- or down-regulated by 10  $\mu$ M compound **10** and 89 proteins by 30  $\mu$ M compound **10** (data can be

reviewed in the appendix (Table 17)). 10  $\mu$ M compound **11** led to a significant up- or down-regulation of 93 proteins and 30  $\mu$ M to the modulation of 69 proteins (data can be reviewed in the appendix (Table 18)). 30  $\mu$ M compound **10** induced the upregulation of FDFT1 (Epoxyqualene Biosynthesis, Figure 41A) involved in the biosynthesis of cholesterol. Besides this, the top pathway for 10 and 30  $\mu$ M compound **10** is again the protein ubiquitination pathway containing, amongst others, several subunits of the proteasome.

Collectively, the proteome profiling revealed predominantly proteins involved or related to cholesterol homeostasis for the most active derivatives **12** and **13**, providing a starting point for further biological investigations towards the MoA.

#### 6.2.4.1 Validation of cholesterol-modulating activity of tetrahydroindolo[2,3-a]quinolizines

The proteome profiling suggested modulated cholesterol biosynthesis upon treatment with tetrahydroindolo[2,3-a]quinolizine derivatives. The biosynthesis of cholesterol and fatty acids is regulated by transcription factors of the sterol regulatory element (SRE) binding proteins (SREBPs) family.<sup>[161, 162]</sup> To investigate the influence of compounds **10-13** on the biosynthesis of cholesterol, a reporter gene assay was performed using the 3-hydroxy-3-methylglutaryl-coenzyme A synthase (HMG-CoA) promoter, which is regulated by SREBP.

## RESULTS

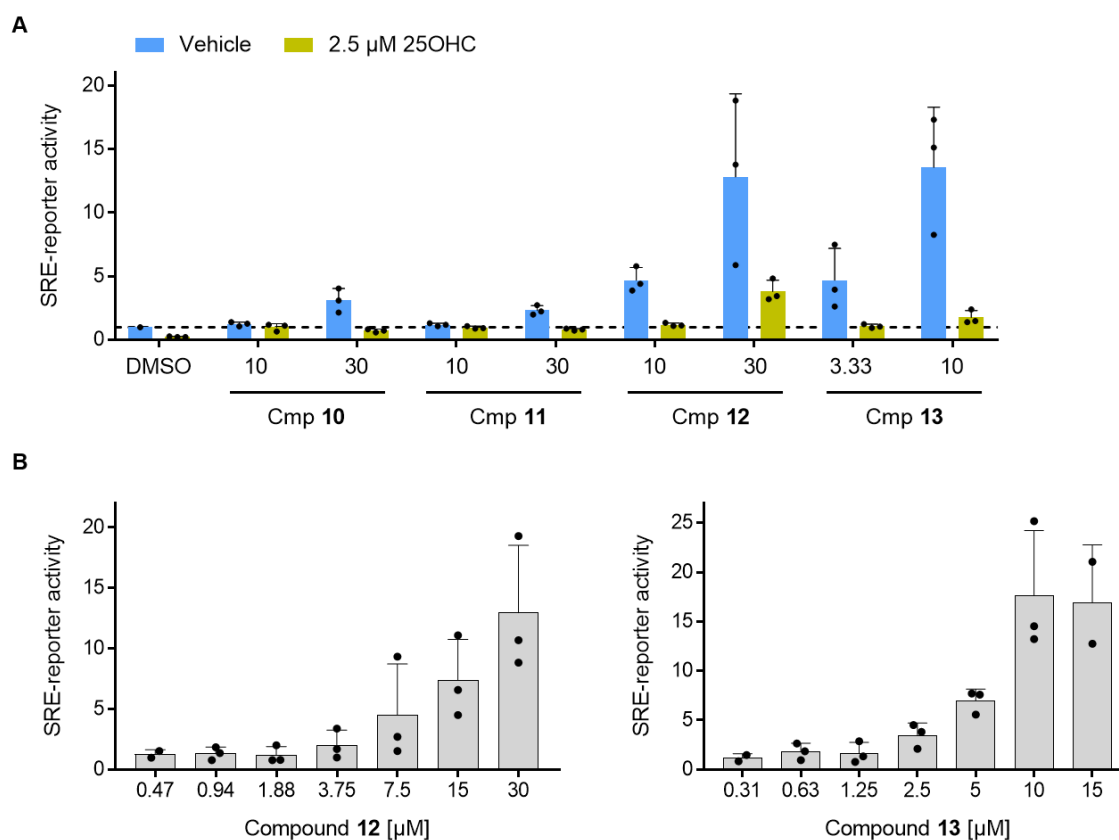


**Figure 42: Influence of compounds 10-13 on SREBP-dependent transcriptional activation.**

(A and B) U-2OS cells were transfected with a firefly luciferase construct under the control of the HMG-CoA synthase promoter and a plasmid for constitutive *Renilla* luciferase expression. Cells were treated for 24 h with the compounds or DMSO prior to the determination of both luciferase activities. Data are mean values  $\pm$  SD of three independent experiments. (A) Co-treatment with or without 25-hydroxycholesterol (25OHC). Values are normalized to the DMSO control in the absence of 25OHC. (B) Dose-dependent analysis for compounds **12** and **13** in the absence of 25OHC. Values are normalized to the DMSO control. Data are mean values  $\pm$  SD of three independent replicates.

Figure 42 demonstrates that 25-hydroxycholesterol (25OHC) suppressed the SRE-dependent reporter activity in cells. This was expected as under physiological conditions cholesterol *de novo* synthesis is only induced if sterol levels, sensed at the ER membrane, are too low.<sup>[163]</sup> Compound **13** most potently and dose-dependently activated SREBP-responsive transcription in the absence of 25OHC by 5- and 14-fold at 3.3  $\mu$ M and 10  $\mu$ M, respectively (Figure 42A, B). Compound **12** also led to the activation of SREBP-responsive transcription in the absence of 25OHC by 5- or 13-fold, however, at 10  $\mu$ M and 30  $\mu$ M, respectively (Figure 42A, B). Whereas compound **11** was inactive, compound **10** showed a 3-fold activation at the highest concentration of 30  $\mu$ M (Figure 42A). The presence of 25OHC suppressed the activation by the compounds, indicating a modulation of SREBP-dependent transcription upstream of cholesterol sensing.

Collectively, these results demonstrate that the activity and potency of compounds **10-13** in the SRE-reporter gene assay exactly reflect the activity suggested by the IPA analysis of the proteome profiling. Compound **13** and, less potently, compound **12** activated the SREBP-responsive transcription, whereas compound **11** was inactive and compound **10** only showed a weak activation at 30  $\mu$ M.

### 6.2.5 Investigation of lysosomotropism-related bioactivity

Lysosomotropic agents may disturb various cellular processes.<sup>[44, 146, 164, 165]</sup> The hydrophobic moiety allows intercalation and accumulation in the lysosomal membrane, which may lead to altered activity of inherent membrane proteins and to a disturbed lysosomal lipid homeostasis.<sup>[44, 166]</sup> One example are the intracellular cholesterol transporters NPC1 and NPC2 (Niemann-Pick C1 and C2 proteins), which guide cholesterol out of the lysosomes. Their activity is disturbed by the intercalation of lysosomotropic compounds in membrane structures and by an increased lysosomal pH.<sup>[44, 167, 168]</sup> For this reason, the influence of the tetrahydroindolo[2,3-a]quinolizines **10-13** on the intracellular localization of cholesterol was explored. For this, filipin was used, which binds unesterified cholesterol and is naturally fluorescent.<sup>[169]</sup>

## RESULTS

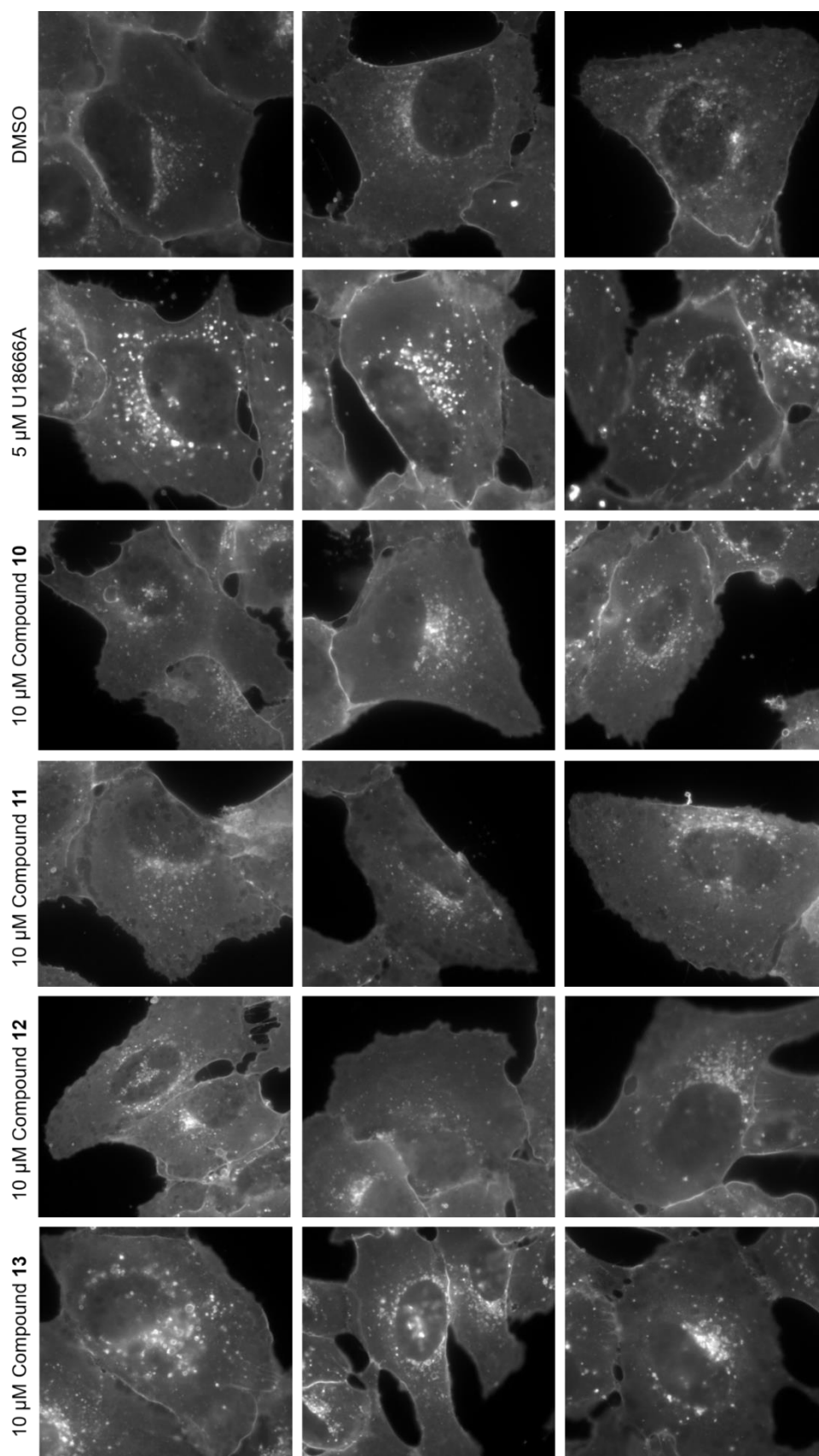


**Figure 43: Influence of compounds 10-13 on cellular cholesterol distribution.**

U-2OS cells were treated with 10  $\mu$ M compound or DMSO or U-18666A as a control for 3 h prior to fixation and staining with filipin. Representative images of three independent experiments.

## RESULTS

The cationic sterol U-18666A was used as a control. U-18666A blocks cholesterol egress by binding to the sterol-sensing domain of NPC1, which results in lysosomal accumulation of cholesterol.<sup>[170]</sup> The images of filipin-stained cells in Figure 43 illustrate that cells, treated with DMSO, exhibited a filipin staining in form of diffuse dots mainly located around the nucleus. In contrast, U-18666A treatment led to an accumulation of cholesterol, visible as bright puncta. Treatment of cells with 10  $\mu$ M compounds **10-12** did not influence the intracellular cholesterol distribution.

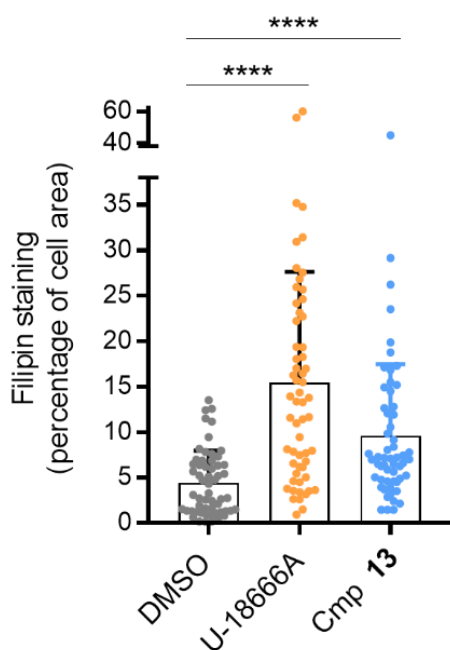


**Figure 44: Quantification of filipin staining for compound 13.**

U-2OS cells were treated with 10  $\mu$ M compound or DMSO or U-18666A as a control for 3 h prior to fixation and staining with filipin. Quantification was performed with Fiji-ImageJ. Significance was determined using a two-tailed, unpaired t-test. \*\*\*\*p < 0.0001.

Treatment of the cells with 10  $\mu$ M compound **13** led, similar to U-18666A, to a significant intracellular accumulation of cholesterol, visible as brighter puncta, primarily located around the nucleus (Figure 43 and Figure 44). Because of the short treatment time of three hours, an accumulation due to the increased *de novo* synthesis can be excluded, and therefore the accumulation can solely be attributed to trapped cholesterol.

Recent studies link cholesterol homeostasis also to autophagy<sup>[171-173]</sup> and report an accumulation of LC3II-labeled autophagosomes after exposure to amphiphilic molecules.<sup>[134, 171, 174-177]</sup> Autophagy is a highly dynamic and evolutionary conserved pathway. It preserves cellular homeostasis by balancing sources of energy via the degradation of cytoplasmic organelles and long-lived and damaged proteins.

## RESULTS

---

The process of autophagy comprises the formation of autophagosomes, which are double-membrane vesicles that sequester the cargo before fusion with lysosomes. Within the lysosomes, acid hydrolases degrade the cargo for recycling.<sup>[178-181]</sup> During this process, the microtubule-associated light chain protein 3 (LC3) plays an important role in autophagosome biogenesis and closure and undergoes lipidation with phosphatidylethanolamine, which yields LC3II, that associates to the surface of the autophagosome and is released upon completion. Monitoring the protein level of LC3II and p62/SQSTM1, an autophagy substrate, is one of the most common methods used to study the autophagic flux.<sup>[180]</sup> Chloroquine inhibits the autophagic flux by interfering with the autophagosome-lysosome fusion. Therefore, the presence of Chloroquine allows quantifying the amplitude of the autophagic flux as it stops the turnover of LC3II and p62/SQSTM1.<sup>[182]</sup>

To investigate the influence of the tetrahydroindolo[2,3-a]quinolizines **10-13** on the autophagic flux, the number of LC3II puncta per cell was monitored in the presence and absence of 50  $\mu$ M Chloroquine.



## RESULTS

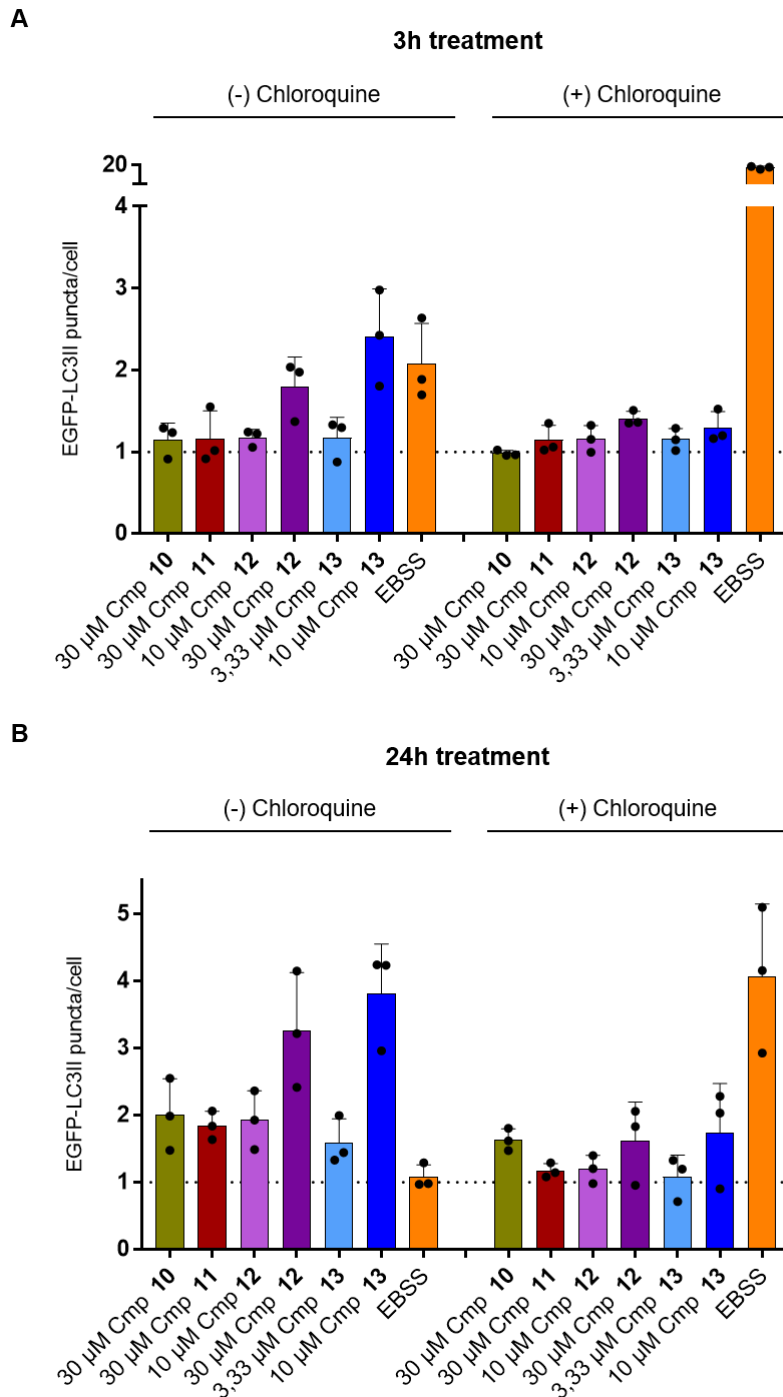


**Figure 45: Influence of compounds 10-13 on the number of LC3II puncta.**

MCF7 cells stably expressing EGFP-LC3 were treated for 3 h (A) and 24 h (B) with compounds (cmp), DMSO or EBSS (for amino acid starvation) as controls, in the absence or presence of 50 μM Chloroquine (CQ) prior to staining with Hoechst for visualizing DNA. The number of LC3II puncta was quantified as a measure of autophagy. Data were normalized to the DMSO control and are mean values  $\pm$  SD of three independent experiments.

Treatment of cells with Earle's Balanced Salt Solution (EBSS), which does not contain amino acids, activates autophagy via amino acid starvation.

## RESULTS

Figure 45 illustrates that EBSS induced autophagy after 3 h and to a lesser extent after 24 h of treatment. As expected, the corresponding increase in LC3II puncta was only visible in the presence of Chloroquine as it blocks the autophagosome-lysosomal fusion and thus, the degradation of EGFP-LC3II. Treatment of cells with 30  $\mu$ M compounds **10** and **11** showed neither an effect in the presence or absence of Chloroquine nor at the different time points. On the contrary, 10  $\mu$ M compound **13** and less potently 30  $\mu$ M compound **12** increased the number of puncta in the absence of Chloroquine, whereas no effect was observed in the presence of Chloroquine. Compared to the 24 h treatment, which increased the number of puncta of approx. 3 and 4- fold for 30  $\mu$ M compound **12** and 10  $\mu$ M compound **13**, respectively, the influence was less pronounced after 3 h of treatment. The lower concentrations of 10  $\mu$ M compound **12** and 3.33  $\mu$ M compound **13** were inactive in all measured conditions.

To distinguish between induction or perturbation of the autophagic flux, the protein levels of LC3II and p62/SQSTM1 upon treatment with compound **12** and **13** were analyzed by immunoblotting, as they possessed an effect in the LC3II puncta assay.

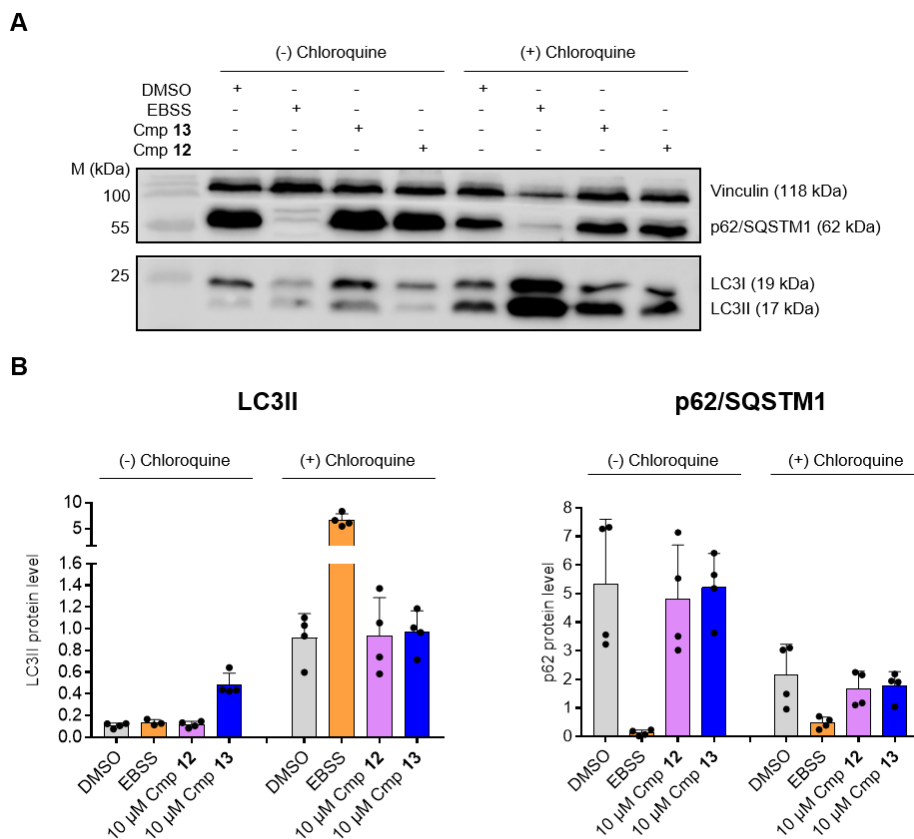


**Figure 46: Influence of compounds 12 and 13 on the protein levels of LC3II and p62/SQSTM1.**

U-2OS cells were treated for 24 h with 10  $\mu$ M compound **12** and **13** or DMSO or EBSS in the absence or presence of 50  $\mu$ M Chloroquine (CQ). Protein levels were determined using immunoblotting. (A)

## RESULTS

---

Images are representative of four independent experiments. (B) Quantified band intensities are mean values  $\pm$  SD of four independent experiments.

As expected, amino acid starvation using EBSS increased the LC3II protein level in the presence of Chloroquine (Figure 46A, B). p62/SQSTM1 functions as an adaptor molecule interacting with polyubiquitinated protein aggregates and LC3II at the phagophore for the selective uptake and degradation of the autophagic cargo.<sup>[183]</sup> p62/SQSTM1 itself is a substrate of autophagy<sup>[184]</sup> and therefore is degraded upon amino acid starvation in the absence of Chloroquine, which can be seen by the decreased protein level compared to the DMSO control. In accordance with the LC3II puncta assay, 10  $\mu$ M compound **12** did not influence the protein levels of LC3II and p62/SQSTM1 compared to the DMSO control. Also, in line with the LC3II puncta assay (Figure 45), 10  $\mu$ M compound **13** increased the LC3II protein level in the absence but not in the presence of Chloroquine. However, compound **13** did not affect the protein levels of p62/SQSTM1 compared to the DMSO control. An increase in the LC3II protein level solely in the absence of Chloroquine without changes in the p62/SQSTM1 level indicates that at 10  $\mu$ M only compound **13** inhibited autophagy at a later stage of the autophagic flux. Hence, compound **13** acts similar to Chloroquine, which may result from their lysosomotropic properties.

Moreover, a disturbed intracellular cholesterol homeostasis upon exposure to amphiphilic molecules may affect the transport and budding of endocytic vesicles. This could be due to an altered lipid raft composition, a change in membrane elasticity or due to a defective calcium homeostasis inside the acidic compartments.<sup>[44]</sup> For this reason, the influence of tetrahydroindolo[2,3-a]quinolizines **10-13** on the endocytic uptake of transferrin was investigated using transferrin conjugated to a fluorophore (AF594-Transferrin).

## RESULTS

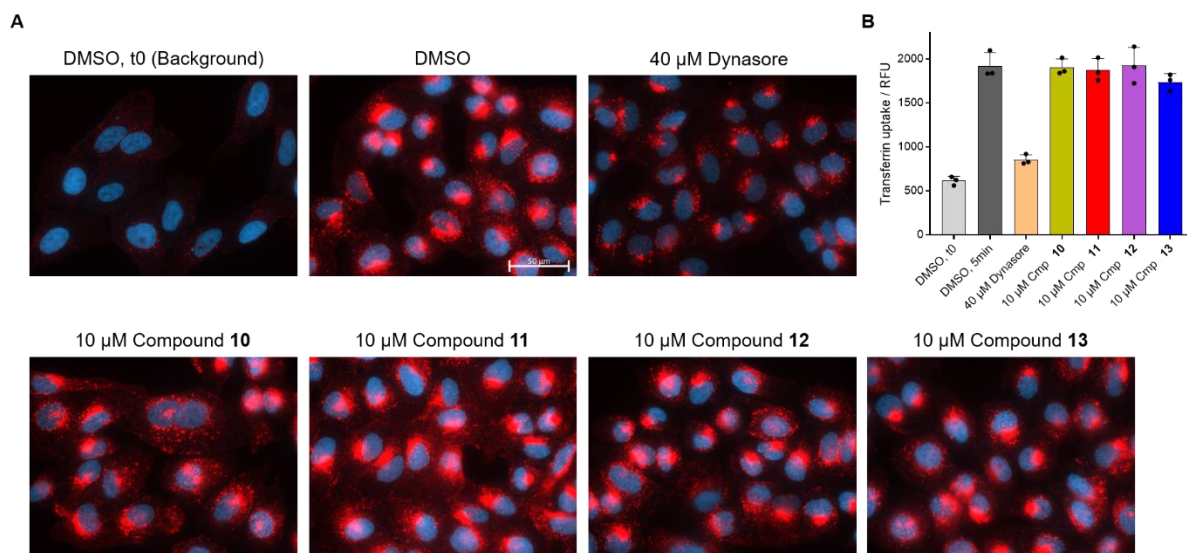


**Figure 47: Influence of compounds 10-13 on the endocytotic uptake of transferrin.**

U-2OS cells were treated for 3 h with the compounds (cmp) or DMSO or dynasore as controls prior to addition of AF594-Transferrin (red) and incubation for 2 min at RT to stop endocytosis. A background DMSO sample (t0) was immediately fixed and stained with DAPI for visualizing DNA (blue). All other samples were incubated for 5 min at 37 °C to initiate endocytosis before fixation and staining with DAPI. (A) Representative images (scale bar: 50 μm) and (B) quantification of three independent experiments.

Dynasore was used as a control as it inhibits the GTPase activity of dynamin, which is responsible for the constriction and fission of endocytic vesicles.<sup>[185]</sup> Figure 47 illustrates that treatment of the cells with dynasore led as expected to a concentration-dependent decrease in the uptake of transferrin compared to the DMSO control. However, none of the compounds affected the transferrin uptake at 10 μM.

Collectively, the experiments to investigate the lysosomotropic-related bioactivity of the tetrahydroindolo[2,3-a]quinolizines **10-13** revealed that compound **13** exhibited the most pronounced effects, which is in line with the lysosomotropic potency of the compounds (Figure 32). Compound **13** led to an accumulation of cholesterol, most likely in acidic organelles, disturbing the intracellular distribution. Furthermore, compound **13** blocked the autophagic flux, similar to the lysosomotropic drug Chloroquine, at a later stage of autophagy. However, compound **13** did not influence the endocytic uptake of transferrin.

### 6.2.6 Analysis of reference compounds biosimilar to compound 13

The morphological fingerprint of compound **13** was biosimilar to 12.5 % of the reference compounds (449 of 3580) and to 8 % of the in-house compounds (768 of 9619), hence a similar effect on lysosomes and cholesterol homeostasis was assumed. For neuronal receptors, morphological profile similarity has been suggested based on their accumulation in

## RESULTS

lysosomes as a consequence of their physicochemical properties.<sup>[84, 186]</sup> Therefore, 32 references, representing different chemical structures and target classes were selected and tested for their modulation of SREBP-dependent transcription and their influence on lysosomal staining. The structures of the selected references can be reviewed in the appendix (Table 19). For most of the references from the cluster, a link to lysosomotropism is already reported. Therefore, references, for which lysosomotropism was not indicated, were selected and comprise compounds targeting GPCRs, enzymes and especially kinases, ion channels and a group of compounds with miscellaneous activities. These compounds were tested at concentrations for which the highest biosimilarity to 10  $\mu\text{M}$  compound **13** was detected in the CPA.

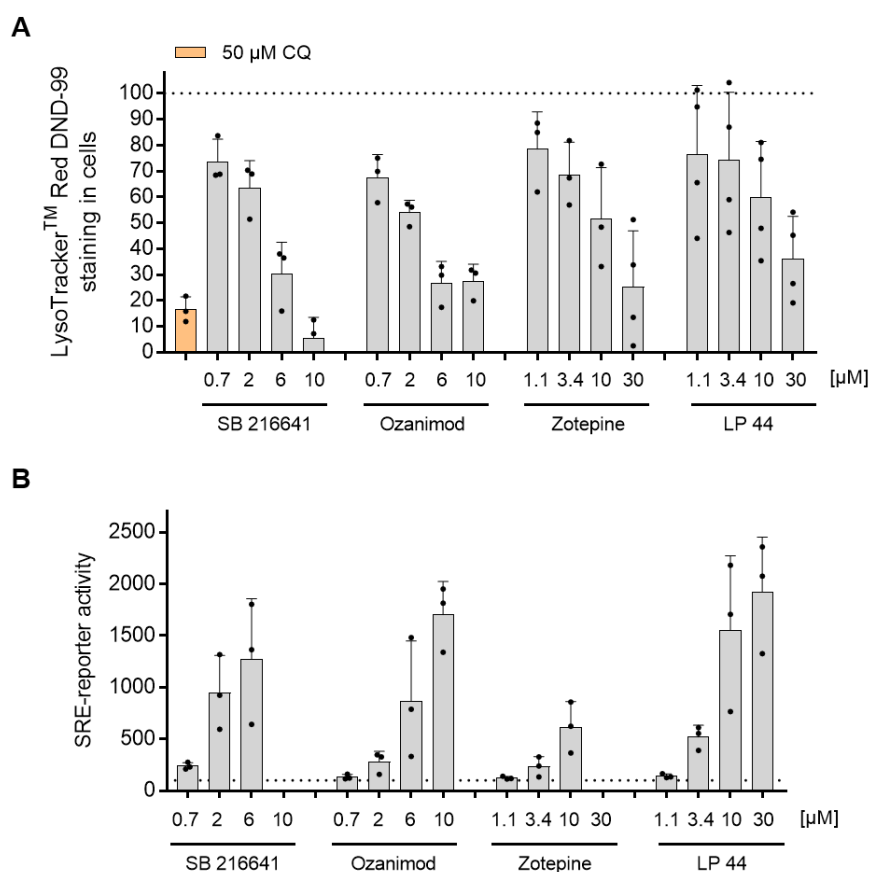


**Figure 48: Influence of selected GPCR-targeting references on SREBP-dependent transcriptional activation and lysosomal staining.**

(A) U-2OS cells incubated for 1 h with the compounds or DMSO or Chloroquine as controls prior to staining with LysoTracker™ Red DND-99. Data are mean values  $\pm$  SD of three or four independent experiments. Values were normalized to DMSO (100 %, dotted line). (B) U-2OS cells were transfected with a firefly luciferase construct under the control of the HMG-CoA synthase promoter and a plasmid for constitutive *Renilla* luciferase expression. Cells were treated for 24 h with the compounds or DMSO prior to the determination of both luciferase activities. Data are mean values  $\pm$  SD of three independent

## RESULTS

experiments. Missing concentrations were toxic and therefore excluded from the data set. Values were normalized to DMSO (100 %, dotted line).

Chloroquine was used as a positive control for the lysosomal staining as it reduces the staining based on its lysosomotropic properties. Figure 48 demonstrates that the four selected GPCR-targeting references SB216641, Ozanimod, Zotepine and LP 44 not only dose-dependently decreased lysosomal staining (Figure 48A) but also activated the SREBP-dependent reporter in a concentration-dependent manner (Figure 48B). Whereas the lowest tested concentrations ( $\leq 1.1 \mu\text{M}$ ) decreased the LysoTracker staining only to a maximum of 30 %, the highest concentrations ( $\geq 10 \mu\text{M}$ ) reduced the staining by at least 60 %. Concentrations  $\geq 6 \mu\text{M}$  activated the reporter to at least 5-fold.

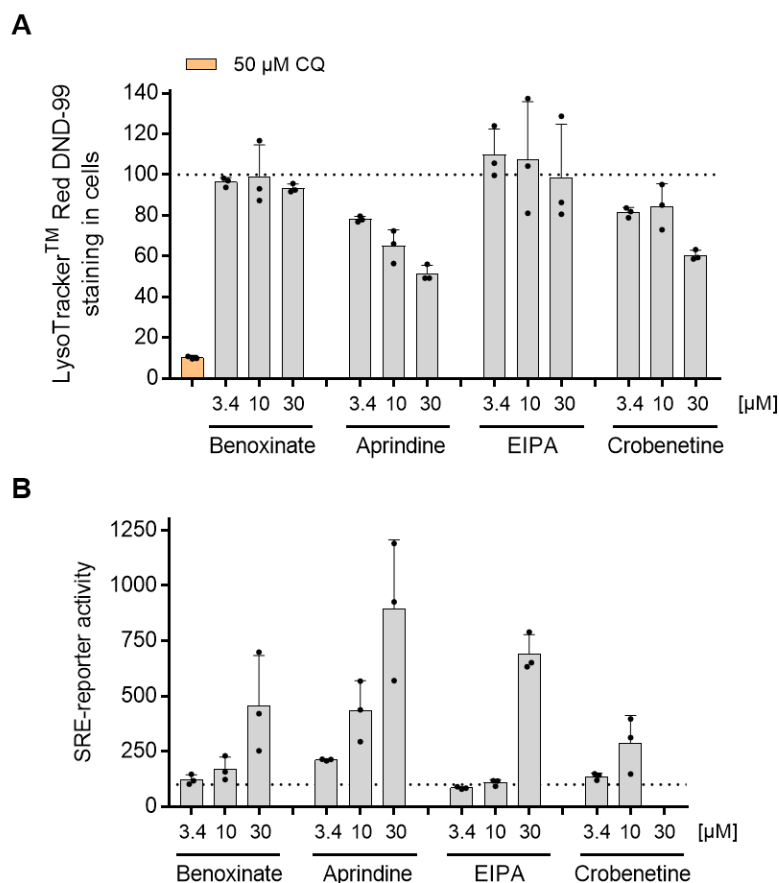


**Figure 49: Influence of selected ion channel-targeting references on SREBP-dependent transcriptional activation and lysosomal staining.**

(A) U-2OS cells incubated for 1 h with the compounds or DMSO or Chloroquine as controls prior to staining with LysoTracker™ Red DND-99. Data are mean values  $\pm$  SD of three independent experiments. Values were normalized to DMSO (100 %, dotted line). (B) U-2OS cells were transfected with a firefly luciferase construct under the control of the HMG-CoA synthase promoter and a plasmid for constitutive *Renilla* luciferase expression. Cells were treated for 24 h with the compounds or DMSO prior to the determination of both luciferase activities. Data are mean values  $\pm$  SD of three independent

## RESULTS

experiments. Missing concentrations were toxic and therefore excluded from the data set. Values were normalized to DMSO (100 %, dotted line).

Figure 49 demonstrates that the four selected ion channel-targeting references Benoxinate, Aprindine, EIPA and Crobenetine displayed different activities in both assays. Benoxinate did not influence the lysosomal staining but activated the SREBP-dependent reporter by 5-fold at the highest concentration of 30  $\mu\text{M}$ . Aprindine treatment induced a concentration-dependent decrease in lysosomal staining with a residual signal of 50 % at the highest concentration of 30  $\mu\text{M}$ . Aprindine also led to a concentration-dependent activation of the SREBP-dependent reporter by 9-fold at 30  $\mu\text{M}$ . EIPA treatment did not influence the lysosomal staining but activated the SREBP-dependent reporter by 8-fold at 30  $\mu\text{M}$ . Crobenetine only showed a slight effect on the lysosomal staining and reduced the signal by 40 % at the highest concentration of 30  $\mu\text{M}$ . On the other hand, treatment for 24 h with 30  $\mu\text{M}$  was toxic and 10  $\mu\text{M}$  Crobenetine only slightly activated the SREBP-dependent reporter by 3-fold.

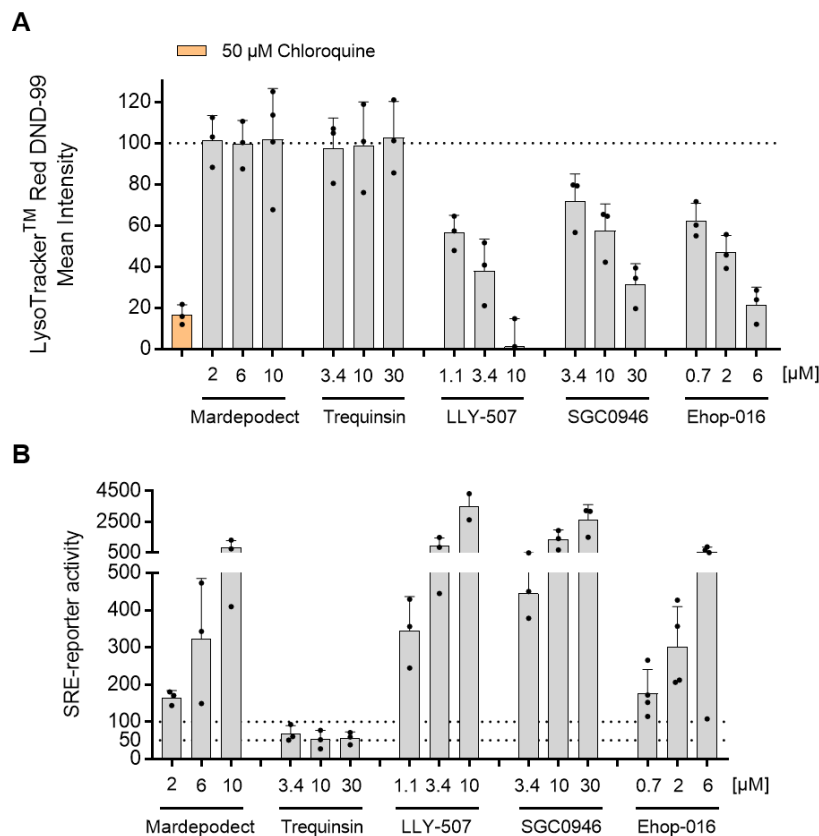


**Figure 50: Influence of selected enzyme-targeting references on SREBP-dependent transcriptional activation and lysosomal staining.**

(A) U-2OS cells incubated for 1 h with the compounds or DMSO or Chloroquine as controls prior to staining with LysoTracker™ Red DND-99. Data are mean values  $\pm$  SD of three independent experiments. Values were normalized to DMSO (100 %, dotted line). (B) U-2OS cells were transfected

## RESULTS

with a firefly luciferase construct under the control of the HMG-CoA synthase promoter and a plasmid for constitutive *Renilla* luciferase expression. Cells were treated for 24 h with the compounds or DMSO prior to the determination of both luciferase activities. Data are mean values  $\pm$  SD of three or four independent experiments. Values were normalized to DMSO (100 %, dotted line).

Figure 50 demonstrates that the five selected enzyme-targeting references Mardepodect, trequinsin, LLY-507, SGC0946 and EHOp-016 displayed different activities in both assays. Mardepodect did not influence the lysosomal staining but activated the SREBP-dependent reporter in a concentration-dependent manner up to 8-fold at 10  $\mu$ M. Trequinsin did not affect the lysosomal staining but inhibited the SREBP-dependent reporter by 50 % at 10 and 30  $\mu$ M. 3.4  $\mu$ M trequinsin inhibited the SREBP-dependent reporter, however, only by 30 %. Treatment with LLY-507, SGC0946 and EHOp-016 led to a concentration-dependent decrease in the lysosomal staining as well as to an activation of the SREBP-dependent reporter in a dose-dependent manner. The highest tested concentration of 10  $\mu$ M LLY-507, 30  $\mu$ M SGC0946 and 6  $\mu$ M EHOp-016 reduced the lysosomal staining by 99, 70 and 80 %, respectively, and activated the SREBP-dependent reporter by 35-, 27- and 5.5-fold, respectively.

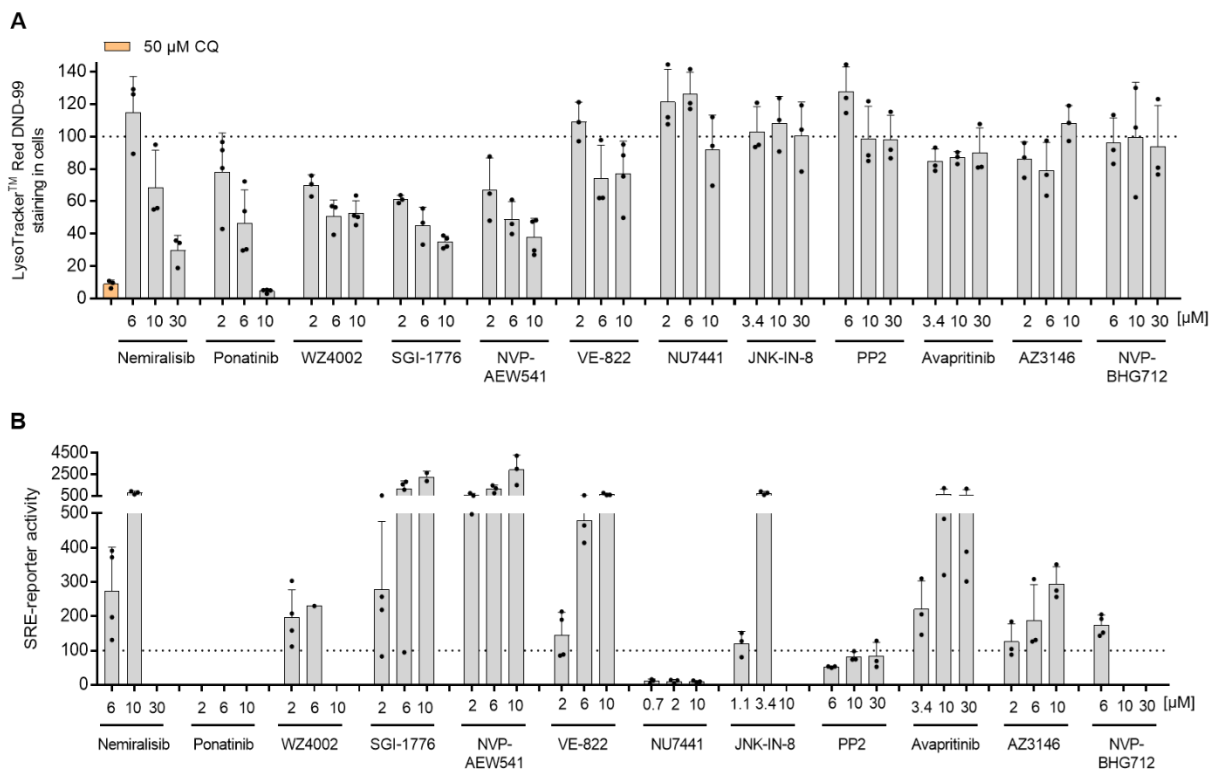


**Figure 51: Influence of selected kinase-targeting references on SREBP-dependent transcriptional activation and lysosomal staining.**

(A) U-2OS cells incubated for 1 h with the compounds or DMSO or Chloroquine as controls prior to staining with LysoTracker™ Red DND-99. Data are mean values  $\pm$  SD of three independent experiments. Values were normalized to DMSO (100 %, dotted line). (B) U-2OS cells were transfected



## RESULTS

---

with a firefly luciferase construct under the control of the HMG-CoA synthase promoter and a plasmid for constitutive *Renilla* luciferase expression. Cells were treated for 24 h with the compounds or DMSO prior to the determination of both luciferase activities. Data are mean values  $\pm$  SD of three independent experiments. Missing concentrations were toxic and therefore excluded from the data set. Values were normalized to DMSO (100 %, dotted line).

Among the enzyme-targeting references of the cluster, 75.4 % were kinase inhibitors (Figure 30). Therefore, 12 kinase inhibitors were selected for testing their influence on the lysosomal staining and SREBP-mediated gene expression. Figure 51 shows that the treatment with Nemiralisib, Ponatinib, WZ4002, SGI-1776 and NVP-AEW541 induced a concentration-dependent decrease in the lysosomal staining. At the highest concentration of 30  $\mu$ M Nemiralisib, 10  $\mu$ M Ponatinib, 10  $\mu$ M WZ4002, 10  $\mu$ M SGI-1776 and 10  $\mu$ M NVP-AEW541, the lysosomal staining was reduced by 70, 95, 50, 65 and 62 %, respectively. VE-822, NU7441, JNK-IN-8, PP2, Avapritinib, AZ3146 and NVP-BHG712 did not influence the staining. 10  $\mu$ M Nemiralisib induced the SREBP-dependent transcription by 8-fold. The 24 h treatment with Ponatinib was toxic at all measured concentrations (2-10  $\mu$ M). WZ4002 induced the SREBP-dependent transcriptional activation by 2-fold at 2  $\mu$ M as well as 6  $\mu$ M. Treatment with SGI-1776, NVP-AEW541 and VE-822 provoked a concentration-dependent increase of SREBP-dependent transcription by 23-, 29- and 6.5-fold at 10  $\mu$ M. All tested concentrations of NU7441 suppressed the SREBP-mediated reporter gene expression. JNK-IN-8 stimulated the SREBP-dependent reporter at 3.4  $\mu$ M by approx. 8-fold, whereas treatment of cells with a higher dose of 10  $\mu$ M was toxic. PP2 did not influence the SREBP-mediated reporter gene expression. Avapritinib and AZ3146 led to a concentration-dependent induction of the SREBP-mediated reporter by 6- and 3- fold at 30 and 10  $\mu$ M, respectively. NVP-BHG712 showed cytotoxic effects at 10 and 30  $\mu$ M and 6  $\mu$ M induced the SREBP-mediated reporter by approx. 2-fold.

## RESULTS

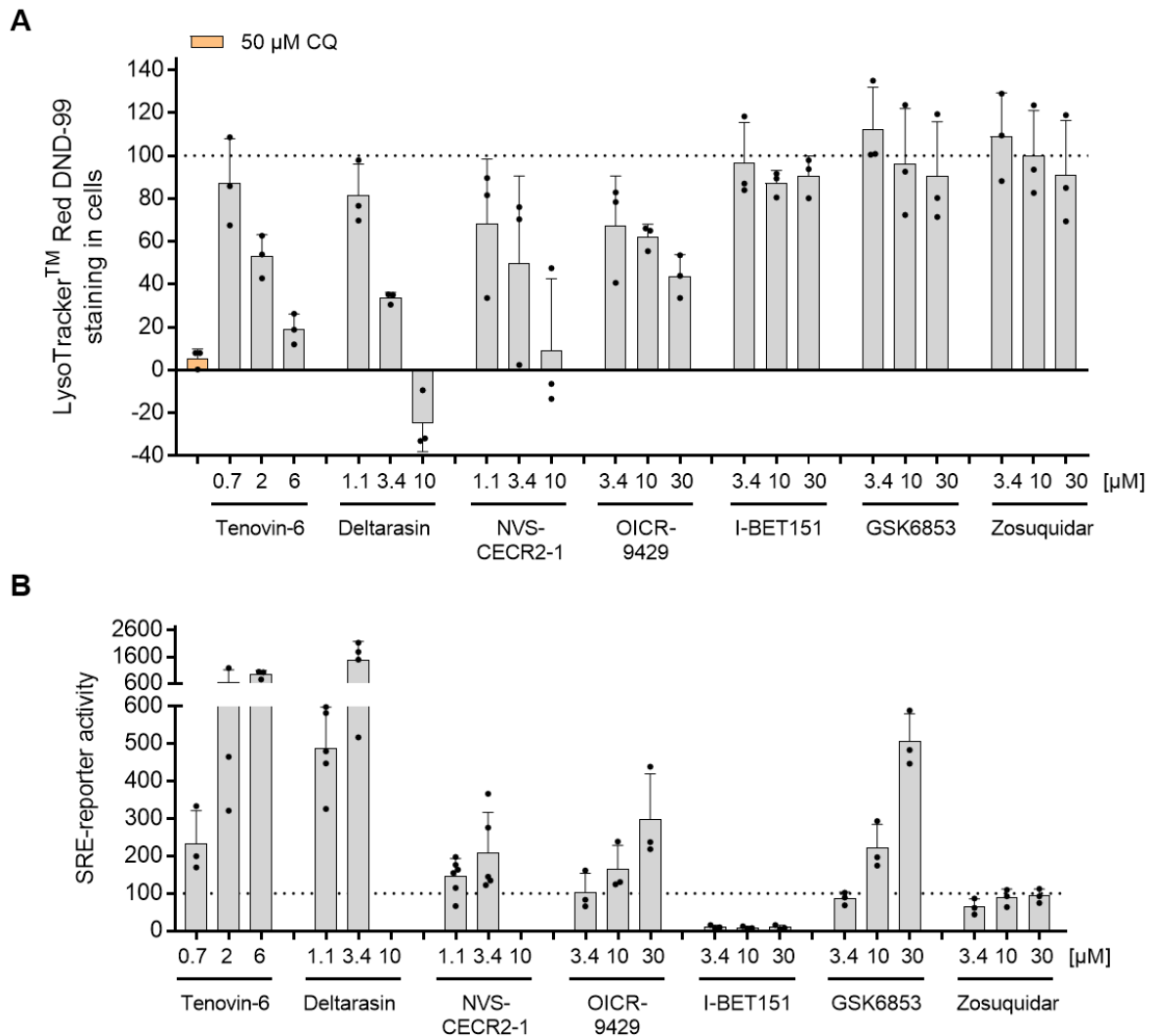


**Figure 52: Influence of selected references with miscellaneous targets and activities on SREBP-dependent transcriptional activation and lysosomal staining.**

(A) U-2OS cells incubated for 1 h with the compounds or DMSO or Chloroquine as controls prior to staining with LysoTracker™ Red DND-99. Data are mean values  $\pm$  SD of three independent experiments. Values were normalized to DMSO (100 %, dotted line). (B) U-2OS cells were transfected with a firefly luciferase construct under the control of the HMG-CoA synthase promoter and a plasmid for constitutive *Renilla* luciferase expression. Cells were treated for 24 h with the compounds or DMSO prior to the determination of both luciferase activities. Data are mean values  $\pm$  SD of three or more independent experiments. Missing concentrations were toxic and therefore excluded from the data set. Values were normalized to DMSO (100 %, dotted line).

Figure 52 demonstrates that the selected references with miscellaneous targets displayed different activities in both assays. Tenovin-6 and deltarasin dose-dependently decreased the lysosomal staining. Deltarasin is an inhibitor of the KRAS-PDE $\delta$  interaction<sup>[187]</sup> and tenovin-6 is a potent activator of p53, but also inhibits the protein deacetylase activity of SIRT1-3 *in vitro*.<sup>[188, 189]</sup> 6  $\mu$ M tenovin-6 reduced the staining by 80 % and 10  $\mu$ M deltarasin decreased the signal down to -25 %.

## RESULTS

---

Since the LysoTracker mean intensity of 100  $\mu$ M Chloroquine was used as a control in this assay and subtracted as a background signal, negative values can emerge from this analysis if a compound reduces the staining more potently than the control of 100  $\mu$ M Chloroquine. 6  $\mu$ M tenovin-6 and 3.4  $\mu$ M deltarasin activated the SREBP-dependent reporter by 9- and 15-fold, respectively. The CECR2 (cat eye syndrome chromosome region, candidate 2) inhibitor NVP-CECR2-1<sup>[190]</sup> and OICR-9429 an antagonist of the interaction between WDR5 (WD repeat domain 5) and MLL1 (mixed lineage leukemia protein 1)<sup>[191]</sup> dose-dependently decreased the lysosomal staining and activated the SREBP-mediated gene expression. 3.4  $\mu$ M NVS-CECR2-1 and 30  $\mu$ M OICR-9429 reduced the lysosomal staining by 90 and 60 %, respectively, and activated the reporter by 2- and 3-fold, respectively. The BET (bromodomain and extra-terminal motif) inhibitor I-BET151<sup>[192]</sup>, the Bromodomain and PHD Finger Containing 1 (BRPF1) inhibitor GSK6853<sup>[193]</sup> and the P-glycoprotein modulator zosuquidar<sup>[194]</sup> did not affect the lysosomal staining. Zosuquidar did also not influence the SREBP-dependent gene expression. However, I-BET151 inhibited the SREBP-dependent gene expression at all measured concentrations (3.4-30  $\mu$ M] by 90 %, whereas GSK6853 dose-dependently activated the gene expression up to 5-fold at 30  $\mu$ M.

Collectively, these results demonstrate that, besides two exceptions namely PP2 and zosuquidar, all references modulated SREBP-dependent gene expression. References that led to a decrease in lysosomal staining also activated the SREBP-dependent gene expression. References that did not influence the lysosomal staining were instead either activating or inhibiting the SREBP-dependent gene expression.

Small molecules may also interfere with the cholesterol homeostasis by directly modulating enzymes involved in the cholesterol biosynthesis (i.e., mevalonate pathway) like statins that inhibit the 3-hydroxy-3-methylglutaryl-coenzyme A reductase (HMGCR), the rate-limiting enzyme of the mevalonate pathway.

## RESULTS

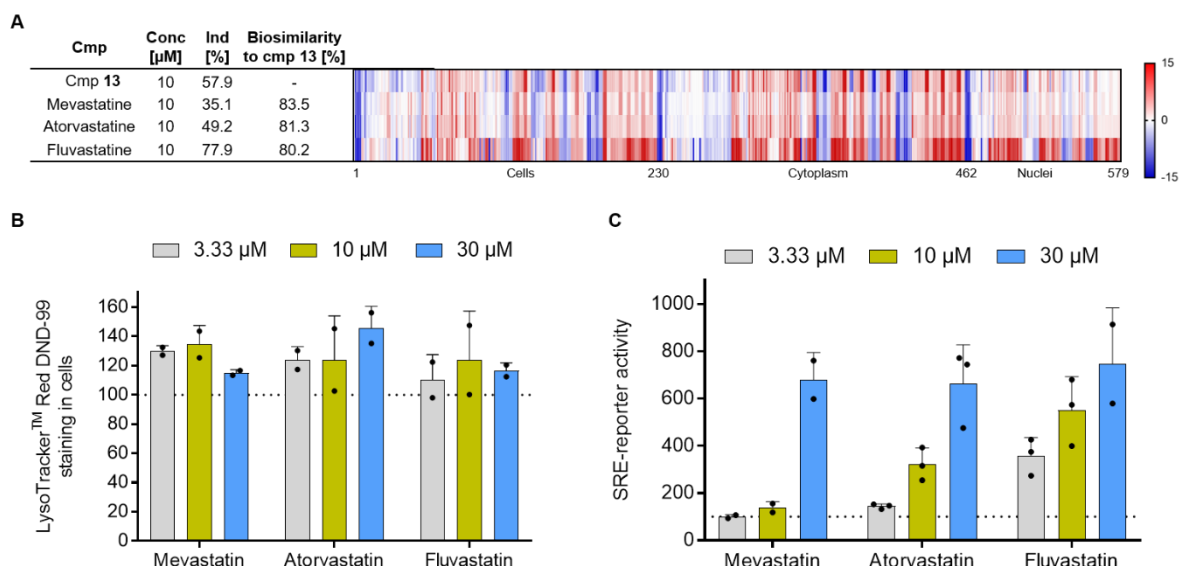


**Figure 53: Morphological fingerprints of statins and their influence on lysosomal staining and SRE-mediated gene expression.**

(A) Morphological fingerprints of statins biosimilar to compound **13**, visualized as heatmap profiles. The top profile is set as a reference (100 % biosimilarity, BioSim) to which the following fingerprints are compared. The set of 579 features is divided into cell (1-229), cytoplasm (230-461) and nuclei (462-579) related features. Values were normalized to the DMSO control. Blue: decreased feature, red: increased feature. (B) U-2OS cells incubated for 1 h with the compounds or DMSO or Chloroquine as controls prior to staining with LysoTracker™ Red DND-99. Data are mean values  $\pm$  SD of two independent experiments. (C) U-2OS cells were transfected with a firefly luciferase construct under the control of the HMG-CoA synthase promoter and a plasmid for constitutive *Renilla* luciferase expression. Cells were treated for 24 h with the compounds or DMSO prior to the determination of both luciferase activities. Data are mean values  $\pm$  SD of two or three independent experiments.

Figure 53 illustrates that the statins Mevastatin, Atorvastatin and Fluvastatin showed high biosimilarity ( $\geq 80$  %) to the fingerprint of compound **13** (Figure 53A). However, without reducing the lysosomal staining (Figure 53B), they activate, as expected, the SRE-dependent reporter gene expression (Figure 53C). The reason may be a negative feedback mechanism that activates SREBP signaling due to reduced cholesterol that is sensed at the ER because of the statin-inhibited cholesterol biosynthesis.

Additionally, SREBP-regulated genes can be explored by the analysis of gene expression profiles. The Broad Institute LINCS Center for Transcriptomics<sup>[41]</sup> (<https://www.ncbi.nlm.nih.gov/geo/query/acc.cgi?acc=GSE70138>) published gene expression profiles (L1000 Connectivity Map (CMap)) for more than 19,000 compounds.

## RESULTS

**Table 5: Modulated genes involved in the biosynthesis of cholesterol upon treatment with indicated compounds.**

Publicly available gene expression profiling data analyzed with IPA. Genes involved in cholesterol biosynthesis were depicted in bold.

| Compound      | Conc. [μM] | Treatment [h] | Cell line   | Genes         | Expr. Log ratio | Expr. p-value |
|---------------|------------|---------------|-------------|---------------|-----------------|---------------|
| SGI1776       | 10         | 24            | A375        | <b>ACAA2</b>  | -1.074          | 7.98E-03      |
|               |            |               |             | HADHA         | 1.07            | 1.97E-02      |
|               |            |               |             | <b>ACAT2</b>  | 1.35            | 4.03E-04      |
|               |            |               |             | HSD17B7       | 1.513           | 1.28E-05      |
|               |            |               |             | <b>MVD</b>    | 1.539           | 4.47E-14      |
|               |            |               |             | SC5D          | 1.969           | 5.34E-04      |
|               |            |               |             | <b>FDPS</b>   | 1.984           | 3.18E-09      |
|               |            |               |             | <b>LSS</b>    | 1.986           | 3.89E-05      |
|               |            |               |             | TM7SF2        | 2.37            | 4.32E-09      |
|               |            |               |             | CYP51A1       | 2.558           | 8.66E-11      |
|               |            |               |             | DHCR7         | 2.925           | 4.42E-12      |
|               |            |               |             | NSDHL         | 2.938           | 2.49E-16      |
|               |            |               |             | <b>IDI1</b>   | 3.068           | 3.17E-09      |
|               |            |               |             | <b>HMGCR</b>  | 3.374           | 3.13E-18      |
|               |            |               |             | <b>FDFT1</b>  | 3.427           | 3.02E-16      |
|               |            |               |             | DHCR24        | 3.757           | 4.28E-08      |
|               |            |               |             | <b>SQLE</b>   | 3.853           | 5.74E-07      |
|               |            |               |             | AEW541        | 10              | 24            |
| EBP           | 0.895      | 3.20E-04      |             |               |                 |               |
| CYP51A1       | 0.944      | 1.31E-02      |             |               |                 |               |
| HSD17B7       | 0.962      | 6.25E-03      |             |               |                 |               |
| <b>ACAT2</b>  | 1.187      | 2.09E-09      |             |               |                 |               |
| <b>FDFT1</b>  | 1.231      | 2.02E-05      |             |               |                 |               |
| <b>SQLE</b>   | 1.242      | 2.78E-03      |             |               |                 |               |
| <b>FDPS</b>   | 1.296      | 5.61E-06      |             |               |                 |               |
| TM7SF2        | 1.3        | 5.52E-04      |             |               |                 |               |
| <b>HMGCR</b>  | 1.307      | 1.46E-12      |             |               |                 |               |
| DHCR24        | 1.427      | 2.20E-02      |             |               |                 |               |
| <b>LSS</b>    | 1.529      | 7.89E-05      |             |               |                 |               |
| NSDHL         | 1.568      | 1.03E-06      |             |               |                 |               |
| <b>HMGCS1</b> | 1.573      | 5.93E-10      |             |               |                 |               |
| SC5D          | 1.573      | 2.54E-02      |             |               |                 |               |
| MSMO1         | 1.592      | 7.65E-04      |             |               |                 |               |
| DHCR7         | 1.675      | 9.15E-06      |             |               |                 |               |
| <b>IDI1</b>   | 1.874      | 2.50E-04      |             |               |                 |               |
| I-BET151      | 3.33       | 24            | SKL myocyte | <b>ACAT2</b>  | -1.594          | 2.81E-07      |
|               |            |               |             | <b>HMGCS1</b> | -0.963          | 2.27E-10      |
|               |            |               |             | EBP           | -0.664          | 2.25E-02      |
|               |            |               |             | GGPS1         | -0.538          | 2.95E-02      |
|               |            |               |             | <b>MVK</b>    | -0.431          | 2.75E-02      |

From the 32 selected references, gene expression profiles for the Pim (provirus integration site for Moloney murine leukemia virus) kinase inhibitor SGI1776<sup>[195]</sup>, the IGFIR (Insulin-like

## RESULTS

---

growth factor I receptor) kinase inhibitor NVP-AEW541<sup>[196]</sup> and the bromodomain inhibitor I-BET151<sup>[192]</sup> were found in the CMap database (Table 5). SGI1776 and AEW541 significantly upregulated genes involved in the *de novo* biosynthesis of cholesterol. I-BET151 reduced their expression as already observed in the SREBP-responsive reporter gene assay.

These results demonstrate that modulation of the cholesterol homeostasis leads to a characteristic protein and gene expression signature, which can even be identified without experimental lab work if gene expression profiles are publicly available.

## 7 DISCUSSION

### 7.1 CPA identified a cluster based on a common MoA

Target identification approaches that are usually employed, like affinity-based chemical proteomics, are limited in the detectable bioactivity space and often restricted to protein targets. Unbiased morphological profiling, e.g., using the CPA, represents a promising approach for the identification of compounds that target non-protein biomolecules like metal ions<sup>[197, 198]</sup>, lipids<sup>[199]</sup>, DNA<sup>[31]</sup> or RNA<sup>[32, 33]</sup>, which emerged as a new research field in recent years. This requires morphological fingerprint similarity between reference compounds based on a shared target or MoA. To examine if CPA can be applied to identify iron-chelating activity, the morphological fingerprints of DFO and biosimilar reference compounds were investigated.

The morphological fingerprints generated for different concentrations of the iron chelator DFO revealed that predominantly features related to the Hoechst staining of the nucleus were affected. Among the Hoechst-unrelated features, the induction of only those features, describing the cell and cytoplasm area shape, dose-dependently increased and reached z-score values  $\geq 10$ . The changes in the nucleus and cell size can be explained by the elemental role of iron. Iron is indispensable for many essential cellular processes, including cell growth and replication.<sup>[102, 113, 115]</sup> DNA synthesis and repair processes require enzymes that need iron as a cofactor, hence, iron depletion is known to induce cell cycle arrest in G1/S phase and to act anti-proliferative.<sup>[114, 115]</sup> The fingerprints for the different concentrations of DFO showed a concentration-dependent increase in the induction and exhibited a high biosimilarity among each other indicating that the fingerprint of each concentration is related to the same bioactivity excluding the possibility of an additional off-target activity at higher concentrations.

#### 7.1.1 Annotated iron-chelating ligands are biosimilar to DFO

The investigation of reference compounds with morphological fingerprint similarity to DFO revealed the metal ion chelating references Ciclopirox, 1,10-phenanthroline, catechol and PAC-1 among the compounds with the highest biosimilarity. Chelating agents are in general not entirely specific for certain metal ions<sup>[200]</sup> but they have preferences in binding (Table 6).

## DISCUSSION

**Table 6: Ion binding preferences of metal ion chelators.**

| Chelating agent     | Preference   |
|---------------------|--|
| Deferoxamine        | $\text{Fe}^{3+} \gg \text{Al}^{3+} > \text{Cu}^{2+} > \text{Zn}^{2+} \approx \text{Co}^{2+} > \text{Ni}^{2+} \approx \text{Fe}^{2+} > \text{Mg}^{2+} > \text{Ca}^{2+} \text{ Sr}^{2+}$ <sup>[103, 200-204]</sup> |
| Ciclopirox          | $\text{Fe}^{3+}$ , trivalent > divalent <sup>[204-206]</sup>   |
| 1,10-Phenanthroline | $\text{Fe}^{2+}$ <sup>[203]</sup><br>$\text{Fe}^{3+} \gg \text{Cu}^{2+} \approx \text{Ni}^{2+} \approx \text{Zn}^{2+}$ <sup>[207]</sup>  |
| Catechol            | $\text{Fe}^{3+}$ , trivalent > divalent cations <sup>[203, 208]</sup>  |

In general, DFO, Ciclopirox, 1,10-phenanthroline as well as catechol prefer trivalent over divalent metal ions. Ciclopirox, 1,10-phenanthroline and catechol exhibit the highest affinity for ferric ( $\text{Fe}^{3+}$ ) and ferrous ( $\text{Fe}^{2+}$ ) ions, whereas DFO has a very high selectivity for ferric ions. PAC-1 is known to activate procaspase-3 by chelating zinc ions<sup>[111]</sup> but also iron-chelating activity was reported recently.<sup>[209]</sup> Hence, the morphological fingerprint similarity among the identified metal ion chelators can be ascribed to the complexation of iron rather than other metal ions. Ciclopirox, 1,10-phenanthroline, PAC-1 and catechol did not only exhibit a high biosimilarity to DFO but were also highly biosimilar among each other with a median biosimilarity of 87.2 %, demonstrating that iron chelators form a cluster in the CPA. This led to the assumption that this small cluster can be used to identify not only annotated iron chelators but also novel iron-complexing agents.

Target prediction using cheminformatic methods is often performed after phenotypic screening or morphological profiling. This *in silico* approach is typically based on chemical-structural and structure-sequence similarities among proteins, restricting the identification to protein targets.



## DISCUSSION

**Table 7: Target prediction for iron chelators using web-based cheminformatic tools.<sup>[210]</sup>**

Iron-chelating bioactivity is depicted in bold.

| Website                                     | Top predicted activity/target  |  |  |
|---|--|--|--|
|   | DFO  | Ciclopirox   | 1,10-Phenanthroline  |
| PASS<br>Online                              | <ul style="list-style-type: none"> <li><b>Iron antagonist</b></li> <li>CDP-glycerol glycerophosphotransferase inhibitor</li> <li>Polyamine-transporting ATPase inhibitor</li> <li>Mucositis treatment</li> <li>Antidote</li> </ul>               | <ul style="list-style-type: none"> <li>Antiseborrheic</li> <li>Testosterone 17<math>\beta</math>-dehydrogenase inhibitor</li> <li>Polarization stimulant</li> <li>CYP2J substrate</li> <li>Membrane permeability inhibitor</li> </ul>                | <ul style="list-style-type: none"> <li>Dehydro-L-gulonate decarboxylase inhibitor</li> <li>Glutathione thiolesterase inhibitor</li> <li>Amine dehydrogenase inhibitor</li> <li>Taurine dehydrogenase inhibitor</li> <li>Alkane 1-monoxygenase inhibitor</li> </ul> |
| Similarity<br>ensemble<br>approach<br>(SEA) | <ul style="list-style-type: none"> <li>ATP-dependent molecular chaperone HSP82</li> <li>Glutamate receptor 1</li> <li>Deoxyhypusine synthase</li> <li>Acetylpolyamine amidohydrolase</li> <li>Putative agmatine deiminase</li> </ul>             | <ul style="list-style-type: none"> <li>Heat shock protein 90</li> <li>Acetyl-CoA carboxylase</li> <li>Isocitrate dehydrogenase</li> <li>Taste receptor type 1</li> </ul>   | <ul style="list-style-type: none"> <li>Heat shock protein 90</li> <li>C-C chemokine receptor</li> <li>Mitochondrial import inner membrane translocase</li> <li>Neutrophil collagenase</li> <li>Matrix metalloproteinase-9</li> </ul>                               |
| Swiss<br>Target<br>Prediction               | <ul style="list-style-type: none"> <li>Matrix metalloproteinase 1</li> <li>Endothelin-converting enzyme 1</li> <li>Histone deacetylase 6</li> <li>Histone deacetylase 2</li> <li>Histone deacetylase 3/Nuclear receptor corepressor 2</li> </ul> | <ul style="list-style-type: none"> <li>Isocitrate dehydrogenase</li> <li>Poly [ADP-ribose] polymerase 1</li> <li>Dihydroorotate dehydrogenase</li> <li>Cystic fibrosis transmembrane conductance regulator</li> <li>Nitric oxide synthase</li> </ul> | <ul style="list-style-type: none"> <li>C-C chemokine receptor</li> <li>Monoamine oxidase B</li> <li>Indoleamine 2,3-dioxygenase</li> <li>Quinone reductase 2</li> <li>Serotonin 3a receptor</li> </ul>   |
| SuperPred                                   | <ul style="list-style-type: none"> <li><b>Iron chelating agent</b></li> <li>DNA topoisomerase II alpha</li> <li>Hypoxia-inducible factor 1 alpha</li> <li>DNA polymerase iota</li> <li>Geminin</li> </ul>  | <ul style="list-style-type: none"> <li>Adenosine receptors</li> <li>Adrenergic receptor</li> <li>Angiotensin II type 2 receptor</li> <li>Bradykinin B2 receptor</li> <li>C-C chemokine receptor</li> </ul>   | <ul style="list-style-type: none"> <li>Androgen receptor</li> <li>Arachidonate 5-lipoxygenase</li> <li>C-C chemokine receptor</li> <li>Cytochrome P450</li> <li>Estrogen receptor alpha</li> </ul>   |
| STITCH                                      | <ul style="list-style-type: none"> <li>Transferrin receptor</li> <li>Hypoxia-inducible factor 1 alpha</li> <li>Solute carrier family 11 member</li> <li>Aconitase 1</li> <li>Tumor protein p53</li> </ul>  | <ul style="list-style-type: none"> <li>Prostaglandin-endoperoxide synthase</li> <li>ATPase alpha 1 polypeptide</li> <li>Arachidonate 15-lipoxygenase</li> <li>Hypoxia inducible factor 1</li> <li>Nuclear receptor subfamily 3</li> </ul>            |  |
| PPB2  | <ul style="list-style-type: none"> <li>Matrix metalloproteinase-2</li> <li>Arachidonate 5-lipoxygenase</li> <li>Cannabinoid CB1 receptor</li> <li>Matrix metalloproteinase-3</li> <li>Carbonic anhydrase II</li> </ul>                           | <ul style="list-style-type: none"> <li>Isocitrate dehydrogenase</li> <li>11-beta-hydroxysteroid dehydrogenase</li> <li>Phosphodiesterase 7A</li> <li>Dopamine receptor</li> <li>Adenosine receptor</li> </ul>  | <ul style="list-style-type: none"> <li>Vascular endothelial growth factor receptor 2</li> <li>Serotonin receptor</li> <li>Nuclear factor NF-kappa-B p65 subunit</li> <li>Kappa opioid receptor</li> <li>Egl nine homolog 1</li> </ul>                              |

Table 7 illustrates that several web-based cheminformatic tools failed to predict iron-chelating activity for Ciclopirox and 1,10-phenanthroline. This was not unexpected as those approaches rely on either structural similarity, which is not given for iron chelators, or on known compound-protein interactions. Only the PASS algorithm<sup>[211, 212]</sup> and SuperPred<sup>[213]</sup> proposed an iron-

chelating activity for DFO. This highlights the need to extend the target space of cheminformatic approaches to non-protein targets to enable MoA prediction as early as possible.

### 7.1.2 CPA identified a cluster of iron chelators and cell cycle modulators sharing a common MoA

The CPA revealed not only a high fingerprint similarity between DFO and the iron chelators but also to 35 additional references with diverse annotated targets and activities. Table 8 illustrates that some enzymes, targeted by the references, require a metal ion for their activity.

**Table 8: Targets of references, biosimilar to DFO, that require metal ions for their activity.**

| Target                        | Metal ion binding  |
|-------------------------------|--|
| CDK, MAPK p38, AK             | Mg <sup>2+</sup> [214-216]   |
| Topoisomerase                 | Mg <sup>2+</sup> , Mn <sup>2+</sup> , Ca <sup>2+</sup> , Co <sup>2+</sup> [217, 218] |
| poly(ADP-ribose) polymerase   | Zn <sup>2+</sup> [219, 220]  |
| Lysine specific demethylase 1 | Fe <sup>2+</sup> , Zn [221]  |
| Metalloproteinase-2           | Zn [222]   |

However, only the histone demethylase LSD1 is dependent on Fe(II)<sup>[214]</sup> and therefore iron chelation alone can not be the underlying MoA and explain the biosimilarity within the cluster.

Nucleoside analogs, CDK inhibitors, topoisomerase inhibitors, antifolates, PARP inhibitors and DNA intercalating agents have the modulation of the cell cycle as a common denominator. Nucleoside analogs are incorporated into DNA by DNA polymerase during DNA synthesis, which blocks the extension of the nascent strand and activates the DNA damage checkpoint resulting in an S phase arrest of the cell cycle.<sup>[223]</sup> DFO displayed high biosimilarity to nine nucleoside analogs. The bioactivity of nucleoside analogs was investigated using Trifluridine, Arabinocytidine, Cladribine and Fludarabine as representatives, which did not exhibit an iron-chelating activity but led to the accumulation of cells in S phase. One exception was Fludarabine that increased the number of cells in the G1 phase, which has also been reported in the literature<sup>[224]</sup>. Fludarabine is thought to activate p53<sup>[224]</sup>, which has an essential function in DNA damage-induced G1/S arrest<sup>[225]</sup>.

CDKs are the key regulatory proteins of the cell cycle and ensure the proper transitions from one cell cycle phase to the next. Their activity gets periodically activated and deactivated during cell cycle progression and is controlled by cyclins. Thereby, each cell cycle transition is regulated by a different CDK-cyclin-complex.<sup>[226]</sup> DFO displayed high biosimilarity to nine CDK inhibitors whose bioactivity was exemplified by PHA-793887 and roscovitine. Confirming literature reportings, PHA-79388<sup>[119]</sup> and roscovitine<sup>[120]</sup> led to cell cycle arrest in the G2/M phase. PHA-793882 also showed iron-chelating ability at a concentration of 30  $\mu\text{M}$ , however, cell cycle arrest was already detected at a concentration of 3.33  $\mu\text{M}$  and therefore the cell cycle modulating activity is most likely not a result of the iron-chelating ability.

Topoisomerases control the superhelical density during DNA unwinding for replication by transiently cleaving either one (type I) or both (type II) strands of the helix.<sup>[227]</sup> The three topoisomerase inhibitors, biosimilar to DFO, were represented by Topotecan, which did not possess an iron-chelating ability but led to the accumulation of cells in S phase confirming literature findings<sup>[228]</sup>.

Furthermore, DFO displayed morphological fingerprint similarity to antifolates, PARP inhibitors and one MMP-2 and LSD-1 inhibitor. An iron-chelating activity was experimentally excluded, except for the PARP inhibitors, which have not been tested. Nevertheless, a link to cell cycle modulation for those references is already reported in the literature. Folate is a methyl donor required for DNA synthesis and its deprivation is reported to induce cell cycle arrest in the G1/S phase.<sup>[229, 230]</sup> Also, two PARP inhibitors possessed biosimilarity to DFO. The poly(ADP-ribose)-polymerase is involved in DNA repair processes and catalyzes the transfer of ADP-ribose to target proteins involved in nucleic acid metabolism, modulation of chromatin structure and DNA synthesis and repair.<sup>[231]</sup> PARP inhibitors suppress their enzymatic activity and are reported to lead to cell cycle arrest in the S/G2 phase.<sup>[232, 233]</sup> Matrix metalloproteinases degrade (glycol)proteins, membrane receptors, cytokines and growth factors of the extracellular matrix and at the first glance are not linked to a cell cycle-related activity.<sup>[234]</sup> However, several studies demonstrate that MMPs promote tumor growth and therefore inhibitors have been developed as anticancer agents and shown to induce cell cycle arrest.<sup>[235, 236]</sup> And lastly, the genetic depletion or small molecule inhibition of the histone demethylase LSD1 is reported to lead to an accumulation of cells in the G1 phase of the cell cycle.<sup>[237]</sup>

Thus, the biosimilarity of iron-chelating agents and nucleoside analogs, CDK, topoisomerase, PARP, MMP-2 and LSD1 inhibitors in the CPA can be attributed to the shared MoA of cell cycle arrest in the G1/S or G2 phase.

However, there is no straight association between adenosine kinase, MAP kinase p38 and Wnt/ $\beta$ -catenin inhibition and dopamine 1 receptor activation and cell cycle-related activity.

## DISCUSSION

For A-134974, IQ 1 and ( $\pm$ )-SKF-81297, an iron-chelating ability was experimentally excluded. However, the pyrimidinylimidazole inhibitors-3-5, A-134974, IQ 1 and ( $\pm$ )-SKF-81297 may influence the cell cycle via unknown targets that determine the morphological fingerprint, independent of their primary annotated bioactivity. Interestingly, based on its chemical structure, A-134974 belongs to the group of nucleoside analogs (Table 11), which could explain the classification of this adenosine kinase inhibitor into this cluster. Moreover, additional references inhibiting the adenosine kinase have been profiled in the CPA but do not appear in the Fe/DNA synthesis cluster. Furthermore, they are not highly similar among their target class in the CPA supporting the hypothesis of an additional, not annotated target-related effect on the cell cycle.

Clusters of iron chelators and DNA synthesis modulators have been identified in previous morphological studies. Schulze *et al.*<sup>[64]</sup> performed morphological profiling after 19 h of compound treatment and identified a cluster of DNA modulators and iron siderophores by using EdU and a phospho-histone H3 antibody as a mitotic marker. Breinig *et al.*<sup>[129]</sup> treated cells for 48 h, only stained for DNA and actin, and demonstrated clustering of 1,10-phenanthroline with cell cycle modulators. In contrast, the CPA was able to identify clusters of iron-chelating agents and cell cycle modulators without specific staining for cell cycle markers. Thereby, the assay facilitates the coverage of an even broader range of bioactivity, independent of cytostatic effects as the majority of the references did not display a reduction in cell growth after 24 h of treatment but the cell cycle was already arrested at that time. The results presented in this thesis not only expand the set of references that based on their MoA belong to the Fe/DNA synthesis cluster but also enabled the identification of novel iron-chelating agents and DNA synthesis modulators.

**Table 9: Target prediction for 8-hydroxyquinoline using web-based cheminformatic tools.<sup>[210]</sup>**

| Website                            | Top predicted activity/target  |
|------------------------------------|--|
| PASS Online                        | <ul style="list-style-type: none"><li>• Corticosteroid side-chain-isomerase</li><li>• Rhamnulose-1-phosphate aldolase</li><li>• Glycosylphosphatidylinositol phospholipase D</li><li>• Antiseborrheic</li><li>• Magensium-protoporphyrin IX minimethyl ester cyclase</li></ul> |
| Similarity ensemble approach (SEA) | <ul style="list-style-type: none"><li>• Bacterial leucyl aminopeptidase</li><li>• Methionine aminopeptidase 2</li><li>• Solute carrier family 40 member 1</li><li>• NF-kappa-B inhibitor alpha</li><li>• cAMP-specific 3',5'-cyclic phosphodiesterase 4B</li></ul>             |

## DISCUSSION

| Website               | Top predicted activity/target  |
|-----------------------|--|
| SwissTargetPrediction | <ul style="list-style-type: none"> <li>• Methionine aminopeptidase 2</li> <li>• Indoleamine 2,3-dioxygenase</li> <li>• Mannose-6-phosphate isomerase</li> <li>• Proteasome Macropain subunit MB1</li> <li>• Tryptophan 2,3-dioxygenase</li> </ul>                      |
| SuperPred             | <ul style="list-style-type: none"> <li>• Adenosine receptor</li> <li>• Adrenergetic receptor</li> <li>• Androgen receptor</li> <li>• Angiotensin II type 2 receptor</li> <li>• Arachidonate 5-lipoxygenase</li> </ul>  |
| STITCH                | <ul style="list-style-type: none"> <li>• Glycerol dehydrogenase</li> <li>• Inner membrane protein</li> <li>• tRNA(Ile)-lysidine synthase</li> <li>• Quinone oxidoreductase</li> </ul>  |
| PPB2                  | <ul style="list-style-type: none"> <li>• Induced myeloid leukemia cell differentiation protein</li> <li>• Serotonin receptor</li> <li>• Kappa opioid receptor</li> <li>• Vascular endothelial growth factor receptor 2</li> <li>• P53-binding protein Mdm-2</li> </ul> |

Several uncharacterized 8-hydroxyquinoline derivatives were identified to be biosimilar to DFO. Although this is a known motif for a metal-chelating ligand<sup>[102, 127]</sup>, the applied cheminformatic web-based tools failed to predict iron-chelating activity (Table 9). The macrocycle **8** and the natural product-inspired compound **9** were identified as novel cell cycle modulators and blocked cells in S phase. To investigate the underlying mechanism of action, both compounds were explored for their ability to bind DNA and to modulate the activity of the topoisomerase I and II as well as selected CDK/cyclin-complexes. However, the compounds were inactive in all assays but they may still inhibit these enzymes in cells or target other cell cycle regulating proteins.

Hierarchical clustering of fingerprints, biosimilar to DFO, was performed to examine a potential division into subclusters based on the different mechanisms of action. The analysis revealed a separation of the mimetics, i.e., antifolates and nucleoside analogs from the protein modulating compounds. Also, the so-far uncharacterized compounds **4**, **8** and **9** were assigned to the correct subcluster. Compound **4**, representing the 8-hydroxyquinoline scaffold, was correctly allocated to the second subcluster. Furthermore, it was clearly separated from compounds **8** and **9** but close to the other iron-chelating agents. This finding demonstrates that the CPA predicted iron-chelating activity as a mechanism of action for compound **4**, independent of chemical similarity. To generalize this observation, other annotated iron chelators and cell cycle modulators need to be profiled and experimentally evaluated.

In contrast, hierarchical clustering based on only selected staining, e.g., on DNA, actin and plasma membrane/Golgi staining, did not divide the cluster into useful subgroups of different mechanisms of action. This highlights the benefit of multiplexed morphological profiling, like the CPA, that enables identification of clusters that share a MoA and furthermore, has the potential to offer insight into the different mechanisms of action, predicting even target-related bioactivity.

Collectively, these findings prove that the CPA is able to identify the modulation of non-protein targets such as iron-chelating agents and DNA-targeting compounds. The CPA analysis revealed that iron-chelating agents and DNA synthesis modulators form a cluster based on the shared MoA of cell cycle arrest in the G1, S or G2 phase, irrespective of chemical similarity and annotated targets and activities. Thereby the CPA overcomes the limitation of commonly employed target identification approaches like affinity-based proteomics that can only identify protein targets. Several web-based cheminformatic tools failed to predict iron-chelating activity for the annotated iron chelators Ciclopirox and 1,10-phenanthroline, underlining the need to expand the target space that can be identified in these tools. Furthermore, the cluster can now be used to identify novel iron-chelating compounds and cell cycle modulators of the G1, S, or G2 phase. Finally, the hierarchical clustering of members of the Fe/DNA synthesis cluster highlighted that the CPA is technically able to predict even target-related bioactivity by dividing the cluster into subclusters of different mechanisms of action.

## 7.2 Bioactivity of tetrahydroindolo[2,3-a]quinolizines

### 7.2.1 Tetrahydroindolo[2,3-a]quinolizines accumulate in lysosomes

The four tetrahydroindolo[2,3-a]quinolizine derivatives **10-13** were subjected to the CPA to assess their bioactivity. At 10  $\mu\text{M}$ , **10-12** were only very weakly active in the CPA with an induction below 10 %. Interestingly, 10  $\mu\text{M}$  compound **13** strongly induced a phenotypic change with an induction value of 57.9 %, and, therefore compound **13** was selected for further MoA deconvolution. A comparison of its morphological fingerprint with the reference set revealed biosimilarity to 449 references. This large cluster of references comprised different targets and bioactivities hampering a target or MoA prediction for compound **13** based on the annotated activities of the references. Nevertheless, the cluster provided a first hint towards a potential MoA as it is enriched in GPCR ligands and anti-psychotics, which are known to accumulate in lysosomes based on their physicochemical properties<sup>[44, 140]</sup>. Compounds with a logP value above 2 and a bpKa between 6.5 and 11 are prone, and therefore predictive, to accumulate in lysosomes and increase lysosomal pH.<sup>[140]</sup> Most of the references are based on their physicochemical properties most likely lysosomotropic. Compound **13** has these properties with a clogP of 3.7 and a bpKa of 9.1. For this reason, the tetrahydroindolo[2,3-a]quinolizines **10-13** were tested for their influence on lysosomal staining. Compound **11** was inactive in the lysosomotropism assay and also compound **10** was only active at the highest concentration of 30  $\mu\text{M}$ . However, compound **12** and, more potently, compound **13** decreased the lysosomal staining already at 10  $\mu\text{M}$ . Although compound **11** was inactive, its physicochemical properties are predictive of lysosomal accumulation. However, the clogP of compound **11** (clogP: 2.1; bpKa: 7.97) is only slightly higher than 2, which could be an explanation for the weak lysosomotropic effect. In contrast, compound **10** and **12** have a bpKa of 9.64 and 9.65, respectively, and a clogP of 2.95 and 2.75, respectively. Of note, the ion-trapping behavior of the so-called lysosomotropic compounds as well as the LysoTrackerRed DND-99 staining are not selective for lysosomes but concern all organelles with an acidic lumen like the Golgi and endosomes.<sup>[140, 147]</sup> To differentiate between lysosomes and other acidic organelles, one would need a fluorescently-labeled version of the compound. Then, a co-staining could be performed using a lysosomal marker, e.g., an antibody against the lysosome-associated membrane glycoprotein 2 (LAMP2), together with the fluorescently-labeled compound to localize both, lysosomes, and the compound. Interestingly, the trend in activity observed in the lysosomotropism assay reflects the trend in activity in the CPA as assessed by the induction values. At 10  $\mu\text{M}$ , compound **10** and **11** possessed very low induction values and were inactive or only very weakly active in the lysosomotropism assay. Compound **12** and, more potently, compound **13** were active in the CPA as well as in the

lysosomotropism assay. This is also reflected by the biosimilarity values among the four derivatives, where only compound **12** and **13** were biosimilar (85 %) at 10  $\mu\text{M}$  (Figure 29), suggesting that the morphological fingerprint of 10  $\mu\text{M}$  compound **12** and **13** originate from the lysosomotropic activity.

Lysosomotropism is largely cell-type and species independent. As only compound **13** was lysosomotropic at 10  $\mu\text{M}$  and was also the only derivative that affected the growth behavior of U-2OS, HeLa and L-cells, the effect could be related to the lysosomotropic activity. Moreover, a dose of 20  $\mu\text{M}$  compound **13** was toxic after 30 min of treatment. Lysosomotropism has been linked to cell death<sup>[238]</sup>, however, the mechanisms are not well studied and understood. The more hydrophobic the basic molecules are, the lower the concentration at which they are cytotoxic. Hydrophilic basic amines are well tolerated up to millimolar concentrations whereas amphiphilic molecules are able to induce cell death at micromolar concentrations.<sup>[44]</sup> The most frequently observed feature of lysosomotropism is cytoplasmic vacuolization, which has also been observed for compound **13**. As a consequence of lysosomotropic accumulation, compartments become enlarged (vacuolated) due to the influx of water to relieve osmotic pressure and prevent bursting of lysosomes. The exact role in cytotoxicity is unsolved but a prolonged duration of cytoplasmic vacuolization may also lead to irreversible cellular injuries and eventually to cell death.<sup>[146, 147]</sup> Another potential mechanism that could lead to cytotoxicity is via inhibition of autophagy upon exposure to lysosomotropic agents. A blocked autophagic flux was also observed for 10  $\mu\text{M}$  compound **13**. As the autophagic cargo gets degraded by lysosomal acid hydrolases, an increased pH would inhibit the degradation of autophagolysosomes, which has the potential to initiate cell death.<sup>[44, 140, 238]</sup> Furthermore, lysosomal cell death is induced by a permeabilized lysosomal membrane, which leads to the efflux of lysosomal content into the cytosol. Lysosomal membrane permeabilization by lysosomotropic compounds cannot be clearly assigned to a certain mechanism but most likely reflects multiple ways to permeabilize the lysosomal membrane.<sup>[144, 239]</sup>

Treatment with compound **13** at a dose of 10  $\mu\text{M}$  led to cell shrinkage and rounding within the first 30 min after compound addition. Cell shrinkage and rounding goes along with changes in the actin cytoskeleton. Although compound **13** did not influence the actin polymerization *in vitro*, formation of retraction fibers and deformed nuclei were observed. The nuclear shape is preserved by the cytoskeleton.<sup>[240]</sup> The formation of retraction fibers and the deformed nuclei could be a result of a partial loss of adhesion due to the cell rounding induced by compound **13**, similar to cells that undergo mitosis<sup>[241]</sup>. Furthermore, compound **12**, which did not lead to initial cell shrinkage and rounding, did also not lead to the formation of fibers or deformed nuclei.



To examine a potential link between the cell shrinkage and rounding and the lysosomotropic activity, a co-treatment with the v-ATPase inhibitor Bafilomycin A, responsible for the acidic pH in lysosomes, was explored. Therefore, it was expected that lysosomotropic activities of the compound will be rescued by the treatment with Bafilomycin A1. However, the co-treatment did neither reverse the initial cell shrinkage and rounding nor the cytotoxicity induced by compound **13**, suggesting a lysosomotropism-unrelated effect. However, the actual cause remains unsolved. Although Bafilomycin A1 is commonly used as a control inhibitor for the v-ATPase activity<sup>[242-244]</sup>, it is also reported to disrupt mitochondrial function by acting as a potassium ionophore<sup>[245]</sup>. Therefore, more selective v-ATPase inhibitors like concanamycin A or salicylhalamide A, which do not have other known targets<sup>[246]</sup> could be tested.

### **7.2.2 Tetrahydroindolo[2,3-a]quinolizines modulate cholesterol homeostasis**

The lysosomotropic activity of compound **13** seems to influence its morphological fingerprint, hampering a MoA prediction that goes beyond this secondary effect, as compound **13** was biosimilar to more than 400 reference compounds with diverse annotated targets and activities. Therefore, a global proteome profiling was performed to gain more insight into the bioactivity of the tetrahydroindolo[2,3-a]quinolizines. Compound **13** and, less potently, compound **12** led to an upregulation of proteins involved in cholesterol biosynthesis. The upregulation of SREBP-dependent target genes was afterwards experimentally confirmed.

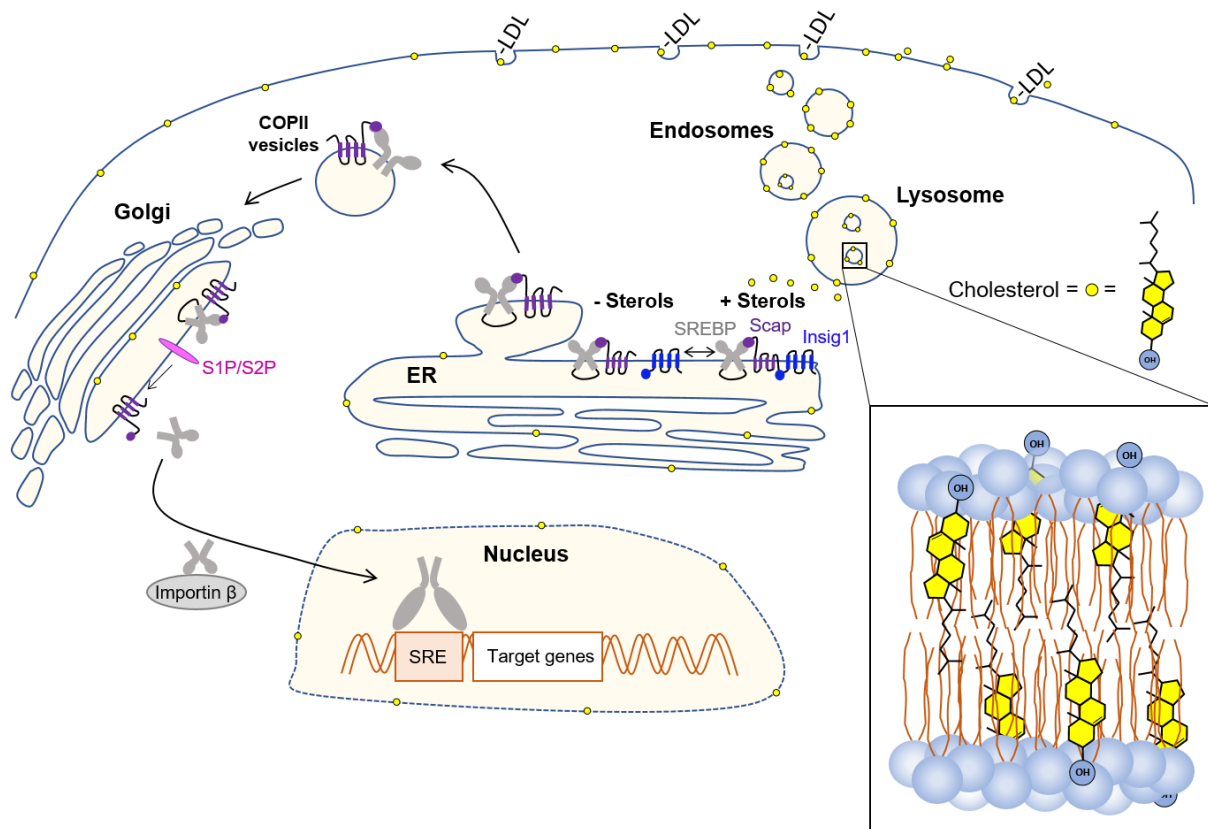


**Figure 54: Regulation of cholesterol homeostasis adapted from P. J. Espenshade.<sup>[247]</sup>**

Cholesterol is taken up via endocytosis in form of low-density-lipoprotein (LDL)-bound cholesteryl esters. Arrived at the lysosomes, cholesterol is hydrolyzed and exported out of the lysosomes. SREBPs are synthesized as inactive precursors anchored in the ER, where cellular cholesterol levels are sensed. SREBP interacts with the sterol-sensor Scap (SREBP cleavage-activating protein) that only binds to the ER-resident protein Insig1 (Insulin-induced gene protein-1) when cholesterol is bound to Scap. The absence of cholesterol disrupts this binding and SREBP-Scap is loaded onto COPII-coated vesicles and transported to the Golgi, where two proteases site-1 (S1P) and site-2 (S2P) release the transcription factor domain of SREBP that is guided into the nucleus by importin  $\beta$ . Transcription is activated by binding of SREBP to the SRE in the promoter region of target genes.

Cholesterol is biosynthesized by all mammalian cells and is a crucial cellular component. It is an important regulator of membrane permeability and fluidity, transmembrane signaling pathways and for the synthesis of steroid hormones, bile acid and vitamin D. Cholesterol is predominantly localized to cell membranes and the majority resides in the plasma membrane. The levels of cholesterol are regulated by the interplay between the *de novo* biosynthesis, uptake, and storage. A tight regulation of these mechanisms is crucial as a disturbed cholesterol homeostasis can cause several human diseases like the neurodegenerative Niemann-Pick type C (NPC) disease, where cholesterol is accumulated in lysosomes. Furthermore, a high plasma concentration of cholesterol can lead to an increased risk for atherosclerotic heart disease. Mammalian cells obtain cholesterol via receptor-mediated endocytosis in form of low-density-lipoprotein (LDL) bound cholesteryl esters.

LDL-cholesterol is then transported through the early and late endosomes to the lysosomes. The lysosomal acid cholesterol esterase lipase A hydrolyses the ester to the unesterified free cholesterol, which subsequently is distributed to the ER and the PM via interacting with sterol transport proteins. The two lysosomal proteins NPC1 and NPC2 are responsible for the export of cholesterol out of the lysosomes. NPC2 is localized inside the lumen of lysosomes and late endosomes and extracts and shuffles cholesterol from internal membranes to the NPC1 protein that is localized at the limiting membrane. Cellular cholesterol levels are sensed at the ER as it is very sensitive to changes in cholesterol level due to its low cholesterol content of less than 1 % of the cell's total cholesterol. Excess cholesterol is esterified by the acyl coenzyme A:cholesterol acyltransferase (ACAT) and stored as reservoirs in cytosolic lipid droplets or released as a component of plasma lipoproteins. The *de novo* biosynthesis of cholesterol occurs at the ER, requiring more than 30 chemical reactions, and is regulated by the transcription factor sterol regulatory element binding protein 2 (SREBP2) via a negative feedback mechanism that senses cholesterol and oxysterols. SREBP2 is attached to the ER membrane and associated with the SREBP cleavage-activating protein (Scap) and the Insulin-induced gene protein-1 (Insig-1). Scap has a sterol-sensing domain, which is also the cholesterol-dependent binding site for Insig-1. Insig-1 is stabilized by Scap as the binding to Scap prevents Insig-1 ubiquitination and degradation. Under cholesterol depleted conditions, the binding of Scap to Insig-1 is disrupted and the SREBP2-Scap complex is sorted onto COPII-coated vesicles and transported to the Golgi. At this site, the transcription factor domain of SREBP gets released via proteolytic cleavage by the two proteases site-1 (S1P) and site-2 (S2P). The active transcription factor domain is escorted into the nucleus by importin  $\beta$  where it activates the transcription by binding to the SRE sequence in the promoter region of target genes. Under cholesterol-replete conditions, the SREBP2-Scap-Insig-1 complex is retained in the ER membrane as the presence of cholesterol or 25-hydroxycholesterol prevents binding of coat proteins to Scap, obviating the assembly of COPII-coated vesicles. [157, 161, 162, 248, 249]

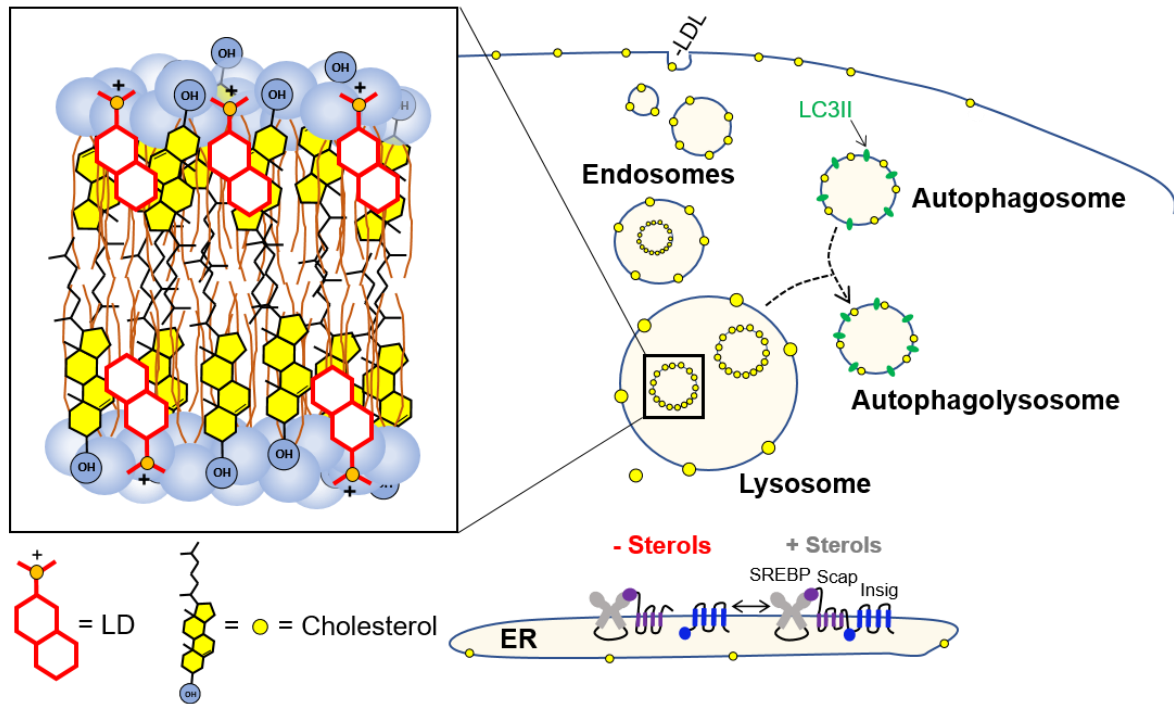


**Figure 55: Possible influences of lysosomotropic compounds on cholesterol homeostasis.**

Lysosomotropic drugs (LD) increase the lysosomal pH and the hydrophobic part of amphiphilic molecules may intercalate within membranes of vesicles in acidic organelles disturbing their composition and elasticity. Both can lead to an altered activity of lysosomal proteins, which can result in an accumulation of cholesterol within lysosomal membranes as the activity of the proteins, responsible for the export of cholesterol, is disturbed. As a result, low cholesterol levels are sensed at the ER and the biosynthesis of cholesterol gets activated. Changes in the membrane elasticity and an altered lipid raft composition can also inhibit endocytotic uptake. In addition, the degradation of the autophagic cargo and the autophagic marker LC3II depends on an acidic pH in lysosomes and may be perturbed by lysosomotropic compounds.

Lysosomotropic compounds are reported to alter cholesterol homeostasis and activate SREBP signaling (Figure 55).<sup>[44, 171, 250-256]</sup> As a result of the basicity of lysosomotropic compounds, the pH in acidic organelles increases and the hydrophobic part of amphiphilic molecules may intercalate within their membranes. The increased pH as well as the altered membrane structure can lead to a perturbed activity of lysosomal membrane proteins such as the acid sphingomyelinase (ASM)<sup>[165]</sup>, NPC1, phospholipases<sup>[164]</sup> and the acid ceramidase.<sup>[44]</sup> NPC1 and NPC2 are responsible for the export of cholesterol out of the lysosomes and inhibition of their activity by an increased pH<sup>[167, 168]</sup> leads to an accumulation of cholesterol inside lysosomal membranes, mimicking the phenotype of the NPC disease<sup>[257]</sup>. This in turn lowers cholesterol levels at the ER, activating the *de novo* biosynthesis of cholesterol. In addition, a change in the membrane structure and fluidity, as well as an altered lipid raft composition due to cholesterol accumulation, may lead to an inhibited uptake of endocytic substrates, which has been observed upon exposure of amphiphilic molecules as well as in NPC deficient cells.<sup>[171, 258, 259]</sup>

Furthermore, the degradation of the autophagic cargo and the autophagic marker LC3II is dependent on an acidic pH<sup>[260]</sup>. Therefore, the autophagic flux is perturbed upon exposure to lysosomotropic compounds and was also observed in NPC deficient cells.<sup>[176, 261, 262]</sup>

Only the most active compound **13** led to an accumulation of intracellular cholesterol, most likely in acidic organelles like lysosomes, endosomes, and Golgi, and thereby to a disturbed cholesterol localization. The data confirmed the hypothesis that the activation of SREBP-mediated gene expression is not a result of a low total cholesterol level but rather cholesterol is hidden from the ER-sensing machinery due to the accumulation in acidic membrane compartments. At 10  $\mu$ M, only compound **13** led to an accumulation of LC3II in the absence of Chloroquine without changes in the protein level of p62/SQSTM1, neither in the presence nor the absence of Chloroquine. This indicates a perturbation of the autophagic flux and excludes an autophagy-enhancing effect as this would have led to a decreased protein level of p62/SQSTM1.

Hence, compound **13** either inhibits the degradation of the autophagic cargo due to an increased lysosomal pH or it might act similar to Chloroquine and blocks the fusion of autophagosomes and lysosomes. The precise mechanism of how Chloroquine blocks the fusion is not completely understood but it is suggested that the impact of Chloroquine on some functions of the Golgi and endosomes contribute to the impairment of the fusion.<sup>[182]</sup> To determine if the fusion between autophagosomes and lysosomes is blocked, a tandem mCherry-EGFP-LC3 expression cell line can be used to simultaneously monitor autophagosomes and autolysosomes.<sup>[84, 263]</sup>

The endocytic uptake of transferrin was not affected upon exposure of compounds **10-13**. Compound **13** might not be hydrophobic enough to alter the membrane composition and elasticity in a way that it affects the vesicular transport system because an increased pH alone could block cholesterol egress from lysosomes<sup>[167, 168]</sup>. This result suggests that compound **13** most likely blocks the autophagic flux by increasing the pH in lysosomes rather than by blocking the fusion of autophagosomes and lysosomes as compound **13** does not interfere with the endosomal-lysosomal transport system.

Based on the connection between lysosomotropism and the activation of SREBP-mediated gene expression, further proteins related to lysosomal function were identified among the proteins modulated by compound **13** supporting the lysosomotropic effect. The three lysosomal hydrolases SCPEP1 (retinoid-inducible serine carboxypeptidase), Neu1 (Sialidase-1) and PPT1 (palmitoyl-protein thioesterase 1) were modulated by compound **13** (Table 15), which are direct targets of the master gene transcription factor EB (TFEB).

TFEB regulates lysosomal biogenesis and function and is the master transcriptional regulator of the CLEAR (Coordinated Lysosomal Expression and Regulation) gene network.<sup>[264]</sup>

Considering the connection between lysosomotropism and SREBP-mediated gene expression, the proteome profiling data mirrors and confirms the CPA data. Comparing the concentration of 10  $\mu$ M, only compound **13** showed an appropriate induction, the highest activity in the lysosomotropism assay and the strongest activation of SREBP-mediated gene expression. Although the proteome profiling revealed a manifestation of lysosomotropism, i.e., a disturbed cholesterol homeostasis, it can still be seen as a complementary approach, as each approach alone gave different hints towards the MoA.<sup>[74]</sup> The CPA pointed towards lysosomotropism and the proteome profiling towards a disturbed cholesterol homeostasis. Therefore, the integration of both profiling approaches was necessary to link the findings and assign a correct MoA to compound **13**. The proteome profiling data alone could have been misleading if one is not aware of the connection between lysosomotropism and cholesterol modulation.

Ultimately, the analysis of the proteome profiling data for the most active derivatives **12** and **13** was dominated by the enrichment of pathways related to cholesterol homeostasis hindering a target or MoA prediction which would have gone beyond this adverse effect determined by the physicochemical properties. However, for compound **10** and **12** the protein ubiquitination pathway was the top predicted pathway, enriched in modulated subunits of the proteasome, providing another starting point for MoA identification besides the lysosomotropic activity. For this, ubiquitinated proteins could be isolated and identified.<sup>[265]</sup> Isolation could be performed by pull-down approaches using tagged ubiquitin derivatives or affinity reagents that recognize endogenous ubiquitin. Ubiquitinated and isolated proteins can be identified via antibodies or mass spectrometry and deliver a next hint towards the MoA.

### **7.3 Many well-known drugs and tool compounds modulate cholesterol homeostasis**

The morphological fingerprint of compound **13** shared similarity to the fingerprints of 12.5 % of the references (449 of 3580) and 8 % (768 of 9619) of the research compounds, which were synthesized by chemists of the MPI, Dortmund. Fingerprint similarity based on lysosomotropism has been suggested for modulators of neuronal receptors.<sup>[84, 186]</sup> Therefore, a similar influence was assumed for the references biosimilar to compound **13**. 32 structurally diverse references with different annotated targets were selected and tested for their influence on lysosomal staining and cholesterol homeostasis.

Whereas only 18 references were identified as lysosomotropic, 29 references modulated the SREBP-dependent gene expression. Except for Ponatinib, which was toxic at all measured concentrations, and NU7441 and I-BET151, which strongly inhibited the SREBP-mediated gene expression, all other references had an activating effect. The inhibiting activity of the DNA-dependent protein kinase inhibitor NU7441 may be attributed to its additional target mTOR as the mTOR complex 1 promotes the function of SREBP.<sup>[266-268]</sup> A possible link between the bromodomain inhibitor I-BET151 and cholesterol homeostasis was provided by a recent study that highlighted a novel epigenetic mechanism involved in the regulation of lipid homeostasis and a decrease in the protein level of HMGCR by the BET inhibitor JQ1.<sup>[269]</sup> As only half of the tested references were lysosomotropic, but the majority modulated the SREBP-dependent gene expression, the MoA of this cluster is most likely a disturbed cholesterol homeostasis rather than lysosomotropism.

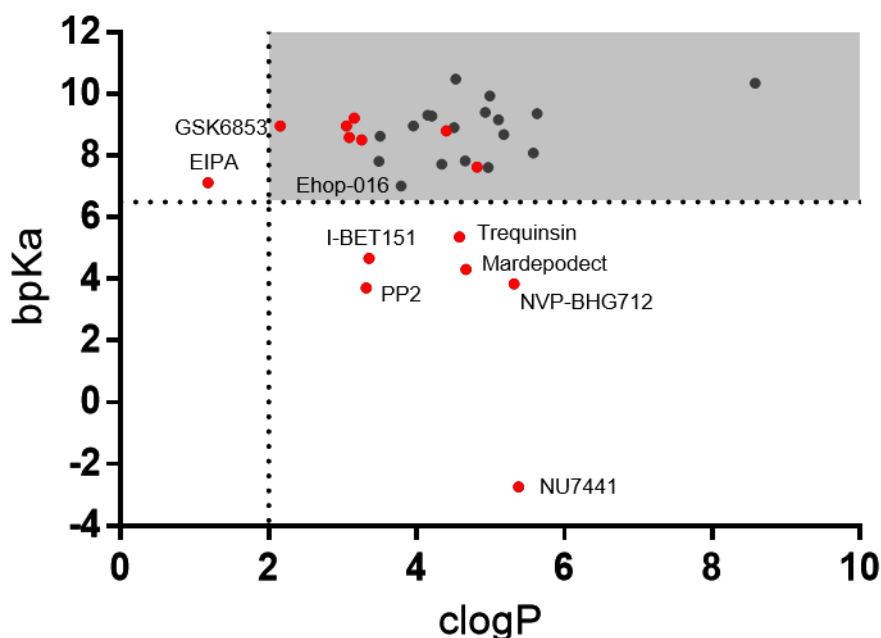


**Figure 56: Physicochemical properties of selected references biosimilar to compound 13.**

Calculated<sup>[141]</sup> logP value of selected references biosimilar ( $\geq 75\%$ ) to 10  $\mu\text{M}$  compound **13** plotted against their calculated basic pKa (bpKa) value. Grey region corresponds to  $\text{clogP} > 2$  and  $\text{bpKa} > 6.5$ , i.e., potentially lysosomotropic. References depicted in red did not decrease the LysoTrackerRed DND-99 staining (see 6.2.6).

Only two out of the 32 references, the src kinase inhibitor PP2<sup>[270]</sup> and the P-glycoprotein modulator zosuquidar<sup>[194]</sup>, did neither influence the lysosomal staining nor the SREBP-mediated gene expression.

Whereas PP2 did not possess the physicochemical properties predictive for lysosomotropism, zosuquidar was predicted as lysosomotropic (Figure 56). In general, compounds may require a longer incubation time to accumulate in acidic compartments, e.g., up to four hours, before the effect is reversed at later time points due to adaptation to lysosomal stress<sup>[142]</sup>, and/or a higher concentration. However, as the fingerprint similarity in the CPA was detected after 20 hours at 10  $\mu$ M and also the readout of the reporter gene assay was after 24 h at an even higher concentration of 30  $\mu$ M, this could be excluded. The anti-psychotic drug Risperidone and the anti-histamine Chlorpheniramine were as well identified to be inactive in the lysosomotropism assay although they possess physicochemical properties predictive of lysosomotropism.<sup>[140]</sup> However, the authors of this study did not mention a possible explanation that went beyond the incubation time and tested concentration. For PP2 and zosuquidar, another possibility could be that they interfere in a different way, e.g., related to their nominal target, with the cholesterol homeostasis but without affecting the cholesterol biosynthesis. For example, the P-glycoprotein mediates cholesterol redistribution in cell membranes and its inhibition may affect cellular cholesterol trafficking.<sup>[271]</sup> However, the reason for the morphological fingerprint similarity between compound **13** and PP2 and zosuquidar remains to be clarified.

Figure 56 shows that all 7 references without predicted physicochemical properties for lysosomotropism also did not influence the lysosomal staining although all of them possess either a clogP above 2 or a bpKa above 6.5. This points out the importance of these two physicochemical properties as compounds with neither a clogP  $\geq$  2 alone nor a bpKa  $\geq$  6.5 alone reduced the lysosomal staining, which was also observed in previous studies<sup>[140, 272]</sup>. However, they all modulate the SRE-mediated gene expression, except for PP2, supporting the hypothesis, that the bioactivity of this cluster is most likely based on an altered cholesterol homeostasis and not solely based on lysosomotropism.

Within the whole cluster of references, which were biosimilar to compound **13**, 109 references did not exhibit physicochemical properties predictive of lysosomotropism, and known cholesterol modulators and sterol-like compounds can be found among them. The sterol-like compounds 4-Androsten-4-ol-3,17-dione, 5-alpha-THDOC, alfadolone acetate, Epiandrosterone, equilin, estrone, Formestane, Melengestrol acetate and Progesterone displayed biosimilarity to compound **13** but do not possess a clogP  $\geq$  2 and a bpKa  $\geq$  6.5. Also, the statins Mevastatine, Atorvastatine and Fluvastatine, which inhibit the HMG CoA reductase, the rate-limiting enzyme of the mevalonate pathway, were not lysosomotropic but activated the SRE-dependent gene expression. In addition, the three anti-fungals Isoconazole, Itraconazole and Ketoconazole can be found among the references without predicted properties for lysosomotropism.



## DISCUSSION

Isoconazole inhibits the sterol 14 $\alpha$ -demethylase that is required for cholesterol biosynthesis<sup>[273]</sup>, the triazole Itraconazole is reported to inhibit cholesterol export from lysosomes by binding to NPC1<sup>[274]</sup> and also Ketoconazole is known to inhibit cholesterol synthesis<sup>[275, 276]</sup>. Furthermore, the v-ATPase inhibitor Bafilomycin A1 (Baf A1) is among the references without physicochemical properties predictive of lysosomotropism. Baf A1 leads to an increase in lysosomal pH, however, independent of its physicochemical properties. Furthermore, Baf A1 is reported to activate SREBP signaling and to activate genes involved in lipid synthesis and storage.<sup>[242, 277-279]</sup> Moreover, morphological clusters based on the inhibition of the v-ATPase by Baf A1 or concanamycin derivatives have been identified in human cell lines.<sup>[64, 280]</sup>

**Table 10: Connectivity Map (CMap)<sup>[41]</sup> analysis for Chlorpromazine.**

Top 5 data for chlorpromazine obtained using the summary of cell line results of CLUE (CMap linked user environment) (<https://clue.io>) with connectivity based on perturbagen or gene knockdown. Connectivity to cholesterol-regulating compounds or knockdown of v-ATPase and the lysosomal and pH-dependent enzyme acid ceramidase is detected (shown in bold).

|                          | Name   | Score |
|--------------------------|--|-------|
| <b>Perturbagen class</b> | Dopamine receptor antagonist   | 99.92 |
|                          | Tricyclic antidepressant   | 99.90 |
|                          | T-type calcium channel blocker   | 99.80 |
|                          | <b>Sterol demethylase inhibitor</b>  | 99.71 |
|                          | <b>HMGCR inhibitor</b>   | 99.62 |
| <b>Genetic knockdown</b> | poly (ADP-ribose) glycohydrolase   | 99.22 |
|                          | Protein S (alpha)  | 97.51 |
|                          | <b>Acid ceramidase, N-acylsphingosine<br/>amidohydrolase</b>                                 | 96.86 |
|                          | <b>ATP6V0B (ATPases / V-type, ATPase, H+<br/>transporting, lysosomal 21 kDa, V0 subunit)</b> | 96.79 |
|                          | <b>ATP6V0C (ATPases / V-type, ATPase, H+<br/>transporting, lysosomal 16 kDa, V0 subunit)</b> | 96.72 |

Furthermore, similar to SGI1776, AEW541 and I-BET151 (Table 5), the CMAP<sup>[41, 281]</sup> is able to reveal a connection between small molecules and v-ATPase knockdown as well as the regulation of genes involved in cholesterol biosynthesis as exemplified by the lysosomotropic agent Chlorpromazine<sup>[143]</sup>.

These findings highlight the connectivity based on the shared MoA, i.e., an altered cholesterol homeostasis, which leads to a characteristic protein and gene expression signature that can even be identified without experimental lab work if gene expression profiles are publicly available. This bioactivity can even be expanded to different species as morphological profiling in yeast revealed a link between profiles of v-ATPase deletion mutants and the v-ATPase inhibitor concanamycin A.<sup>[76]</sup>

Prior studies report on modulators of neuronal receptors that cluster based on their morphological fingerprint and proposed lysosomal accumulation as a MoA.<sup>[84, 186]</sup> The analysis of the references biosimilar to compound **13** builds on this observation as also many of the 449 references have a reported lysosomotropic activity like Lapatinib, Sertraline, Bepidil and Tamoxifen.<sup>[140]</sup> However, the observed phenotype was expanded to the modulation of cholesterol homeostasis as a common underlying MoA, which has hardly been described for most of the compounds in this cluster. Therefore, this cluster can be used to identify not only annotated but also novel modulators of cholesterol homeostasis. However, the prediction based on morphological fingerprint similarity needs further experimental proof, especially because SREBP activation might not be the primary bioactivity if it is caused by the physicochemical properties of the compounds.

Recently, the group of Prof. Waldmann developed a PDE $\delta$  proteolysis targeting chimera (PROTAC), in analogy to the PDE $\delta$  inhibitor deltasonamide 1, and demonstrated that deltasonamide 1, as well as the active and inactive PROTAC, led to the activation of SREBP.<sup>[282]</sup> This bioactivity was at that time linked to the primary target PDE $\delta$ , however, based on the present state of knowledge, it is most likely an off-target effect caused by the lysosomotropic properties of deltasonamide 1. Deltasonamide 1 has physicochemical properties predictive of lysosomotropism (clogP: 3.9; bpKa: 10.05), which was also experimentally confirmed (Figure 57C).

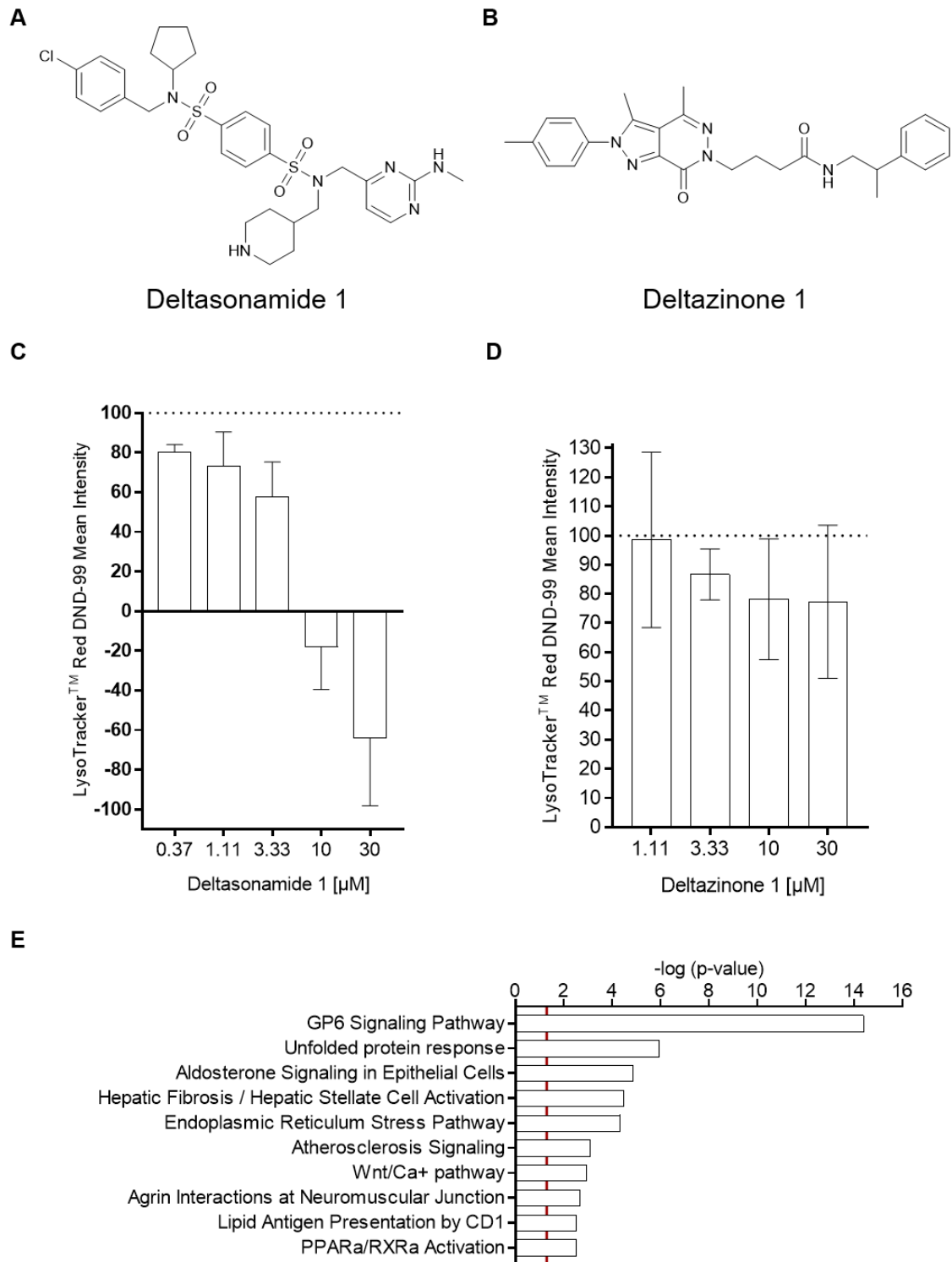


**Figure 57: Influence of deltasonamide 1 and deltazinone 1 on lysosomal staining.**

(A and B) Chemical structures of deltasonamide 1 (A) and deltazinone 1 (B). (C and D) U-2OS cells incubated for 1 h with deltasonamide 1 (C), deltazinone 1 (D) or DMSO or Chloroquine as controls prior to staining with LysoTracker™ Red DND-99. Data are mean values  $\pm$  SD of three independent experiments. (E) U-2OS cells were treated for 24 h with 1  $\mu$ M deltazinone 1 prior to proteome profiling using tandem mass tags for quantification by nanoHPLC-MS/MS. Data are mean values  $\pm$  SD of three independent experiments. Experiment performed by Dr. Michael Winzker. Pathway enrichment analysis was performed using IPA to determine significantly (FDR < 0.05, Benjamini-Hochberg corrected) affected pathways. Top 10 enriched pathways. Red line:  $p = 0.05$ .

To strengthen this finding, deltazinone 1<sup>[283]</sup>, a PDE $\delta$  inhibitor with different scaffold and chemotype (Figure 57B) was analyzed, which in contrast has a clogP of 4.04 and a bpKa of - 1.29 that are not predictive of lysosomotropism. This matches with the experimental data (Figure 57C). Furthermore, Figure 57E illustrates that a proteome profiling of cells treated with deltazinone 1, conducted by Dr. Michael Winzker, did not reveal modulation of proteins involved in cholesterol homeostasis. This example demonstrates the importance to raise awareness for the frequent modulation of cholesterol homeostasis by the physicochemical properties of small molecules to assign correct mode-of-actions.

In line with that, similar examples may be described in the literature as especially the number of high-content imaging and 'omics studies strongly increased over the last years.<sup>[284]</sup> For example, proteome profiles of the kinase inhibitors Lapatinib, Bosutinib, Sunitinib, and Gefitinib formed an unexpected cluster regulating the (chole)sterol synthesis pathway.<sup>[285]</sup> However, these kinase inhibitors are described as lysosomotropic agents in the literature, indicating that, in line with the results presented in this thesis, the observed cholesterol modulation is most likely caused by the physicochemical properties of the kinase inhibitors.<sup>[140, 286]</sup> In addition, Ravindranath *et al.*<sup>[287]</sup> analyzed gene expression data from the CMap and identified anti-psychotics and calcium channel binders upregulating genes responsible for the sterol synthesis and linked this effect to the primary target/MoA. However, well-known lysosomotropic drugs like Amitriptyline, Chlorpromazine and Verapamil<sup>[142]</sup> are among the identified compounds and the results may as well be explained by the findings presented in this thesis. Furthermore, Zhao *et al.*<sup>[209]</sup> screened the Prestwick library for the presence of pharmacological inhibitors of the conventional protein secretion pathway that transports proteins from the ER to the Golgi and afterwards to the plasma membrane via secretory vesicles. They identified 30 compounds (2.5 % of the library) that inhibited protein secretion > 50 % at 10  $\mu$ M. However, the transport of proteins between intracellular membrane compartments relies on a balanced cholesterol homeostasis<sup>[288]</sup> and several FDA-approved drugs, reported to be lysosomotropic, are among the identified hits like Perhexiline<sup>[289]</sup>, Quinacrine<sup>[290]</sup>, Sertraline<sup>[140]</sup>, Terfenadine<sup>[272]</sup>, Mefloquine<sup>[291]</sup>, Suloctidil<sup>[272]</sup> and Monensin<sup>[292]</sup>. Hence, their identification as inhibitors of the conventional protein secretion pathway, which relies on a balanced cholesterol homeostasis, might as well be a result of their physicochemical properties.

Therefore, the herein identified cluster might additionally be used to explain the regulation of genes or proteins involved in cholesterol homeostasis by small molecules, which have so far not been linked to the physicochemical properties of the used compounds. As SREBP activation is not necessarily linked to the modulation of a compounds' primary target, biological

processes linked to the physicochemical properties need to be carefully evaluated to assign a correct MoA.

The findings presented in this thesis highlight the obviously frequent occurrence of a modulated cholesterol homeostasis and lysosomal function by small molecules. Despite the frequent appearance, the modulated cholesterol homeostasis is rarely linked to lysosomotropism, i.e., to the physicochemical properties of the compounds. There is a need to increase the awareness for this type of bioactivity as it can be, and most likely for the majority of the cases will be, induced by the physicochemical properties and therefore often represents an off-target activity. But the lysosomotropic activity can also be part of the therapeutic effect of a drug. Chloroquine, for example, exerts its antimalarial activity mainly by increasing pH and accumulation in the food vacuole of the parasites.<sup>[293]</sup>

The modulation of cholesterol homeostasis seems to generate a specific gene and protein signature and therefore can be identified by profiling approaches. However, the results of both profiling strategies, used to investigate the bioactivity of the tetrahydroindolo[2,3-a]quinolizines, were dominated by this off-target effect. This, firstly, can be misleading towards the assignment of incorrect bioactivity if there is low awareness for the connection between lysosomotropism and cholesterol homeostasis, and secondly, makes it difficult to identify a potential lysosomotropic-independent target or MoA. Furthermore, bioactivity induced by physicochemical properties cannot be detected by protein-centric approaches, which are commonly used to identify targets of small molecules. Moreover, this kind of bioactivity is often unfavorable due to promiscuity for non-therapeutic targets associated with preclinical findings of toxicity.<sup>[135, 136]</sup> Lysosomes are essential organelles responsible for the digestion of old organelles, macromolecules and engulfed microbes to keep up cellular homeostasis. They play a key role in cellular processes like autophagy, endo- and exocytosis, membrane repair and cell death. The importance of lysosomes is also reflected in the number of diseases where lysosomal dysfunction is a major contributor such as disorders of the lipid and glucose metabolism, infectious diseases, bone diseases, disorders of the immune system and neurodegenerative diseases like Alzheimer<sup>[294, 295]</sup> or Niemann-Pick disease type C (NPC)<sup>[296]</sup>. Lysosomotropic compounds can lead to cytoplasmic vacuolization, induction of oxidative or ER stress, impaired intracellular vesicle trafficking, perturbed autophagy<sup>[44]</sup> and to phospholipidosis, where intracellular phospholipids accumulate and induce the formation of lamellar bodies<sup>[164]</sup>. Moreover, the lysosomal and endosomal accumulation of unesterified cholesterol and sphingolipids in cells throughout the body is also the hallmark of the NPC disease and leads to symptoms like progressive neurodegeneration, enlargement of liver and spleen, often resulting in death at an early age.<sup>[296, 297]</sup>

## DISCUSSION

---

The concentration of the tested drugs, at which an influence on lysosomal pH and SRE-mediated gene expression was observed, is for many of them higher than their therapeutic dose. Therefore, the drugs might not suffer from the lysosomotropism, however, it can often be observed that compound concentrations in phenotypic studies are increased until a phenotype can be detected. Hence, caution is advised when using compounds at high concentrations (i.e., micromolar range) as this increases the chance to impair lysosomal function and/or cholesterol homeostasis. Lysosomotropic compounds have been shown to accumulate in lysosomes to concentrations that are 100fold higher than their cytosolic concentration.<sup>[143, 298]</sup> Duvvuri and Krise<sup>[299]</sup> demonstrated that around 40 % of a model lysosomotropic amine is associated with lysosomes and thus, this might still decrease the effective drug concentration and hence, affect target binding<sup>[139]</sup> and should therefore be considered during drug design and hit optimization.

## 8 CONCLUSION AND PERSPECTIVE

Profiling the bioactivity of small molecules in an unbiased way using the Cell Painting Assay is a powerful approach to predict, investigate and identify mode-of-action based on morphological fingerprint similarity to reference compounds and is independent of chemical similarity. Not only chemical similarity or similar targets lead to a shared physiological response in cells, but also structurally different compounds with different annotated targets may induce similar morphological changes due to a shared MoA, defining a cluster.

This thesis demonstrates that the CPA is able to identify not only annotated but also novel iron-chelating agents and cell cycle modulators of the G1/S or G2 phase as they cluster together based on the shared MoA of cell cycle arrest. Hierarchical clustering using their morphological fingerprints delivered a first insight into the different mechanisms of action demonstrating that the CPA would be able to predict even target-related bioactivity within a cluster that shares a MoA. However, to generalize this statement, more annotated compounds would need to be profiled in the CPA and the bioactivity would need to be experimentally confirmed. The mechanism for the two novel DNA synthesis modulators identified in this thesis remains unsolved, however, the compounds could be further tested against more CDK/cyclin complexes or other proteins involved in DNA synthesis, replication and repair. Of note, iron chelators and DNA synthesis modulators are also being investigated as anti-cancer agents because of their cytostatic and cytotoxic activity.<sup>[300-304]</sup> Therefore, the iron chelators **1-7** and the two DNA synthesis modulators **8** and **9**, identified in this thesis, could be interesting tool compounds to study the cytostatic effect and selectivity to cancer cells as potential anti-cancer agents.

Furthermore, a second cluster of references was identified in this thesis, that shared a modulated cholesterol homeostasis as a MoA. For the most part, this cluster consists of lysosomotropic compounds, whose physicochemical properties lead to cholesterol accumulation in membranes of acidic organelles thereby disturbing cholesterol localization and activating its *de novo* biosynthesis. Numerous well-characterized drugs share this MoA, which is not related to their annotated primary targets and, importantly, impossible to identify by commonly applied, target identification procedures designed to determine protein targets. The cluster enables the identification of new modulators of cholesterol homeostasis and can be used to associate the regulation of corresponding genes or proteins to an effect induced by the physicochemical properties of the compounds rather than to their annotated primary targets. How cells respond to the exposure of lysosomotropic compounds is not well characterized.<sup>[142]</sup> However, an effect determined by the physicochemical properties is mostly unwanted and can be considered as adverse. Moreover, this kind of bioactivity often leads to

promiscuity for non-therapeutic targets associated with preclinical findings of toxicity<sup>[135, 136]</sup> further decreasing the success rate of clinical trials in a drug discovery program.<sup>[305, 306]</sup> Therefore, the pharmaceutical industry establishes early safety evaluations of new chemical entities more and more to lower compound attrition due to toxicity. Although it is not fully understood how lysosomotropism contributes to toxicity, a connection has been established<sup>[238]</sup>, and hence, assays that detect lysosomal impairment as early as possible are desired.<sup>[140]</sup> Furthermore, the physicochemical properties should be more intensively considered in the hit optimization process to avoid cation trapping and membrane intercalation.

Lysosomotropic activity might not always be undesired as lysosomotropic compounds are currently heavily investigated as actors on the endolysosomal host-pathogen interface for the inhibition of the Severe Acute Respiratory Syndrome Related Coronavirus 2 (SARS-CoV-2) to enter its host cells<sup>[307, 308]</sup> and to combat the virus-mediated suppression of cholesterol synthesis.<sup>[309]</sup> Moreover, a genome-scale CRISPR loss-of-function screen<sup>[309]</sup> identified genes that are part of the endosomal entry pathway as essential for SARS-CoV-2 infection, including subunits of the v-ATPase and NPC1, whose loss of function led to an induction of cholesterol biosynthesis. Therefore, loss-of-function mutants of those genes may combat the virus-mediated suppression of cholesterol synthesis. In line with this, the study demonstrated that seven tested inhibitors reduced the viral load by over 100-fold. Six of those hits were also biosimilar to compound **13** in the CPA including GSK6853 that led to an approx. 10-fold reduction in viral load. Therefore, the herein identified references that modulate cholesterol homeostasis, as well as compound **13**, could very well be used for the study as anti-SARS-CoV-2 agents. Moreover, there are several FDA-approved drugs among the herein identified cholesterol modulators, which may accelerate the process to identify anti-SARS-CoV-2 agents by drug repurposing.

In general, the identification of on- and off-target interaction networks of promiscuous compounds is an important resource to raise awareness, to better understand and make use of those poly-pharmacological effects to, e.g., optimize compound selectivity or repurpose well-tolerated drugs. This underlines the benefit of unbiased approaches that cover a broad range of bioactivity.<sup>[1, 35]</sup> Furthermore, unbiased profiling is especially important for small molecules with non-protein targets as those targets or MoAs are difficult to identify with commonly used target identification approaches. The results presented in this thesis demonstrate that the CPA is able to overcome this limitation by the successful identification of iron-chelating agents and lysosomotropic compounds as non-protein targets. Taken together, the CPA and the combination with other profiling approaches can cover the demand for a detailed mapping of the bioactivity space to identify potential off-target activity and toxicity as



early as possible and to expand the annotation of available reference compounds beyond their primary targets. The findings presented in this thesis emphasize the predictive value of the CPA to configure the target/MoA identification and validation process more efficiently in terms of time, throughput, and covered bioactivity space.

## 9 REFERENCES

1. Schenone, M., Dančik, V., Wagner, B.K. & Clemons, P.A. Target identification and mechanism of action in chemical biology and drug discovery. *Nature chemical biology* **9**, 232-240 (2013).
2. Kawasumi, M. & Nghiem, P. Chemical Genetics: Elucidating Biological Systems with Small-Molecule Compounds. *Journal of Investigative Dermatology* **127**, 1577-1584 (2007).
3. Laraia, L., Robke, L. & Waldmann, H. Bioactive Compound Collections: From Design to Target Identification. *Chem* **4**, 705-730 (2018).
4. Kapoor, S., Waldmann, H. & Ziegler, S. Novel approaches to map small molecule-target interactions. *Bioorg Med Chem* **24**, 3232-45 (2016).
5. Stockwell, B.R. Frontiers in chemical genetics. *Trends in Biotechnology* **18**, 449-455 (2000).
6. Hannon, G.J. RNA interference. *Nature* **418**, 244-251 (2002).
7. Caicedo, J.C., Singh, S. & Carpenter, A.E. Applications in image-based profiling of perturbations. *Curr Opin Biotechnol* **39**, 134-142 (2016).
8. Agrawal, N., *et al.* RNA Interference: Biology, Mechanism, and Applications. *Microbiology and Molecular Biology Reviews* **67**, 657-685 (2003).
9. Hall, B., Limaye, A. & Kulkarni, A.B. Overview: generation of gene knockout mice. *Current protocols in cell biology* **Chapter 19**, Unit-19.12.17 (2009).
10. Britsch, S., *Transgenic and Knock-out Animals in Encyclopedic Reference of Genomics and Proteomics in Molecular Medicine*, 2006, Springer Berlin Heidelberg, 1900-1903.
11. Al-Ali, H. The evolution of drug discovery: from phenotypes to targets, and back. *MedChemComm* **7**, 788-798 (2016).
12. Proschak, E., Stark, H. & Merk, D. Polypharmacology by Design: A Medicinal Chemist's Perspective on Multitargeting Compounds. *Journal of Medicinal Chemistry* **62**, 420-444 (2019).
13. Reddy, A.S. & Zhang, S. Polypharmacology: drug discovery for the future. *Expert review of clinical pharmacology* **6**, 41-47 (2013).
14. Croston, G.E. The utility of target-based discovery. *Expert Opin Drug Discov* **12**, 427-429 (2017).
15. Nussinov, R., Tsai, C.J. & Jang, H. Protein ensembles link genotype to phenotype. *PLoS Comput Biol* **15**, e1006648 (2019).
16. Deans, A.R., *et al.* Finding our way through phenotypes. *PLoS biology* **13**, e1002033-e1002033 (2015).
17. Swinney, D.C. Phenotypic vs. target-based drug discovery for first-in-class medicines. *Clin Pharmacol Ther* **93**, 299-301 (2013).
18. Stockwell, B.R. Chemical genetics: ligand-based discovery of gene function. *Nature reviews. Genetics* **1**, 116-125 (2000).
19. Swinney, D.C. The Contribution of Mechanistic Understanding to Phenotypic Screening for First-in-Class Medicines. *Journal of Biomolecular Screening* **18**, 1186-1192 (2013).
20. Ziegler, S., Pries, V., Hedberg, C. & Waldmann, H. Target Identification for Small Bioactive Molecules: Finding the Needle in the Haystack. *Angewandte Chemie International Edition* **52**, 2744-2792 (2013).
21. Baell, J. & Walters, M.A. Chemistry: Chemical con artists foil drug discovery. *Nature* **513**, 481-483 (2014).
22. Gilberg, E., *et al.* Highly Promiscuous Small Molecules from Biological Screening Assays Include Many Pan-Assay Interference Compounds but Also Candidates for Polypharmacology. *Journal of Medicinal Chemistry* **59**, 10285-10290 (2016).
23. Lee, J. & Bogoy, M. Target deconvolution techniques in modern phenotypic profiling. *Curr Opin Chem Biol* **17**, 118-26 (2013).

## REFERENCES

24. Wagner, B.K. & Schreiber, S.L. The Power of Sophisticated Phenotypic Screening and Modern Mechanism-of-Action Methods. *Cell chemical biology* **23**, 3-9 (2016).
25. Byrne, R. & Schneider, G. In Silico Target Prediction for Small Molecules. *Methods Mol Biol* **1888**, 273-309 (2019).
26. Awale, M. & Reymond, J.-L. The polypharmacology browser: a web-based multi-fingerprint target prediction tool using ChEMBL bioactivity data. *Journal of cheminformatics*, 2017. **9**, 11 DOI: 10.1186/s13321-017-0199-x.
27. Raedler, L.A. Lonsurf (Trifluridine plus Tipiracil): A New Oral Treatment Approved for Patients with Metastatic Colorectal Cancer. *American health & drug benefits* **9**, 97-100 (2016).
28. Mobarra, N., *et al.* A Review on Iron Chelators in Treatment of Iron Overload Syndromes. *Int J Hematol Oncol Stem Cell Res* **10**, 239-247 (2016).
29. Santos, R., *et al.* A comprehensive map of molecular drug targets. *Nat Rev Drug Discov* **16**, 19-34 (2017).
30. Gray, K.C., *et al.* Amphotericin primarily kills yeast by simply binding ergosterol. *Proc Natl Acad Sci U S A* **109**, 2234-9 (2012).
31. Ralph, R.K., Marshall, B. & Darkin, S. Anti-cancer drugs which intercalate into DNA: How do they act? *Trends in Biochemical Sciences* **8**, 212-214 (1983).
32. Hong, W., Zeng, J. & Xie, J. Antibiotic drugs targeting bacterial RNAs. *Acta pharmaceutica Sinica. B* **4**, 258-265 (2014).
33. Disney, M.D. Targeting RNA with Small Molecules To Capture Opportunities at the Intersection of Chemistry, Biology, and Medicine. *Journal of the American Chemical Society* **141**, 6776-6790 (2019).
34. Schneidewind, T., *et al.* Morphological Profiling Identifies a Common Mode of Action for Small Molecules with Different Targets. *ChemBioChem* **21**, 3197-3207 (2020).
35. Giri, A.K., Ianevski, A. & Aittokallio, T. Genome-wide off-targets of drugs: risks and opportunities. *Cell Biology and Toxicology* **35**, 485-487 (2019).
36. Ziegler, S., Sievers, S. & Waldmann, H. Morphological profiling of small molecules. *Cell Chemical Biology*(2021) DOI: <https://doi.org/10.1016/j.chembiol.2021.02.012>.
37. Chandrasekaran, S.N., Ceulemans, H., Boyd, J.D. & Carpenter, A.E. Image-based profiling for drug discovery: due for a machine-learning upgrade? *Nature Reviews Drug Discovery* **20**, 145-159 (2021).
38. Richards, M.P., *Techniques for Gene Expression Profiling in Medical Biomethods Handbook*, 2005, Humana Press, 507-518.
39. Shendure, J., *et al.* DNA sequencing at 40: past, present and future. *Nature* **550**, 345-353 (2017).
40. Lamb, J., *et al.* The Connectivity Map: Using Gene-Expression Signatures to Connect Small Molecules, Genes, and Disease. *Science* **313**, 1929 (2006).
41. Subramanian, A., *et al.* A Next Generation Connectivity Map: L1000 Platform and the First 1,000,000 Profiles. *Cell* **171**, 1437-1452 e17 (2017).
42. Ravindranath, A.C., *et al.* Connecting gene expression data from connectivity map and in silico target predictions for small molecule mechanism-of-action analysis. *Molecular BioSystems* **11**, 86-96 (2015).
43. Musa, A., *et al.* A review of connectivity map and computational approaches in pharmacogenomics. *Briefings in bioinformatics* **19**, 506-523 (2018).
44. Kuzu, O.F., Toprak, M., Noory, M.A. & Robertson, G.P. Effect of lysosomotropic molecules on cellular homeostasis. *Pharmacological Research* **117**, 177-184 (2017).
45. Shigemizu, D., *et al.* Using Functional Signatures to Identify Repositioned Drugs for Breast, Myelogenous Leukemia and Prostate Cancer. *PLOS Computational Biology* **8**, e1002347 (2012).
46. Iorio, F., *et al.* Discovery of drug mode of action and drug repositioning from transcriptional responses. *Proceedings of the National Academy of Sciences* **107**, 14621 (2010).

## REFERENCES

47. Iwata, M., *et al.* Elucidating the modes of action for bioactive compounds in a cell-specific manner by large-scale chemically-induced transcriptomics. *Scientific Reports* **7**, 40164 (2017).
48. Lowe, R., *et al.* Transcriptomics technologies. *PLoS computational biology* **13**, e1005457-e1005457 (2017).
49. Barglow, K.T. & Cravatt, B.F. Activity-based protein profiling for the functional annotation of enzymes. *Nature Methods* **4**, 822-827 (2007).
50. Kwon, H.J. & Karuso, P. Chemical proteomics, an integrated research engine for exploring drug-target-phenotype interactions. *Proteome science* **16**, 1-1 (2018).
51. Savitski, M.M., *et al.* Tracking cancer drugs in living cells by thermal profiling of the proteome. *Science* **346**, 1255784 (2014).
52. Wright, M.H. & Sieber, S.A. Chemical proteomics approaches for identifying the cellular targets of natural products. *Natural Product Reports* **33**, 681-708 (2016).
53. Rix, U. & Superti-Furga, G. Target profiling of small molecules by chemical proteomics. *Nature Chemical Biology* **5**, 616-624 (2009).
54. Saei, A.A., *et al.* ProTargetMiner as a proteome signature library of anticancer molecules for functional discovery. *Nature Communications* **10**, 5715 (2019).
55. Available from: <http://protargetminer.genexplain.com/> Access date: 27.01.2021.
56. Willis, C., Nyffeler, J. & Harrill, J. Phenotypic Profiling of Reference Chemicals across Biologically Diverse Cell Types Using the Cell Painting Assay. **25**, 755-769 (2020).
57. Cox, M.J., *et al.* Tales of 1,008 small molecules: phenomic profiling through live-cell imaging in a panel of reporter cell lines. *Scientific Reports* **10**, 13262 (2020).
58. Bougen-Zhukov, N., Loh, S.Y., Lee, H.K. & Loo, L.H. Large-scale image-based screening and profiling of cellular phenotypes. *Cytometry A* **91**, 115-125 (2017).
59. Pahl, A. & Sievers, S. The Cell Painting Assay as a Screening Tool for the Discovery of Bioactivities in New Chemical Matter. *Methods Mol Biol* **1888**, 115-126 (2019).
60. Boland, M.V. & Murphy, R.F. A neural network classifier capable of recognizing the patterns of all major subcellular structures in fluorescence microscope images of HeLa cells. *Bioinformatics* **17**, 1213-23 (2001).
61. Tanaka, M., *et al.* An Unbiased Cell Morphology-Based Screen for New, Biologically Active Small Molecules. *PLOS Biology* **3**, e128 (2005).
62. Futamura, Y., *et al.* Morphobase, an Encyclopedic Cell Morphology Database, and Its Use for Drug Target Identification. *Chemistry & Biology* **19**, 1620-1630 (2012).
63. Woehrmann, M.H., *et al.* Large-scale cytological profiling for functional analysis of bioactive compounds. *Molecular BioSystems* **9**, 2604-2617 (2013).
64. Schulze, C.J., *et al.* "Function-First" Lead Discovery: Mode of Action Profiling of Natural Product Libraries Using Image-Based Screening. *Chemistry & Biology* **20**, 285-295 (2013).
65. Simm, J., *et al.* Repurposing High-Throughput Image Assays Enables Biological Activity Prediction for Drug Discovery. *Cell chemical biology* **25**, 611-618.e3 (2018).
66. Gibson, C.C., *et al.* Strategy for identifying repurposed drugs for the treatment of cerebral cavernous malformation. *Circulation* **131**, 289-99 (2015).
67. Mullard, A. Machine learning brings cell imaging promises into focus. *Nat Rev Drug Discov* **18**, 653-655 (2019).
68. Scheeder, C., Heigwer, F. & Boutros, M. Machine learning and image-based profiling in drug discovery. *Current Opinion in Systems Biology* **10**, 43-52 (2018).
69. Sommer, C. & Gerlich, D.W. Machine learning in cell biology - teaching computers to recognize phenotypes. *J Cell Sci* **126**, 5529-39 (2013).
70. Reisen, F., *et al.* Linking phenotypes and modes of action through high-content screen fingerprints. *Assay Drug Dev Technol* **13**, 415-27 (2015).
71. Melillo, B., *et al.* Synergistic Effects of Stereochemistry and Appendages on the Performance Diversity of a Collection of Synthetic Compounds. *J Am Chem Soc* **140**, 11784-11790 (2018).
72. Hippman, R.S., *et al.* Multiple Chemical Features Impact Biological Performance Diversity of a Highly Active Natural Product-Inspired Library. **21**, 3137-3145 (2020).

## REFERENCES

73. Christoforow, A., *et al.* Design, Synthesis, and Phenotypic Profiling of Pyrano-Furo-Pyridone Pseudo Natural Products. *Angewandte Chemie International Edition* **58**, 14715-14723 (2019).
74. Wawer, M.J., *et al.* Toward performance-diverse small-molecule libraries for cell-based phenotypic screening using multiplexed high-dimensional profiling. *Proceedings of the National Academy of Sciences of the United States of America* **111**, 10911-10916 (2014).
75. Singh, S., *et al.* Morphological Profiles of RNAi-Induced Gene Knockdown Are Highly Reproducible but Dominated by Seed Effects. *PLOS ONE* **10**, e0131370 (2015).
76. Ohnuki, S., Oka, S., Nogami, S. & Ohya, Y. High-content, image-based screening for drug targets in yeast. *PLoS One* **5**, e10177 (2010).
77. Gustafsdottir, S.M., *et al.* Multiplex Cytological Profiling Assay to Measure Diverse Cellular States. *PLOS ONE* **8**, e80999 (2013).
78. Bray, M.A., *et al.* Cell Painting, a high-content image-based assay for morphological profiling using multiplexed fluorescent dyes. *Nat Protoc* **11**, 1757-74 (2016).
79. *Handbook of Assay Development in Drug Discovery*. 2006.
80. Warchal, S.J., *et al.* High content phenotypic screening identifies serotonin receptor modulators with selective activity upon breast cancer cell cycle and cytokine signaling pathways. *Bioorg Med Chem* **28**, 115209 (2020).
81. Carpenter, A.E., *et al.* CellProfiler: image analysis software for identifying and quantifying cell phenotypes. *Genome Biol* **7**, R100 (2006).
82. Available from:  
<https://docs.scipy.org/doc/scipy/reference/generated/scipy.spatial.distance.correlation.html> Access date: 28.12.2020.
83. Foley, D.J., *et al.* Phenotyping Reveals Targets of a Pseudo-Natural-Product Autophagy Inhibitor. *Angewandte Chemie (International ed. in English)* **59**, 12470-12476 (2020).
84. Laraia, L., *et al.* Image-Based Morphological Profiling Identifies a Lysosomotropic, Iron-Sequestering Autophagy Inhibitor. *Angewandte Chemie International Edition in press* (2020).
85. Zimmermann, S., *et al.* A Scaffold-Diversity Synthesis of Biologically Intriguing Cyclic Sulfonamides. *Chemistry* **25**, 15498-15503 (2019).
86. Kang, J., *et al.* Improving drug discovery with high-content phenotypic screens by systematic selection of reporter cell lines. *Nature Biotechnology* **34**, 70-77 (2016).
87. Dückert, H., *et al.* Natural product-inspired cascade synthesis yields modulators of centrosome integrity. *Nature Chemical Biology* **8**, 179-184 (2012).
88. Saxton, J.E. Recent progress in the chemistry of the monoterpene indole alkaloids. *Natural Product Reports* **14**, 559-590 (1997).
89. Takayama, H., *et al.* Discovery of anti-influenza A virus activity of a corynanthe-type indole alkaloid, hirsutine, in vitro and the structure-activity relationship of natural and synthetic analogs. *Bioorganic & Medicinal Chemistry Letters* **7**, 3145-3148 (1997).
90. Smith, J.R., *et al.* Multiple sterol regulatory elements in promoter for hamster 3-hydroxy-3-methylglutaryl-coenzyme A synthase. *J Biol Chem* **263**, 18480-7 (1988).
91. Dooley, K.A., Millinder, S. & Osborne, T.F. Sterol regulation of 3-hydroxy-3-methylglutaryl-coenzyme A synthase gene through a direct interaction between sterol regulatory element binding protein and the trimeric CCAAT-binding factor/nuclear factor Y. *J Biol Chem* **273**, 1349-56 (1998).
92. Yang, A., Pantoom, S. & Wu, Y.W. Elucidation of the anti-autophagy mechanism of the Legionella effector RavZ using semisynthetic LC3 proteins. *Elife* **6**(2017).
93. Nikfarjam, L. & Farzaneh, P. Prevention and detection of Mycoplasma contamination in cell culture. *Cell journal* **13**, 203-212 (2012).
94. Pahl, A. & Sievers, S., *The Cell Painting Assay as a Screening Tool for the Discovery of Bioactivities in New Chemical Matter in Systems Chemical Biology: Methods and Protocols*, 2019, Springer New York, 115-126.

## REFERENCES

---

95. Available from: <https://docs.scipy.org/doc/scipy/reference/cluster.hierarchy.html#module-scipy.cluster.hierarchy> Access date: 01.03.2021.
96. Available from: <https://seaborn.pydata.org/generated/seaborn.clustermap.html> Access date: 01.03.2021.
97. Buck, S.B., *et al.* Detection of S-phase cell cycle progression using 5-ethynyl-2'-deoxyuridine incorporation with click chemistry, an alternative to using 5-bromo-2'-deoxyuridine antibodies. *Biotechniques* **44**, 927-9 (2008).
98. Cox, J. & Mann, M. MaxQuant enables high peptide identification rates, individualized p.p.b.-range mass accuracies and proteome-wide protein quantification. *Nature Biotechnology* **26**, 1367-1372 (2008).
99. Tyanova, S. & Cox, J. Perseus: A Bioinformatics Platform for Integrative Analysis of Proteomics Data in Cancer Research. *Methods Mol Biol* **1711**, 133-148 (2018).
100. Stookey, L.L. Ferrozine---a new spectrophotometric reagent for iron. *Analytical Chemistry* **42**, 779-781 (1970).
101. Lowry, O.H., Rosebrough, N.J., Farr, A.L. & Randall, R.J. Protein measurement with the Folin phenol reagent. *J Biol Chem* **193**, 265-75 (1951).
102. Heather C Hatcher, R.N.S., Frank M Torti, Suzy V Torti Synthetic and natural iron chelators: therapeutic potential and clinical use. *Future Med. Chem* **9**, 1643-1670 (2009).
103. Keberle, H. The Biochemistry of Desferrioxamine and its Relation to Iron Metabolism. *Annals of the New York Academy of Sciences* **119**, 758-768 (1964).
104. Available from: <https://www.prestwickchemical.com/screening-libraries/prestwick-chemical-library/> Access date: 29.12.2020.
105. Abrams, B.B., Hanel, H. & Hoehler, T. Ciclopirox Olamine - a Hydroxypyridone Antifungal Agent. *Clinics in Dermatology* **9**, 471-477 (1991).
106. Eberhard, Y., *et al.* Chelation of intracellular iron with the antifungal agent ciclopirox olamine induces cell death in leukemia and myeloma cells. *Blood* **114**, 3064-3073 (2009).
107. Zhou, H., *et al.* The antitumor activity of the fungicide ciclopirox. *International journal of cancer* **127**, 2467-2477 (2010).
108. Margerum, D.W. Kinetics of 1,10-Phenanthroline Chelation .2. Effect of Hydroxide Ion on the Dissociation Rate of Tris-(1,10-Phenanthroline)-Iron(li). *Journal of the American Chemical Society* **79**, 2728-2733 (1957).
109. Eizric, D.L., de Lúcio, M.A., Boschero, A.C. & Hoffmann, M.E. 1, 10 Phenanthroline, a metal chelator, protects against alloxan- but not streptozotocin-induced diabetes. *Journal of Free Radicals in Biology & Medicine* **2**, 189-192 (1986).
110. de Avellar, I.G.J., *et al.* Reevaluating the role of 1,10-phenanthroline in oxidative reactions involving ferrous ions and DNA damage. *Biochimica et Biophysica Acta (BBA) - General Subjects* **1675**, 46-53 (2004).
111. Peterson, Q.P., *et al.* PAC-1 Activates Procaspace-3 in Vitro through Relief of Zinc-Mediated Inhibition. *Journal of Molecular Biology* **388**, 144-158 (2009).
112. Franz, K.J. Application of inorganic chemistry for non-cancer therapeutics. *Dalton Trans* **41**, 6333-4 (2012).
113. Puig, S., Ramos-Alonso, L., Romero, A.M. & Martinez-Pastor, M.T. The elemental role of iron in DNA synthesis and repair. *Metallomics* **9**, 1483-1500 (2017).
114. Siriwardana, G. & Seligman, P.A. Two cell cycle blocks caused by iron chelation of neuroblastoma cells: separating cell cycle events associated with each block. *Physiol Rep* **1**, e00176 (2013).
115. Yu, Y., Kovacevic, Z. & Richardson, D.R. Tuning Cell Cycle Regulation with an Iron Key. *Cell Cycle* **6**, 1982-1994 (2007).
116. Kataoka, Y., *et al.* Cytotoxicity of trifluridine correlates with the thymidine kinase 1 expression level. *Scientific Reports* **9**, 7964 (2019).

## REFERENCES

117. Rechkoblit, O., *et al.* Structural insights into mutagenicity of anticancer nucleoside analog cytarabine during replication by DNA polymerase  $\eta$ . *Scientific Reports* **9**, 16400 (2019).
118. Van den Neste, E., Cardoen, S., Offner, F. & Bontemps, F. Old and new insights into the mechanisms of action of two nucleoside analogs active in lymphoid malignancies: fludarabine and cladribine (review). *Int J Oncol* **27**, 1113-24 (2005).
119. Brasca, M.G., *et al.* Optimization of 6,6-dimethyl pyrrolo[3,4-c]pyrazoles: Identification of PHA-793887, a potent CDK inhibitor suitable for intravenous dosing. *Bioorg Med Chem* **18**, 1844-53 (2010).
120. Węsierska-Gądek, J., *et al.* Roscovitine, a selective CDK inhibitor, reduces the basal and estrogen-induced phosphorylation of ER- $\alpha$  in human ER-positive breast cancer cells. *J Cell Biochem* **112**, 761-72 (2011).
121. Kollmannsberger, C., *et al.* Topotecan - A novel topoisomerase I inhibitor: pharmacology and clinical experience. *Oncology* **56**, 1-12 (1999).
122. Usha, S., Johnson, I.M. & Malathi, R. Modulation of DNA intercalation by resveratrol and genistein. *Molecular and Cellular Biochemistry* **284**, 57-64 (2006).
123. Agudelo, D., Bourassa, P., Bérubé, G. & Tajmir-Riahi, H.A. Intercalation of antitumor drug doxorubicin and its analogue by DNA duplex: structural features and biological implications. *Int J Biol Macromol* **66**, 144-50 (2014).
124. Laraia, L. & Waldmann, H. Natural product inspired compound collections: evolutionary principle, chemical synthesis, phenotypic screening, and target identification. *Drug Discovery Today: Technologies* **23**, 75-82 (2017).
125. Kumar, K. & Waldmann, H. Synthesis of Natural Product Inspired Compound Collections. *Angewandte Chemie (International ed. in English)* **48**, 3224-42 (2009).
126. Karageorgis, G., Foley, D.J., Laraia, L. & Waldmann, H. Principle and design of pseudo-natural products. *Nature Chemistry* (2020).
127. Liu, Z.D. & Hider, R.C. Design of iron chelators with therapeutic application. *Coordination Chemistry Reviews* **232**, 151-171 (2002).
128. Dow, M., *et al.* Modular Synthesis of Diverse Natural Product-Like Macrocycles: Discovery of Hits with Antimycobacterial Activity. *Chemistry – A European Journal* **23**, 7207-7211 (2017).
129. Breinig, M., Klein, F.A., Huber, W. & Boutros, M. A chemical–genetic interaction map of small molecules using high-throughput imaging in cancer cells. *Molecular Systems Biology* **11**, 846 (2015).
130. Sankar, M.G., *et al.* Stereoselective synthesis of a natural product inspired tetrahydroindolo[2,3-a]-quinolizine compound library. *Bioorganic & Medicinal Chemistry* **23**, 2614-2620 (2015).
131. Urs, N.M., Nicholls, P.J. & Caron, M.G. Integrated approaches to understanding antipsychotic drug action at GPCRs. *Current opinion in cell biology* **27**, 56-62 (2014).
132. Sriram, K. & Insel, P.A. G Protein-Coupled Receptors as Targets for Approved Drugs: How Many Targets and How Many Drugs? *Molecular pharmacology* **93**, 251-258 (2018).
133. Alavijeh, M.S., Chishty, M., Qaiser, M.Z. & Palmer, A.M. Drug metabolism and pharmacokinetics, the blood-brain barrier, and central nervous system drug discovery. *NeuroRx : the journal of the American Society for Experimental NeuroTherapeutics* **2**, 554-571 (2005).
134. Vater, M., *et al.* New insights into the intracellular distribution pattern of cationic amphiphilic drugs. *Scientific Reports* **7**, 44277 (2017).
135. Tarcsay, Á. & Keserű, G.M. Contributions of Molecular Properties to Drug Promiscuity. *Journal of Medicinal Chemistry* **56**, 1789-1795 (2013).
136. Peters, J.-U., *et al.* Can we discover pharmacological promiscuity early in the drug discovery process? *Drug Discovery Today* **17**, 325-335 (2012).
137. Lu, S., Jessen, B., Strock, C. & Will, Y. The Contribution of Physicochemical Properties To Multiple In Vitro Cytotoxicity Endpoints. *Toxicology in vitro : an international journal published in association with BIBRA* **26**, 613-20 (2012).

## REFERENCES

138. De Duve, C., *et al.* Lysosomotropic agents. *Biochemical Pharmacology* **23**, 2495-2531 (1974).
139. Marceau, F., *et al.* Cation trapping by cellular acidic compartments: Beyond the concept of lysosomotropic drugs. *Toxicology and Applied Pharmacology* **259**, 1-12 (2012).
140. Nadanaciva, S., *et al.* A high content screening assay for identifying lysosomotropic compounds. *Toxicology in Vitro* **25**, 715-723 (2011).
141. Available from: <https://chemaxon.com> Access date: 01.03.2021.
142. Lu, S., *et al.* Lysosomal adaptation: How cells respond to lysosomotropic compounds. *PLOS ONE* **12**, e0173771 (2017).
143. Villamil Giraldo, Ana M., Appelqvist, H., Ederth, T. & Öllinger, K. Lysosomotropic agents: impact on lysosomal membrane permeabilization and cell death. *Biochemical Society Transactions* **42**, 1460-1464 (2014).
144. Aits, S. & Jäättelä, M. Lysosomal cell death at a glance. *Journal of Cell Science* **126**, 1905 (2013).
145. Pagliero, R.J., *et al.* Discovery of Small Molecules That Induce Lysosomal Cell Death in Cancer Cell Lines Using an Image-Based Screening Platform. *ASSAY and Drug Development Technologies* **14**, 489-510 (2016).
146. Aki, T., Nara, A. & Uemura, K. Cytoplasmic vacuolization during exposure to drugs and other substances. *Cell Biology and Toxicology* **28**, 125-131 (2012).
147. Goldman, S.D.B., Funk, R.S., Rajewski, R.A. & Krise, J.P. Mechanisms of amine accumulation in, and egress from, lysosomes. *Bioanalysis* **1**, 1445-1459 (2009).
148. Yoshimori, T., *et al.* Bafilomycin A1, a specific inhibitor of vacuolar-type H(+)-ATPase, inhibits acidification and protein degradation in lysosomes of cultured cells. *J Biol Chem* **266**, 17707-12 (1991).
149. Fletcher, D.A. & Mullins, R.D. Cell mechanics and the cytoskeleton. *Nature* **463**, 485-492 (2010).
150. MacLean-Fletcher, S. & Pollard, T.D. Mechanism of action of cytochalasin B on actin. *Cell* **20**, 329-341 (1980).
151. Holzinger, A. Jasplakinolide: an actin-specific reagent that promotes actin polymerization. *Methods Mol Biol* **586**, 71-87 (2009).
152. Ramsey, W.S. Retraction fibers and leucocyte chemotaxis. *Exp Cell Res* **86**, 184-7 (1974).
153. Sims, J.R., Karp, S. & Ingber, D.E. Altering the cellular mechanical force balance results in integrated changes in cell, cytoskeletal and nuclear shape. *J Cell Sci* **103 (Pt 4)**, 1215-22 (1992).
154. Lee, H., *et al.* Cytoskeletal prestress regulates nuclear shape and stiffness in cardiac myocytes. *Experimental Biology and Medicine* **240**, 1543-1554 (2015).
155. Schug, Z.T., *et al.* Acetyl-CoA synthetase 2 promotes acetate utilization and maintains cancer cell growth under metabolic stress. *Cancer Cell* **27**, 57-71 (2015).
156. Scott, N.A., *et al.* The cholesterol synthesis enzyme lanosterol 14 $\alpha$ -demethylase is post-translationally regulated by the E3 ubiquitin ligase MARCH6. *The Biochemical journal* **477**, 541-555 (2020).
157. Luo, J., Yang, H. & Song, B.-L. Mechanisms and regulation of cholesterol homeostasis. *Nature Reviews Molecular Cell Biology* **21**, 225-245 (2020).
158. Nakamura, K., *et al.* Isopentenyl diphosphate isomerase, a cholesterol synthesizing enzyme, is localized in Lewy bodies. *Neuropathology* **35**, 432-40 (2015).
159. Rodriguez-Agudo, D., *et al.* Intracellular cholesterol transporter StarD4 binds free cholesterol and increases cholesteryl ester formation. *Journal of lipid research* **49**, 1409-1419 (2008).
160. Tanaka, S., *et al.* Fatty acid desaturase 2 is up-regulated by the treatment with statin through geranylgeranyl pyrophosphate-dependent Rho kinase pathway in HepG2 cells. *Scientific Reports* **9**, 10009 (2019).



## REFERENCES

161. Horton, J.D., Goldstein, J.L. & Brown, M.S. SREBPs: activators of the complete program of cholesterol and fatty acid synthesis in the liver. *J Clin Invest* **109**, 1125-31 (2002).
162. Ye, J. & DeBose-Boyd, R.A. Regulation of cholesterol and fatty acid synthesis. *Cold Spring Harbor perspectives in biology* **3**, a004754 (2011).
163. Shimano, H. & Sato, R. SREBP-regulated lipid metabolism: convergent physiology — divergent pathophysiology. *Nature Reviews Endocrinology* **13**, 710-730 (2017).
164. Halliwell, W.H. Cationic Amphiphilic Drug-Induced Phospholipidosis. *Toxicologic Pathology* **25**, 53-60 (1997).
165. Kornhuber, J., et al. Functional Inhibitors of Acid Sphingomyelinase (FIASMA): A Novel Pharmacological Group of Drugs with Broad Clinical Applications. *Cellular Physiology and Biochemistry* **26**, 9-20 (2010).
166. Stark, M., et al. The Lysosomotropic Activity of Hydrophobic Weak Base Drugs is Mediated via Their Intercalation into the Lysosomal Membrane. *Cells* **9**, 1082 (2020).
167. Qian, H., et al. Structural Basis of Low-pH-Dependent Lysosomal Cholesterol Egress by NPC1 and NPC2. *Cell* **182**, 98-111.e18 (2020).
168. Deffieu, M.S. & Pfeffer, S.R. Niemann–Pick type C 1 function requires luminal domain residues that mediate cholesterol-dependent NPC2 binding. *Proceedings of the National Academy of Sciences* **108**, 18932 (2011).
169. Maxfield, F.R. & Wüstner, D. Analysis of cholesterol trafficking with fluorescent probes. *Methods in cell biology* **108**, 367-393 (2012).
170. Lu, F., et al. Identification of NPC1 as the target of U18666A, an inhibitor of lysosomal cholesterol export and Ebola infection. *eLife* **4**, e12177 (2015).
171. Kuzu, O.F., Gowda, R., Sharma, A. & Robertson, G.P. Leelamine Mediates Cancer Cell Death through Inhibition of Intracellular Cholesterol Transport. *Molecular Cancer Therapeutics* **13**, 1690 (2014).
172. Ouimet, M., et al. Autophagy regulates cholesterol efflux from macrophage foam cells via lysosomal acid lipase. *Cell Metab* **13**, 655-67 (2011).
173. Elrick, M.J., Yu, T., Chung, C. & Lieberman, A.P. Impaired proteolysis underlies autophagic dysfunction in Niemann-Pick type C disease. *Human molecular genetics* **21**, 4876-4887 (2012).
174. Zschocke, J., et al. Antidepressant Drugs Diversely Affect Autophagy Pathways in Astrocytes and Neurons—Dissociation from Cholesterol Homeostasis. *Neuropsychopharmacology* **36**, 1754-1768 (2011).
175. Rossi, M., et al. Desmethylclomipramine induces the accumulation of autophagy markers by blocking autophagic flux. *Journal of cell science* **122**, 3330-3339 (2009).
176. Ashoor, R., Yafawi, R., Jessen, B. & Lu, S. The contribution of lysosomotropism to autophagy perturbation. *PloS one* **8**, e82481-e82481 (2013).
177. Pacheco, C.D., Kunkel, R. & Lieberman, A.P. Autophagy in Niemann-Pick C disease is dependent upon Beclin-1 and responsive to lipid trafficking defects. *Hum Mol Genet* **16**, 1495-503 (2007).
178. Glick, D., Barth, S. & Macleod, K.F. Autophagy: cellular and molecular mechanisms. *The Journal of pathology* **221**, 3-12 (2010).
179. Levine, B. & Klionsky, D.J. Development by Self-Digestion: Molecular Mechanisms and Biological Functions of Autophagy. *Developmental Cell* **6**, 463-477 (2004).
180. Orhon, I. & Reggiori, F. Assays to Monitor Autophagy Progression in Cell Cultures. *Cells* **6**, 20 (2017).
181. Shintani, T. & Klionsky, D.J. Autophagy in Health and Disease: A Double-Edged Sword. *Science* **306**, 990 (2004).
182. Mauthe, M., et al. Chloroquine inhibits autophagic flux by decreasing autophagosome-lysosome fusion. *Autophagy* **14**, 1435-1455 (2018).
183. Liu, W.J., et al. p62 links the autophagy pathway and the ubiquitin-proteasome system upon ubiquitinated protein degradation. *Cell Mol Biol Lett* **21**, 29 (2016).
184. Bjørkøy, G., et al., *Chapter 12 Monitoring Autophagic Degradation of p62/SQSTM1 in Methods in Enzymology*, 2009, Academic Press, 181-197.

## REFERENCES

185. Kirchhausen, T., Macia, E. & Pelish, H.E. Use of dynasore, the small molecule inhibitor of dynamin, in the regulation of endocytosis. *Methods in enzymology* **438**, 77-93 (2008).
186. Gustafsdottir, S.M., *et al.* Multiplex cytological profiling assay to measure diverse cellular states. *PLoS one* **8**, e80999-e80999 (2013).
187. Zimmermann, G., *et al.* Small molecule inhibition of the KRAS-PDE $\delta$  interaction impairs oncogenic KRAS signalling. *Nature* **497**, 638-42 (2013).
188. Yuan, H., *et al.* Tenovin-6 inhibits proliferation and survival of diffuse large B-cell lymphoma cells by blocking autophagy. *Oncotarget* **8**, 14912-14924 (2017).
189. Dai, W., Zhou, J., Jin, B. & Pan, J. Class III-specific HDAC inhibitor Tenovin-6 induces apoptosis, suppresses migration and eliminates cancer stem cells in uveal melanoma. *Scientific Reports* **6**, 22622 (2016).
190. Park, S.G., *et al.* Cytotoxic activity of bromodomain inhibitor NVS-CECR2-1 on human cancer cells. *Scientific Reports* **10**, 16330 (2020).
191. Grebien, F., *et al.* Pharmacological targeting of the Wdr5-MLL interaction in C/EBP $\alpha$  N-terminal leukemia. *Nature Chemical Biology* **11**, 571-578 (2015).
192. Long, J., *et al.* The BET bromodomain inhibitor I-BET151 acts downstream of smoothed protein to abrogate the growth of hedgehog protein-driven cancers. *J Biol Chem* **289**, 35494-502 (2014).
193. Bamborough, P., *et al.* GSK6853, a Chemical Probe for Inhibition of the BRPF1 Bromodomain. *ACS Medicinal Chemistry Letters* **7**, 552-557 (2016).
194. Cripe, L.D., *et al.* Zosuquidar, a novel modulator of P-glycoprotein, does not improve the outcome of older patients with newly diagnosed acute myeloid leukemia: a randomized, placebo-controlled trial of the Eastern Cooperative Oncology Group 3999. *Blood* **116**, 4077-4085 (2010).
195. Chen, L.S., *et al.* Pim kinase inhibitor, SGI-1776, induces apoptosis in chronic lymphocytic leukemia cells. *Blood* **114**, 4150-4157 (2009).
196. García-Echeverría, C., *et al.* In vivo antitumor activity of NVP-AEW541-A novel, potent, and selective inhibitor of the IGF-IR kinase. *Cancer Cell* **5**, 231-9 (2004).
197. Weekley, C.M. & He, C. Developing drugs targeting transition metal homeostasis. *Current opinion in chemical biology* **37**, 26-32 (2017).
198. Chen, A.Y., *et al.* Targeting Metalloenzymes for Therapeutic Intervention. *Chemical reviews* **119**, 1323-1455 (2019).
199. Gray, K.C., *et al.* Amphotericin primarily kills yeast by simply binding ergosterol. *Proceedings of the National Academy of Sciences* **109**, 2234 (2012).
200. Maclean, K.H., Cleveland, J.L. & Porter, J.B. Cellular zinc content is a major determinant of iron chelator-induced apoptosis of thymocytes. *Blood* **98**, 3831-3839 (2001).
201. Liu, G., Men, P., Perry, G. & Smith, M.A., *Nanoparticle and Iron Chelators as a Potential Novel Alzheimer Therapy in Free Radicals and Antioxidant Protocols*, 2010, Humana Press, 123-144.
202. Crisponi, G., *et al.* A Speciation Study on the Perturbing Effects of Iron Chelators on the Homeostasis of Essential Metal Ions. *PLOS ONE* **10**, e0133050 (2015).
203. Crisponi, G., Nurchi, V. & Lachowicz, J. Iron Chelation for Iron Overload in Thalassemia. *Metal ions in life sciences* **19** (2019).
204. Linden, T., *et al.* The antimycotic ciclopirox olamine induces HIF-1 $\alpha$  stability, VEGF expression, and angiogenesis. *The FASEB Journal* **17**, 761-763 (2003).
205. Subissi, A., Monti, D., Togni, G. & Mailland, F. Ciclopirox Recent Nonclinical and Clinical Data Relevant to its Use as a Topical Antimycotic Agent. *Drugs* **70**, 2133-52 (2010).
206. Bohn, M. & Kraemer, K.T. Dermatopharmacology of ciclopirox nail lacquer topical solution 8% in the treatment of onychomycosis. *Journal of the American Academy of Dermatology* **43**, S57-S69 (2000).
207. McCann, M., *et al.* Deciphering the Antimicrobial Activity of Phenanthroline Chelators. *Current Medicinal Chemistry* **19**, 2703-2714 (2012).

## REFERENCES

208. Hider, R. Recent developments centered on orally active iron chelators. *Thalassemia Reports* **4**:2261(2014).
209. Li, F., *et al.* Procaspase-3-activating compound 1 stabilizes hypoxia-inducible factor 1 $\alpha$  and induces DNA damage by sequestering ferrous iron. *Cell Death Dis* **9**, 1025 (2018).
210. *Systems Chemical Biology - Methods and Protocols*, ed. Waldmann, S.Z.a.H. 2019.
211. Filimonov, D.A., *et al.* [The computerized prediction of the spectrum of biological activity of chemical compounds by their structural formula: the PASS system. Prediction of Activity Spectra for Substance]. *Eksp Klin Farmakol* **58**, 56-62 (1995).
212. Lagunin, A., Stepanchikova, A., Filimonov, D. & Poroikov, V. PASS: prediction of activity spectra for biologically active substances. *Bioinformatics* **16**, 747-8 (2000).
213. Nickel, J., *et al.* SuperPred: update on drug classification and target prediction. *Nucleic Acids Research* **42**, W26-W31 (2014).
214. Jacobsen, D.M., *et al.* Price To Be Paid for Two-Metal Catalysis: Magnesium Ions That Accelerate Chemistry Unavoidably Limit Product Release from a Protein Kinase. *Journal of the American Chemical Society* **134**, 15357-15370 (2012).
215. Yu, L., *et al.* Role of Mg<sup>2+</sup> ions in protein kinase phosphorylation: insights from molecular dynamics simulations of ATP-kinase complexes. *Molecular Simulation* **37**, 1143-1150 (2011).
216. Wang, Z. & Cole, P.A. Catalytic mechanisms and regulation of protein kinases. *Methods in enzymology* **548**, 1-21 (2014).
217. Deweese, J.E. & Osheroff, N. The use of divalent metal ions by type II topoisomerases. *Metallomics* **2**, 450-459 (2010).
218. Sissi, C. & Palumbo, M. Effects of magnesium and related divalent metal ions in topoisomerase structure and function. *Nucleic acids research* **37**, 702-711 (2009).
219. Hegedűs, C. & Virág, L. Inputs and outputs of poly(ADP-ribose)ation: Relevance to oxidative stress. *Redox Biology* **2**, 978-982 (2014).
220. Gradwohl, G., *et al.* The second zinc-finger domain of poly(ADP-ribose) polymerase determines specificity for single-stranded breaks in DNA. *Proceedings of the National Academy of Sciences of the United States of America* **87**, 2990-2994 (1990).
221. Anand, R. & Marmorstein, R. Structure and Mechanism of Lysine-specific Demethylase Enzymes. *Journal of Biological Chemistry* **282**, 35425-35429 (2007).
222. Yao, C., *et al.* Binding, selectivity and sequence recognition of matrix metalloproteinase-2 to oligopeptides. *Journal of Biomolecular Structure and Dynamics* **38**, 275-282 (2020).
223. Ewald, B., Sampath, D. & Plunkett, W. Nucleoside analogs: molecular mechanisms signaling cell death. *Oncogene* **27**, 6522-6537 (2008).
224. Baran-Marszak, F., *et al.* Differential roles of STAT1 $\alpha$  and STAT1 $\beta$  in fludarabine-induced cell cycle arrest and apoptosis in human B cells. *Blood* **104**, 2475-2483 (2004).
225. Dasika, G.K., *et al.* DNA damage-induced cell cycle checkpoints and DNA strand break repair in development and tumorigenesis. *Oncogene* **18**, 7883-7899 (1999).
226. Vermeulen, K., Van Bockstaele, D.R. & Berneman, Z.N. The cell cycle: a review of regulation, deregulation and therapeutic targets in cancer. *Cell Prolif* **36**, 131-49 (2003).
227. Margarete, M.S.H., Hittelman, W.N. & Earnshaw, W.C. Differential Expression of DNA Topoisomerases I and II during the Eukaryotic Cell Cycle. *Proceedings of the National Academy of Sciences of the United States of America* **85**, 1086-1090 (1988).
228. Zhang, F.-L., *et al.* Topoisomerase I Inhibitors, Shikonin and Topotecan, Inhibit Growth and Induce Apoptosis of Glioma Cells and Glioma Stem Cells. *PLOS ONE* **8**, e81815 (2013).
229. Yang, Y., *et al.* Folate deprivation induces cell cycle arrest at G<sub>0</sub>/G<sub>1</sub> phase and apoptosis in hippocampal neuron cells through down-regulation of IGF-1 signaling pathway. *Int J Biochem Cell Biol* **79**, 222-230 (2016).
230. Huang, R.-F.S., *et al.* Folate Deficiency Induces a Cell Cycle-Specific Apoptosis in HepG2 Cells. *The Journal of Nutrition* **129**, 25-31 (1999).

## REFERENCES

---

231. Morales, J., *et al.* Review of poly (ADP-ribose) polymerase (PARP) mechanisms of action and rationale for targeting in cancer and other diseases. *Critical reviews in eukaryotic gene expression* **24**, 15-28 (2014).
232. Michelena, J., *et al.* Analysis of PARP inhibitor toxicity by multidimensional fluorescence microscopy reveals mechanisms of sensitivity and resistance. *Nature Communications* **9**, 2678 (2018).
233. Jelinic, P. & Levine, D.A. New Insights into PARP Inhibitors; Effect on Cell Cycle and Homology-Directed DNA Damage Repair. *Molecular Cancer Therapeutics* **13**, 1645 (2014).
234. Laronha, H. & Caldeira, J. Structure and Function of Human Matrix Metalloproteinases. *Cells* **9**, 1076 (2020).
235. Nyormoi, O., Mills, L. & Bar-Eli, M. An MMP-2/MMP-9 inhibitor, 5a, enhances apoptosis induced by ligands of the TNF receptor superfamily in cancer cells. *Cell Death & Differentiation* **10**, 558-569 (2003).
236. Daniel, C., *et al.* Matrix metalloproteinase inhibitors cause cell cycle arrest and apoptosis in glomerular mesangial cells. *J Pharmacol Exp Ther* **297**, 57-68 (2001).
237. He, Y., *et al.* LSD1 promotes S-phase entry and tumorigenesis via chromatin co-occupation with E2F1 and selective H3K9 demethylation. *Oncogene* **37**, 534-543 (2018).
238. Walls, K.C., *et al.* Lysosome dysfunction triggers Atg7-dependent neural apoptosis. *The Journal of biological chemistry* **285**, 10497-10507 (2010).
239. Wang, F., Gómez-Sintes, R. & Boya, P. Lysosomal membrane permeabilization and cell death. *Traffic* **19**, 918-931 (2018).
240. Ermis, M., *et al.* A high throughput approach for analysis of cell nuclear deformability at single cell level. *Scientific reports* **6**, 36917-36917 (2016).
241. Dix, C.L., *et al.* The Role of Mitotic Cell-Substrate Adhesion Re-modeling in Animal Cell Division. *Dev Cell* **45**, 132-145.e3 (2018).
242. Weber, R.A., *et al.* Maintaining Iron Homeostasis Is the Key Role of Lysosomal Acidity for Cell Proliferation. *Molecular Cell* **77**, 645-655.e7 (2020).
243. Matsumoto, N. & Nakanishi-Matsui, M. Proton pumping V-ATPase inhibitor bafilomycin A1 affects Rab7 lysosomal localization and abolishes anterograde trafficking of osteoclast secretory lysosomes. *Biochem Biophys Res Commun* **510**, 421-426 (2019).
244. Mauvezin, C. & Neufeld, T.P. Bafilomycin A1 disrupts autophagic flux by inhibiting both V-ATPase-dependent acidification and Ca-P60A/SERCA-dependent autophagosome-lysosome fusion. *Autophagy* **11**, 1437-1438 (2015).
245. Teplova, V.V., *et al.* Bafilomycin A1 is a potassium ionophore that impairs mitochondrial functions. *Journal of Bioenergetics and Biomembranes* **39**, 321 (2007).
246. Zoncu, R., *et al.* mTORC1 senses lysosomal amino acids through an inside-out mechanism that requires the vacuolar H(+)-ATPase. *Science* **334**, 678-83 (2011).
247. Espenshade, P.J. SREBPs: sterol-regulated transcription factors. *Journal of Cell Science* **119**, 973 (2006).
248. Afonso, M.S., *et al.* Molecular Pathways Underlying Cholesterol Homeostasis. *Nutrients* **10**, 760 (2018).
249. Howe, V., *et al.* Cholesterol homeostasis: How do cells sense sterol excess? *Chem Phys Lipids* **199**, 170-178 (2016).
250. Raeder, M., *et al.* Antidepressant drugs activate SREBP and up-regulate cholesterol and fatty acid biosynthesis in human glial cells. *Neuroscience letters* **395**, 185-90 (2006).
251. Fernø, J., *et al.* Antipsychotic drugs activate SREBP-regulated expression of lipid biosynthetic genes in cultured human glioma cells: a novel mechanism of action? *The Pharmacogenomics Journal* **5**, 298-304 (2005).
252. Kristiana, I., *et al.* Antipsychotic drugs upregulate lipogenic gene expression by disrupting intracellular trafficking of lipoprotein-derived cholesterol. *The Pharmacogenomics Journal* **10**, 396-407 (2010).

## REFERENCES

253. Skrede, S., Steen, V.M. & Fernø, J. Antipsychotic-induced increase in lipid biosynthesis: activation through inhibition? *Journal of lipid research* **54**, 307-309 (2013).
254. Fernø, J., *et al.* Drug-induced activation of SREBP-controlled lipogenic gene expression in CNS-related cell lines: marked differences between various antipsychotic drugs. *BMC neuroscience* **7**, 69-69 (2006).
255. Vik-Mo, A.O., Fernø, J., Skrede, S. & Steen, V.M. Psychotropic drugs up-regulate the expression of cholesterol transport proteins including ApoE in cultured human CNS- and liver cells. *BMC pharmacology* **9**, 10-10 (2009).
256. Lange, Y. & Steck, T.L. Cholesterol homeostasis. Modulation by amphiphiles. *J Biol Chem* **269**, 29371-4 (1994).
257. Lange, Y., Ye, J., Rigney, M. & Steck, T. Cholesterol movement in Niemann-Pick type C cells and in cells treated with amphiphiles. *J Biol Chem* **275**, 17468-75 (2000).
258. Sobo, K., *et al.* Late endosomal cholesterol accumulation leads to impaired intra-endosomal trafficking. *PLoS one* **2**, e851-e851 (2007).
259. Zhang, M., *et al.* Cessation of rapid late endosomal tubulovesicular trafficking in Niemann-Pick type C1 disease. *Proc Natl Acad Sci U S A* **98**, 4466-71 (2001).
260. Kawai, A., *et al.* Autophagosome-lysosome fusion depends on the pH in acidic compartments in CHO cells. *Autophagy* **3**, 154-7 (2007).
261. Liao, G., *et al.* Cholesterol accumulation is associated with lysosomal dysfunction and autophagic stress in Npc1 *-/-* mouse brain. *Am J Pathol* **171**, 962-75 (2007).
262. Guo, H., *et al.* Niemann-Pick type C2 deficiency impairs autophagy-lysosomal activity, mitochondrial function, and TLR signaling in adipocytes. *Journal of lipid research* **57**, 1644-1658 (2016).
263. Laraia, L., *et al.* Discovery of Novel Cinchona-Alkaloid-Inspired Oxazastatane Autophagy Inhibitors. *Angewandte Chemie International Edition* **56**, 2145-2150 (2017).
264. Sardiello, M., *et al.* A gene network regulating lysosomal biogenesis and function. *Science* **325**, 473-7 (2009).
265. *MATER METHODS* **2014**;4:827.
266. Eid, W., *et al.* mTORC1 activates SREBP-2 by suppressing cholesterol trafficking to lysosomes in mammalian cells. *Proc Natl Acad Sci U S A* **114**, 7999-8004 (2017).
267. Peterson, T.R., *et al.* mTOR complex 1 regulates lipin 1 localization to control the SREBP pathway. *Cell* **146**, 408-20 (2011).
268. Wang, B.T., *et al.* The mammalian target of rapamycin regulates cholesterol biosynthetic gene expression and exhibits a rapamycin-resistant transcriptional profile. *Proc Natl Acad Sci U S A* **108**, 15201-6 (2011).
269. Tonini, C., *et al.* Inhibition of Bromodomain and Extraterminal Domain (BET) Proteins by JQ1 Unravels a Novel Epigenetic Modulation to Control Lipid Homeostasis. *Int J Mol Sci* **21**(2020).
270. Dai, X., *et al.* Src kinase inhibitor PP2 regulates the biological characteristics of A549 cells via the PI3K/Akt signaling pathway. *Oncology letters* **16**, 5059-5065 (2018).
271. Garrigues, A., Escargueil, A.E. & Orłowski, S. The multidrug transporter, P-glycoprotein, actively mediates cholesterol redistribution in the cell membrane. *Proceedings of the National Academy of Sciences* **99**, 10347 (2002).
272. Kornhuber, J., *et al.* Identification of new functional inhibitors of acid sphingomyelinase using a structure-property-activity relation model. *J Med Chem* **51**, 219-37 (2008).
273. Warrilow, A.G., Parker, J.E., Kelly, D.E. & Kelly, S.L. Azole affinity of sterol 14 $\alpha$ -demethylase (CYP51) enzymes from *Candida albicans* and *Homo sapiens*. *Antimicrobial agents and chemotherapy* **57**, 1352-1360 (2013).
274. Trinh, M.N., *et al.* Triazoles inhibit cholesterol export from lysosomes by binding to NPC1. *Proc Natl Acad Sci U S A* **114**, 89-94 (2017).
275. Kraemer, F.B. & Pont, A. Inhibition of cholesterol synthesis by ketoconazole. *Am J Med* **80**, 616-22 (1986).
276. Kraemer, F.B. & Spilman, S.D. Effects of ketoconazole on cholesterol synthesis. *J Pharmacol Exp Ther* **238**, 905-11 (1986).

## REFERENCES

277. Séité, S., *et al.* The Autophagic Flux Inhibitor Bafilomycin A1 Affects the Expression of Intermediary Metabolism-Related Genes in Trout Hepatocytes. *Frontiers in Physiology* **10** (2019).
278. Snodgrass, R.G., *et al.* A Novel Function for 15-Lipoxygenases in Cholesterol Homeostasis and CCL17 Production in Human Macrophages. *Frontiers in Immunology* **9** (2018).
279. Furuchi, T., Aikawa, K., Arai, H. & Inoue, K. Bafilomycin A1, a specific inhibitor of vacuolar-type H(+)-ATPase, blocks lysosomal cholesterol trafficking in macrophages. *J Biol Chem* **268**, 27345-8 (1993).
280. Young, D.W., *et al.* Integrating high-content screening and ligand-target prediction to identify mechanism of action. *Nat Chem Biol* **4**, 59-68 (2008).
281. Wassermann, A.M., Tudor, M. & Glick, M. Deorphanization strategies for dark chemical matter. *Drug Discov Today Technol* **23**, 69-74 (2017).
282. Winzker, M., *et al.* Development of a PDE $\delta$ -Targeting PROTACs that Impair Lipid Metabolism. *Angewandte Chemie International Edition* **59**, 5595-5601 (2020).
283. Papke, B., *et al.* Identification of pyrazolopyridazinones as PDE $\delta$  inhibitors. *Nat Commun* **7**, 11360 (2016).
284. Calvert, M.E., Ward, A.M., Wright, G.D. & Bard, F. New developments and novel applications in high throughput and high content imaging. *Cytometry A* **89**, 705-7 (2016).
285. Saei, A.A., *et al.* ProTargetMiner: A proteome signature library of anticancer molecules for functional discovery. *bioRxiv*, 421115 (2018).
286. Noguchi, S., *et al.* Bosutinib, an SRC inhibitor, induces caspase-independent cell death associated with permeabilization of lysosomal membranes in melanoma cells. *Vet Comp Oncol* **16**, 69-76 (2018).
287. Ravindranath, A.C., *et al.* Connecting gene expression data from connectivity map and in silico target predictions for small molecule mechanism-of-action analysis. *Molecular bioSystems* **11**, 86-96 (2015).
288. Stüven, E., *et al.* Intra-Golgi Protein Transport Depends on a Cholesterol Balance in the Lipid Membrane. *The Journal of biological chemistry* **278**, 53112-22 (2004).
289. Shacoori, V., *et al.* Inhibition of (Na<sup>+</sup>,K<sup>+</sup>)-ATPase and Mg<sup>++</sup>-ATPase by a lysosomotropic drug: perhexiline maleate. *Res Commun Chem Pathol Pharmacol* **59**, 161-72 (1988).
290. Lüllmann-Rauch, R., Pods, R. & von Witzendorff, B. The antimalarials quinacrine and chloroquine induce weak lysosomal storage of sulphated glycosaminoglycans in cell culture and in vivo. *Toxicology* **110**, 27-37 (1996).
291. Zhitomirsky, B., *et al.* Lysosomotropic drugs activate TFEB via lysosomal membrane fluidization and consequent inhibition of mTORC1 activity. *Cell Death & Disease* **9**, 1191 (2018).
292. Baxt, B. Effect of lysosomotropic compounds on early events in foot-and-mouth disease virus replication. *Virus Res* **7**, 257-71 (1987).
293. Zhou, W., *et al.* Chloroquine against malaria, cancers and viral diseases. *Drug Discovery Today* **25**, 2012-2022 (2020).
294. Settembre, C., Fraldi, A., Medina, D.L. & Ballabio, A. Signals from the lysosome: a control centre for cellular clearance and energy metabolism. *Nat Rev Mol Cell Biol* **14**, 283-96 (2013).
295. Settembre, C. & Ballabio, A. Lysosomal adaptation: how the lysosome responds to external cues. *Cold Spring Harbor perspectives in biology* **6**, a016907 (2014).
296. Bi, X. & Liao, G. Cholesterol in Niemann-Pick Type C disease. *Sub-cellular biochemistry* **51**, 319-335 (2010).
297. Tamura, A. & Yui, N. Lysosomal-specific Cholesterol Reduction by Biocleavable Polyrotaxanes for Ameliorating Niemann-Pick Type C Disease. *Scientific Reports* **4**, 4356 (2014).
298. Kornhuber, J., *et al.* Lipophilic cationic drugs increase the permeability of lysosomal membranes in a cell culture system. *J Cell Physiol* **224**, 152-64 (2010).

## REFERENCES

---

299. Duvvuri, M. & Krise, J.P. A Novel Assay Reveals That Weakly Basic Model Compounds Concentrate in Lysosomes to an Extent Greater Than pH-Partitioning Theory Would Predict. *Molecular Pharmaceutics* **2**, 440-448 (2005).
300. Kelley, M.R. & Fishel, M.L. DNA repair proteins as molecular targets for cancer therapeutics. *Anti-cancer agents in medicinal chemistry* **8**, 417-425 (2008).
301. Ibrahim, O. & O'Sullivan, J. Iron chelators in cancer therapy. *BioMetals* **33**, 201-215 (2020).
302. Berdis, A.J. Inhibiting DNA Polymerases as a Therapeutic Intervention against Cancer. *Frontiers in Molecular Biosciences* **4** (2017).
303. Feng, D., Tu, Z., Wu, W. & Liang, C. Inhibiting the expression of DNA replication-initiation proteins induces apoptosis in human cancer cells. *Cancer Res* **63**, 7356-64 (2003).
304. Lange, S.S., Takata, K.-i. & Wood, R.D. DNA polymerases and cancer. *Nature reviews. Cancer* **11**, 96-110 (2011).
305. Hughes, J.P., Rees, S., Kalindjian, S.B. & Philpott, K.L. Principles of early drug discovery. *British journal of pharmacology* **162**, 1239-1249 (2011).
306. Lin, A., *et al.* Off-target toxicity is a common mechanism of action of cancer drugs undergoing clinical trials. *Science Translational Medicine* **11**, eaaw8412 (2019).
307. Schloer, S., *et al.* Targeting the endolysosomal host-SARS-CoV-2 interface by clinically licensed functional inhibitors of acid sphingomyelinase (FIASMA) including the antidepressant fluoxetine. *Emerg Microbes Infect* **9**, 2245-2255 (2020).
308. Ballout, R.A., Sviridov, D., Bukrinsky, M.I. & Remaley, A.T. The lysosome: A potential juncture between SARS-CoV-2 infectivity and Niemann-Pick disease type C, with therapeutic implications. *The FASEB Journal* **34**, 7253-7264 (2020).
309. Daniloski, Z., *et al.* Identification of Required Host Factors for SARS-CoV-2 Infection in Human Cells. *Cell* (2020).

**10 FIGURES**

Figure 1: Classical versus chemical genetics to study biological systems. Adapted from Kawasumi and Nghiem.<sup>[2]</sup> .....6

Figure 2: Schematic illustration of the central dogma of molecular biology. Adapted from M. P. Richards.<sup>[38]</sup> ..... 10

Figure 3: General workflow of morphological profiling of small molecules adapted from Ziegler *et al.*<sup>[36]</sup>..... 13

Figure 4: Target or mode-of-action prediction for uncharacterized compounds (cmp) based on comparison of morphological profiles to annotated reference (ref) compounds. .... 14

Figure 5: Schematic representation of morphological profiles subjected to hierarchical clustering or dimensionality reduction used for the clustering of low-dimensional profiles.... 16

Figure 6: Schematic representation of morphological profiling for small molecules to reverse disease phenotype..... 17

Figure 7: Workflow of the CPA and data analysis performed at the COMAS and MPI, Dortmund adapted from Ziegler *et al.*<sup>[36, 59]</sup> ..... 19

Figure 8: Workflow for bioactivity prediction performed at the MPI, Dortmund. .... 21

Figure 9: Morphological fingerprints of DFO. .... 49

Figure 10: Selected features of the morphological fingerprints of DFO. .... 50

Figure 11: Morphological profiling of different metal-chelating agents with high biosimilarity to DFO..... 52

Figure 12: Morphological fingerprints of reference compounds with high biosimilarity (> 75 %) to 10  $\mu$ M DFO. .... 53

Figure 13: Influence of DFO on cell growth, iron chelation and cell cycle..... 55

Figure 14: Influence of selected nucleoside analogs on cell growth, iron chelation and cell cycle. .... 57

Figure 15: Influence of PHA-793887, roscovitine and Topotecan on cell growth, iron chelation and cell cycle..... 59

Figure 16: Images of U-2OS cells treated with PHA-793887 and roscovitine..... 61

Figure 17: Influence of Ciclopirox, resveratrol and Doxorubicin on cell growth, iron chelation and cell cycle..... 62

Figure 18: Images of U-2OS cells treated with 0.37  $\mu$ M Doxorubicin..... 63

Figure 19: Iron chelation by compounds with high biosimilarity to DFO..... 64

Figure 20: Morphological profiling of 8-hydroxyquinoline derivatives 1-7 with high biosimilarity to DFO..... 65

Figure 21: Influence of compounds 1-7 on cell growth. .... 67

Figure 22: Influence of compounds 1-7 on iron chelation and cell cycle..... 68



## FIGURES

---

|  |     |
|--|-----|
| Figure 23: Morphological profiling of compounds 8 and 9 with high biosimilarity to DFO. ....   | 69  |
| Figure 24: Influence of compounds 8 and 9 on cell growth, iron chelation and cell cycle. ....  | 71  |
| Figure 25: DNA binding of compounds 8 and 9. ....  | 72  |
| Figure 26: Hierarchical clustering of fingerprints from compounds biosimilar (> 80 %) to 10 $\mu$ M DFO.....                                 | 75  |
| Figure 27: Hierarchical clustering of fingerprints from compounds biosimilar (> 80 %) to DFO based on selected features. ....                | 76  |
| Figure 28: Morphological fingerprints of tetrahydroindolo[2,3-a]quinolizines 10-13.....  | 77  |
| Figure 29: Morphological profiling of compounds 10-13.....   | 78  |
| Figure 30: Distribution of target classes among references biosimilar to 10 $\mu$ M compound 13. ....  | 79  |
| Figure 31: Physicochemical properties of references biosimilar to compound 13. ....  | 80  |
| Figure 32: Influence of compounds 10-13 on lysosomal accumulation of LysoTracker™ Red DND-99. ....   | 81  |
| Figure 33: Influence of compounds 10-13 on cell growth and morphology.....   | 83  |
| Figure 34: Influence of compound 13 on cell morphology. ....   | 84  |
| Figure 35: Influence of compound 13 on the growth of HeLa and L cells. ....  | 85  |
| Figure 36: Influence of Bafilomycin A1 co-treatment on cell morphology and viability of U-2OS cells that were treated with compound 13.....  | 86  |
| Figure 37: Influence of compound 13 on actin dynamics. ....  | 88  |
| Figure 38: Influence of compounds 12 and 13 on the actin cytoskeleton. ....  | 90  |
| Figure 39: Proteome profiling analysis of compound 13.....   | 92  |
| Figure 40: Proteome profiling analysis of compound 12.....   | 93  |
| Figure 41: Proteome profiling analysis of compounds 10 and 11.....   | 95  |
| Figure 42: Influence of compounds 10-13 on SREBP-dependent transcriptional activation. ....  | 97  |
| Figure 43: Influence of compounds 10-13 on cellular cholesterol distribution. ....   | 99  |
| Figure 44: Quantification of filipin staining for compound 13.....   | 100 |
| Figure 45: Influence of compounds 10-13 on the number of LC3II puncta. ....  | 102 |
| Figure 46: Influence of compounds 12 and 13 on the protein levels of LC3II and p62/SQSTM1. ....  | 103 |
| Figure 47: Influence of compounds 10-13 on the endocytotic uptake of transferrin. ....   | 105 |
| Figure 48: Influence of selected GPCR-targeting references on SREBP-dependent transcriptional activation and lysosomal staining. ....        | 106 |
| Figure 49: Influence of selected ion channel-targeting references on SREBP-dependent transcriptional activation and lysosomal staining. .... | 107 |
| Figure 50: Influence of selected enzyme-targeting references on SREBP-dependent transcriptional activation and lysosomal staining. ....      | 108 |

## FIGURES

---

|  |     |
|--|-----|
| Figure 51: Influence of selected kinase-targeting references on SREBP-dependent transcriptional activation and lysosomal staining. ....                          | 109 |
| Figure 52: Influence of selected references with miscellaneous targets and activities on SREBP-dependent transcriptional activation and lysosomal staining. .... | 111 |
| Figure 53: Morphological fingerprints of statins and their influence on lysosomal staining and SRE-mediated gene expression. ....                                | 113 |
| Figure 54: Regulation of cholesterol homeostasis adapted from P. J. Espenshade. <sup>[247]</sup> ....  | 127 |
| Figure 55: Possible influences of lysosomotropic compounds on cholesterol homeostasis. ....  | 129 |
| Figure 56: Physicochemical properties of selected references biosimilar to compound 13. ....   | 132 |
| Figure 57: Influence of deltasonamide 1 and deltazinone 1 on lysosomal staining. ....  | 136 |

## 11 TABLES

|   |     |
|---|-----|
| Table 1: Volumes used to wash, detach and resuspend the cells depending on the flask size.<br>.....   | 33  |
| Table 2: Antibodies, blocking solution and detection method for LC3 and p62 p62/SQSTM1 immunoblot.....  | 42  |
| Table 3: Inhibition of human topoisomerase I relaxation and topoisomerase II $\alpha$ decatenation by 30 $\mu$ M compounds 8 and 9. ....                                      | 73  |
| Table 4: Inhibition or binding of selected CDK/cyclin complexes by 30 $\mu$ M compounds 8 and 9. ....   | 74  |
| Table 5: Modulated genes involved in the biosynthesis of cholesterol upon treatment with indicated compounds.....   | 114 |
| Table 6: Ion binding preferences of metal ion chelators. ....   | 117 |
| Table 7: Target prediction for iron chelators using web-based cheminformatic tools. <sup>[210]</sup> ....   | 118 |
| Table 8: Targets of references, biosimilar to DFO, that require metal ions for their activity.<br>.....   | 119 |
| Table 9: Target prediction for 8-hydroxyquinoline using web-based cheminformatic tools. <sup>[210]</sup><br>.....   | 121 |
| Table 10: Connectivity Map (CMap) <sup>[41]</sup> analysis for Chlorpromazine. ....   | 134 |
| Table 11: Structure of references with high biosimilarity (> 75 %) to DFO. ....   | 166 |
| Table 12: Quantification of the percentage of U-2OS cells in the G1 (DNA content of 2N), S and G2 (4N) phase of the cell cycle upon treatment with annotated references. .... | 168 |
| Table 13: Quantification of the percentage of U-2OS cells in the G1 (DNA content of 2N), S and G2 (4N) phase of the cell cycle upon treatment with compounds 1-9.....         | 168 |
| Table 14: Annotated reference compounds with high morphological biosimilarity ( $\geq$ 75 %) to 10 $\mu$ M compound 13.....   | 169 |
| Table 15: Proteins modulated by 10 $\mu$ M compound 13. ....  | 182 |
| Table 16: Proteins modulated by compound 12. ....   | 185 |
| Table 17: Proteins modulated by compound 10. ....   | 188 |
| Table 18: Proteins modulated by compound 11. ....   | 189 |
| Table 19: Structures of selected annotated reference compounds with high biosimilarity (> 75 %) to 10 $\mu$ M compound 13. ....   | 192 |

## 12 ABBREVIATIONS

| Abbreviation            | Definition   |
|-------------------------|--|
| <b>25OHC</b>            | 25-hydroxycholesterol                                |
| <b>ACAT</b>             | Acyl coenzymeA:cholesterol acyltransferase           |
| <b>ACSS2</b>            | Acetyl-coenzyme A synthetase                         |
| <b>AF</b>               | Alexa fluorophore                                    |
| <b>APS</b>              | Ammonium persulfate                                  |
| <b>ASM</b>              | Acid sphingomyelinase                                |
| <b>ATP</b>              | Adenosine triphosphate                               |
| <b>Baf A1</b>           | Bafilomycin A1                                       |
| <b>BioSim</b>           | Biosimilarity  |
| <b>BRPF1</b>            | Bromodomain and PHD Finger Containing 1              |
| <b>BSA</b>              | Bovine serum albumin                                 |
| <b>CaCl<sub>2</sub></b> | Calcium chloride                                     |
| <b>CDK</b>              | Cyclin-dependent kinase                              |
| <b>cDNA</b>             | Complementary deoxyribonucleic acid                  |
| <b>CECR2</b>            | Cat eye syndrome chromosome region, candidate 2      |
| <b>CLEAR</b>            | Coordinated lysosomal expression and regulation      |
| <b>CMAP</b>             | Connectivity map                                     |
| <b>Cmp</b>              | Compound   |
| <b>COMAS</b>            | Compound Management and Screening Center             |
| <b>Conc.</b>            | Concentration  |
| <b>COP</b>              | Coat protein complex                                 |
| <b>CPA</b>              | Cell Painting Assay                                  |
| <b>CQ</b>               | Chloroquine  |
| <b>CRISPR</b>           | Clustered regulatory interspaced palindromic repeats |
| <b>Cy5</b>              | Cyanine 5  |
| <b>d</b>                | Day  |
| <b>DAPI</b>             | 4',6-diamidino-2-phenylindole                        |

## ABBREVIATIONS

| Abbreviation  | Definition   |
|---------------|--|
| <b>DFO</b>    | Deferoxamine   |
| <b>DMEM</b>   | Dulbecco's modified eagle's medium   |
| <b>DMSO</b>   | Dimethyl sulfoxide   |
| <b>DNA</b>    | Deoxyribonucleic acid  |
| <b>DNase</b>  | Deoxyribonuclease  |
| <b>DTE</b>    | Dithioerythritol   |
| <b>DTT</b>    | Dithiothreitol   |
| <b>EBSS</b>   | Earle's balanced salt solution   |
| <b>EDTA</b>   | Ethylenediaminetetraacetate  |
| <b>EdU</b>    | 5-ethynyl-2'-deoxyuridine  |
| <b>EGFP</b>   | Enhanced green fluorescent protein   |
| <b>EGTA</b>   | Ethylene glycol-bis( $\beta$ -aminoethyl ether)-N,N,N',N'-tetraacetic acid |
| <b>EIPA</b>   | 5-(N-Ethyl-N-isopropyl)amiloride   |
| <b>Em</b>     | Emission   |
| <b>EMEM</b>   | Eagle's minimum essential medium   |
| <b>ER</b>     | Endoplasmic reticulum  |
| <b>Ex</b>     | Excitation   |
| <b>FACS</b>   | Fluorescence activated cell sorting  |
| <b>FADS2</b>  | Fatty acid desaturase 2  |
| <b>FDA</b>    | Food and Drug Administration   |
| <b>FDFT1</b>  | Squalene synthase  |
| <b>FDR</b>    | False discovery rate   |
| <b>FITC</b>   | Fluorescein isothiocyanate   |
| <b>FSC</b>    | Forward scatter  |
| <b>g</b>      | Gravity  |
| <b>G418</b>   | Geneticin  |
| <b>GPCR</b>   | G protein-coupled receptor   |
| <b>GTPase</b> | Guanosine triphosphatase   |
| <b>h</b>      | hour   |

## ABBREVIATIONS

| Abbreviation            | Definition   |
|-------------------------|--|
| <b>HCL</b>              | Hydrochloric acid                                  |
| <b>HEPES</b>            | 4-(2-hydroxyethyl)-1-piperazineethanesulfonic acid |
| <b>HMG-CoA</b>          | 3-hydroxy-3-methylglutaryl-coenzyme A              |
| <b>HMGCR</b>            | 3-hydroxy-3-methylglutaryl-coenzyme A reductase    |
| <b>HMGCS1</b>           | 3-hydroxy-3-methylglutaryl-coenzyme A synthase     |
| <b>HPLC</b>             | High pressure liquid chromatography                |
| <b>HRP</b>              | Horseradish peroxidase                             |
| <b>IDI1</b>             | Isopentyl-diphosphate delta-isomerase 1            |
| <b>Ind</b>              | Induction  |
| <b>Insig-1</b>          | Insulin-induced gene protein-1                     |
| <b>IPA</b>              | Ingenuity pathway analysis                         |
| <b>KRAS</b>             | Kirsten rat sarcoma                                |
| <b>LB</b>               | Lysogeny broth                                     |
| <b>LC3</b>              | Microtubule-associated light chain protein 3       |
| <b>LDL</b>              | Low-density lipoprotein                            |
| <b>LOPAC</b>            | Library of pharmacologically active compounds      |
| <b>LSD1</b>             | Lysine-specific histone demethylase 1              |
| <b>LSS</b>              | Lanosterol synthase                                |
| <b>MAD</b>              | Median absolute deviation                          |
| <b>MAP kinase p38</b>   | Mitogen-activated protein kinase p38               |
| <b>MBP</b>              | Median biosimilarity percentage                    |
| <b>MgCl<sub>2</sub></b> | Magnesium chloride                                 |
| <b>mH<sub>2</sub>O</b>  | Millipore filtered deionized water                 |
| <b>min</b>              | Minute   |
| <b>MLL1</b>             | Mixed lineage leukemia protein 1                   |
| <b>MMoA</b>             | Molecular mechanism of action                      |
| <b>MMP-2</b>            | Matrix metalloproteinase-2                         |
| <b>MoA</b>              | Mode of action                                     |
| <b>mRNA</b>             | Messenger ribonucleic acid                         |

## ABBREVIATIONS

| Abbreviation     | Definition  |
|------------------|---|
| <b>MS</b>        | Mass spectrometry   |
| <b>NaCl</b>      | Sodium chloride   |
| <b>Neu-1</b>     | Sialidase-1   |
| <b>NGS</b>       | Next generation sequencing                                |
| <b>NPC1/2</b>    | Niemann-Pick protein C1 and C2                            |
| <b>PARP</b>      | Poly(ADP-Ribose)-polymerase                               |
| <b>PBS</b>       | Phosphate-buffered saline                                 |
| <b>PCR</b>       | Polymerase chain reaction                                 |
| <b>PDE</b>       | Phosphodiesterase   |
| <b>PFA</b>       | Paraformaldehyde  |
| <b>PI</b>        | Propidium iodide  |
| <b>PIPES</b>     | Piperazine-N,N'-bis(2-ethanesulfonic acid)                |
| <b>PPT1</b>      | Palmitoyl-protein thioesterase 1                          |
| <b>PROTAC</b>    | Proteolysis targeting chimera                             |
| <b>PVDF</b>      | Polyvinylidenfluorid                                      |
| <b>Ref</b>       | Reference   |
| <b>RNA</b>       | Ribonucleic acid  |
| <b>RNAi</b>      | RNA interference  |
| <b>RNase</b>     | Ribonuclease  |
| <b>rpm</b>       | Revolutions per minute                                    |
| <b>RT</b>        | Room temperature  |
| <b>S1P/2</b>     | Proteases site-1 and site-2                               |
| <b>SARS-CoV2</b> | Severe Acute Respiratory Syndrome Related Coronavirus 2   |
| <b>Scap</b>      | SREBP cleavage-activating protein                         |
| <b>SCPEP1</b>    | Retinoid-inducible serine carboxypeptidase                |
| <b>SD</b>        | Standard deviation  |
| <b>SDS</b>       | Sodium dodecyl sulfate                                    |
| <b>SDS-PAGE</b>  | Sodium dodecyl sulfate polyacrylamide gel electrophoresis |
| <b>SEA</b>       | Similarity ensemble approach                              |

## ABBREVIATIONS

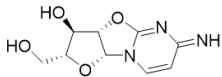
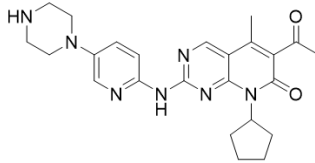
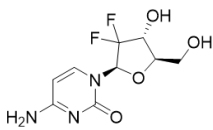
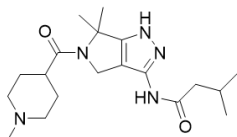
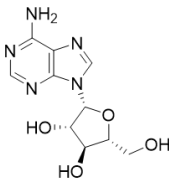
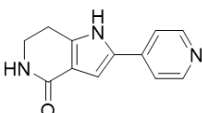
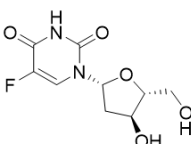
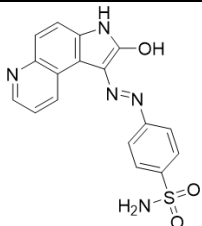
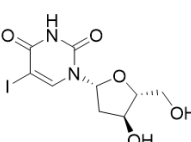
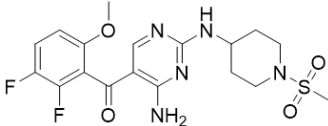
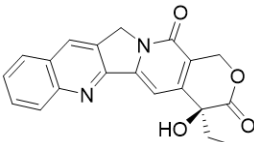
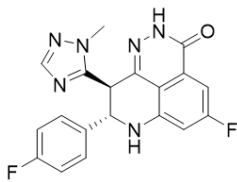
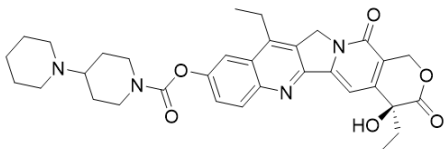
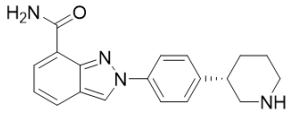
| Abbreviation    | Definition                                |
|-----------------|---|
| <b>s</b>        | Second                                    |
| <b>siRNA</b>    | Small interfering ribonucleic acid        |
| <b>SQSTM1</b>   | Sequestome-1                              |
| <b>SRE</b>      | Sterol regulatory element                 |
| <b>SREBP</b>    | Sterol regulatory element binding protein |
| <b>SSC</b>      | Side scatter                              |
| <b>STARD4</b>   | StAR-related lipid transport protein 4    |
| <b>TCEP</b>     | Tris(2-carboxyethyl)phosphine             |
| <b>TEAB</b>     | Tetraethylammonium bicarbonate            |
| <b>TEMED</b>    | Tetramethylethylenediamine                |
| <b>TFEB</b>     | Transcription factor EB                   |
| <b>TMT</b>      | Tandem mass tag                           |
| <b>Tris</b>     | Tris(hydroxymethyl)aminomethan            |
| <b>TxRed</b>    | Texas red                                 |
| <b>V</b>        | Volt                                      |
| <b>v-ATPase</b> | Vacuolar-adenosine triphosphatase         |
| <b>WDR5</b>     | WD repeat domain 5                        |
| <b>WGA</b>      | Wheat germ agglutinin                     |



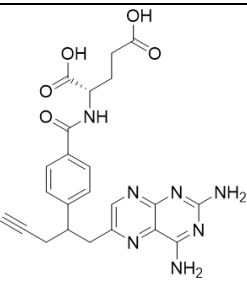
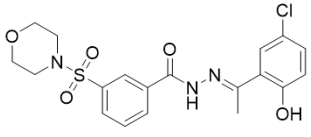
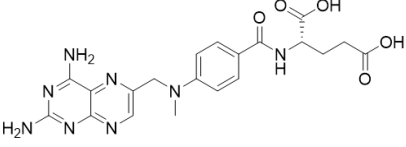
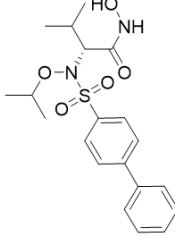
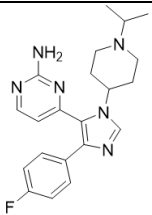
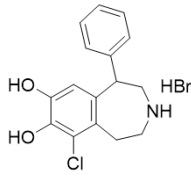
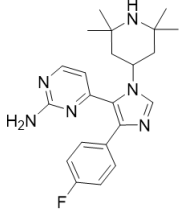
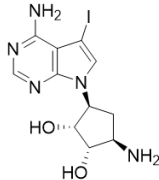
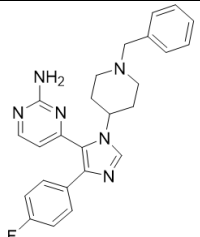
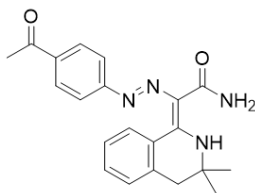
## 13 APPENDIX

## 13.1 Additional data related to 6.1

Table 11: Structure of references with high biosimilarity (&gt; 75 %) to DFO.

| Trivial name         | Structure   | Trivial name               | Structure   |
|----------------------|---|----------------------------|---|
| Ancitabine           |    | Palbociclib                |    |
| Gemcitabine          |    | PHA-793887                 |    |
| Vidarabine           |   | PHA-767491                 |   |
| Floxuridine          |  | Oxindole-based inhibitor-2 |  |
| Idoxuridine          |  | R547                       |  |
| (S)-(+)-Camptothecin |  | BMN-673                    |  |
| Irinotecan           |  | Niraparib                  |  |

APPENDIX

| Trivial name                     | Structure   | Trivial name               | Structure   |
|----------------------------------|---|----------------------------|---|
| Pralatrexate                     |    | SP2509                     |    |
| Methotrexate                     |    | ARP 101                    |    |
| Pyrimidinylimidazole inhibitor-3 |   | (±)-SKF-81297 hydrobromide |    |
| Pyrimidinylimidazole inhibitor-4 |  | A-134974                   |  |
| Pyrimidinylimidazole inhibitor-5 |  | IQ 1                       |  |

**APPENDIX**

**Table 12: Quantification of the percentage of U-2OS cells in the G1 (DNA content of 2N), S and G2 (4N) phase of the cell cycle upon treatment with annotated references.**

Cells were treated with reference compounds or DMSO as a control for 22 h and afterwards pulsed for another 2 h with 10  $\mu$ M EdU (5-ethynyl-2'-deoxyuridine) prior to fixation and staining of DNA with PI. DNA content and EdU incorporation were determined by means of flow cytometry. Data are mean values of three independent experiments.

| Compound                     | Cells / % |      |       |      |      |      |
|------------------------------|-----------|------|-------|------|------|------|
|                              | 2N        |      | 2N-4N |      | 4N   |      |
|                              | Mean      | SD   | Mean  | SD   | Mean | SD   |
| DMSO                         | 46.6      | 3.5  | 38.0  | 6.3  | 15.3 | 8.4  |
| 10 $\mu$ M Deferoxamine      | 18.1      | 10.7 | 78.8  | 13.2 | 2.9  | 2.3  |
| 10 $\mu$ M Trifluridine      | 3.5       | 0.7  | 93.2  | 3.2  | 3.1  | 2.4  |
| 3.33 $\mu$ M Arabinocytidine | 30.6      | 9.6  | 63.3  | 9.4  | 5.5  | 0.5  |
| 3.33 $\mu$ M Cladribine      | 15.5      | 6.6  | 79.6  | 9.6  | 4.5  | 3.0  |
| 10 $\mu$ M Fludarabine       | 70.9      | 9.7  | 14.4  | 11.0 | 15.0 | 3.0  |
| 3.33 $\mu$ M PHA-793887      | 45.8      | 1.3  | 22.4  | 5.3  | 31.7 | 6.2  |
| 30 $\mu$ M Roscovitine       | 34.3      | 5.6  | 34.4  | 15.4 | 29.8 | 10.6 |
| 3.33 $\mu$ M Topotecan       | 26.8      | 11.4 | 62.9  | 16.5 | 9.9  | 5.5  |
| 10 $\mu$ M Ciclopirox        | 21.3      | 2.5  | 73.1  | 4.1  | 5.4  | 2.8  |
| 0.33 $\mu$ M Doxorubicin     | 41.5      | 5.7  | 3.4   | 3.5  | 55.8 | 9.6  |
| 30 $\mu$ M Resveratrol       | 10.8      | 6.2  | 84.4  | 11.1 | 4.4  | 4.5  |

**Table 13: Quantification of the percentage of U-2OS cells in the G1 (DNA content of 2N), S and G2 (4N) phase of the cell cycle upon treatment with compounds 1-9.**

Cells were treated with compounds 1-9 or DMSO as a control for 22 h and afterwards pulsed for another 2 h with 10  $\mu$ M EdU (5-ethynyl-2'-deoxyuridine) prior to fixation and staining of DNA with PI. DNA content and EdU incorporation were determined by means of flow cytometry. Data are mean values of three independent experiments.

| Compound              | Cells / % |      |       |      |      |     |
|-----------------------|-----------|------|-------|------|------|-----|
|                       | 2N        |      | 2N-4N |      | 4N   |     |
|                       | Mean      | SD   | Mean  | SD   | Mean | SD  |
| DMSO                  | 47.1      | 9.3  | 34.2  | 15.6 | 18.3 | 6.8 |
| 10 $\mu$ M Compound 1 | 50.5      | 20.6 | 37.2  | 24.7 | 10.9 | 4.8 |

APPENDIX

|                       |      |      |      |      |      |      |
|-----------------------|------|------|------|------|------|------|
| 10 $\mu$ M Compound 2 | 59.5 | 15.1 | 25.0 | 16.6 | 14.1 | 5.3  |
| 10 $\mu$ M Compound 3 | 27.9 | 18.6 | 58.6 | 28.4 | 11.9 | 8.9  |
| 10 $\mu$ M Compound 4 | 37.7 | 17.9 | 49.4 | 21.6 | 11.5 | 3.3  |
| 10 $\mu$ M Compound 5 | 31.0 | 10.1 | 41.5 | 23.4 | 26.3 | 12.9 |
| 10 $\mu$ M Compound 6 | 30.7 | 11.7 | 59.7 | 16.1 | 8.7  | 4.5  |
| 10 $\mu$ M Compound 7 | 54.8 | 14.3 | 27.4 | 21.7 | 17.0 | 7.2  |
| 10 $\mu$ M Compound 8 | 22.8 | 10.0 | 70.5 | 17.9 | 6.4  | 8.1  |
| 10 $\mu$ M Compound 9 | 28.2 | 5.2  | 68.9 | 5.8  | 2.5  | 0.8  |

### 13.2 Additional data related to 6.2

**Table 14: Annotated reference compounds with high morphological biosimilarity ( $\geq 75\%$ ) to 10  $\mu$ M compound 13.**

| Trivial name  | Induction [%] | Biosimilarity to 10 $\mu$ M cmp 13 [%] | Cell Count [%] |
|---|---------------|--|----------------|
| (-)-cis-(1S,2R)-U-50488 tartrate  | 52.8          | 92.8                                   | 104            |
| (-)-trans-(1S,2S)-U-50488 hydrochloride                                 | 61.8          | 83.2                                   | 92             |
| (+)-Chlorpheniramine maleate  | 18.0          | 78.6                                   | 90             |
| ( $\pm$ ) trans-U-50488 methanesulfonate                                | 68.9          | 87.1                                   | 108            |
| ( $\pm$ )-7-Hydroxy-DPAT hydrobromide                                   | 11.6          | 75.5                                   | 89             |
| ( $\pm$ )-Butaclamol hydrochloride, AY 23028                            | 43.5          | 90.6                                   | 104            |
| ( $\pm$ )-Octoclothepein maleate  | 52.3          | 92.0                                   | 103            |
| ( $\pm$ )-PPHT hydrochloride  | 44.0          | 85.9                                   | 95             |
| ( $\pm$ )-Propranolol hydrochloride                                     | 10.7          | 76.0                                   | 103            |
| (R)-Propranolol hydrochloride   | 6.2           | 79.0                                   | 97             |
| (R,R)-cis-Diethyl tetrahydro-2,8-chrysenediol                           | 85.0          | 76.7                                   | 66             |
| (S)-Propranolol hydrochloride   | 24.4          | 91.1                                   | 98             |
| 1-(1-Naphthyl)piperazine hydrochloride                                  | 61.7          | 81.5                                   | 105            |
| 3-(1H-Imidazol-4-yl)propyl di(p-fluorophenyl)methyl ether hydrochloride | 33.9          | 86.3                                   | 95             |
| 3-Tropanyl-3,5-dichlorobenzoate   | 35.8          | 82.2                                   | 89             |
| Navoban, Tropisetron  | 24.5          | 77.6                                   | 91             |
| 4-Hydroxytamoxifen  | 24.0          | 82.3                                   | 96             |
| 5-alpha-THDOC   | 6.9           | 76.5                                   | 95             |

**APPENDIX**

| <b>Trivial name</b>                         | <b>Induction [%]</b> | <b>Biosimilarity to 10 µM cmp 13 [%]</b> | <b>Cell Count [%]</b> |
|---|----------------------|--|-----------------------|
| 6-Chloromelatonin                           | 3.1                  | 76.0                                     | 99                    |
| A-77636 hydrochloride                       | 40.4                 | 79.1                                     | 84                    |
| Acepromazine maleate                        | 21.8                 | 80.7                                     | 102                   |
| Alaproclate hydrochloride                   | 40.2                 | 78.8                                     | 91                    |
| Alprenolol hydrochloride                    | 19.7                 | 77.6                                     | 105                   |
| Alverine citrate                            | 11.1                 | 81.4                                     | 96                    |
| AM1241                                      | 49.7                 | 86.0                                     | 103                   |
| Aminobenzotropine, ABT                      | 2.8                  | 77.9                                     | 103                   |
| AMN082                                      | 60.1                 | 81.4                                     | 98                    |
| Antazoline hydrochloride                    | 4.7                  | 75.7                                     | 104                   |
| Antozoline hydrochloride                    | 12.8                 | 85.5                                     | 92                    |
| Astemizole                                  | 86.9                 | 84.6                                     | 90                    |
| Azelastine hydrochloride                    | 56.1                 | 87.3                                     | 94                    |
| Benperidol                                  | 20.9                 | 83.4                                     | 99                    |
| Benzotropine mesylate                       | 31.3                 | 83.1                                     | 105                   |
| Benzydamine hydrochloride                   | 18.7                 | 81.4                                     | 103                   |
| Biperiden hydrochloride                     | 67.4                 | 81.1                                     | 102                   |
| BP 897                                      | 84.6                 | 83.4                                     | 81                    |
| BRL 52537 hydrochloride                     | 57.3                 | 88.5                                     | 95                    |
| Bromoacetyl alprenolol menthane             | 14.2                 | 86.3                                     | 86                    |
| BTCP hydrochloride                          | 37.8                 | 75.8                                     | 100                   |
| Bupirone hydrochloride                      | 16.2                 | 87.0                                     | 99                    |
| BW 723C86                                   | 33.2                 | 89.1                                     | 102                   |
| Carbetapentane citrate                      | 12.3                 | 79.5                                     | 98                    |
| Carvedilol                                  | 64.6                 | 87.6                                     | 97                    |
| CGS-12066A maleate                          | 19.3                 | 83.6                                     | 105                   |
| Chlorcyclizine hydrochloride                | 54.9                 | 88.0                                     | 91                    |
| Chloro-IB-MECA                              | 7.1                  | 79.0                                     | 107                   |
| Chloropyramine hydrochloride                | 34.7                 | 94.0                                     | 94                    |
| Cisapride                                   | 35.8                 | 86.3                                     | 97                    |
| Citalopram hydrobromide                     | 29.4                 | 84.7                                     | 102                   |
| Clemastine fumarate                         | 52.5                 | 90.0                                     | 91                    |
| Clomiphene citrate (Z,E)                    | 60.6                 | 90.4                                     | 99                    |
| Cloperastine hydrochloride                  | 27.6                 | 87.1                                     | 100                   |
| CNS-1102, Cerestat, Aptiganel hydrochloride | 53.7                 | 88.1                                     | 96                    |
| Cortexolone maleate                         | 16.6                 | 82.4                                     | 92                    |

**APPENDIX**

| <b>Trivial name</b>                       | <b>Induction [%]</b> | <b>Biosimilarity to 10 µM cmp 13 [%]</b> | <b>Cell Count [%]</b> |
|---|----------------------|--|-----------------------|
| Cyclobenzaprine hydrochloride             | 37.0                 | 89.8                                     | 103                   |
| Cyproheptadine hydrochloride              | 77.0                 | 90.3                                     | 91                    |
| Deptropine citrate                        | 36.3                 | 90.6                                     | 103                   |
| Desloratidine                             | 26.4                 | 80.8                                     | 91                    |
| Dextromethorphan hydrobromide monohydrate | 31.8                 | 86.7                                     | 90                    |
| Dicyclomine hydrochloride                 | 58.7                 | 80.1                                     | 97                    |
| Dihydroergotamine methanesulfonate        | 49.2                 | 78.0                                     | 100                   |
| Dihydroergotamine tartrate                | 68.9                 | 85.6                                     | 100                   |
| Dilazep dihydrochloride                   | 9.5                  | 76.2                                     | 101                   |
| Diphenhydramine hydrochloride             | 8.5                  | 84.4                                     | 95                    |
| Diphenylpyraline hydrochloride            | 27.3                 | 91.6                                     | 98                    |
| DO 897/99                                 | 3.1                  | 76.7                                     | 91                    |
| Domperidone                               | 72.9                 | 83.2                                     | 95                    |
| Doxazosin mesylate                        | 10.0                 | 79.3                                     | 103                   |
| Ebastine                                  | 63.2                 | 88.0                                     | 89                    |
| Endoxifen HCl                             | 37.8                 | 79.7                                     | 94                    |
| Escitalopram                              | 16.1                 | 85.8                                     | 104                   |
| Ethopropazine hydrochloride               | 27.6                 | 76.8                                     | 100                   |
| Fenoterol hydrobromide                    | 7.3                  | 75.1                                     | 104                   |
| Fiduxosin hydrochloride                   | 24.7                 | 83.4                                     | 100                   |
| FLB 131                                   | 11.6                 | 82.9                                     | 101                   |
| Fluoxetine hydrochloride, Prozac          | 47.5                 | 92.7                                     | 101                   |
| Fluspidine                                | 70.8                 | 82.4                                     | 96                    |
| Fluvoxamine maleate                       | 7.3                  | 78.0                                     | 107                   |
| Formoterol                                | 20.0                 | 78.3                                     | 94                    |
| Forskolin                                 | 19.3                 | 79.6                                     | 95                    |
| Fulvestrant                               | 33.5                 | 75.2                                     | 95                    |
| GBR-12909 dihydrochloride                 | 47.2                 | 79.9                                     | 93                    |
| GBR-12935 dihydrochloride                 | 32.6                 | 90.4                                     | 94                    |
| GR 113808                                 | 49.1                 | 80.7                                     | 94                    |
| GR 127935 hydrochloride                   | 40.9                 | 85.2                                     | 99                    |
| GR 4661                                   | 68.2                 | 84.9                                     | 96                    |
| GR 55562 dihydrobromide                   | 87.7                 | 79.0                                     | 100                   |
| Guanabenz acetate, WY-8678                | 42.0                 | 84.0                                     | 96                    |
| GW405833 hydrochloride                    | 50.9                 | 85.1                                     | 86                    |
| Hexahydro-sila-difenidol hydrochloride    | 48.2                 | 88.5                                     | 92                    |

APPENDIX

| Trivial name   | Induction [%] | Biosimilarity to 10 µM cmp 13 [%] | Cell Count [%] |
|--|---------------|-----------------------------------|----------------|
| Homochlorcyclizine dihydrochloride                     | 42.0          | 85.7                              | 95             |
| Hydroxyzine dihydrochloride                            | 37.5          | 83.7                              | 90             |
| Ifenprodil tartrate                                    | 37.7          | 89.4                              | 107            |
| Indatraline hydrochloride, Lu 19-005                   | 55.1          | 89.9                              | 93             |
| Ketanserin tartrate hydrate                            | 29.5          | 76.5                              | 100            |
| L-687,384 hydrochloride                                | 25.7          | 90.1                              | 101            |
| L-703,606, oxalate                                     | 5.2           | 77.3                              | 108            |
| L-741,626  | 4.0           | 79.5                              | 106            |
| L-750,667 trihydrochloride                             | 37.0          | 75.8                              | 105            |
| L-765,314  | 45.8          | 86.2                              | 101            |
| Levallorphan tartrate                                  | 12.6          | 77.2                              | 111            |
| LP 12 hydrochloride hydrate                            | 41.3          | 87.7                              | 101            |
| LP44   | 53.2          | 86.6                              | 101            |
| Mebhydroline 1,5-naphtalenedisulfonate                 | 36.6          | 84.6                              | 96             |
| Memantine hydrochloride                                | 4.8           | 75.8                              | 99             |
| Mesoridazine besylate                                  | 11.7          | 78.5                              | 95             |
| Metergoline  | 28.5          | 81.7                              | 99             |
| Methiothepin maleate                                   | 68.0          | 89.1                              | 93             |
| Methotrimeprazine maleat salt                          | 28.2          | 87.9                              | 96             |
| Methoxy-6-harmalan                                     | 43.4          | 88.8                              | 95             |
| Metixene hydrochloride                                 | 8.6           | 81.1                              | 105            |
| MRS 1523   | 21.2          | 75.2                              | 86             |
| Naftopidil dihydrochloride, KT-611 dihydrochloride     | 52.2          | 84.5                              | 101            |
| Naloxonazine dihydrochloride                           | 34.7          | 86.9                              | 89             |
| Naltriben methanesulfonate, NTB                        | 17.3          | 83.6                              | 105            |
| Naltrindole hydrochloride, NTI hydrochloride           | 37.1          | 92.6                              | 105            |
| NAN-190 hydrobromide                                   | 12.3          | 76.1                              | 85             |
| N-Desmethylozapine                                     | 40.1          | 87.9                              | 98             |
| Nebivolol HCl  | 57.5          | 85.7                              | 98             |
| Nefazodone HCl   | 52.5          | 78.9                              | 97             |
| Nisoxetine hydrochloride, LY-94,939                    | 14.9          | 82.8                              | 110            |
| N-Methyl dopamine hydrochloride, Epinine hydrochloride | 14.3          | 75.9                              | 100            |
| N-Methylhistaprodifen dioxalate salt                   | 72.7          | 84.2                              | 86             |
| Nylidrin   | 41.3          | 85.0                              | 102            |
| Orphenadrine hydrochloride                             | 25.7          | 89.1                              | 102            |

**APPENDIX**

| <b>Trivial name</b>                       | <b>Induction [%]</b> | <b>Biosimilarity to 10 µM cmp 13 [%]</b> | <b>Cell Count [%]</b> |
|---|----------------------|--|-----------------------|
| Oxybutynin Chloride                       | 7.3                  | 80.9                                     | 103                   |
| Oxymetazoline hydrochloride               | 36.1                 | 79.3                                     | 98                    |
| Ozanimod (RPC1063)                        | 2.9                  | 79.1                                     | 98                    |
| Paroxetine hydrochloride                  | 37.0                 | 85.9                                     | 99                    |
| Penbutolol sulfate                        | 26.4                 | 87.1                                     | 107                   |
| Pergolide mesylate                        | 9.0                  | 78.8                                     | 107                   |
| Phenylephrine hydrochloride               | 11.1                 | 76.1                                     | 92                    |
| Pimethixene maleate                       | 30.4                 | 86.1                                     | 94                    |
| Piperidolate hydrochloride                | 35.2                 | 86.1                                     | 97                    |
| Pirenperone, R-47,465                     | 15.2                 | 83.0                                     | 104                   |
| Pizotiline malate                         | 59.9                 | 92.8                                     | 102                   |
| p-MPPI hydrochloride                      | 28.3                 | 81.6                                     | 104                   |
| PPT                                       | 17.4                 | 75.2                                     | 92                    |
| Prochlorperazine dimaleate                | 69.3                 | 87.0                                     | 97                    |
| Procyclidine hydrochloride                | 40.6                 | 77.4                                     | 96                    |
| Promethazine hydrochloride                | 18.5                 | 79.2                                     | 110                   |
| R-(+)-8-Hydroxy-DPAT hydrobromide         | 10.2                 | 76.5                                     | 100                   |
| Raloxifene hydrochloride, LY 139481       | 70.3                 | 84.7                                     | 97                    |
| Ritanserlin                               | 54.2                 | 86.9                                     | 85                    |
| Ro 8-4304                                 | 13.0                 | 79.1                                     | 91                    |
| S(-)Eticlopride hydrochloride             | 47.2                 | 84.0                                     | 93                    |
| S-(+)-Fluoxetine hydrochloride            | 25.0                 | 90.6                                     | 108                   |
| Salmeterol                                | 39.9                 | 84.4                                     | 90                    |
| Salmeterol xinafoate, GR 33343X xinafoate | 15.9                 | 84.9                                     | 102                   |
| SB 216641                                 | 44.7                 | 87.0                                     | 94                    |
| SB 242084 dihydrochloride hydrate         | 27.8                 | 75.4                                     | 101                   |
| SCH58261                                  | 13.1                 | 78.4                                     | 101                   |
| SDZ-205,557 hydrochloride                 | 16.6                 | 79.4                                     | 95                    |
| Sertindole                                | 83.1                 | 84.1                                     | 92                    |
| Siramesine fumarate salt                  | 50.6                 | 80.4                                     | 98                    |
| SKF 95282 dimaleate, Zolantidine          | 48.7                 | 91.0                                     | 96                    |
| Spiperone hydrochloride                   | 38.9                 | 77.3                                     | 94                    |
| SR 59230A oxalate                         | 52.5                 | 82.1                                     | 102                   |
| Tamoxifen citrate                         | 69.3                 | 89.8                                     | 92                    |
| Terfenadine                               | 80.3                 | 88.5                                     | 84                    |
| Thiethylperazine malate                   | 59.4                 | 86.8                                     | 103                   |



**APPENDIX**

| <b>Trivial name</b>   | <b>Induction [%]</b> | <b>Biosimilarity to 10 µM cmp 13 [%]</b> | <b>Cell Count [%]</b> |
|---|----------------------|--|-----------------------|
| Thiopropazine dimesylate  | 50.3                 | 89.4                                     | 96                    |
| Tomoxetine  | 28.3                 | 84.0                                     | 88                    |
| Toremifene  | 8.5                  | 87.2                                     | 101                   |
| Trihexyphenidyl hydrochloride                                       | 29.0                 | 80.0                                     | 97                    |
| Trimeprazine tartrate   | 87.7                 | 81.9                                     | 88                    |
| U-62066, Spiradoline mesylate                                       | 69.4                 | 77.0                                     | 96                    |
| U-69593   | 3.1                  | 75.3                                     | 103                   |
| VER-3323 hemifumarate salt  | 8.5                  | 82.8                                     | 103                   |
| WB-4101 hydrochloride   | 31.1                 | 77.9                                     | 95                    |
| Xylometazoline hydrochloride  | 16.8                 | 88.5                                     | 102                   |
| Zimelidine dihydrochloride monohydrate                              | 24.2                 | 86.7                                     | 101                   |
| Zotepine  | 12.3                 | 79.9                                     | 102                   |
| highly selective Sigma 1 receptor. Ki for S1R: 1.3 nM; S2R: 837 nM. | 59.4                 | 87.0                                     | 97                    |
| Amoxapine   | 25.4                 | 85.5                                     | 107                   |
| Amperozide hydrochloride  | 48.4                 | 77.4                                     | 92                    |
| Aripiprazole  | 61.1                 | 82.2                                     | 110                   |
| Bromperidol   | 10.9                 | 81.7                                     | 96                    |
| Chlorpromazine hydrochloride  | 43.4                 | 90.6                                     | 91                    |
| Chlorprothixene hydrochloride                                       | 53.4                 | 89.8                                     | 88                    |
| cis-(Z)-Flupenthixol dihydrochloride                                | 35.6                 | 84.0                                     | 102                   |
| Clomipramine hydrochloride  | 53.7                 | 87.3                                     | 94                    |
| Clozapine   | 18.0                 | 81.6                                     | 103                   |
| Desipramine hydrochloride   | 20.7                 | 84.5                                     | 101                   |
| Dosulepin hydrochloride   | 24.4                 | 88.7                                     | 92                    |
| Doxepin hydrochloride   | 5.2                  | 79.4                                     | 108                   |
| Drofenine hydrochloride   | 19.3                 | 76.3                                     | 113                   |
| Fluphenazine dihydrochloride  | 7.6                  | 84.4                                     | 98                    |
| Fluspirilene, R 6218  | 29.9                 | 87.7                                     | 108                   |
| Haloperidol   | 68.4                 | 90.6                                     | 93                    |
| Imipramine hydrochloride  | 13.1                 | 88.0                                     | 100                   |
| Maprotiline hydrochloride   | 42.0                 | 88.9                                     | 98                    |
| Norcyclobenzaprine  | 67.0                 | 85.8                                     | 96                    |
| Nortriptyline hydrochloride   | 52.3                 | 88.2                                     | 105                   |
| Olanzapine  | 39.0                 | 89.3                                     | 94                    |
| Opipramol, dihydrochloride  | 9.5                  | 76.9                                     | 87                    |

**APPENDIX**

| <b>Trivial name</b>              | <b>Induction [%]</b> | <b>Biosimilarity to 10 µM cmp 13 [%]</b> | <b>Cell Count [%]</b> |
|----------------------------------|----------------------|--|-----------------------|
| Perphenazine                     | 10.7                 | 83.7                                     | 91                    |
| Pimozide                         | 30.7                 | 81.1                                     | 101                   |
| Piperacetazine                   | 54.1                 | 88.0                                     | 100                   |
| Promazine hydrochloride          | 24.5                 | 91.2                                     | 101                   |
| Propionylpromazine hydrochloride | 43.2                 | 92.1                                     | 90                    |
| Protriptyline hydrochloride      | 32.1                 | 85.3                                     | 101                   |
| Reserpine, Methyl reserpate      | 42.7                 | 84.9                                     | 87                    |
| Sertraline hydrochloride         | 56.1                 | 89.6                                     | 103                   |
| Spiperone                        | 15.0                 | 81.7                                     | 105                   |
| Trazodone hydrochloride          | 17.4                 | 86.4                                     | 101                   |
| Trifluoperidol hydrochloride     | 4.7                  | 80.2                                     | 91                    |
| Triflupromazine hydrochloride    | 45.3                 | 95.0                                     | 100                   |
| Trimipramine maleate             | 26.3                 | 85.5                                     | 102                   |
| Zuclopenthixol hydrochloride     | 58.4                 | 88.3                                     | 102                   |
| SB590885                         | 40.4                 | 87.4                                     | 98                    |
| A3 hydrochloride                 | 37.5                 | 82.1                                     | 100                   |
| ABT-702 dihydrochloride          | 21.9                 | 85.7                                     | 101                   |
| Asciminib (ABL001)               | 35.8                 | 78.5                                     | 97                    |
| ASP3026                          | 67.2                 | 75.1                                     | 71                    |
| AT101                            | 35.1                 | 75.7                                     | 91                    |
| Aurora A Inhibitor I             | 21.9                 | 85.7                                     | 90                    |
| Ro 31-8220 Mesylate              | 82.2                 | 77.7                                     | 42                    |
| Autophinib                       | 55.3                 | 75.3                                     | 58                    |
| AZ191                            | 50.1                 | 82.0                                     | 94                    |
| AZD4547                          | 63.7                 | 89.9                                     | 85                    |
| AZD7762                          | 74.8                 | 76.8                                     | 76                    |
| AZD9291                          | 32.6                 | 78.5                                     | 95                    |
| Bafetinib                        | 48.9                 | 80.8                                     | 100                   |
| BLU-285, Avapritinib             | 75.1                 | 90.3                                     | 98                    |
| BMS-536924                       | 60.6                 | 75.5                                     | 91                    |
| Cediranib (AZD2171)              | 24.7                 | 78.1                                     | 92                    |
| CGP-74514A hydrochloride         | 68.7                 | 77.2                                     | 56                    |
| DDR1-IN-1                        | 40.6                 | 83.3                                     | 101                   |
| DL-Stearoylcarnitine chloride    | 34.7                 | 78.8                                     | 94                    |
| Epiblastin A                     | 77.4                 | 76.7                                     | 79                    |
| ERK5-IN-1                        | 19.7                 | 80.6                                     | 108                   |

**APPENDIX**

| <b>Trivial name</b>              | <b>Induction [%]</b> | <b>Biosimilarity to 10 µM cmp 13 [%]</b> | <b>Cell Count [%]</b> |
|----------------------------------|----------------------|--|-----------------------|
| Fimepinostat, CUDC-907           | 64.4                 | 75.6                                     | 67                    |
| Golvatinib (E7050)               | 32.6                 | 81.1                                     | 99                    |
| GSK2292767                       | 33.3                 | 75.7                                     | 100                   |
| GSK583                           | 26.4                 | 79.3                                     | 96                    |
| GSK'872 (GSK2399872A)            | 41.6                 | 77.1                                     | 102                   |
| GW2974                           | 36.4                 | 89.2                                     | 103                   |
| GZD824                           | 77.9                 | 84.3                                     | 74                    |
| HG-9-91-01                       | 63.6                 | 81.2                                     | 105                   |
| HTH-01-015                       | 74.4                 | 75.2                                     | 70                    |
| IKK-16 (IKK Inhibitor VII)       | 48.0                 | 93.3                                     | 101                   |
| Imatinib (STI571)                | 20.2                 | 78.6                                     | 92                    |
| Imatinib Mesylate (STI571)       | 75.5                 | 84.2                                     | 90                    |
| IPI-3063                         | 32.0                 | 78.7                                     | 98                    |
| JNK-IN-8                         | 69.4                 | 89.4                                     | 94                    |
| KN-62                            | 40.8                 | 87.0                                     | 94                    |
| KN-93 Phosphate                  | 9.3                  | 80.6                                     | 96                    |
| Lapatinib (GW-572016) Ditosylate | 32.1                 | 82.9                                     | 103                   |
| Masitinib (AB1010)               | 13.1                 | 75.7                                     | 92                    |
| Miransertib HCl, ARQ 092         | 88.8                 | 77.9                                     | 87                    |
| MK-2206 2HCl                     | 36.8                 | 78.8                                     | 98                    |
| ML347, LDN-193719, VU0469381     | 10.5                 | 76.0                                     | 93                    |
| Foretinib                        | 82.7                 | 75.9                                     | 37                    |
| ML-7                             | 17.6                 | 78.9                                     | 99                    |
| ML-9                             | 70.8                 | 85.0                                     | 99                    |
| Naquotinib(ASP8273)              | 44.4                 | 76.4                                     | 108                   |
| Nemiralisib, GSK2269557          | 43.5                 | 89.5                                     | 98                    |
| NU7441 (KU-57788)                | 25.6                 | 87.8                                     | 94                    |
| NVP-ADW742                       | 30.2                 | 84.4                                     | 90                    |
| NVP-AEW541                       | 29.7                 | 90.4                                     | 102                   |
| NVP-BHG712                       | 48.0                 | 88.0                                     | 100                   |
| NVP-BSK805 2HCl                  | 27.5                 | 85.0                                     | 90                    |
| Opaganib (ABC294640)             | 63.7                 | 80.9                                     | 95                    |
| OSI-906 (Linsitinib)             | 35.1                 | 76.3                                     | 94                    |
| PD173074                         | 24.2                 | 83.5                                     | 92                    |
| PHA-665752                       | 42.1                 | 80.9                                     | 94                    |
| PI-103                           | 52.8                 | 83.4                                     | 88                    |

APPENDIX

| Trivial name  | Induction [%] | Biosimilarity to 10 µM cmp 13 [%] | Cell Count [%] |
|---|---------------|-----------------------------------|----------------|
| PIK-III   | 48.7          | 80.8                              | 96             |
| Pipinib   | 65.3          | 92.4                              | 91             |
| Ponatinib, AP24534  | 64.6          | 89.8                              | 63             |
| PP2, AG 1879  | 52.3          | 77.2                              | 101            |
| PRT-060318 2HCl   | 55.3          | 76.9                              | 85             |
| PRT062607 (P505-15, BIIB057) HCl  | 79.1          | 82.4                              | 74             |
| Regorafenib (BAY 73-4506)   | 16.8          | 83.1                              | 93             |
| SGI-1776 free base  | 42.7          | 88.2                              | 96             |
| Sunitinib, free base  | 73.4          | 75.2                              | 59             |
| T-00127-HEV1  | 34.7          | 77.9                              | 97             |
| Tepotinib (EMD 1214063)   | 37.3          | 76.9                              | 94             |
| TWS119  | 46.3          | 76.0                              | 92             |
| URMC-099  | 61.7          | 75.3                              | 95             |
| Varlitinib  | 7.3           | 80.6                              | 101            |
| Vatalanib   | 37.0          | 76.6                              | 95             |
| VE-822  | 46.1          | 85.7                              | 109            |
| Vemurafenib (PLX4032, RG7204)   | 0.7           | 77.1                              | 97             |
| VPS34 inhibitor 1   | 68.9          | 80.3                              | 85             |
| VPS34-IN1   | 21.9          | 82.4                              | 88             |
| WAY-600   | 44.9          | 83.0                              | 98             |
| WZ4002  | 61.8          | 91.7                              | 98             |
| WZ4003  | 75.3          | 85.7                              | 90             |
| YM201636  | 29.2          | 82.0                              | 93             |
| inhibitor of GSK3-beta. Bioorg Med Chem Lett. (2004), 14(9), 2121-2125.                               | 73.4          | 89.3                              | 93             |
| inhibitor of Insulin-like growth factor I receptor. Bioorg Med Chem Lett. (2009), 19(2), 373-7.       | 15.2          | 85.8                              | 95             |
| inhibitor of Insulin-like growth factor I receptor. Bioorg Med Chem Lett. (2009), 19(2), 360-364.     | 16.2          | 83.7                              | 100            |
| inhibitor of PERK. J. Med. Chem. 2012   | 11.2          | 82.8                              | 99             |
| inhibitor of Epidermal growth factor receptor erbB1. Bioorg Med Chem Lett. (2006), 16(17), 4686-4691. | 14.9          | 82.8                              | 98             |
| inhibitor of PLK1 kinase. Bioorg Med Chem Lett. 2009 Feb 1;19(3):1018-21.                             | 14.5          | 81.3                              | 102            |
| GSK-3 inhibitor. Bioorg Med Chem Lett. (2006), 16(8), 2091-2094.                                      | 39.2          | 81.1                              | 87             |
| ATP-competitive Raf kinase inhibitor. Nature. 2010 May 20;465(7296):305-10.                           | 25.0          | 80.8                              | 96             |
| inhibitor of Akt1. Bioorg Med Chem Lett. 2009 Apr 15;19(8):2244-8.                                    | 17.3          | 80.4                              | 100            |
| binder of B-Raf kinase. Bioorg Med Chem Lett. (2008), 18(15), 4373-4376.                              | 21.2          | 79.9                              | 88             |

**APPENDIX**

| <b>Trivial name</b>   | <b>Induction [%]</b> | <b>Biosimilarity to 10 µM cmp 13 [%]</b> | <b>Cell Count [%]</b> |
|---|----------------------|--|-----------------------|
| inhibitor of cRaf1 kinase. Bioorg Med Chem Lett. (2000), 10(3), 223-226.                          | 19.0                 | 79.6                                     | 98                    |
| Inhibitor of B-Raf V600E mutant. Bioorg Med Chem Lett. 2011 Aug 1;21(15):4436-40.                 | 83.9                 | 79.5                                     | 95                    |
| dual EGFR/ErbB-2 inhibitor. Bioorg Med Chem Lett. (2009), 19(5), 1332-1336.                       | 1.6                  | 79.2                                     | 96                    |
| inhibitor of PIP4K2A. Bioorg Med Chem Lett. (2000), 10(3), 223-226.                               | 24.9                 | 78.7                                     | 104                   |
| inhibitor of Akt1. Bioorg Med Chem Lett. 2009 Apr 15;19(8):2244-8.                                | 74.3                 | 78.3                                     | 55                    |
| Inhibitor of B-Raf V600E mutant. Bioorg Med Chem Lett. 2011 Aug 1;21(15):4436-40.                 | 75.3                 | 77.1                                     | 83                    |
| inhibitor of Vascular endothelial growth factor receptor 2. J Med Chem (2007), 50(18), 4453-4470. | 55.3                 | 77.0                                     | 73                    |
| inhibitor of MAP kinase p38 alpha. Organic Letters (2005), 7(21), 4753-4756.                      | 9.0                  | 76.1                                     | 88                    |
| dual EGFR/ErbB-2 inhibitor. Bioorg Med Chem Lett. (2009), 19(3), 817-820.                         | 9.8                  | 75.7                                     | 101                   |
| inhibitor of Yes1 kinase. Bioorg Med Chem Lett. (2007), 17(21), 5886-5893.                        | 77.5                 | 75.6                                     | 91                    |
| AZ 3146   | 51.8                 | 77.8                                     | 109                   |
| (R)-PFI-2   | 63.9                 | 89.1                                     | 98                    |
| AZ6102  | 67.9                 | 82.5                                     | 88                    |
| AZ82, TS-574-B  | 29.5                 | 81.4                                     | 98                    |
| BIX01294 (hydrochloride hydrate)  | 44.2                 | 86.2                                     | 103                   |
| CB-839  | 38.7                 | 76.4                                     | 94                    |
| CONH hydrochloride  | 2.8                  | 78.2                                     | 104                   |
| Ellipticine   | 73.7                 | 77.6                                     | 49                    |
| GSK126  | 76.5                 | 83.8                                     | 95                    |
| GSK343  | 42.7                 | 91.7                                     | 102                   |
| GSK484 (hydrochloride)  | 58.2                 | 87.4                                     | 93                    |
| GSK-LSD1 (Hydrochloride)  | 3.6                  | 78.5                                     | 102                   |
| JQEZ5   | 32.0                 | 75.9                                     | 101                   |
| Ketoconazole  | 21.4                 | 84.1                                     | 92                    |
| LB42708   | 40.8                 | 78.8                                     | 98                    |
| LLY-507   | 43.0                 | 92.1                                     | 111                   |
| Mardepodect (PF-2545920)  | 26.6                 | 80.6                                     | 96                    |
| Mebeverine hydrochloride  | 18.1                 | 84.4                                     | 110                   |
| MS023   | 48.0                 | 81.1                                     | 107                   |
| MS049 (hydrochloride)   | 43.0                 | 77.7                                     | 99                    |
| Nafronyl oxalate  | 34.4                 | 76.0                                     | 100                   |
| Pirlindole mesylate   | 21.2                 | 90.1                                     | 96                    |

APPENDIX

| Trivial name  | Induction [%] | Biosimilarity to 10 µM cmp 13 [%] | Cell Count [%] |
|---|---------------|-----------------------------------|----------------|
| Rifabutin   | 36.4          | 84.9                              | 95             |
| Romidepsin  | 69.1          | 76.6                              | 74             |
| SGC0946   | 45.9          | 86.3                              | 97             |
| SGI-1027  | 32.5          | 76.2                              | 76             |
| SKF-525A hydrochloride, Proadifen hydrochloride   | 29.7          | 86.1                              | 104            |
| SRT 1720  | 81.5          | 76.8                              | 89             |
| Tazemetostat, EPZ6438   | 34.2          | 88.8                              | 99             |
| Trequinsin hydrochloride HL 725   | 29.5          | 85.5                              | 93             |
| UNC0638   | 56.5          | 87.9                              | 95             |
| UNC0642   | 45.8          | 86.2                              | 93             |
| UNC1999   | 47.3          | 86.0                              | 100            |
| it is a very potent and highly selective inhibitor of the enzymatic activity of Cathepsin C | 39.7          | 85.4                              | 95             |
| EHop-016  | 61.5          | 90.2                              | 101            |
| (±)-Verapamil hydrochloride   | 11.1          | 79.0                              | 103            |
| 5-(N-Ethyl-N-isopropyl)amiloride, EIPA  | 72.2          | 81.4                              | 94             |
| AMG 9810  | 33.3          | 85.5                              | 94             |
| Amlodipine  | 15.2          | 76.7                              | 98             |
| Aprindine hydrochloride, Amidonal   | 32.1          | 91.0                              | 100            |
| Benoxinate hydrochloride  | 16.1          | 85.0                              | 103            |
| Benzamil hydrochloride  | 38.3          | 85.4                              | 88             |
| Bepriidil hydrochloride   | 54.2          | 86.9                              | 89             |
| Cinacalcet HCl  | 57.9          | 75.6                              | 109            |
| Crobenetine   | 46.5          | 76.8                              | 94             |
| Dibucaine   | 30.6          | 85.6                              | 107            |
| Fendiline hydrochloride   | 7.4           | 79.0                              | 101            |
| Flunarizine dihydrochloride   | 40.1          | 84.7                              | 100            |
| IMID-4F hydrochloride   | 10.4          | 82.4                              | 103            |
| Lercanidipine hydrochloride hemihydrate   | 82.2          | 79.0                              | 80             |
| Lidoflazine   | 70.1          | 90.0                              | 103            |
| Loperamide hydrochloride  | 63.7          | 92.1                              | 98             |
| Mibefradil dihydrochloride, Ro 40-5967  | 10.5          | 80.5                              | 97             |
| Nicardipine hydrochloride, YC-93 hydrochloride  | 74.4          | 78.9                              | 87             |
| NNC 55-0396   | 38.2          | 88.7                              | 103            |
| Oxethazaine   | 79.3          | 78.9                              | 97             |
| Phenamyl methanesulfonate   | 68.2          | 88.9                              | 94             |

**APPENDIX**

| <b>Trivial name</b>   | <b>Induction [%]</b> | <b>Biosimilarity to 10 µM cmp 13 [%]</b> | <b>Cell Count [%]</b> |
|---|----------------------|--|-----------------------|
| Prenylamine lactate   | 59.9                 | 89.1                                     | 86                    |
| Propafenone hydrochloride   | 32.8                 | 83.5                                     | 92                    |
| Quinidine sulfate   | 66.3                 | 78.9                                     | 83                    |
| Quinine sulfate   | 57.5                 | 80.5                                     | 81                    |
| 4-Androsten-4-ol-3,17-dione, 4-OH-A                                   | 16.2                 | 80.8                                     | 96                    |
| Alfadolone acetate  | 10.9                 | 84.9                                     | 104                   |
| Epiandrosterone   | 22.1                 | 84.0                                     | 101                   |
| Equilin   | 16.4                 | 85.8                                     | 96                    |
| Estrone, Folliculin   | 14.5                 | 86.3                                     | 87                    |
| Formestane  | 21.8                 | 77.6                                     | 110                   |
| Melengestrol acetate  | 21.1                 | 77.0                                     | 104                   |
| Progesterone  | 46.3                 | 79.2                                     | 94                    |
| U-73343   | 27.1                 | 87.0                                     | 101                   |
| Fluvastatin sodium salt   | 77.9                 | 80.2                                     | 102                   |
| Atorvastatin  | 49.2                 | 81.3                                     | 105                   |
| Mevastatin  | 55.8                 | 82.7                                     | 92                    |
| Isoconazole   | 15.2                 | 82.6                                     | 91                    |
| Terconazole   | 42.1                 | 83.3                                     | 102                   |
| Butoconazole nitrate  | 40.8                 | 81.7                                     | 88                    |
| (-)-Epinephrine bitartrate, Adrenaline bitartrate                     | 14.0                 | 77.9                                     | 105                   |
| (S)-crizotinib  | 46.6                 | 84.4                                     | 93                    |
| 3-Methoxy-morphanin hydrochloride, nor-Dextromethorphan hydrochloride | 25.4                 | 78.6                                     | 98                    |
| 5-(N,N-hexamethylene)amiloride  | 85.5                 | 82.6                                     | 86                    |
| A-395   | 31.3                 | 80.0                                     | 92                    |
| Amodiaquin dihydrochloride ;dihydrate                                 | 16.2                 | 81.9                                     | 103                   |
| Aumitin   | 25.7                 | 82.6                                     | 98                    |
| Azithromycin  | 10.4                 | 83.4                                     | 110                   |
| Bafilomycin A1, Baf-A1  | 79.3                 | 82.6                                     | 91                    |
| Beta-Escin  | 81.7                 | 80.5                                     | 82                    |
| Ceramide  | 10.4                 | 76.9                                     | 106                   |
| Chromopynone 1  | 21.6                 | 82.0                                     | 97                    |
| CPI-637   | 74.1                 | 77.6                                     | 89                    |
| Cyclopamine, V. californicum  | 20.4                 | 75.2                                     | 97                    |
| Deltarasin  | 85.5                 | 87.5                                     | 81                    |
| Dibucaine hydrochloride, ;Cinchocaine hydrochloride                   | 17.1                 | 85.5                                     | 98                    |

**APPENDIX**

| <b>Trivial name</b>                             | <b>Induction [%]</b> | <b>Biosimilarity to 10 µM cmp 13 [%]</b> | <b>Cell Count [%]</b> |
|---|----------------------|--|-----------------------|
| Dirithromycin                                   | 8.5                  | 79.3                                     | 100                   |
| Erythromycin                                    | 4.8                  | 78.5                                     | 104                   |
| Fingolimod (FTY720) HCl                         | 15.0                 | 78.6                                     | 98                    |
| GSK-5959  | 78.9                 | 75.6                                     | 76                    |
| GSK6853   | 49.9                 | 84.7                                     | 91                    |
| GX15-070, Obatoclox (mesylate)                  | 92.4                 | 76.1                                     | 73                    |
| Halofantrine hydrochloride                      | 52.7                 | 76.2                                     | 90                    |
| I-BET151  | 28.5                 | 79.2                                     | 93                    |
| lofetamine hydrochloride                        | 39.6                 | 81.3                                     | 102                   |
| Itraconazole                                    | 73.1                 | 88.3                                     | 96                    |
| JK 184  | 84.5                 | 79.8                                     | 45                    |
| Lipoxygenin                                     | 28.3                 | 88.1                                     | 84                    |
| MDL 28170, Z-Val-Phe-CHO                        | 44.0                 | 82.9                                     | 95                    |
| Mefloquine                                      | 26.8                 | 76.0                                     | 101                   |
| Monensin A sodium salt, Rumensin, ;Coban 45     | 81.9                 | 78.8                                     | 79                    |
| MRK-740   | 18.0                 | 88.7                                     | 108                   |
| NVS-CECR2-1                                     | 80.1                 | 76.4                                     | 73                    |
| OICR-9429                                       | 24.4                 | 86.1                                     | 103                   |
| PDMP hydrochloride                              | 68.4                 | 79.9                                     | 89                    |
| Perhexiline maleate                             | 22.5                 | 79.7                                     | 108                   |
| Phenazopyridine hydrochloride                   | 5.9                  | 77.1                                     | 99                    |
| PIK-93  | 28.8                 | 80.1                                     | 96                    |
| Quinacrine dihydrochloride                      | 52.0                 | 75.1                                     | 88                    |
| SAG   | 43.9                 | 91.8                                     | 97                    |
| Saquinavir mesylate                             | 40.1                 | 76.5                                     | 87                    |
| SAR405  | 47.3                 | 90.0                                     | 88                    |
| SGC-CBP30                                       | 76.2                 | 78.3                                     | 82                    |
| Smoothib  | 8.1                  | 78.7                                     | 88                    |
| Sonidegib (Erismodegib, NVP-LDE225)             | 26.1                 | 76.9                                     | 101                   |
| Spiramycin I, Spiramycin II and, Spiramycin III | 35.4                 | 86.5                                     | 99                    |
| Tariquidar                                      | 46.5                 | 78.2                                     | 96                    |
| Tenovin-6                                       | 50.8                 | 80.3                                     | 96                    |
| Tetracaine hydrochloride                        | 29.9                 | 78.1                                     | 97                    |
| TMB-8 hydrochloride                             | 20.0                 | 84.9                                     | 106                   |
| U-73122   | 70.3                 | 76.3                                     | 78                    |
| U-74389G maleate                                | 32.8                 | 84.9                                     | 91                    |



APPENDIX

| Trivial name                    | Induction [%] | Biosimilarity to 10 $\mu$ M cmp 13 [%] | Cell Count [%] |
|---------------------------------|---------------|--|----------------|
| Zosuquidar (LY335979) 3HCl      | 47.5          | 75.6                                   | 98             |
| Dimethisoquin hydrochloride     | 59.8          | 92.8                                   | 95             |
| Dipivefrin hydrochloride        | 50.6          | 84.0                                   | 90             |
| Levopropoxyphene napsylate      | 9.5           | 81.7                                   | 104            |
| Glafenine hydrochloride         | 17.8          | 85.4                                   | 90             |
| Diperodon hydrochloride         | 14.3          | 81.3                                   | 106            |
| Suloctidil                      | 47.5          | 86.9                                   | 105            |
| Nitrarine dihydrochloride       | 14.2          | 76.5                                   | 88             |
| BI-167107                       | 53.0          | 75.4                                   | 102            |
| negative control of BI 1002494. | 51.6          | 77.5                                   | 75             |

**Table 15: Proteins modulated by 10  $\mu$ M compound 13.**

U-2OS cells were treated for 24 h with 10  $\mu$ M compound **13** prior to proteome profiling using tandem mass tags for quantification by nanoHPLC-MS/MS. Data are mean values  $\pm$  SD of three independent experiments. Log<sub>2</sub> (ratio) and p-values ( $p < 0.05$  Benjamini-Hochberg corrected) of up- and down-regulated proteins. Gene names of proteins involved in the regulation of cholesterol homeostasis and lysosomal function were depicted in bold.

| Gene name   | 10 $\mu$ M Compound 13   |             |
|-------------|--------------------------|-------------|
|             | Log <sub>2</sub> (ratio) | p-value     |
| GMEB2       | -0.514083743             | 7.73841E-14 |
| EXOC6       | -0.472540617             | 6.34912E-12 |
| COG7        | -0.466577172             | 1.16076E-11 |
| DTL         | -0.44222784              | 1.26334E-10 |
| CEP131      | -0.440257907             | 1.52432E-10 |
| <b>PPT1</b> | -0.395532012             | 8.73579E-09 |
| FAM49B      | -0.390654147             | 1.32511E-08 |
| DYM         | -0.381377518             | 2.88757E-08 |
| HNRNPD      | -0.372069716             | 6.19797E-08 |
| EID2        | -0.346938074             | 4.46125E-07 |
| FIGNL1      | -0.341621369             | 6.66231E-07 |
| PCTP        | -0.326981902             | 1.95107E-06 |
| DCP2        | -0.324651927             | 2.30566E-06 |
| TGFB2       | -0.315437198             | 4.41494E-06 |
| SAMD4B      | -0.309584945             | 6.61028E-06 |
| SDF4        | -0.303456366             | 1.00129E-05 |
| PDCD2       | -0.290772885             | 2.3084E-05  |

APPENDIX

| Gene name     | 10 $\mu$ M Compound 13 |             |
|---------------|------------------------|-------------|
|               | Log2 (ratio)           | p-value     |
| SNAPC1        | -0.289370954           | 2.52663E-05 |
| TFAM          | -0.288827926           | 2.61632E-05 |
| KBTBD4        | -0.288166195           | 2.72971E-05 |
| HMG2          | -0.283088326           | 3.76905E-05 |
| CDKN2AIP      | -0.272970557           | 7.05824E-05 |
| TPM2          | -0.269599378           | 8.65956E-05 |
| KLHL11        | -0.268964052           | 8.99746E-05 |
| PSMB10        | -0.262168556           | 0.000134814 |
| SMARCA1       | -0.262094021           | 0.000135406 |
| HSPA13        | -0.26199472            | 0.000136199 |
| UPF3A         | -0.258494407           | 0.000167113 |
| EEF1D         | -0.257168114           | 0.000180465 |
| ANO10         | -0.252502561           | 0.000235838 |
| CLSPN         | -0.252315432           | 0.000238361 |
| PTPN18        | -0.251427948           | 0.000250677 |
| GALK2         | -0.248995692           | 0.000287559 |
| <b>SCPEP1</b> | -0.244628653           | 0.000366839 |
| NCOA6         | -0.236630738           | 0.000567378 |
| SKP2          | -0.234966815           | 0.000620272 |
| CPSF3L        | -0.233643487           | 0.000665576 |
| TAF6L         | -0.232634395           | 0.00070217  |
| LYAR          | -0.231650233           | 0.000739653 |
| TAF5          | -0.224628955           | 0.001065968 |
| ERBB2IP       | -0.224144593           | 0.001092791 |
| C5orf22       | -0.223571777           | 0.001125317 |
| SPTY2D1       | -0.223408714           | 0.001134739 |
| CDC123        | -0.222762451           | 0.001172801 |
| PPP1R14C      | -0.221746519           | 0.001235027 |
| MRPL14        | -0.221562833           | 0.001246598 |
| hCG_2043597   | 0.280741721            | 0.001334606 |
| ANXA4         | 0.280886441            | 0.001326929 |
| CLEC16A       | 0.282538235            | 0.001242145 |
| DDOST         | 0.282674968            | 0.001235356 |
| ENO2          | 0.282857507            | 0.001226346 |
| STXBP1        | 0.284472942            | 0.001149212 |
| GNB1          | 0.288570613            | 0.00097322  |
| ARHGAP31      | 0.288840652            | 0.000962547 |
| <b>LSS</b>    | 0.289235234            | 0.000947147 |
| HGH1          | 0.289774179            | 0.000926482 |
| MAPK7         | 0.290355593            | 0.000904657 |
| CEP152        | 0.29109323             | 0.000877653 |
| RTN1          | 0.292014092            | 0.000844991 |

## APPENDIX

| Gene name         | 10 $\mu$ M Compound 13 |             |
|-------------------|------------------------|-------------|
|                   | Log2 (ratio)           | p-value     |
| CAMK2D            | 0.297675759            | 0.000667708 |
| TMEM33            | 0.300340652            | 0.000596837 |
| GRN               | 0.301309228            | 0.000572862 |
| QPRT              | 0.302353263            | 0.000548025 |
| CALM2;CALM1;CALM3 | 0.306556672            | 0.000457832 |
| PHACTR4           | 0.307595253            | 0.000437788 |
| <b>FADS2</b>      | 0.309862942            | 0.000396836 |
| <b>GNPDA1</b>     | 0.310678869            | 0.000382999 |
| CRIPT             | 0.316090256            | 0.000302036 |
| NADSYN1           | 0.316307336            | 0.00029915  |
| LRRC49            | 0.320201308            | 0.000251564 |
| LMAN1             | 0.321120709            | 0.000241415 |
| TBC1D2B           | 0.321267605            | 0.000239829 |
| CNRIP1            | 0.323652059            | 0.000215421 |
| NIN               | 0.32386142             | 0.000213393 |
| CSTB              | 0.329619884            | 0.000164162 |
| PTAR1             | 0.334618062            | 0.000130302 |
| PANK2             | 0.335514665            | 0.000124972 |
| TIMP1             | 0.34388575             | 8.42069E-05 |
| MEAF6             | 0.348755479            | 6.66579E-05 |
| <b>ACSS2</b>      | 0.35573256             | 4.74445E-05 |
| <b>IDI1</b>       | 0.355847836            | 4.71763E-05 |
| KLHL25            | 0.360750526            | 3.70122E-05 |
| <b>HMGCS1</b>     | 0.360870302            | 3.67921E-05 |
| FER;Pe1Fe10       | 0.361872017            | 3.4999E-05  |
| UBXN2B            | 0.362488627            | 3.39369E-05 |
| TRIP11            | 0.362581044            | 3.37804E-05 |
| YES1              | 0.372843236            | 2.00826E-05 |
| MORF4L2           | 0.380703419            | 1.33644E-05 |
| OSGEPL1           | 0.383294702            | 1.16654E-05 |
| BAG1              | 0.38496837             | 1.06798E-05 |
| UTP14A            | 0.389561921            | 8.36682E-06 |
| KIF2C             | 0.396593034            | 5.72886E-06 |
| LPXN              | 0.401644439            | 4.34728E-06 |
| APP               | 0.402385622            | 4.17363E-06 |
| GABARAP           | 0.408535093            | 2.96803E-06 |
| TRAPPC2B;TRAPPC2  | 0.419963479            | 1.5553E-06  |
| SAMD9L            | 0.420131803            | 1.54038E-06 |
| ASCC2             | 0.436769366            | 5.83496E-07 |
| KCMF1             | 0.437207729            | 5.68491E-07 |
| RBFA              | 0.44029364             | 4.72906E-07 |
| <b>STARD4</b>     | 0.451436609            | 2.40829E-07 |

APPENDIX

| Gene name    | 10 $\mu$ M Compound 13 |             |
|--------------|------------------------|-------------|
|              | Log2 (ratio)           | p-value     |
| HS1BP3       | 0.466895074            | 9.19979E-08 |
| <b>FDFT1</b> | 0.472195894            | 6.56781E-08 |
| GOLGB1       | 0.48451972             | 2.95895E-08 |
| CDK5         | 0.486164004            | 2.65643E-08 |
| DBI          | 0.487911582            | 2.36784E-08 |
| EYA3         | 0.507926226            | 6.16937E-09 |
| KLHL18       | 0.519226074            | 2.82247E-09 |
| <b>NEU1</b>  | 0.550253808            | 3.03071E-10 |
| PCBD1        | 0.567700386            | 8.1857E-11  |
| KDELR2       | 0.569868684            | 6.93771E-11 |
| GPNMB        | 0.570561588            | 6.57966E-11 |
| CCM2         | 0.67520237             | 1.08238E-14 |
| KHNYN        | 0.797926903            | 6.49975E-20 |
| TNFSF13B     | 0.851840854            | 1.78102E-22 |
| PARP12       | 0.860564709            | 6.61678E-23 |
| RPRD1A       | 0.883647799            | 4.59285E-24 |
| HAUS2        | 0.923579454            | 3.86152E-26 |

**Table 16: Proteins modulated by compound 12.**

U-2OS cells were treated for 24 h with 10  $\mu$ M and 30  $\mu$ M compound **12** prior to proteome profiling using tandem mass tags for quantification by nanoHPLC-MS/MS. Data are mean values  $\pm$  SD of three independent experiments. Log2 (ratio) and p-values ( $p < 0.05$  Benjamini-Hochberg corrected) of up- and down-regulated proteins. Gene names of proteins involved in the regulation of cholesterol homeostasis and lysosomal function were depicted in bold.

| 10 $\mu$ M compound 12 |              |             | 30 $\mu$ M compound 12 |              |             |
|------------------------|--------------|-------------|------------------------|--------------|-------------|
| Gene name              | log2 (ratio) | p-value     | Gene name              | log2 (ratio) | p-value     |
| ZMYND8                 | 0.275106     | 4.41544E-06 | ARFIP2                 | 0.363874912  | 3.50003E-05 |
| ZBTB8OS                | -0.1511      | 0.00074765  | CCM2                   | 0.516362131  | 4.1351E-09  |
| CCM2                   | 0.331239     | 3.38521E-08 | hCG_2043597            | 0.576957464  | 5.02057E-11 |
| ING1                   | 0.287063     | 1.67795E-06 | GCSH                   | 0.316507041  | 0.0003212   |
| CTSD                   | -0.16555     | 0.000216832 | <b>PPT1</b>            | -0.523840964 | 3.71933E-15 |
| <b>PPT1</b>            | -0.36348     | 2.87743E-16 | GPNMB                  | 0.442945629  | 4.63762E-07 |
| AP1S1                  | -0.20632     | 3.81588E-06 | GEMIN2                 | -0.294866025 | 9.19822E-06 |
| UHRF1BP1L              | 0.257038     | 1.77374E-05 | EYA3                   | 0.475179911  | 6.35025E-08 |
| VWA8                   | 0.217128     | 0.00028256  | CENPK                  | 0.36173898   | 3.89122E-05 |
| GTPBP10                | -0.49932     | 2.23567E-29 | HMGB3                  | -0.26044628  | 8.86278E-05 |
| PIP5K1A                | -0.1722      | 0.000118602 | APP                    | 0.521319985  | 2.93336E-09 |
| PSMD10                 | 0.218746     | 0.000254602 | <b>NEU1</b>            | 0.570569158  | 8.1715E-11  |
| CDC37L1                | 0.205907     | 0.000571059 | MTMR1                  | 0.406395733  | 3.77223E-06 |

APPENDIX

| 10 $\mu$ M compound 12 |              |             | 30 $\mu$ M compound 12 |              |             |
|------------------------|--------------|-------------|------------------------|--------------|-------------|
| Gene name              | log2 (ratio) | p-value     | Gene name              | log2 (ratio) | p-value     |
| BRD8                   | -0.17075     | 0.00013549  | ARAP3                  | 0.299667478  | 0.000660748 |
| NIN                    | 0.29252      | 1.06551E-06 | PPP2R5D                | -0.299114853 | 6.83266E-06 |
| EEFSEC                 | -0.17931     | 6.07512E-05 | UQCRC2                 | 0.62341696   | 1.24209E-12 |
| UBE2F                  | 0.224507     | 0.000174752 | GABARAP                | -0.304501593 | 4.66087E-06 |
| PPP1R9B                | 0.213158     | 0.000363777 | FCHO2                  | 0.335772157  | 0.000134831 |
| NCALD                  | 0.209428     | 0.000459535 | CLUH                   | -0.344180197 | 2.29533E-07 |
| SNCA                   | 0.195426     | 0.001069989 | BAG1                   | 0.310493052  | 0.000417242 |
| EXOC6                  | -0.34463     | 9.06721E-15 | HMGN4                  | -0.219782293 | 0.000930115 |
| FBXO3                  | 0.218738     | 0.000254744 | STK25                  | 0.318064779  | 0.000299938 |
| LMO7                   | -0.27955     | 3.4157E-10  | UBE2C                  | -0.221224949 | 0.000860825 |
| DTL                    | -0.14571     | 0.001156513 | KHNYN                  | 0.878137767  | 1.4062E-23  |
| FAH                    | -0.19242     | 1.65816E-05 | ARPC3                  | -0.23409985  | 0.000423074 |
| RPS2                   | -0.27706     | 4.89919E-10 | FANCG                  | 0.463371992  | 1.33574E-07 |
| UQCRC2                 | 0.204948     | 0.000605553 | CALU                   | -0.256512105 | 0.000112983 |
| GABARAP                | 0.276932     | 3.81839E-06 | LPXN                   | 0.592305422  | 1.52496E-11 |
| MSL1                   | -0.27581     | 5.85874E-10 | SIN3B                  | 0.35595414   | 5.16973E-05 |
| WWP2                   | -0.22568     | 4.2037E-07  | KLHL18                 | 0.374186128  | 2.08195E-05 |
| HMGN4                  | 0.305076     | 3.63703E-07 | PCNT                   | 0.380778402  | 1.48326E-05 |
| KHNYN                  | 0.447827     | 9.28312E-14 | NFATC1                 | -0.275994152 | 3.28704E-05 |
| RIPK2                  | -0.14944     | 0.000856456 | AIFM1                  | 0.302716017  | 0.000581361 |
| SH3BGRL                | 0.250096     | 2.95796E-05 | <b>FADS2</b>           | 0.346008539  | 8.34394E-05 |
| GFPT2                  | -0.14791     | 0.000969443 | TIMP1                  | 0.314513564  | 0.000350469 |
| HMGN2                  | 0.239076     | 6.49094E-05 | CSTB                   | 0.339213014  | 0.000114911 |
| DBI                    | 0.247932     | 3.46018E-05 | TYMS                   | -0.249908492 | 0.00016857  |
| PSAP                   | -0.15159     | 0.000718362 | HMGN2                  | -0.315710187 | 2.06103E-06 |
| ERCC1                  | 0.217834     | 0.000270028 | S100A6                 | 0.33475849   | 0.000141293 |
| TRAPPC2B               | 0.280591     | 2.84629E-06 | TPM2                   | -0.248078302 | 0.00018803  |
| CPS1                   | 0.236401     | 7.81809E-05 | PSMB1                  | 0.340834856  | 0.000106516 |
| MAN1A1                 | -0.17764     | 7.12589E-05 | APC                    | 0.319837004  | 0.000277354 |
| <b>FDFT1</b>           | 0.267719     | 7.87752E-06 | HMGB2                  | -0.31854251  | 1.66982E-06 |
| CETN2                  | 0.222689     | 0.000196967 | PSMB4                  | 0.314677268  | 0.000347974 |
| HSPA13                 | -0.17867     | 6.45875E-05 | PSMB6                  | 0.307700396  | 0.000470424 |
| PSMB3                  | -0.16706     | 0.000189468 | PSMB5                  | 0.30887568   | 0.000447315 |
| SMARCA2                | 0.247667     | 3.52704E-05 | GRN                    | 0.30088675   | 0.000627858 |
| SNRPF                  | 0.279688     | 3.06127E-06 | DDT                    | 0.398378044  | 5.84169E-06 |
| TMSB4X                 | 0.675114     | 3.47475E-29 | CPS1                   | -0.23813273  | 0.000336244 |
| COG7                   | -0.18416     | 3.79247E-05 | HSPA1L                 | 0.35444963   | 5.56238E-05 |
| RHOG                   | -0.1474      | 0.001009926 | <b>FDFT1</b>           | 0.474306732  | 6.71326E-08 |
| RBM3                   | 0.198138     | 0.000912001 | <b>LSS</b>             | 0.352422774  | 6.13618E-05 |
| TFAM                   | -0.2252      | 4.45365E-07 | PSMB3                  | 0.328369737  | 0.000189233 |
| CDK5                   | 0.369912     | 7.24681E-10 | PSMB2                  | 0.38454175   | 1.21927E-05 |
| HNRNPU                 | 0.221732     | 0.000209707 | POLR2J                 | -0.230415195 | 0.000520305 |

APPENDIX

| 10 $\mu$ M compound 12 |              |             | 30 $\mu$ M compound 12 |              |             |
|------------------------|--------------|-------------|------------------------|--------------|-------------|
| Gene name              | log2 (ratio) | p-value     | Gene name              | log2 (ratio) | p-value     |
| MAPK7                  | 0.583439     | 3.12905E-22 | TPD52                  | -0.236843273 | 0.000362005 |
| HNRNPD                 | 0.396475     | 4.09931E-11 | GFER                   | -0.237237275 | 0.000353944 |
| ESPL1                  | 0.39714      | 3.80562E-11 | PSMA6                  | 0.343377203  | 9.45116E-05 |
| NCOA6                  | -0.1742      | 9.85261E-05 | TGFB2                  | -0.243875504 | 0.000240996 |
| GOLGB1                 | 0.535912     | 5.13804E-19 | RPL39P5                | -0.236115605 | 0.000377345 |
| HSP90AB4P              | -0.19701     | 1.03074E-05 | TFAM                   | -0.247313604 | 0.00019677  |
| HSP90AB2P              | -0.17476     | 9.34427E-05 | <b>HMGCS1</b>          | 0.335415244  | 0.000137074 |
| C3orf38                | 0.217032     | 0.000284302 | <b>IDI1</b>            | 0.440250009  | 5.44409E-07 |
| RIF1                   | 0.207543     | 0.000516442 | NCOA6                  | -0.239774838 | 0.000305917 |
| HAUS6                  | -0.16081     | 0.000329207 | LPIN1                  | 0.422102123  | 1.56444E-06 |
| DENND4C                | -0.17423     | 9.82275E-05 | SNAPC1                 | -0.432466894 | 8.26248E-11 |
| RNF123                 | 0.223067     | 0.000192142 | TWISTNB                | -0.225566283 | 0.000680125 |
| SPTY2D1                | 0.206045     | 0.000566272 | UQCC2                  | -0.333920062 | 5.16625E-07 |
| RLTPR                  | 0.292202     | 1.0943E-06  | YOD1                   | 0.295317501  | 0.00079159  |
| LDOC1L                 | -0.16535     | 0.000220763 | FOCAD                  | 0.315857649  | 0.000330473 |
| FIGNL1                 | -0.18712     | 2.8297E-05  | FAM160B1               | 0.303207397  | 0.000569428 |
| PRUNE                  | -0.18814     | 2.55705E-05 | SPTY2D1                | 2.999686003  | 1.0976E-256 |
| PABPN1                 | -0.18016     | 5.60086E-05 | FIGNL1                 | -0.243370399 | 0.00024823  |
| NAA40                  | 0.244429     | 4.44884E-05 | DYM                    | -0.321462572 | 1.34163E-06 |
| NR2C2AP                | 0.37771      | 3.18029E-10 | NAA40                  | 0.310219228  | 0.000422197 |
| DCP2                   | 0.287675     | 1.59533E-06 | RBFA                   | 0.475215495  | 6.33587E-08 |
| MYO18B                 | 0.318687     | 1.08182E-07 | MNS1                   | -0.25172475  | 0.000151143 |
| SAMD9L                 | 0.404892     | 1.58595E-11 | YIPF5                  | -0.263744563 | 7.21215E-05 |
| DHX37                  | -0.18649     | 3.01359E-05 | <b>STARD4</b>          | 0.391470641  | 8.46001E-06 |
| RPTOR                  | -0.21671     | 1.1953E-06  | PAWR                   | -0.220360562 | 0.000901743 |
| APITD1                 | 0.219565     | 0.000241473 | RPRD1A                 | 0.318413734  | 0.000295359 |
| ZCCHC7                 | 0.211991     | 0.000391534 | PSMB7                  | 0.292536169  | 0.000887448 |
| LEPREL4                | -0.22838     | 3.04649E-07 | SDF2                   | -0.279891968 | 2.54266E-05 |
| DVL3                   | 0.40306      | 1.95328E-11 | LARP6                  | 0.354127288  | 5.6501E-05  |
| WBSCR16                | 0.194091     | 0.001156709 | LLPH                   | -0.324252605 | 1.08662E-06 |
| CHAMP1                 | 0.257642     | 1.69553E-05 | KLHL25                 | 0.299264342  | 0.00067197  |
| UBE2E2                 | 0.256329     | 1.86988E-05 | PARP12                 | 0.785046577  | 3.70506E-19 |
| NDNL2                  | -0.14823     | 0.000944678 | ASCC2                  | 0.375219375  | 1.9749E-05  |
| NEDD4L                 | -0.19007     | 2.10502E-05 | OSGEPL1                | 0.396136463  | 6.59198E-06 |
| TEFM                   | 0.314722     | 1.54802E-07 | EPB41L5                | 0.326093733  | 0.000209733 |
| KCTD15                 | 0.324022     | 6.63647E-08 | <b>ACSS2</b>           | 0.298487365  | 0.0006941   |
| PSMB7                  | -0.17853     | 6.54393E-05 | HAUS2                  | 0.799909294  | 7.86191E-20 |
| LARP6                  | 0.259766     | 1.4457E-05  | CDKN2AIP               | -0.294218361 | 9.62136E-06 |
| TTYH3                  | -0.204       | 4.90537E-06 | ZAK                    | -0.238468647 | 0.00032982  |
| PARP12                 | 0.568155     | 3.61808E-21 | CRIPT                  | 0.337803841  | 0.000122708 |
| PLEKHA4                | 0.200599     | 0.000787625 | PDP1                   | -0.490825713 | 1.71079E-13 |
| C2orf44                | 0.33055      | 3.61185E-08 | GNG12                  | 0.395233631  | 6.9195E-06  |

**APPENDIX**

| 10 $\mu$ M compound 12 |              |             | 30 $\mu$ M compound 12 |              |             |
|------------------------|--------------|-------------|------------------------|--------------|-------------|
| Gene name              | log2 (ratio) | p-value     | Gene name              | log2 (ratio) | p-value     |
| MEAF6                  | 0.211249     | 0.000410186 | CTSZ                   | -0.260291249 | 8.94854E-05 |
| <b>SCPEP1</b>          | -0.14619     | 0.001113106 | TNFSF13B               | -0.498197854 | 7.42977E-14 |
| CHD8                   | -0.16711     | 0.000188615 |                        |              | 1           |
| STARD5                 | -0.20099     | 6.77389E-06 |                        |              | 1           |
| PDP1                   | 0.220348     | 0.000229509 |                        |              | 1           |
| PALD1                  | -0.18009     | 5.6371E-05  |                        |              | 1           |
| TNFSF13B               | 0.597883     | 2.92108E-23 |                        |              | 1           |
| TMED5                  | -0.16542     | 0.000219384 |                        |              | 1           |
| STARD13                | -0.16088     | 0.000327323 |                        |              | 1           |
| PCLO                   | 0.467785     | 7.18421E-15 |                        |              | 1           |

**Table 17: Proteins modulated by compound 10.**

U-2OS cells were treated for 24 h with 10  $\mu$ M and 30  $\mu$ M compound **10** prior to proteome profiling using tandem mass tags for quantification by nanoHPLC-MS/MS. Data are mean values  $\pm$  SD of three independent experiments. Log2 (ratio) and p-values ( $p < 0.05$  Benjamini-Hochberg corrected) of up- and down-regulated proteins. Gene names of proteins involved in the regulation of cholesterol homeostasis and lysosomal function were depicted in bold.

| 10 $\mu$ M compound 10 |             |             | 30 $\mu$ M compound 10 |             |          |
|------------------------|-------------|-------------|------------------------|-------------|----------|
| Gene names             | log2(ratio) | p-value     | Gene names             | log2(ratio) | p-value  |
| CCM2                   | 0.674834    | 8.85478E-09 | CCM2                   | 0.396467    | 1.57E-08 |
| hCG_2043597            | -0.4212     | 4.56108E-06 | STXBP1                 | 0.278254    | 7.22E-05 |
| FAM49B                 | 0.619818    | 1.28544E-07 | hCG_2043597            | 0.539353    | 1.48E-14 |
| EYA3                   | 0.394194    | 0.000803118 | <b>PPT1</b>            | -0.27903    | 1.66E-07 |
| NIN                    | 0.731661    | 4.45408E-10 | GPNMB                  | 0.246968    | 0.000427 |
| KHNYN                  | 0.806981    | 5.93329E-12 | EYA3                   | 0.320612    | 4.82E-06 |
| LPXN                   | 0.464159    | 7.81684E-05 | NIN                    | 0.414543    | 3.4E-09  |
| HMGN2                  | 0.508677    | 1.487E-05   | EXOC6                  | -0.2229     | 2.91E-05 |
| TRAPPC2B               | 0.414175    | 0.000427393 | DTL                    | -0.20799    | 9.6E-05  |
| PCBD1                  | -0.41549    | 6.11978E-06 | CEP131                 | -0.1917     | 0.000325 |
| TFAM                   | -0.34399    | 0.000178166 | KHNYN                  | 0.917727    | 4.2E-39  |
| CDK5                   | 0.450923    | 0.000124658 | TRAPPC2B               | 0.418881    | 2.33E-09 |
| HNRNPD                 | 0.471276    | 6.05125E-05 | <b>FDFT1</b>           | 0.247628    | 0.000412 |
| GOLGB1                 | 0.412058    | 0.000457531 | HSPA13                 | -0.18872    | 0.000402 |
| CLEC16A                | -0.39783    | 1.48414E-05 | COG7                   | -0.21725    | 4.61E-05 |
| SPTY2D1                | 0.547391    | 3.13728E-06 | CDK5                   | 0.440947    | 3.23E-10 |
| FIGNL1                 | -0.34737    | 0.000153898 | MAPK7                  | 0.537709    | 1.77E-14 |

APPENDIX

| 10 $\mu$ M compound 10 |                          |             | 30 $\mu$ M compound 10 |                          |          |
|------------------------|--------------------------|-------------|------------------------|--------------------------|----------|
| Gene names             | log <sub>2</sub> (ratio) | p-value     | Gene names             | log <sub>2</sub> (ratio) | p-value  |
| RBFA                   | 0.421443                 | 0.000337454 | HNRNPD                 | 0.397678                 | 1.42E-08 |
| PARP12                 | 0.830905                 | 1.3824E-12  | NCOA6                  | -0.37097                 | 3.38E-12 |
| CDKN2AIP               | -0.44222                 | 1.49697E-06 | GOLGB1                 | 0.54073                  | 1.27E-14 |
| CRIP1                  | 0.398381                 | 0.000705286 | SPTY2D1                | 3.141836                 | NaN      |
| TNFSF13B               | 0.513                    | 1.25638E-05 | MRPL14                 | -0.17732                 | 0.000886 |
|                        |                          |             | FIGNL1                 | -0.30627                 | 9.15E-09 |
|                        |                          |             | DYM                    | -0.1865                  | 0.000471 |
|                        |                          |             | DCP2                   | 0.327255                 | 3.05E-06 |
|                        |                          |             | SAMD9L                 | 0.263197                 | 0.000174 |
|                        |                          |             | PARP12                 | 0.356544                 | 3.68E-07 |
|                        |                          |             | MEAF6                  | 0.247989                 | 0.000404 |
|                        |                          |             | HAUS2                  | 0.36299                  | 2.26E-07 |
|                        |                          |             | CDKN2AIP               | -0.38032                 | 9.58E-13 |
|                        |                          |             | TNFSF13B               | 0.643716                 | 4.44E-20 |

**Table 18: Proteins modulated by compound 11.**

U-2OS cells were treated for 24 h with 10  $\mu$ M and 30  $\mu$ M compound **11** prior to proteome profiling using tandem mass tags for quantification by nanoHPLC-MS/MS. Data are mean values  $\pm$  SD of three independent experiments. Log<sub>2</sub> (ratio) and p-values ( $p < 0.05$  Benjamini-Hochberg corrected) of up- and down-regulated proteins. Gene names of proteins involved in the regulation of cholesterol homeostasis and lysosomal function were depicted in bold.

| 10 $\mu$ M compound 11 |                          |           | 30 $\mu$ M compound 11 |                          |          |
|------------------------|--------------------------|-----------|------------------------|--------------------------|----------|
| Gene names             | log <sub>2</sub> (ratio) | p-value   | Gene names             | log <sub>2</sub> (ratio) | p-value  |
| ZMYND8                 | 0.375299                 | 5.165E-05 | OTUD5                  | 0.389652                 | 0.000233 |
| CDC42BPA               | -0.47973                 | 4.371E-12 | CIC                    | 0.403387                 | 0.000139 |
| CCM2                   | 0.480232                 | 2.249E-07 | CDC42BPA               | -0.50527                 | 2.15E-09 |
| TTN                    | -0.27401                 | 7.805E-05 | CCM2                   | 0.497852                 | 2.56E-06 |
| SCOC                   | 0.304865                 | 0.0010021 | TTN                    | -0.30962                 | 0.000241 |
| RASSF7                 | -0.34158                 | 8.339E-07 | RASSF7                 | -0.40974                 | 1.2E-06  |
| EIF4G3                 | -0.23475                 | 0.0007179 | hCG_2043597            | 1.460789                 | 2.1E-43  |
| <b>PPT1</b>            | -0.26608                 | 0.0001253 | <b>PPT1</b>            | -0.42411                 | 5.01E-07 |
| AP1S1                  | -0.28996                 | 2.904E-05 | EPS8                   | 0.389948                 | 0.000231 |
| GTPBP10                | -0.95879                 | 1.251E-43 | AP1S1                  | -0.3198                  | 0.00015  |
| VBP1                   | 0.538751                 | 6.348E-09 | GTPBP10                | -1.03344                 | 2.02E-34 |
| NIN                    | 0.623737                 | 1.792E-11 | APOBEC3B               | 0.40281                  | 0.000142 |
| TMEM33                 | -0.35612                 | 2.785E-07 | RIOK3                  | 0.467603                 | 9.99E-06 |



**APPENDIX**

| 10 $\mu$ M compound 11 |             |           | 30 $\mu$ M compound 11 |             |          |
|------------------------|-------------|-----------|------------------------|-------------|----------|
| Gene names             | log2(ratio) | p-value   | Gene names             | log2(ratio) | p-value  |
| PHLDB2                 | 0.322637    | 0.0004992 | NIN                    | 0.672574    | 2.06E-10 |
| NEDD8-MDP1             | 0.373444    | 5.624E-05 | TANGO2                 | 0.410951    | 0.000104 |
| LMO7                   | -0.4323     | 4.405E-10 | PPP1R9B                | 0.410761    | 0.000105 |
| NAT1                   | 0.30558     | 0.0009751 | LMO7                   | -0.5625     | 2.68E-11 |
| PPP2R5D                | -0.3786     | 4.695E-08 | PPP2R5D                | -0.47332    | 2.05E-08 |
| MSL1                   | -0.32321    | 3.136E-06 | MSL1                   | -0.43762    | 2.15E-07 |
| STXBP3                 | 0.405139    | 1.247E-05 | STXBP3                 | 0.374567    | 0.000404 |
| STK25                  | 0.397111    | 1.846E-05 | KHNYN                  | 0.700989    | 3.46E-11 |
| KHNYN                  | 0.776296    | 6.058E-17 | LPXN                   | 0.596353    | 1.74E-08 |
| FANCG                  | 0.526879    | 1.351E-08 | SAP30                  | -0.28383    | 0.000762 |
| GYG2                   | 0.369188    | 6.826E-05 | MYCBP2                 | -0.31091    | 0.000227 |
| LPXN                   | 0.442366    | 1.843E-06 | TRAPPC2B               | 0.548577    | 2.18E-07 |
| SAP30                  | -0.24194    | 0.0004892 | MAN1A1                 | -0.38006    | 6.64E-06 |
| MYCBP2                 | -0.277      | 6.511E-05 | SMARCA2                | 0.370857    | 0.000461 |
| YEATS4                 | 0.321164    | 0.0005295 | RBM5                   | -0.30042    | 0.000367 |
| HMGN1                  | -0.28527    | 3.904E-05 | PCBD1                  | -0.3227     | 0.00013  |
| TRAPPC2B               | 0.553436    | 2.441E-09 | TMSB4X                 | 0.69082     | 6.61E-11 |
| EEF1A                  | 0.36909     | 6.857E-05 | PPIA                   | -0.51695    | 9.11E-10 |
| HIST1H1C               | 0.308303    | 0.0008781 | RBM3                   | 0.380056    | 0.000332 |
| STMN1                  | 0.309552    | 0.0008367 | TFAM                   | -0.28426    | 0.000748 |
| MAN1A1                 | -0.31301    | 6.356E-06 | CDK5                   | 0.503605    | 1.95E-06 |
| NUP153                 | 0.399443    | 1.648E-05 | HNRNPU                 | 0.362921    | 0.00061  |
| SMARCA2                | 0.379642    | 4.226E-05 | DNAJC3                 | 0.800352    | 3.86E-14 |
| RBM5                   | -0.26255    | 0.000154  | HNRNPD                 | 0.580688    | 4.08E-08 |
| CLTCL1                 | -0.24249    | 0.000475  | ESPL1                  | 0.392193    | 0.000212 |
| TPD52                  | -0.27075    | 9.494E-05 | NCOA6                  | -0.45508    | 6.95E-08 |
| PCBD1                  | -0.33556    | 1.297E-06 | LRRC14                 | 0.395729    | 0.000186 |
| TMSB4X                 | 0.782417    | 3.457E-17 | FAM98C                 | 0.362854    | 0.000612 |
| PPIA                   | -0.45242    | 6.586E-11 | EDRF1                  | 0.358501    | 0.000711 |
| TFAM                   | -0.23696    | 0.0006387 | ARID4B                 | -0.30469    | 0.000303 |
| CDK5                   | 0.339108    | 0.0002537 | HSP90AB4P              | -0.47783    | 1.5E-08  |
| HNRNPU                 | 0.395036    | 2.04E-05  | C3orf38                | 0.4901      | 3.65E-06 |
| MAPK7                  | 0.42711     | 4.111E-06 | RIF1                   | 0.401328    | 0.00015  |
| HNRNPD                 | 0.560403    | 1.538E-09 | YOD1                   | 0.372391    | 0.000437 |
| ESPL1                  | 0.363705    | 8.737E-05 | SPTY2D1                | 0.556556    | 1.45E-07 |
| NCOA6                  | -0.37818    | 4.86E-08  | RLTPR                  | 0.381738    | 0.000312 |
| LRRC14                 | 0.389529    | 2.655E-05 | FIGNL1                 | -0.33237    | 8.13E-05 |
| FAM98C                 | 0.337785    | 0.0002682 | NR2C2AP                | 0.507455    | 1.63E-06 |
| ARID4B                 | -0.32164    | 3.503E-06 | ZCCHC7                 | 0.450354    | 2.1E-05  |
| HSP90AB4P              | -0.33492    | 1.359E-06 | RPP25L                 | 0.375317    | 0.000394 |
| C3orf38                | 0.467504    | 4.644E-07 | DOCK8                  | -0.34611    | 4.08E-05 |
| RARS2                  | -0.25465    | 0.0002423 | NUP35                  | 0.413372    | 9.45E-05 |

**APPENDIX**

| 10 $\mu$ M compound 11 |             |           | 30 $\mu$ M compound 11 |             |          |
|------------------------|-------------|-----------|------------------------|-------------|----------|
| Gene names             | log2(ratio) | p-value   | Gene names             | log2(ratio) | p-value  |
| RIF1                   | 0.374214    | 5.429E-05 | CHAMP1                 | 0.42489     | 5.99E-05 |
| YOD1                   | 0.478514    | 2.483E-07 | UBE2E2                 | 0.357716    | 0.000731 |
| SPTY2D1                | 0.57939     | 4.245E-10 | NDNL2                  | -0.36561    | 1.47E-05 |
| FIGNL1                 | -0.30807    | 8.883E-06 | CFAP54                 | 0.639724    | 1.49E-09 |
| DPP8                   | -0.23765    | 0.0006159 | KCTD15                 | 0.579874    | 4.26E-08 |
| GTF2H5                 | 0.341613    | 0.0002283 | LGMN                   | 0.503561    | 1.96E-06 |
| NR2C2AP                | 0.514085    | 2.993E-08 | ACBD6                  | 0.36123     | 0.000647 |
| MYO18B                 | 0.605165    | 6.931E-11 | PARP12                 | 0.68586     | 9.03E-11 |
| RPAP2                  | -0.27893    | 5.785E-05 | RWDD1                  | 0.438552    | 3.43E-05 |
| RPTOR                  | -0.23252    | 0.000807  | CDKN2AIP               | -0.38457    | 5.16E-06 |
| APITD1                 | 0.34471     | 0.0002002 | CALCOCO1               | -0.32589    | 0.000112 |
| ZCCHC7                 | 0.529495    | 1.145E-08 | TNFSF13B               | 0.917605    | 4.14E-18 |
| RPP25L                 | 0.316998    | 0.000625  | MAGED1                 | 0.503856    | 1.93E-06 |
| SMC1B                  | -0.24056    | 0.000527  | PCLO                   | 0.377678    | 0.000361 |
| DOCK8                  | -0.33547    | 1.306E-06 |                        |             |          |
| NUP35                  | 0.392705    | 2.282E-05 |                        |             |          |
| RDH11                  | -0.25429    | 0.0002472 |                        |             |          |
| DVL3                   | 0.306508    | 0.000941  |                        |             |          |
| CHAMP1                 | 0.394449    | 2.098E-05 |                        |             |          |
| UBE2E2                 | 0.415321    | 7.506E-06 |                        |             |          |
| NDNL2                  | -0.35309    | 3.512E-07 |                        |             |          |
| CFAP54                 | 0.629236    | 1.192E-11 |                        |             |          |
| NACC1                  | -0.2364     | 0.0006581 |                        |             |          |
| KCTD15                 | 0.548652    | 3.341E-09 |                        |             |          |
| PARP12                 | 0.735483    | 2.285E-15 |                        |             |          |
| TMX1                   | 0.309767    | 0.0008297 |                        |             |          |
| RWDD1                  | 0.371918    | 6.03E-05  |                        |             |          |
| BRD7                   | 0.314459    | 0.0006908 |                        |             |          |
| AASDHPPT               | -0.23296    | 0.0007886 |                        |             |          |
| CDKN2AIP               | -0.47124    | 1.032E-11 |                        |             |          |
| PDP1                   | 0.309997    | 0.0008223 |                        |             |          |
| CALCOCO1               | -0.33206    | 1.672E-06 |                        |             |          |
| ARMCX3                 | -0.2783     | 6.014E-05 |                        |             |          |
| DDX19B                 | 0.316956    | 0.0006261 |                        |             |          |
| TNFSF13B               | 0.806804    | 3.547E-18 |                        |             |          |
| TMED5                  | -0.23777    | 0.000612  |                        |             |          |
| MRFAP1                 | 0.312651    | 0.0007416 |                        |             |          |
| PCLO                   | 0.388744    | 2.756E-05 |                        |             |          |

APPENDIX

Table 19: Structures of selected annotated reference compounds with high biosimilarity (> 75 %) to 10  $\mu$ M compound 13.

| Trivial name | Structure | Trivial name | Structure |
|--------------|-----------|--------------|-----------|
| SB 216641    |           | Benoxinate   |           |
| Ozanimod     |           | Aprindine    |           |
| Zotepine     |           | EIPA         |           |
| LP44         |           | Crobenetine  |           |
| Mardepodect  |           | VE-822       |           |
| LLY-507      |           | Ponatinib    |           |
| SGC0946      |           | Nemiralisib  |           |

APPENDIX

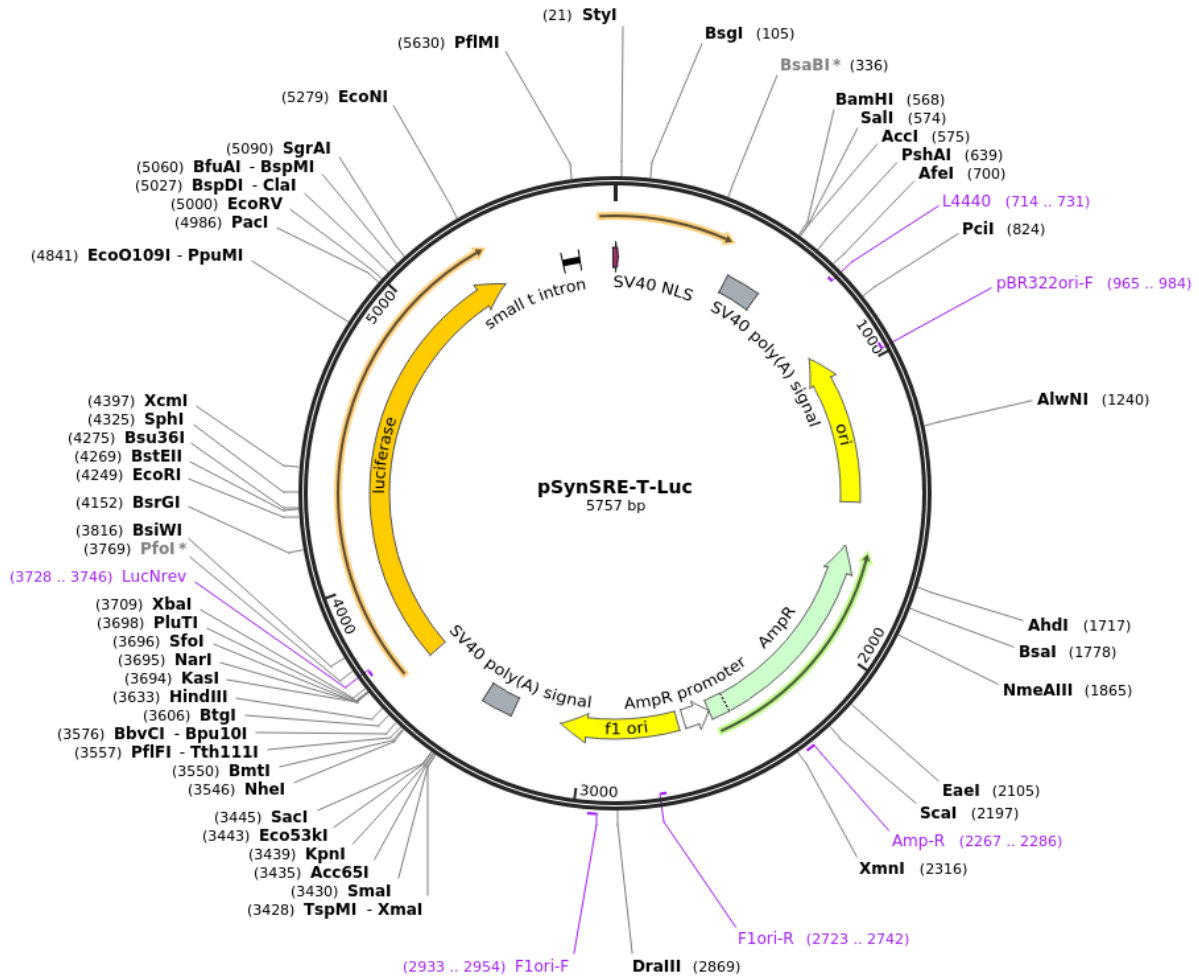
| Trivial name | Structure | Trivial name | Structure |
|--------------|-----------|--------------|-----------|
| EHop-016     |           | WZ4002       |           |
| SGI-1776     |           | Tenovin-6    |           |
| NVP-AEW541   |           | Deltarasin   |           |
| NU7441       |           | I-BET151     |           |
| JNK-IN-8     |           | OICR-9429    |           |
| Avapritinib  |           | GSK6853      |           |
| Trequinsin   |           | PP2          |           |



### 13.2.1 Vector maps

#### pSyn-SRE-T-Luc

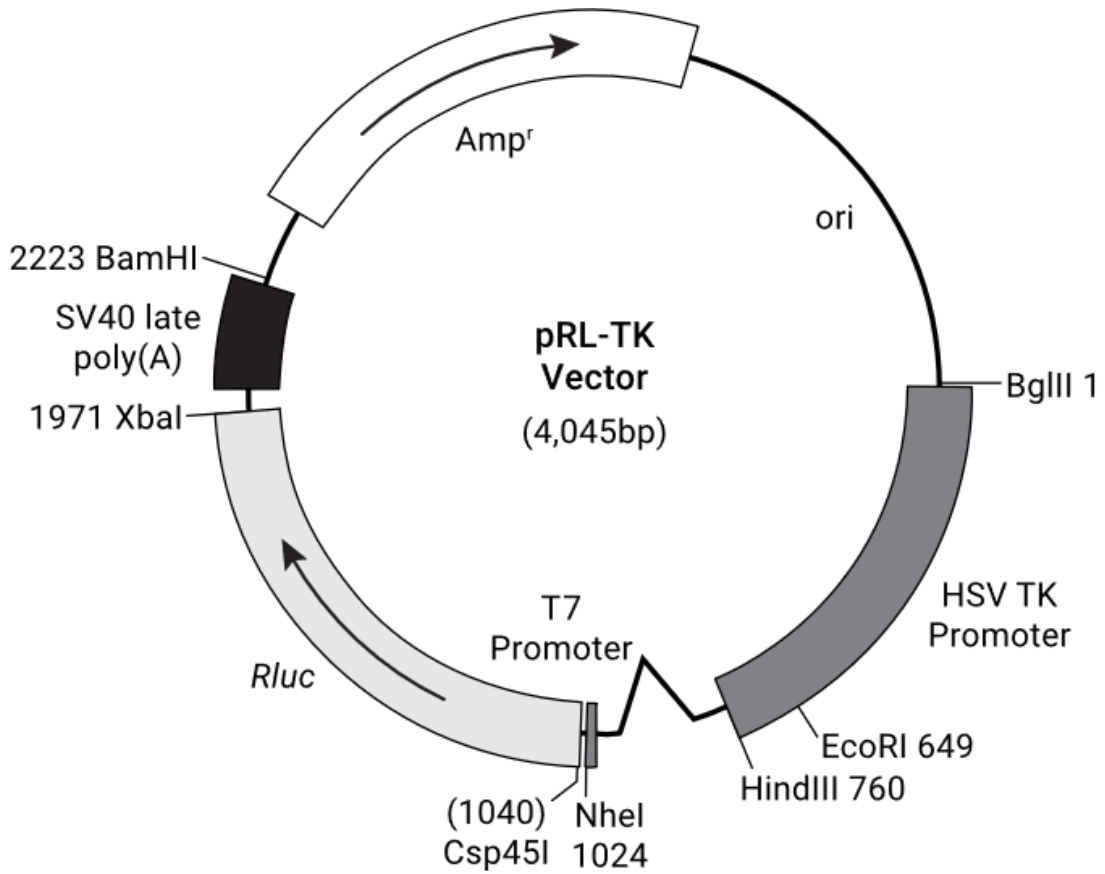
The pSyn-SRE-T-Luc plasmid was obtained from Addgene (#60444) where it was deposited by Timothy Osborne.<sup>[91]</sup>





**pRL-TK**

The pRL-TK plasmid was obtained from Promega (E2241).





## 14 EIDESSTATTLICHE VERSICHERUNG (AFFIDAVIT)

## Eidesstattliche Versicherung (Affidavit)

Schneidewind, Tabea

Name, Vorname  
(Surname, first name)

149201

Matrikel-Nr.  
(Enrolment number)

## Belehrung:

Wer vorsätzlich gegen eine die Täuschung über Prüfungsleistungen betreffende Regelung einer Hochschulprüfungsordnung verstößt, handelt ordnungswidrig. Die Ordnungswidrigkeit kann mit einer Geldbuße von bis zu 50.000,00 € geahndet werden. Zuständige Verwaltungsbehörde für die Verfolgung und Ahndung von Ordnungswidrigkeiten ist der Kanzler/die Kanzlerin der Technischen Universität Dortmund. Im Falle eines mehrfachen oder sonstigen schwerwiegenden Täuschungsversuches kann der Prüfling zudem exmatrikuliert werden, § 63 Abs. 5 Hochschulgesetz NRW.

Die Abgabe einer falschen Versicherung an Eides statt ist strafbar.

Wer vorsätzlich eine falsche Versicherung an Eides statt abgibt, kann mit einer Freiheitsstrafe bis zu drei Jahren oder mit Geldstrafe bestraft werden, § 156 StGB. Die fahrlässige Abgabe einer falschen Versicherung an Eides statt kann mit einer Freiheitsstrafe bis zu einem Jahr oder Geldstrafe bestraft werden, § 161 StGB.

Die oben stehende Belehrung habe ich zur Kenntnis genommen:

## Official notification:

Any person who intentionally breaches any regulation of university examination regulations relating to deception in examination performance is acting improperly. This offence can be punished with a fine of up to EUR 50,000.00. The competent administrative authority for the pursuit and prosecution of offences of this type is the chancellor of the TU Dortmund University. In the case of multiple or other serious attempts at deception, the candidate can also be unenrolled, Section 63, paragraph 5 of the Universities Act of North Rhine-Westphalia.

The submission of a false affidavit is punishable.

Any person who intentionally submits a false affidavit can be punished with a prison sentence of up to three years or a fine, Section 156 of the Criminal Code. The negligent submission of a false affidavit can be punished with a prison sentence of up to one year or a fine, Section 161 of the Criminal Code.

I have taken note of the above official notification.

Dortmund, 15.03.2021

Ort, Datum  
(Place, date)Unterschrift  
(Signature)Titel der Dissertation:  
(Title of the thesis):

Morphological Profiling of Small Molecules for Mode-of-Action Studies using  
the Cell Painting Assay

Ich versichere hiermit an Eides statt, dass ich die vorliegende Dissertation mit dem Titel selbstständig und ohne unzulässige fremde Hilfe angefertigt habe. Ich habe keine anderen als die angegebenen Quellen und Hilfsmittel benutzt sowie wörtliche und sinngemäße Zitate kenntlich gemacht.

Die Arbeit hat in gegenwärtiger oder in einer anderen Fassung weder der TU Dortmund noch einer anderen Hochschule im Zusammenhang mit einer staatlichen oder akademischen Prüfung vorgelegen.

I hereby swear that I have completed the present dissertation independently and without inadmissible external support. I have not used any sources or tools other than those indicated and have identified literal and analogous quotations.

The thesis in its current version or another version has not been presented to the TU Dortmund University or another university in connection with a state or academic examination.\*

\*Please be aware that solely the German version of the affidavit ("Eidesstattliche Versicherung") for the PhD thesis is the official and legally binding version.

Dortmund, 15.03.2021

Ort, Datum  
(Place, date)Unterschrift  
(Signature)